The hepatic response following infection with *Listeria monocytogenes*

BENJAMIN IZAR

INAUGURALDISSERTATION
zur Erlangung des Grades eines **Doktors der Medizin**
des Fachbereichs Medizin der Justus-Liebig-Universität Gießen

édition scientifique
VVB LAUFERSWEILER VERLAG

1. Auflage 2013

1st Edition 2013

Printed in Germany

édition scientifique
VVB LAUFERSWEILER VERLAG

STAUFENBERGRING 15, D-35396 GIESSEN
Tel: 0641-5599888 Fax: 0641-5599890
email: redaktion@doktorverlag.de

www.doktorverlag.de

The hepatic response following infection with *Listeria monocytogenes*

INGURALDISSERTATION

zur Erlangung des Grades eines
Doktors der Medizin
des Fachbereichs Medizin der
Justus-Liebig-Universität Gießen

vorgelegt von

Benjamin Izar

aus Aschaffenburg

Gießen 2013

Aus der Medizinischen Mikrobiologie
Universitätsklinikum Gießen und Marburg GmbH
Standort Gießen
Direktor: Prof. Dr. Trinad Chakraborty

Gutachter: Prof. Dr. Trinad Chakraborty
Gutachter: Prof. Dr. Elke Roeb
Tag der Disputation: 14.03.2013

Dedicated to my parents,

Samun & Basima

TABLE OF CONTENTS

ABBREVIATIONS

°C	Degree Celcius
BHI	Brain heart infusion
BSA	Bovine serum albumine
CCL	Chemokine (C-C motif) ligand
cDNA	Complementary desoxyriboneucleic acid
CFU	Colony-forming unit
CHE	Cholinesterase
cRNA	Complementary riboneucleic acid
CT	Cycle values
CTL	Cytotoxic T Lymphocytes
d p.i.	Day(s) post infection
DAPI	4',6-Diamidino-2-phenylindole dihydrochloride
DAVID	Database for Annotation, Visualization and Integrated Discovery
DEF	Defensin
DMEM	Dulbecco's modified Eagle's medium
DMSO	Dimethyl sulphoxide
DNA	Deoxyribonucleic acid
EDTA	Ethylenediaminetetraacetic acid
FBS	Fetal bovine serum
FC	Fold Change
FDR	False Discovery Rate
GGT	Glutamyl-gamma transaminase
GO	Gene Ontology
GOT	Glutamate-oxalacetic transaminase
GPT	Glutamate-pyruvate transaminase
h	Hour
h p.i.	Hours post infection
HepG2	Human Hepatoma Cells
HuH-7	Human Hepatocellular Carcinoma Cells
IFN-γ	Interferon gamma
IL	Interleukin
IPA	Ingenuity Pathway Analysis

KEGG	Kyoto Encyclopedia of Genes and Genomes
KNN	K Nearest Neighbor
l	Litre
L. monocytogenes	*Listeria monocytogenes*
LD	Lipid droplet
LDH	lactate dehydrogenase
LLO	Listeriolysin
LPS	Lipopolysaccharide
LXR-α	Liver X Receptor alpha
LXR-αP	Phosphorylated Liver X Receptor alpha
mg	Milligram
MHC	Major histocompatibility complex
MHC-Ia	Major histocompatibility complex Class Ia
MHC-Ib	Major histocompatibility complex Class Ib
min	Minute
ml	Millilitre
mM	10-3 mol/l
mRNA	messenger RNA
MVA	Mean versus Average
NF-κB	Nuclear factor kappa-light-chain-enhancer of activated B cells
NK	Natural Kille Cell
OD600	Optical density at 600 nm wavelength
PBS	Phosphate buffered saline
pH	-log10[H+]
PRR	Pathogen Recognition Receptor
QC	Quality Control
RNA	Ribonucleic acid
Rpm	Revolutions per minute
RT-PCR	Reverse Transcriptase-Polymerase-Chain-Reaction
s	Second
SD	Standard deviation
SDS	Sodium dodecyl sulphate
SKNN	Sequential K Nearest Neighbor
TAE buffer	Tris-acetate-EDTA buffer

TAG	Triglyceride
TF	Transcription factor
TLR	Toll-like receptor
Tris	Tris(hydroxymethyl)aminomethane
wt	Wild-type
µg	Microgram
µl	Microlitre
µM	10-6 mol

1. INTRODUCTION

1.1 General Microbiology of *Listeria* ssp.

Listeriae are present ubiquitously in nature and may be isolated from water, soil, plant but also in the gastrointestinal tract of human and animals. The genus *Listeria* consists of a group of bacteria of low G+C content closely related to *Bacillus*, *Clostridium*, *Enterococcus*, *Streptococcus* and *Staphylococcus* [1]. Listerial morphology is described to be bacillary with a length from 0.5 – 2µm and a diameter of 0.4 – 0.5 µm, owning the typical cell wall of Gram-positive bacteria. *Listeria* ssp. are facultative anaerobic, non-sporulating, facultative intracellular living bacteria with high motility at 20-25°C [2]. Decomposing plant material is the native habitat, where *Listeria* ssp. lives saprophytic [3]. On the basis of DNA-DNA hybridization, multilocus enzyme analysis, and 16S rRNA sequencing, the genus *Listeria* presently consists of six species: *Listeria monocytogenes*, *L. ivanovii, L. innocua, L. seeligeri, L. welshimeri* and *L. gray*. The species can be distinguished by cultivation, biochemical markers and microscopy. *Listeria* ssp. possess a remarkably resistance against extreme environment conditions. The optimal growth temperature is considered 30°C – 37°C, but *Listeria* ssp. may survive a temperature range from -0.4°C up to 50°C. *Listeria* ssp. tolerate pH from 4.5 up to 9.6 and common salt concentration of about 10 % [4]. The reproduction time of the strains is nearly identical [1].

Within the genus *Listeria*, only *L. monocytogenes* and *L. ivanovii* are considered virulent, because these species are able to survive and proliferate within the host cells. Particularly *L. monocytogenes* is a public health concern [5]. By virtue of their ability to continue to exist after conventional food conservation, they are potential food-borne pathogens. By phenotypic subtyping of *L. monocytogenes* by serotyping, thirteen serovars have been identified in *L. monocytogenes*. Three of them 1/2a, 1/2b and 4b are mainly isolated from clinical cases [5]. *L. monocytogenes* owns sophisticated virulence factors, which facilitate to cross the intestinal barrier, the feto-placental barriers and the blood brain barrier. In order to maintain its intracellular lifestyle, *L. monocytogenes* has evolved a number of mechanisms to take advantage of host processes to grow and spread from cell to cell without damaging host cells [1]. In this manner it is able to cause an infection disease known as *listeriosis*.

1.2 Virulence factors

By interacting with host immune effectors, bacteria may develop the ability to modulate and use the host environment to improve their own survival. Virulence factors define and characterize the capability of bacteria to survive within host organisms and damage the host. Several listerial virulence factors were described, including factors that enhance the ability of *Listeria* to adhere and invade host cells, escape from the phagosomal vacuole into the cellular cytosol and the complex interplay with the cellular cytoskeleton architecture to move within cells. The virulence of *Listeriae* depends on the ability to express these factors. *L. monocytogenes* possesses a plethora of virulence factors that are essential for its pathogenicity, such as LLO, ActA, Phospholipases, Internalins and ClpCs.

1.2.1 Listeriolysin (LLO)

As *Listeriae* are internalized or phagocyted into cells, they are enclosed within a vacuole that is surrounded by the phagosomal membrane. Professional phagocytic cells immediately begin to kill bacteria within these vacuoles, and survival of *L. monocytogenes* depends on a rapid escaping from this hostile environment. Listeriolysin (hemolysin), encoded by the gene *hly*, is essential for an efficient and rapid disruption of the vacuole after phagocytosis [6, 7]. Thus, it plays a key role not only in intracellular parasitism but also in several vital functions for the interaction of *L. monocytogenes* with the mammalian host.

1.2.1.1 Characterization of LLO and its role in escape from the phagosome

Listeriolysin O (LLO) belongs to a family of cholesterol-dependent pore-forming cytolysins, also including streptolysin O formed by *Streptococcus pyogenes* and perfringolysin O expressed by *Clostridium perfringens* [8]. The fundamental role of LLO in the pathophysiology of listeriosis is demonstrated by double knockout bacteria, lacking the ability to produce LLO, which are not capable to escape into cytosol and unable to survive within invaded cells [6]. In this manner, LLO ensures the survival and proliferation in macrophages and non-professional phagocytes, thereby preserving the intracellular niche for bacterial proliferation. As a mediator of phagosome membrane

disruption, LLO is also required for the efficient escape from the double-membrane vacuole that forms upon cell-to-cell spread [9].

The pore-forming activity of LLO depends on the phagosomal acid level showing high activity at pH conditions ranging from 4.5 to <6 [10], but not at neutral pH, which nearly comes upon the cytoplasmatic pH. Further experimental evidence indicates rapid and irreversible denaturation of LLO structure at neutral pH leading to the conclusion that LLO is active in phagocytic vacuoles, but not in the cytoplasm. Compartmentalization of LLO also requires a PEST-like sequence [11]. PEST sequences direct eukaryotic proteins for proteasomal degradation [12]. This led to the hypothesis of *L. monocytogenes* adopted the PEST motif to advance viability in the host cell without damaging it. LLO-ΔPEST mutants were shown to be able to escape from phagosome, but subsequently destroyed the host cell [11], leading to the suggestion that PEST sequence is required for the LLO-degradation when occurring in the host cytosol and thus preventing precocious cytolysis. However, there is still experimental discrepancy concerning the role of the PEST sequence in LLO [13]. The pores or membrane lesions caused by LLO may facilitate the access of *Listeria* phospholipases, leading to total dissolution of the physical barrier that delimits the phagosomal compartment [1, 13]

1.2.1.2 Other roles of LLO in infection

In addition to its pore-forming activity, LLO is essential in the host-bacterium interaction. LLO induces signaling pathways in the host cells that strongly influence the course of infection. These events include modulation of bacterial uptake [13] cytokine and chemokines expression, induction of mucus exocytosis in intestinal cells [14], suppression of macrophage phagocytosis [15], activation of MAP kinase pathway in epithel cells, NF-κB activation [1], expression of cell adhesion molecules in infected endothelial cells and induction of apoptosis [1, 16]. Studies by Repp et al. further suggest that signaling could be due to direct Ca 2+ influx via the LLO pores [17]. Further investigations demonstrated that proteaosome-mediated degradation of LLO for MHC-I restriction is essential to produce immunodominant T lymphocyte epitope. Moreover induction of MHC-I restriction of intracellular bacteria by LLO-mediated releasing plays a key role in the protective immune response by cytotoxic T

lymphocytes. LLO also initiates a potent humoral response, thus, LLO-specific antibodies can be used in the serodiagnosis of *L. monocytogenes*.

1.2.2 Phospholipases

L. monocytogenes produces two distinct phospholipases C, PC-PLC (lecithinase), encoded by plcB, is a broad-range PLC, whereas PI-PLC, encoded by the plcA, is specific for phosphatidylinositol.

PlcB is active at a pH range from 5.5 to 8.0. It is required for efficient lysis of the secondary phagosomes formed after listerial actin-based cell-to-cell spread [18]. PlcB is secreted as proenzyme that is processed in the extracellular medium by proteolytic cleavage. PlcB must be secreted in an inactive form to prevent bacterial membrane damage due to degradation of its own phospholipids [19]. PlcB is also shown to be required for intercellular spread from macrophages to different types of mammalian cells, including microvascular endothelial cells [20]. In this manner, the PlcA/PlcB tandem supports the LLO-membrane-pore-forming function. Furthermore PLCs also play an important role in pathogenesis by inducing host cell signaling pathways mediated by phospholipid hydrolysis products such as diacylglycerol (DAG), ceramide (CER) and inositol phosphates. These metabolites regulate key cell processes, including cell growth, apoptosis, differentiation and production of cytokines and chemokines [21].

1.2.3 ActA and actin-based motility

Pathogenic *Listeria* ssp., such as *L. monocytogenes* are able to use actin-based (myosin-independent) motility to move intracellularly and spread from cell to cell. ActA, the product of the actA gene, plays a major role in recruitment and polymerization of host actin [22]. ActA is a surface protein, which is polarly distributed on the bacterial exterior and is co-localized with actin at the onset of the actin polymerization process [23].

Two approaches established the key motor function of ActA, the expression of actA in the non-pathogenic *L. innocua* and observation of the capacity of the transformed bacterium to move in cellular extracts and transfection of actA in mammalian cells and detection of F-actin-filament formation [22]. Further factors were identified, which are

not essential for actin-polymerization, but may enhance effectivity of ActA function, including Mena, Profilin and WASP [24] and accelerate listerial movement.
After escaping from the phagosome into the cytoplasm, immediately the bacteria are surrounded by an actin-cloud, formed by Arp2/3 complex activity. There is evidence that interactions between Arp2/3 complex and ActA increases actin nucleation radically [25, 26]. In concert with ActA, these molecules lead to a continuous deposition and re-organization of actin monomers, which is essential for the intracellular movement. This cooperation is localized at just one end of the bacterial surface, thus, unidirectional actin reconstruction guides the prokaryote forward [1].

1.2.4 Internalins

The reason that *L. monocytogenes* causes severe diseases can be traced to its ability to induce its own uptake by host cells, which normally are not-phagocytic, such as endothelia, hepatocytes or cells that belong to the immune system. The proteins that mediate this internalization belong to the Internalin (Inl) family. InlA and InlB, are encoded by the inlAB operon [27]. The primary protein structure contains LRR units (leucine-rich repeat). They are involved in specific protein-protein interactions with the host cell. All internalins, excluding InlB, contain a distal (C-terminal) LPTXG-motif, which is responsible for stimulating sortase A and the covalent attachment to the peptidoglycan in Gram-positive bacteria [28].
Both InlA and InlB are sufficient to trigger internalization into appropriate host cells. They mediate invasion by a similar method, referred as zipper type mechanism, but precise observation revealed that they follow different signaling pathways to achieve entry [29]. The host cell receptor for InlA is E-Cadherin, a calcium-dependent intercellular adhesion glycoprotein. E-cadherin is present on the surface of several cells, including hepatocytes, brain microvascular endothelial cells and placental chorionic villi, all of which are potential targets during *Listeria* infection. E-cadherin contains two extracellular domains (EC1/2), which establish direct connection between neighboring cells. Interaction between InlA and E-Cadherin requires the recognition of prolin residue at position 16. In contrast to human and guinea pig E-Cadherin, mouse E-Cadherin has a glutamate at this position and therefore cannot be invaded by *Listeria* by InlA interaction [29, 30], but may still be invaded by interaction of InlB with the Met-receptor.

Via its LRR region *L. monocytogenes* binds EC1, then intracellular actin cytoskeleton rearrangement via α/β-catenins mediate entry into host cell [31]. Internalin B is necessary for uptake to hepatocytes and non-epithelial cells. Instead of a LPTXG motif, InlB contains a C-terminal GW sequence, which is known to be responsible for association to the bacterial surface [29]. InlB utilizes the hepatocyte growth factor receptor (HGFR or Met) for bacterial adherence to the host cells. Met is a receptor with tyrosine kinase activity. Since initiating its own endocytosis into host cells by Internalins is crucial in the pathophysiology of listeriosis, it is important to identify molecules and receptors in mice that facilitate entry of *Listeria* organisms.

1.2.5 P60 (murein hydrolase)

P60 is a 60kDa extracellular protein of *L. monocytogenes*, encoded by the iap-gene (invasion-associated protein), which influences the bacterial invasion in non-phagocytic cells, especially the intestinal Caco-2 cells. P60 owns a murein hydrolysis activity, which is necessary for septum formation and therefore essential for bacterial proliferation. It has also been shown, that p60 is a major antigen in protective response against *L. monocytogenes*, that is crucial for mediating immunity, but also activating the innate IFN-γ synthesis by NK-cells [32]. However, the receptors for p60 or its antigenic peptides and the mechanism of NK-cell activation remain unclear.

1.2.6 ClpC

A small portion of ingested *L. monocytogenes* survives the hostile environment of phagocytic vacuoles. Survival under stress involves an adaptive response mediated by a set of conserved proteins that are upregulated *in vitro* upon exposure to heat shock, low pH, oxidative agents, toxic chemical compounds, starvation, and, in general, any situation in which bacterial growth is arrested [1, 32], including ClpC proteins. The HSP-100/Clp family is encoded by the clpC gene, which is upregulated in heat shock conditions (42°C) and high osmolarity, preferentially expressed during stationary phase [1, 32]. Further studies suggest a requirement of ClpC for adhesion and invasion of *L. monocytogenes*, possibly by modulating the expression of InlA, InlB and ActA.

1.2.7 Regulation of the virulence gene cluster

LIP-1 (for *Listeria* Pathogenicity Island 1) includes the majority of the known listerial virulence genes. They are regulated by PrfA (positive regulatory factor A), which itself is encoded by LIP-1 (Figure 1). The LIP-1 is present at the same chromosomal localization in the genes of the two pathogen strains *L. monocytogenes* and *L. ivanovii*, indicating that virulence gene cluster was acquired by pathogenic *Listeriae* before speciation [1].

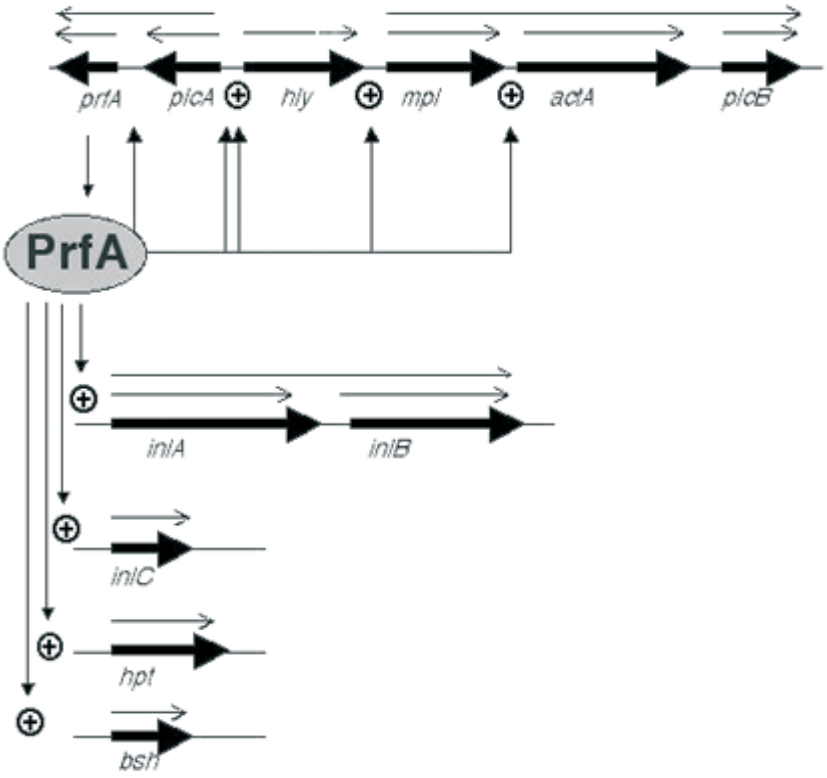

Figure 1: Control of virulence factors by the positive regulatory factor A (PrfA) in *L. monocytogenes* (with permission) [1]. Virulence factors that are located within the *Listeria pathogenicity island*, including listeriolysin (encoded by *hly*), InlA, InlB and actA are regulated by PrfA. This gene cluster is found in all clinical isolates of *L. monocytogenes* and represents the most important virulence determinant.

1.3 Intracellular infectious cycle of *L. monocytogenes*

Besides multiplying within macrophages *L. monocytogenes* is able initiate its own phagocytosis into various cell types that are usually not phagocytic cells, including epithelial cells [33], hepatocytes [34], neurons [35] , dendritic cells [36] and fibroblasts

[36, 37].Upon entry into the cell, *L. monocytogenes* is present in a vacuole that is lysed in less than thirty minutes bay LLO. The so escaped bacterium owns mechanisms to move within the cytoplasm by inducing ActA dependent actin-polymerization in the host cell. By propelling itself, it is also able to spread from cell to cell. In this case, a two-membrane vacuoles is formed consisting of the donor cell membrane and the penetrated cell phospholipid double layer (Figure 2).

1.3.1 Internalization

Upon adhesion to the host cell surface, the *Listeria* penetrates the eukaryote cell. A so-called zipper-type mechanism is needed for invasion of nonphagocytic cells, in which the bacterium is progressively enveloped by the host cell.

The eukaryote cell receptors used by *L. monocytogenes* are various, including the transmembrane glycoprotein E-Cadherin [38], the C1q complement fraction receptor [39], the Met receptor for hepatocyte growth factor (HGF) [40], components of the extracellular matrix such as heparin sulphate proteoglycans (HSPG) [41] and fibronectin [42]. The bacterial ligands identified to date, are surface proteins, such as Internalin A and B (InlA/InlB), p60 and the actin-polymerizing protein ActA.

1.3.2 Intracellular proliferation and intercellular spread

During invasion, *L. monocytogenes* becomes totally engulfed within a phagocytic vacuole, which becomes acidified soon after uptake. Thirty minutes after entry, the bacteria begin to disrupt the phagosome membrane. This escape from phagosome is necessarily required for listerial intracellular survival and proliferation and is mediated by LLO in combination with phospholipases [33].

Within 2 hours, about half the bacteria are present free in the permissive cytoplasm and begin multiplying with a doubling rate time of about 1h.

Intracellular bacteria are instantly encircled by actin, which later rearranges to form an actin tail at one pole of the bacterium. The polar assembly composed of F-actin and some regulator proteins, including the essential listerial surface protein ActA (see below), propels the bacterium with a mean speed of 0.3 μm/s. This movement is non-direceted, so that *L. monocytogenes* potentially reaches the cell periphery, leading to finger-like protrusions with a bacterium at the tip. These protuberances penetrate

uninfected neighbour-cells and are consecutively engulfed by phagocytosis. Thereby a secondary phagosome results in which the pathogen is surrounded by a double membrane, with the inner membrane originating from the donor cell. *L. monocytogenes* escapes rapidly (within 5 minutes) from the newly formed vacuole by dissolving its double membrane, reach the cytoplasm, and initiate a new round of intracellular proliferation and intercellular spread.

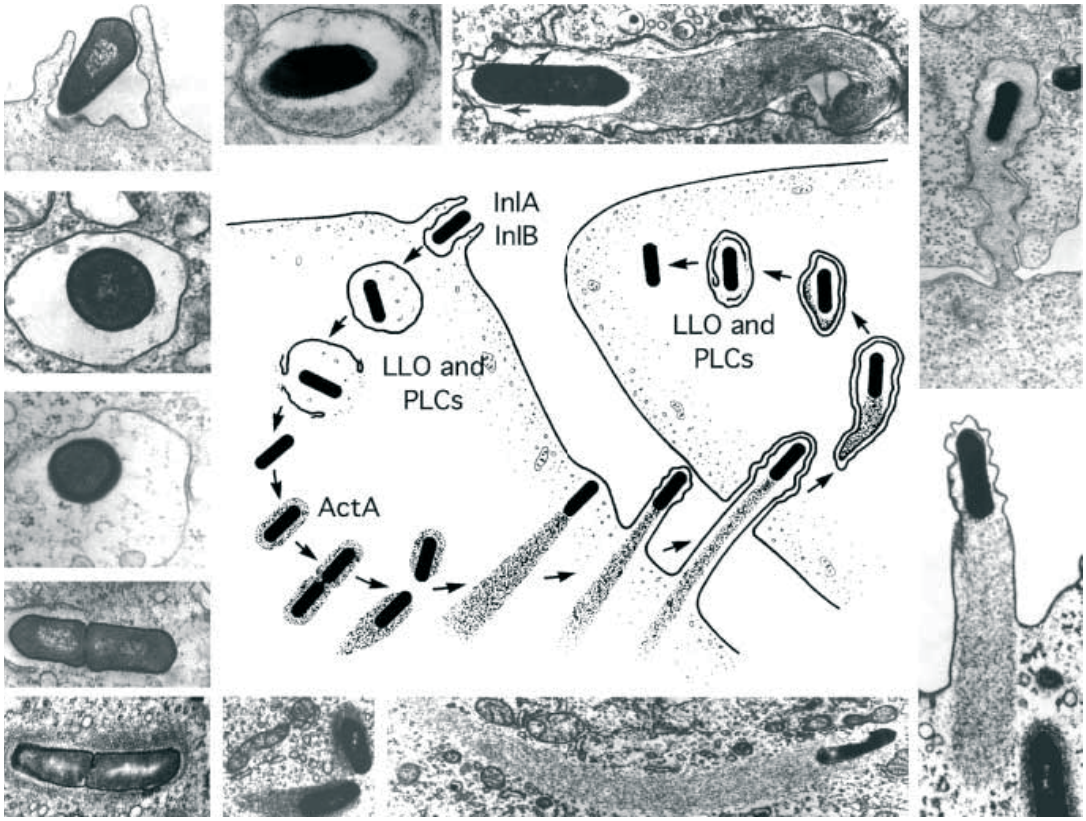

Figure 2: Intracellular lifestyle of *L. monocytogenes* (with permission) [1]. *L. monocytogenes* adheres to the non-phagocytic cell via internalins (mainly internalin A and B) or is actively internalized by macrophages. Within the phagosomal vacuole, induction of virulence factors, such as LLO and PLCs occurs. These virulence factors lead to disruption of the phagosomal vacuole. Bacteria then escape into the cytoplasm and utilize ActA based motility for unidirectional movement within the host cell. By doing so, *L. monocytogenes* is able to spread from one cell to a neighbored cell, in which it is in turn able to escape from the engulfing membrane. Cell-to-cell spread results in engulfment by a double layer of cell membranes. Disruption of this double-layer membrane requires a high activity of PLCs.

\

1.4 Host response upon infection with *L. monocytogenes*

L. monocytogenes is one of the best characterized pathogens in the world. Apart from its role as a food borne pathogen it has been used as model to study innate and adaptive immune response since the early 1960s when Mackaness demonstrated that cell mediated immunity was critical for control of infection in mice [43]. In this model, bacteria were intravenously injected into the bloodstream of mice. Within minutes, most bacteria can be found in the liver and the spleen where they are quickly internalized by resident macrophages [44]. Using *L. monocytogenes* as a model pathogen in mice infection, several studies revealed fundamental knowledge about immunity. Therefore, it is essential to utilize this tool to clarify the pathophysiology of listeriosis and generate essential knowledge in this complex field.

1.4.1 Course of infection in liver and spleen

The majority of injected bacteria are cleared from bloodstream by phagocytic and non-phagocytic cells in liver and spleen within 30 minutes. These organs are crucial for the elimination of *L. monocytogenes* from the organism.

The natural course of an experimental *Listeria* infection in mice is such that the liver captures over 90% of an i.v. injected inoculums of bacteria and the remaining 10% can be found in the spleen [45]. In the liver, bacteria are cleared rapidly during the first hours of infection, but a small number of bacteria is able to escape from early control in the liver. This very small portion is then able to proliferate during the first 24-48h p.i.. During this interval of infection, the amount of *L. monocytogenes* reaches numbers that are thousand fold higher than the initially injected burden. With the onset of innate and especially adaptive immune response the number of viable *Listeriae* in the liver subsequently decreases rapidly.

In spleen, an initial explosive growth of *Listeria* can be observed. After this early phase of proliferation, which occurs within the first 24h – 48hours upon infection, the immune response in the spleen leads to an effective clearance of *Listeria monocytogenes*. Several studies contributed to the attempt to clarify the above described infectious course. However, the global complexity remains largely unknown and is subject of intensive investigations.

1.4.2 Innate immune response

The immune system of vertebrates can be divided into two compartments whose borders became increasingly vague during the last years: innate immunity is a more ancient structure upon which adaptive immunity was subsequently built [46]. Multiple components of both, the innate and adaptive immune systems are crucial to the recognition and elimination of *L. monocytogenes* from the host. The ability of T cell depleted mice to counteract *L. monocytogenes* infection during the first days upon infection emphasizes the importance of innate immune mechanism in the defense response. Macrophages, Neutrophils and Kupffer cells represent phagocytes that are essential in the clearance of *L. monocytogenes*.

These cells contain several functions, such as phagocytosis, autophagy, detection of pathogen by pathogen pattern recognition patterns (PRRs), generation of reactive oxygen intermediates, extracellular traps (called NETs) and cytokine production that contribute to the resistance against pathogens [47].

1.4.2.1 Neutrophils

In mice, neutrophils represent approximately 15% of peripheral white blood cells, and 1-2% of non-parenchymal cells (NPC) in liver. Bacterial infection leads to neutrophil efflux from bone marrow to the site of infection via blood. Within hours, 30-50% of blood cells and 20-45% of NPC are neutrophils that are attracted by chemotaxis. Once localized at the focus of infection, neutrophils contribute to antibacterial resistance by killing bacteria, lysis of infected host cells and secretion of cytokines that suppress intracellular replication of pathogens [48]. The correlation between the magnitude of neutrophil infiltration and the decline in pathogens within the liver between 10 min and 6 hours p.i. supports the role of neutrophil effector function towards extracellular organisms. In the absence of neutrophils extracellular bacterial load is markedly increased. Neutrophils are able to counteract extracellular bacteria by producing reactive oxygen species and induction of influx of immunocompetent cells by synthesis of TNFα, IL-12, MIP-1 and IL-8.

In addition, a study suggested that antimicrobial effects of neutrophils are effective against extracellular bacteria bound to liver cell populations, such as Kupffer cells [49]. However, proteins that are involved in the cell-to-cell interactions between neutrophils

and Kupffer cells and the antimicrobial peptides released by neutrophils upon adhesion of these remain unknown.

1.4.2.2 Macrophages

Macrophages have been the focus of studies investigating the innate immunity during *L. monocytogenes* infection, because replication occurs primarily within these cells. Macrophages are indispensable in the rapid clearance of *Listeria* pathogen from the bloodstream to the liver and the spleen. In spleen *Listeriae* are phagocyted by macrophages of the marginal zone, which is localized between B cell rich red and the T cell rich white pulp. The bacteria loaded cells then migrate to the white pulp and form the beginning focus of infection. Some studies revealed that *L. monocytogenes* uses intercellular spread to invade neighbored T and NK cells in the white pulp and induces apoptosis of these cells. Thereby, *Listeria* suppresses the primary source of early IFN-γ synthesis. In response to infection, macrophages also secrete cytokines such as TNFα and IL-12 [50] which drive natural killer (NK) and CD8+ T cells to produce IFN-γ, which in turn leads to activation of the macrophages and increases their bactericidal activity. As with neutrophils, generation of reactive oxygen and nitrogen intermediates is important for macrophage-mediated killing of *L. monocytogenes*. Mice deficient in phagocyte oxidase have slightly greater bacterial burden than wild-type controls, and mice deficient in nitric oxide synthase have even greater bacterial burdens [51]. Other interferon-inducible genes, such as the p47 GTPases, are also involved in macrophage killing of bacteria through mechanisms that are yet to be determined. However, *L. monocytogenes* evolved mechanisms to escape from killing within macrophages. The pathogen was shown to impair the function of macrophages by mechanisms such as disturbing the phagocytotic activity and the maturation of phagolysosomal vacuoles [51, 52]. Furthermore, *L. monocytogenes* was suggested to trigger a cascade that leads to increased IL-10 production by macrophages, and with respect to the function of this cytokine down modulate the inflammatory response [53]. Recent studies also indicate involvement of genes involved in the regulation of lipid metabolism, such as the orphan nuclear receptor *liver x receptor*, also known as LXR. Importantly, the functions and importance of these newly described pathways that show a clear cross-relation of metabolic pathways and immune response in different organs during listeriosis have not yet been determined.

1.4.2.3 Kupffer cells

Kupffer cells are the resident tissue macrophages of the liver. They account for 80-90% of total fixed tissue macrophages in the liver. Kupffer cells are preferentially located around the periportal region and therefore optimally positioned to response to systemic bacteria and bacterial products that are transported from the gut to the liver via portal vein, but also to intravenous inoculation [54]. In addition, Kupffer cells produce cytokines, such as IL-12 and IL-6, which are crucially involved in the inflammatory response [55]. Kupffer cell deficient mice display an increase in the number of *Listeriae* and decrease in liver and were therefore suggested to be important for phagocytosis of this pathogen. However, following studies refute this idea by showing Kupffer cells indeed were crucial for clearance and trapping of *Listeria* from blood, but did not exhibit phagocyte activity [56]. Rather Kupffer cells were suggested to bind *Listeria* on their cell surface and interact with Neutrophils via intercellular receptors and thereby somehow contribute to the clearance of the pathogen. However, the underlying receptors binding *L. monocytogenes* and interacting mechanisms remain undefined.

1.4.2.4 Pathogen recognition receptors

The interior of the host organism is a sterile environment, and pathogens often gain initial access through the skin, respiratory or gastrointestinal routes. A central role of cells of innate immunity is the recognition chemical structures or invading microorganisms that are detected by pathogen recognition patterns (PRRs). Engagement of PRRs results in secretion of soluble defense factors, maturation of antigen presentation cells and production on inflammatory cytokines. PRRs that recognize microbial products are highly conserved and were present before the evolutionary divergence of the plant and animal kingdom [57]. Key aspect of PRRs is that recognition is limited to an individual motif, such as the peptidoglycan of Gram-positive bacteria or the endotoxin of Gram-negative microorganisms, and PRR coding genes do not undergo rearrangement.

At the cell surface many immune cells, including macrophages express Toll-like receptors (TLRs). Different bacterial-, viral- and protozoan-derived ligands, as well as synthetic ligands, have been identified to bind to TLRs expressed by mice. In the case of *Listeria*, the most important one is TLR2, which recognizes not only the bacterial

peptidoglycan, but also lipoproteins secreted by *Listeria* [58]. TLR recognition of pathogen-derived products leads to cell activation resulting in upregulation of expression of TNFα, IFN-γ, IL-1β and IL-12 [59]. As a Gram-positive bacterium, *L. monocytogenes* does not express the prototypical TLR ligand lipopolysaccharide (LPS), but it does express a myriad of other TLR ligands, including peptidogylcan, flagellin, and bacterial DNA which can activate macrophages. TLR signalling contributes to the immune response against *L. monocytogenes*, as studies with mice deficient in MYD88, the most important adaptor of the TLR pathway show, in which mice are highly susceptible to *Listeria* infection [60].

In the case of an intracellular pathogen such as *L. monocytogenes* another family of PRRs, the recently discovered NOD-like receptors (NLRs) also play a critical role in recognition and innate immunity. The NLR family of cytosolic localized proteins contains about 20 members and includes both nucleotide-binding oligomerization domain (NOD) proteins and NACHT-, LRR- and pyrin-domain-containing proteins (NALPs) [61]. NOD receptors recognize bacterial structures, such as the peptidoglycan of Gram-positive bacteria. These receptors are mainly expressed by dendritic cells (DCs) and macrophages, but also found in small amounts in other blood leukocytes. Activation of NOD-receptors induces maturation of dendritic cells. *In vitro* studies showed that *L. monocytogenes* exposed DCs express greater amounts of surface co-stimulatory molecules CD80 and CD86 for T cell activation than mature DCs. Similar effects were observed in macrophages [62]. Macrophages deficient in a further member of NLRs named NALP3 infected with *L. monocytogenes* showed significantly reduced levels of inflammatory cytokines, indicating an important role of NLR in the regulation of inflammatory response [61, 62]. Thus, recognition of *L. monocytogenes* and its constituents may crucially be involved in the course of infection and the inflammatory response.

1.4.2.5 Inflammatory cytokines

Cytokines represent the medium for leukocytes to communicate with each other and induce an orchestrated and balanced immune response to an external stimulus.

Production of IFN-γ is crucial to restrain intracellular pathogens and initiate an effective innate and adaptive immunity. Its significance is emphasized by mice and humans in defects of IFN-γ or IFN-γ -receptor gene resulting in critical susceptibility to

intracellular bacteria [63, 64]. While NK cells are the most important source for the early IFNγ synthesis, T cells are responsible for the synthesis of IFNγ during the later phase of infection temporally beginning 2-3days upon listerial infection. Among other biological functions in infection, IFNγ induces several genes involved in the anti-microbial activity of macrophages, PRRs and the antigen presentation apparatus and therefore accounts not only for resistance against primary infection, but also drives the arrangement of an immune memory. However, IFNγ plays a less important role for protective immunity during re-infection [65]. Several cytokines are involved in the regulation of IFNγ induction in NK and Th1 cells, of which IL-12 is the most important. Macrophages and Dendritic cells (DC) produce considerable amounts of IFNγ in an IL-12-dependent manner in the initial phase of challenge. Both, IL-12 and IFN-γ in turn boost the production of inflammatory cytokines in these cells. IL-12 preferentially binds to the IL12RB1 receptor that is expressed on NK, TH1, Macrophages and DC. Mature DCs were identified to bet the main producers of IL-12 and is depending on a microbial priming signal via pathogen recognition receptors or phagocytosis [66].

Furthermore, *in vitro* experiments using cDNA microarrays have shown that *L. monocytogenes* infection of macrophages triggers two distinct, temporally separate waves of gene induction, of which the later one is mainly associated with gene induction by interferons [67]. The earlier wave induces genes dependent on NF-κB, which is mediated by TLRs, and is not dependent on the invasion of cells by viable bacteria. However, the second wave of induced genes is dependent on *L. monocytogenes* escaping from the phagolysosome. It remains to be determined what known or unknown intracellular recognition pathway is responsible for inducing this interferon response, but recent data indicate that members of the NOD and NALP family play a central role in intracellular recognition of *L. monocytogenes* and induction of these inflammatory pathways [68, 69].

1.4.2.6 Autophagy

Autophagy or cellular self-digestion is a cellular pathway involved in protein and organelle degradation. It was first discovered as a way for cells to recycle their own intracellular organelles and cytoplasmic contents, a double membrane vacuole forms in the cytosol around the target. In response to environmental signals such as nutrients and hormones, autophagy is induced in cells [70]. ATG proteins (autophagy proteins)

mediate and regulate the autophagosome conformation. Rich et al. demonstrated that cytoplasmatic bacteria can be targets for autophagy [71]. This phenomenon has been well described for intracellular pathogens including invasive group A *Streptococcus* and *Mycobacterium tuberculosis* [71]. In addition, most recent studies with *Drosophila* revealed that induction of the autophagy machinery by Gram-positive bacteria is mediated by the peptidoglycan recognition pattern (PGRP) [72]. Intracellular *L. monocytogenes* can be a target of autophagy as observed in macrophages that were pretreated with chloramphenicol [71]. A recent study provides evidence that autophagy may also be involved in the limitation of acute liver damage that presents as microscopic accumulation of intracellular lipid droplets [73].

1.4.3 Adaptive immune response

Although cells of the innate immune system are necessary for the initial primary response against *L. monocytogenes*, T cells are crucial for the final clearance of the pathogen that begins 2-3days upon infection. The link between innate and adaptive immunity occurs through presentation of listerial peptides associated with MHC molecules. Most important for this connection are dendritic cells and macrophages that express the peptide-load MHC molecules on the cell surface which are recognized by T cells. Additionally, the professional antigen-presentation cells express co-stimulatory molecules that have the ability to enhance the T cell stimulation. Priming of T cells leads to an adaptive immune response and development of T cell memory cells.

1.4.3.1 Antigen presentation

Listeria-derived antigens are associated to MHC class I or MHC class II molecules and presented on the cell surface of antigen presenting cells to CD8 and CD4 T cells, respectively. In addition to the classical antigen presentation pathway, *L. monocytogenes* antigens may be presented by MHC class Ib (MHC-Ib) molecules. MHC-Ib lack the polymorphism of MHC-Ia molecules and bind N-formylated methionine (*f-peptides*), which are mainly limited to bacteria. MHC-Ib restricted T cells are suggested to have a distinct role in the control of infection compared to T cells restricted to MHC-Ia molecules. These T cells are important for the primary antibacterial cellular resistance, while MHC-Ia restricted T cells are responsible for the

generation of a robust protective immunity. Generally, some virulence factors and peptides of *Listeria* were identified as potent antigens for MHC-Ib associated presentation [74]. In response to *L. monocytogenes* infection, DCs are critical in priming the T cell response since mice depleted of these cells are unable to generate a CD8 T cell response to infection. DCs detect the pathogen or listerial products via PRRs, such as NLRs, and then, as some studies revealed, undergo maturation, upregulate the expression of co-stimulatory molecules and induce effective T cell response.

1.4.3.2 T cell response and protective immunity

T cells are indispensable for the final clearance of *L. monocytogenes* from the organism. While both CD4 and CD8 T cells contribute to protective immunity, *in vivo* depletion and adoptive transfer studies have clearly demonstrated that memory CD8 T cells are the most effective T cell subset for cell mediated protection [75] and CD4 cells are crucial for the priming of CD8 memory T cells during primary infection [76]. Interestingly, once T cells were primed, no further antigen presentation is necessary to induce development to cytolytic T cells (CTLs). The extent of proliferation and differentiation upon transient antigen-contact is independent of antigen, since as T cell stop to proliferate, although bacteria are still detectable [77]. T cells undergo maturation upon priming and a portion is detectable as CTLs 4 days post infection.

1.5 Pathogenesis of infection *with L. monocytogenes*

1.5.1 Entry and colonization of host tissues crossing the intestinal barrier

Before ingested *L. monocytogenes* reaches the intestine, it has to endure the acid environment of the stomach, in which a big part of the bacterial burden is eliminated. People using antacids and H2-blocking agents, have a higher risk for listeriosis, because the natural acidic barrier in the stomach is deteriorated [80]. First, *L. monocytogenes* penetrates the host by invading the intestinal epithelium or uses the M-cell epithelium as entry portal; later the bacteria are mainly detected in underlying macrophages. *L. monocytogenes* replicates intracellular in the Peyer's patches at which it establishes a local infection [81]. Intestinal translocation of pathogenic *Listeriae* occurs without the formation of macroscopic or histological lesion in the mouse gut [82]. This suggests

that *Listeria* crosses the intestinal barrier without replication within the epithelium and reaches deep organs very rapidly [83]. Invasion of intestinal epithelium seems to cause an upregulation of IL15 which in turn activates lymphocytes producing Th1-type cytokine. Among others, IFN-γ mediates NO and ROS production in macrophages, which are known to powerfully destroy *L. monocytogenes*, indicating an interaction between the pathogen and host immunity may be a relevant local defense system in the gut [84].

1.5.2 Infection of the liver

Listeria organisms that cross the intestinal barrier are carried to mesenteric lymph nodes, the spleen and the liver by the lymph or blood (Figure 3). About 90% of the bacteria load is captured by Kupffer cells in the liver and hepatocyte within 30 minutes after inoculation, thus the duration of presence in the blood is very short [85] . It is however unclear by which mechanisms Kupffer cells contribute to the killing of *L. monocytogenes*, since they were shown not to internalize the pathogen. Within a few hours the bacteria are killed to a large extend in the liver [86]. Only a small portion outlasts the unspecific and intrinsic cell defense response, but surviving bacteria start to proliferate for 48hours after infection [87]. The principal sites of bacterial proliferation within the liver are hepatocytes [44]. They use two possible ways to gain access to the liver parenchyma: via Kupffer cells by cell-to-cell spread or by using the zipper mechanism to invade hepatocytes directly. Furthermore *L. monocytogenes* utilizes actin-based intercellular spread to infect neighbor hepatocytes [35]. However, it is unclear why a small portion of the bacterial load is able to proliferate during this phase of infection, although innate immunity should be capable to eliminate the small number of *Listeria* organisms.

Neutrophils play an essential role at the spot of infection in the hepatocytes in controlling the acute phase of *L. monocytogenes* infection and in mediating the annihilation of *L. monocytogenes* infected hepatocytes. During the infectious process neutrophils are substituted by blood-delivered mononuclear cells including lymphocytes to form characteristic granulomas. These structures are the histomorphological correlate of cell-mediated immunity and act supposeably as a physical barrier to prevent the lsiterial direct cell-to-cell spread. Subsequently, as a result of γ -Interferon mediated macrophage activation and CD8+ mediated primary immune response, *L.*

monocytogenes is completely cleared from the liver. This elimination procedure calls for a running host immune system.

Furthermore non-pathogenic L. innocua qualifies and enhances the specific *L. monocytogenes* -T-cell-memory via recognition of cross-reactive p60 epitopes shared by the two species [32], indicating listerial toxins to be an important substrate for long-term-mediated immunity. In this manner repeated contact with L. innocua may amplify protective immunity against *L. monocytogenes*. This may possibly explain in part the relatively rare occurrence of clinical disease despite high frequent exposure *L. monocytogenes*. Inadequate immune response in the liver comes along with unlimited proliferation of *L. monocytogenes* with following release of bacteria into the circulation. *L. monocytogenes* can infect wide range of host tissues as indicated by its ability to cause septicaemia involving multiple organs. Most frequent sites that are invaded by *L. monocytogenes* are the gravid uterus, fetus and the CNS.

1.5.3 Infection of the spleen

Besides the elimination of *Listeria* organisms in the liver, the immune response in spleen is most important for an effective clearance of the pathogen from mice [88].

Within 2-12h of infection, *L. monocytogenes* is initially trapped in the marginal zone of the spleen [89], which separates the red and the white pulp. Tapped in the macrophages of the marginal zone, the bacteria are taken to the T cell zones of spleen during the first 24h p.i. leading to depletion from the marginal zone and the red pulp [62]. Bacteria load macrophages are important for trapping the circulating pathogen, but are dispensable for antigen presentation. Rather dendritic cells are important for induction of T cell mediated immunity [90]. Priming of CD8+ T cells appears to be predominantly mediated by dendritic cells (DC) [62]. Entry of the bacteria into the white pulp leads to controlled cell death of the splenic lymphocytes, possibly mediated by LLO [16]. In addition, infected macrophages and dendritic cells undergo apoptosis or necrosis by mechanisms suggested also to be triggered by LLO [91]. Although only 10% of the bacterial burden is initially located in the spleen, *L. monocytogenes* is able to proliferate during the first 24h p.i. and reach CFU concentrations as high as in liver, which contains 90% of the initial pathogen. The spleen seems to be an organ in which *L. monocytogenes* is able to survive and proliferate during the early phase of infection. Consistent with these observations, studies revealed that splenectomized mice show

increased resistance to *Listeria* infection during the early phase of infection, indicating a immunological gap during this phase. Although this phenomenon is known for decades, the underlying mechanisms are not yet resolved. However, after this vulnerable phase of infectious progress, splenic cells somehow acquire the ability to clear the virulent organisms, demonstrated by decreasing count of viable CFU in the progress of infection.

1.5.4 Infection of the gravid uterus, fetus and the CNS

L. monocytogenes gains access to the fetus by blood-borne transplacental infiltration. The bacteria recognize and date specific surface receptor of the placental villous explants. They presumably penetrate via the apical membrane in an internalin-E-cadherin-dependent manner. Translocation across the endothelial barrier enables the bacteria to reach the fetal bloodstream, leading to generalized infection which results in numerous military pyogranulomatous lesions (granulomatosis infantiseptica) and subsequent death or premature birth [92].

Invasion of the brain *L. monocytogenes* has a striking predilection for invading the CNS in humans by crossing the brain blood barrier, this primarily results in the form of meningitis. Active surveillance revealed that *L. monocytogenes* is the second leading cause of bacterial meningitis in patients younger than 1 month or older than 60 years. Moreover appearance of brain lesions in *Listeria*l meningoencephalitis is typical for CNS infection. The frequent listeriosis manifestation in CNS may be in part explicated by listerial ability to invade it in four various ways, (i) invasion by blood-borne, (ii) direct invasion of endothelial cells, (iii) invasion via infected phagocytes or (iv) sui generis by retrograde transport within neurons. Different lines of evidence support the concept that CNS invasion by blood-borne by *L. monocytogenes* is the predominant route of infection in humans [1]. An exciting point is that CNS invasion occurs relatively late in systemic disease, not until an overwhelming replication of *L. monocytogenes* in liver and spleen leaded to a secondary bacteremia. This suggests that *L. monocytogenes* by blood-borne are not particularly tropic for the brain endothelium the same way that they are for other cells, especially hepatocytes. However, *Listeria* organisms are able to spread from phagocytes to endothelial cells and maintain colonization in the CNS. Inference out of observations is that bacteria require a combination of duration and density of bacteremia to penetrate effectively. [36]. Thus,

infection of the CNS in a secondary bacteremia is dependent on the host ability to counteract the pathogen within the primary site of infection and replication, which was clearly shown to be the liver [1].

1.5.5 Pathogenicity of *Listeria* infection

Summarizing the information presented above, three major variables define the clinical outcome of listeriosis: (i) the ingested bacteria load, (ii) the pathogenic attributes of the strain, and (iii) the immunological status of the host. While immunocompetent individuals develop a protective immunity, ingestion of *L. monocytogenes* by immunocompromised and debilitated patients causes unlimited proliferation in the liver and spleen, the primary target organs of *L. monocytogenes*. The susceptible bacteremia results in local infections in secondary target organs, particularly the brain and placenta compartment [1].

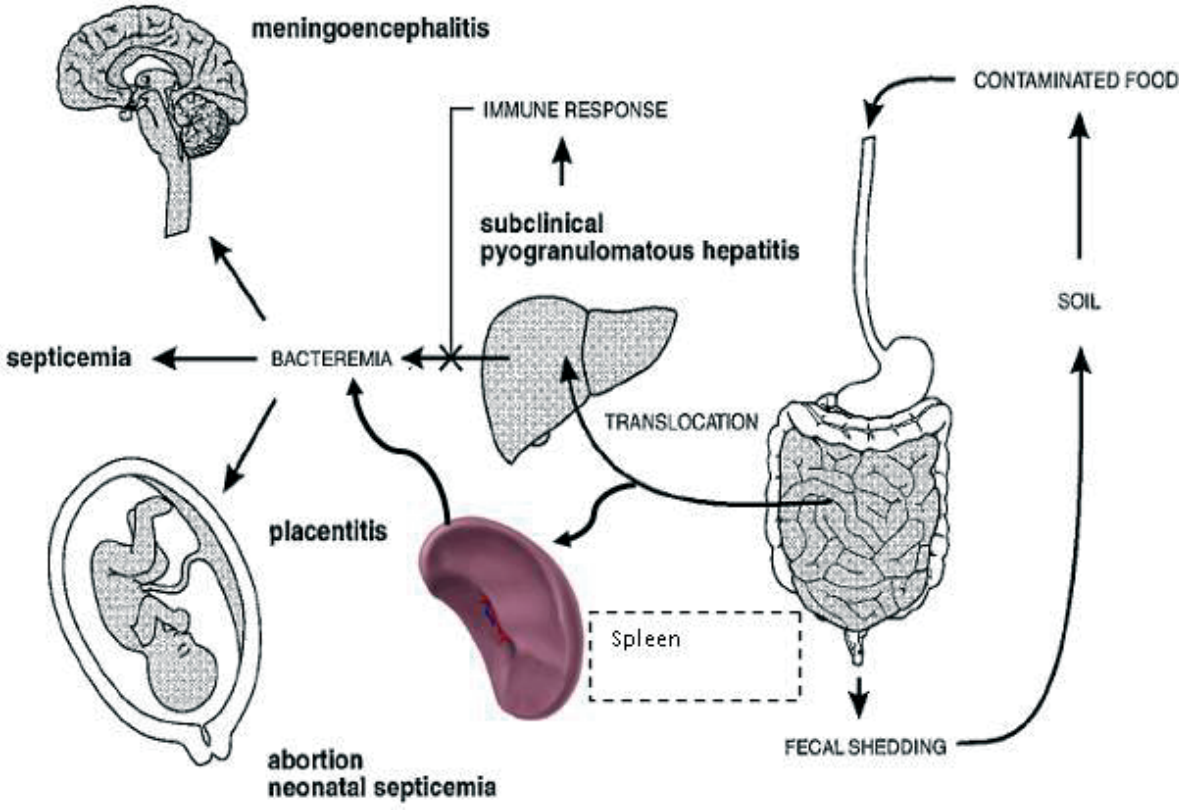

Figure 3: (modified, with permission[1]): Pathogenesis of listeriosis. Naturally, *L. monocytogenes* is ingested with contaminated food. Bacteria surviving the stomach environment reach the gut, translocate into the blood stream and reach the liver via the portal vein or are transported from Peyer plaques to the spleen within macrophages.

90% of the bacterial burden is localized in the liver in this initial phase of infection. In susceptible hosts that are not able to clear the infection in the liver, a secondary systemic bacteremia occurs, which allows the pathogen to spread into other organs. The barrier function of the liver is therefore crucial to prevent a systemic, life-threatening infection.

1.6 Epidemiological aspects of listeriosis

Listeriosis is a world-wide occurring disease associated with a high mortality in individuals without access to adequate antibiotic drugs. Ingestion of *L. monocytogenes* is a very common event, but the incidence of human listeriosis in Europe and the USA is low, ranging from 2 – 8 per million [93, 94]. However, the infection rate is probably underestimated, because in many cases the pathogen is not assumed to be responsible or verified [93]. Development of highly immunosuppressive regimes for organ or bone marrow transplantation and infection with the human immunodeficiency virus (HIV) has significantly increased the incidence for listeriosis in these patients during the last decades. Immunosuppression was detected to be the major risk factor for *listerial* infection; the progression to systemic listeriosis is almost 500 times higher in these patients as compared to the general population [95, 96]. Approximately 30% of all listeriosis affect pregnant woman and new-born infants [97]. Up to 40 cases of neonatal listeriosis are registered in Germany per year. Furthermore, *L. monocytogenes* is responsible for 3 - 6% of bacterial infections of the CNS, such as meningitis. The mean mortality of all listeriosis is high and ranges between 20% and 30%; CNS infections end lethally in up to 5% of registered cases. The most important sources for a *listerial* infection in humans are dairy products, raw and industrially processed foods. The infectious dose depends on the immunity status, pathogen virulence and individual circumstances. In prior healthy persons the infectious dose ranges from 10^5 to 10^9 CFU/ml. Apparently, repetitive ingestion of 10^2 CFU/ml of *L. monocytogenes* may also cause a severe *Listeria*l infection [98]. The immunological niches used by *L. monocytogenes* in an increasing number of immunocompromised individuals worldwide are yet to be fully understood.

1.7 Clinical phenotype of listeriosis

About 10% of the population bears *L. monocytogenes* in their gut flora, without being impaired in health [99]. However, infectious doses of *L. monocytogenes* cause the systemic infection that is also known as listeriosis. *L. monocytogenes* infects human through the ingestion of contaminated food. If not controlled properly by the immune system notably at the liver and spleen level, *L. monocytogenes* infection causes prolonged and asymptomatic bacteremia [88]. It may then reach nearly all organs. Clinical syndromes described for *L. monocytogenes* infection are CNS disease (meningitis, meningoencephalitis, abscess), sepsis, endocarditis, gastroenteritis and some focal localized disease for example hepatitic abscess, lymphadenitis and arthritis [100]. Healthy adults infected with *L. monocytogenes* might have influenza-like illness with fever, gastroenteritis, nausea, aqueous or bloody diarrhoea, abdominal pain, myalgias, headache and backache, arthralgias but might also be clinically silent [101-104]. Systemic Listeriosis becomes clinically apparent in immunocompromised people with underlying diseases, pregnant woman, new-born infants and individuals older than 65 years.

Although *L. monocytogenes* is first and foremost an animal pathogen, infection of mice and rats via the oral route do not cause a reproducible infection. However, other routes of infection, such as the intravenous inoculation were used to determine and investigate *Listeria*l toxins and were shown to produce robust infectious course [105].

1.8 *Listeria* as a model

Infection is a complex interplay between the host and the pathogen. The model of murine listeriosis allows for careful dissection of both host and bacterial factors that are important during infection and in immunity. Infection outcome depends on the effectiveness of the host immune response against a particular pathogen. In the case of *L. monocytogenes*, both innate and adaptive immunity are critical for controlling infection of the intracellular bacterium. Infection is first recognized by the innate immune system, leading to the rapid production of anti-microbial factors, as well as chemokines and cytokines that aid in initiation of the adaptive immune response. *L. monocytogenes* antigen presented by DCs drives strong CD4 and CD8 T cell responses that result in a stable population of *L. monocytogenes*-specific memory T cells. This has

made *L. monocytogenes* infection a useful model for recent vaccine-related studies in the generation, maintenance, and challenge responses of memory T cells. In addition, as a cytosolic intracellular pathogen, *L. monocytogenes* is an ideal model for the growing field of researchers investigating intracellular recognition.

Even though *L. monocytogenes* has been used as a model pathogen for over forty years, the recent studies highlighted suggest there are still unidentified immunological aspects of *L. monocytogenes* infection and immunity. Many of the immune system mechanisms elucidated in murine listeriosis serve homologous functions in other hosts, including humans. In the future, *L. monocytogenes* will continue to be a key pathogen in the identification of new molecules in the regulation of the innate and adaptive immune responses.

1.9 Microarray technology

Whole genome gene expression profiling became an indispensable methodology to capture dynamic changes and to deliver comprehensive biological information following a controlled intervention. It has been successfully applied to nearly every field of biological and medical research, including cancer, metabolic, neurological and infectious diseases worldwide. This led to an exponential increase in number of experiments and studies using microarrays over the last decade (Figure 4). Microarrays provide a possibility to measure the transcript levels of thousands of transcripts at one time. The quality and reliability of microarrays impressively developed during the last years. Sophisticated bioinformatics tools are required to ensure the array quality. In order to make biological interpretation from the massive amount of data gathered from a single microarray study complex tools are required for clustering, enrichment analysis and pathway analysis.

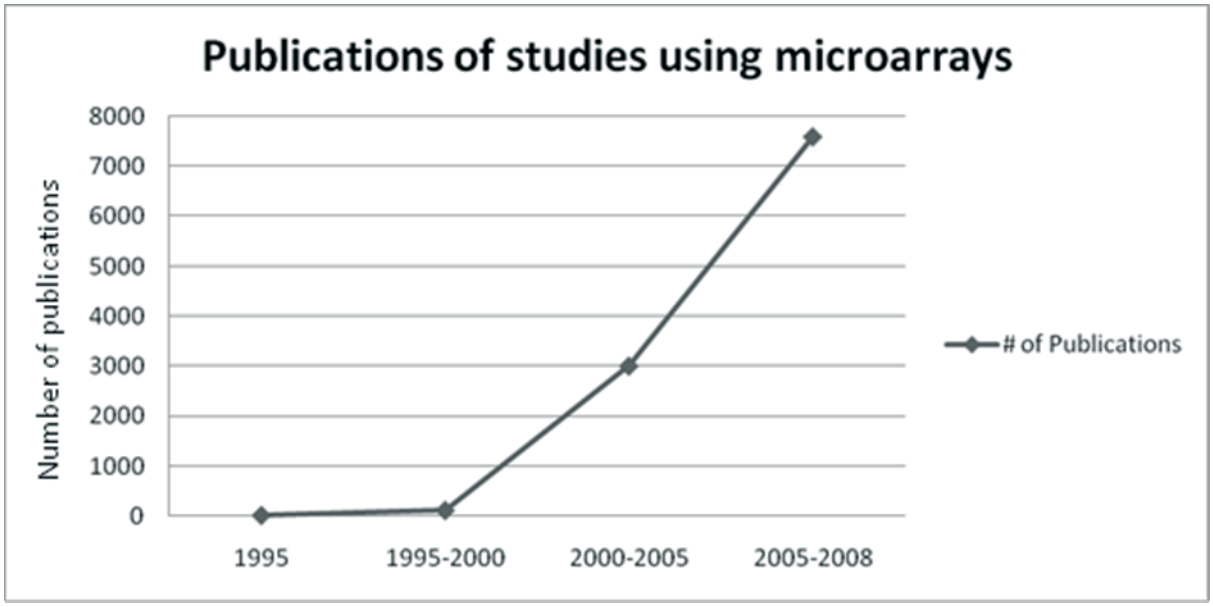

Figure 4: Number of studies that used transcriptional profiling by microarrays as a investigational method. Starting with the development of this innovative technology in 1995, the number of investigators all over the world that used microarrays increased rapidly. The graph demonstrates the increasing use of microarrays over the last 15 years. In the interval from 2005-2008 the number increased to ~7500/year, demonstrating that microarrays are now an established technology that is used in all fields of biomedical research.

1.10 Aims of this work

Most studies focus on a cell based approach or the systemic inflammatory response to describe the host response following infection with *L. monocytogenes*. However, the systemic response does not reflect the pathophysiology and the site specific response in organs that are crucial for the clearance of *L. monocytogenes*. Although it is known that the liver carries the major pathogen burden during infection and is essential for the defence against *L. monocytogenes*, the organ specific mechanisms that lead to the observed phenotype during listeriosis are undetermined. At the same time, it is important to put the resulting local response into the context of signal cascades and intracellular pathways that appear on a cellular level. The complex intracellular mechanisms that lead to the hepatic response which in turn influence the systemic reaction to *L. monocytogenes* are yet to be determined.

It is furthermore unknown how this response behaves over the time course of the infection.

In order to investigate and understand the dynamic changes on both, the global hepatic response and the microscopic level following infection with *L. monocytogenes* in a time dependent manner we applied whole genome microarrays.

The aims of this work are to

1. establish a workflow to obtain raw data from microarray experiments using mRNA isolated from total organs
2. establish a quality control workflow to ensure high and robust quality of data that is used for biological interpretation
3. establish an analytic workflow for the subsequent biological interpretation of high quality transcriptomic data using and improving bioinformatics interpretation tools and based on this analysis to generate testable biological hypotheses
4. validate microarray data with an independent RNA analysis method (quantitative real-time PCR)
5. validate biological hypotheses generated by microarray and qRT-PCR data in functional *in vivo* and cell culture based *in vitro* assays, including immunohistochemistry, immunofluorescence and biochemical serum analysis
6. set results into the context of the pathophysiology of infection with *L. monocytogenes,* fill gaps in the knowledge about the systemic and organ specific response during listeriosus and draw connections to other infection models, including the hepatic acute phase response to LPS stimulation

2. MATERIAL AND METHODS

2.1 Study Design

We infected mice via tail vein with a sublethal dose counting 1500 CFU of *L. monocytogenes* EGD and compared those to non-infected mice (control mice) (Figure 5). Infected mice were killed to the time points 4h, 1d, 2d, 3d and 5d p.i and livers were harvested, mRNA was isolated and given to the microarray analysis pipeline.

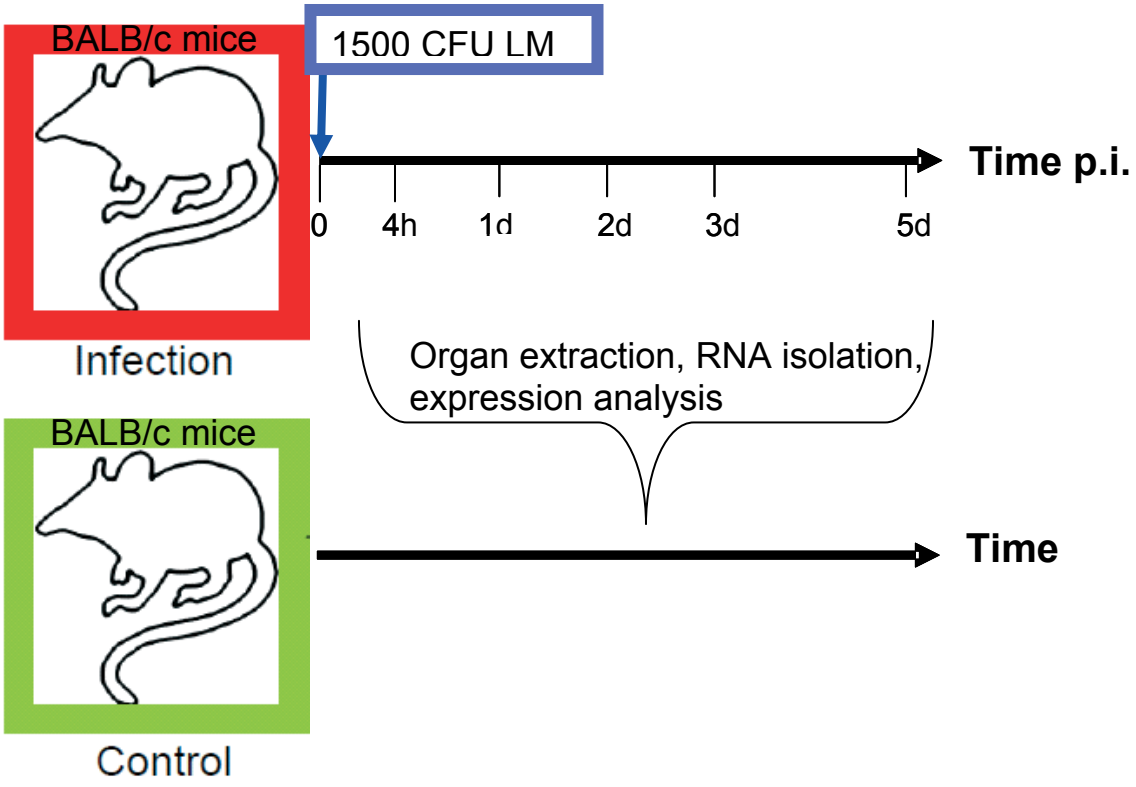

Figure 5: Study design. A total of 18 mice were used in this study. 14 mice were infected with *L.monocytogenes* in the "infection" group. At each time point, three mice (except for time point 5d p.i with two mice) were killed and organs were extracted for further investigation. The infection group was paired with mice that were not infected ("control" group). We used four control mice for comparison. All mice were held under same conditions.

2.1.1 Animals

In the following study, we used 4-5 weeks old female BALB/c mice. Mice were purchased from Harlan Winkelmann GmbH, Borchen, Germany and infected by inoculation of bacteria via the tail vein**.**
In this study four livers harvested from control mice were compared to three livers from independently infected mice, excluding timepoint 5d p.i. with two experimental mice. All work conducted in this study is covered by license GI15/5-26/2004 and approved by the regional board overseeing studies involving animals.

2.1.2 Bacterial cultures and infection assay

L. monocytogenes EGD-e is a serotype 1/2a wild type isolate as described by Glaser P *et al.* 200 [106] *L. monocytogenes* EGD-e were grown in brain-heart infusion (BHI) or on BHI agar plates (Difco) at 37°C. When appropriate, antibiotics were added to the following concentrations: erythromycin 5 µg/ml, chloramphenicol 8 µg/ml on agar plates and 5 µg/ml in broth, 0.5µg/ml gallidermin and 20 µg/ml polymyxin B. For infection assays, bacteria were grown on BHI and harvested at exponential phase (OD_{600} ~ 1.0) and bacterial concentration was adjusted by OD.

2.1.3 Isolation of Total RNA from Organs

1.5ml Eppendorf tubes were filled with 1ml RNAlater RNA stabilization reagent. At least two tubes were prepared for each tissue specimen that was processed. After killing the animals organs were immediately isolated and washed in cold 1xPBS. Organs were cut into slices not thicker than 5mm. A maximum of 100mg of tissue was then put in RNAlater prefilled tubes with a minimum ratio of tissue to RNAlater of at least 1:10 (approximately 10µl reagent per 1mg tissue) and stored for 30 min at RT to allow the stabilizing reagent to penetrate the tissues. We then proceeded with RNA-islolation or transferred the tissue at -80°C for long-term storage. RNA isolation was prepared in following steps:

1. 4ml tubes were filled with RLT lysis Buffer and ß-ME was added to the Buffer RLT in a ratio of 1:1000
2. <50mg RNAlater stabilized tissue was transferred in the RLT lysis Buffer prefilled tubes.
3. Prepared tissue was then disrupted and homogenized in Buffer RLT usind Polytron PT 1300D with 7mm Agregat (PT-DA 1307/2EC) 18 000 rpm on ice. The homogenisator was cleaned after every sample in 0.05% SDS and then in 70% Et-OH.
4. The homogenized lysate was transferred in a new 2ml tube and 0.9 of volume of 70% ethanol was added and mixed.
5. Up to 700µl of the sample was applied to an RNeasy mini column placed in a 2ml collection tube, which then was centrifuges for 15 s at 10000 rpm; flow-through was discarded.
6. 350µl Buffer RW1 was pipetted into the RNeasy mini column and centrifuged for 15 s at 10000 rpm to wash; flow-through was discarded.
7. We added 10µl DNase I stock solution to 70 µl Buffer RDD, mixed and briefly centrifuged.
8. Then 80 µl DNase incubation mix was pipetted directly onto the RNeasy silica-gel membrane and placed on the benchtop (20-30°C) for 20 min.
9. 350µl Buffer RW1 was pipetted into the RNeasy mini column and centrifuged for 15 s at 10000 rpm to wash; flow-through was discarded.
10. RNeasy column was transferred into a new 2 ml collection tube and added 500µl Buffer RPE onto the RNeasy column. The tube was centrifuged for 15 s at 10000 rpm, flow-through was discarded.
11. Another 500 µl of Buffer RPE was added to the RNeasy column and centrifuged for 2 min at 10000 rpm to dry the silica-gel membrane.
12. The RNeasy column was placed in a new 2ml collection tube and centrifuged in a microcentrifuged at full speed for 1 min. The old tube with flow-through was discarded.
13. To elute, the RNeasy column was transferred to a new 1.5 ml collection tube and 50 µl RNase-free water was transferred directly to onto the RNeasy silica-gel membrane depending on the expected RNA yield.

14. If RNA was used for microarray targeting and labeling the it was prepared as following:
    a. 0.1 volumes of 3 M sodium acetate, pH 5.2 and 3 volumes of ethanol 98% were added to the sample.
    b. The sample was mixed and incubated at -20°C for 4h to precipitate the RNA.
    c. It was then centrifuged at 12000rpm for 30 min at 4°C
    d. The RNA pellet was washed with 2 volumes of 75% (v/v) ethanol for 2min and centrifuged at 12000rpm for 5 min at 4°C.
    e. Using speedvac without heating, the pellet was air-dried and the RNA dissolved in 33-55µl water.
15. The sample was incubated at 65°C for 5 min, followed by subsequent cooling on ice.
16. Using the NanoDrop, 1µl aliqouts of RNA were measured and RNA concentration was measured using the Agilent bioanalyzer (RNA 6000 Nano Chip).

2.1.4 CodeLink Whole Genome Mouse Chip details

The basis of every CodeLink™ Microarray is a proprietary three dimensional polyacrylamide aqueous gel matrix. In contrast to two-dimensional surfaces, the specially designed attachment chemistry immobilizes amine-terminated oligonucleotides probes, allowing greater target access to probes.

CodeLink Mouse Whole Genome Bioarray contains single stranded oligonucleotides probes derived from a large majority of publicly available, well annotated mRNA sequences in the Mouse UniGene set of unique clusters. All probes are oligonucleotides, 30 bases in length. Each bioarray contains probes for an independent assay of all ~36 000 genes. Each single probe is specific for one gene, pre-screened and functionally validated. The bioarray contains a set of 50 housekeeping genes that may be used for baseline normalization. Furthermore, the microarray includes 300 positive control probes and 320 negative control probes with corresponding spikes in the cDNA Synthesis Kit to monitor but also contribute to baseline normalization. CodeLink™ bioarray gene probes are carefully screened to minimize gene redundancy and design high-quality, highly specific probes. Each probe is furthermore functionally validated

against several tissues to ensure best representation of the gene so that results will be biologically relevant. Every bioarray undergoes further validation and functional quality tests to ensure high quality and performance.

2.1.5 Array Design and Fabrication

The core of the CodeLink platform is a glass slide coated with a polyacrylamide gel matrix forming a three-dimensional aqueous hybridization environment pattern.
Within this system, each of the ~36 000 probes within an array has an individual single reaction chamber. The probes, which are 5`-amine-terminated modified oligonucleotides, are deposited onto the polymer using piezoelectric dispensing robots and then covalently attached to activated functional groups within the gel matrix. A special fluorescein-derivate dye is co-dispensed to the oligonucleotides, which enables scanning and inspection of every feature element on every slide after the dispensing. The slides are then washed and dried prior to attachment of an individual hybridization chamber. All ~36k probes on the final product have been screened and pre-validated for performance.

2.1.6 Microarray Hybridization and Scanning

MRNA quantity was measured with Nanodrop (NanoDrop Technologies, Rockland DE, USA) and quality was evaluated by the Agilent 2100 Bioanalyzer (Agilent Technologies GmbH, Böblingen, Germany). If mRNA quantity was > 2µ, exhibited wavelength quotient of 260/280 >1.9 and the electrophoresis profile exhibits clean and sharp spikes, which represent the ribosomal RNA, the mRNA is transferred into cRNA. Starting with the isolated mice mRNA (sense), a complementary deoxyribonucleic acid is synthesized to the consecutive sense strand nucleotide sequence (antisense). Following, these strands are separated, the mRNA is rejected and sense cDNA is built during the second strand synthesis. Again, these strands are detached and antisense cRNA is synthesized. Then, after lysing the cDNA strand, cRNA is separated into fragments, which have the capacity to attach to the corresponding fixed probe on the microarray. Fragmentation and hybridization of cRNA to the CodeLink Mouse Whole Genome Bioarray (GE Healthcare, Freiburg, Germany) was executed as described in the CodeLink Expression Assay Kit (GE Healthcare, Freiburg, Germany). Upon ligation to

the corresponding array probe, the cRNA fragments stained via the fluorescence marker Cy5TM-Streptavadin and scanned with the GenePix 4000B Scanner and the GenePix Pro 4.0 Software (Axon Instruments, Arlington, USA). According to the quantity of bound cRNA to the microarray probes, the fluorescence intensity increases equivalently and may be distinguished by the background intensity (Figure 6).

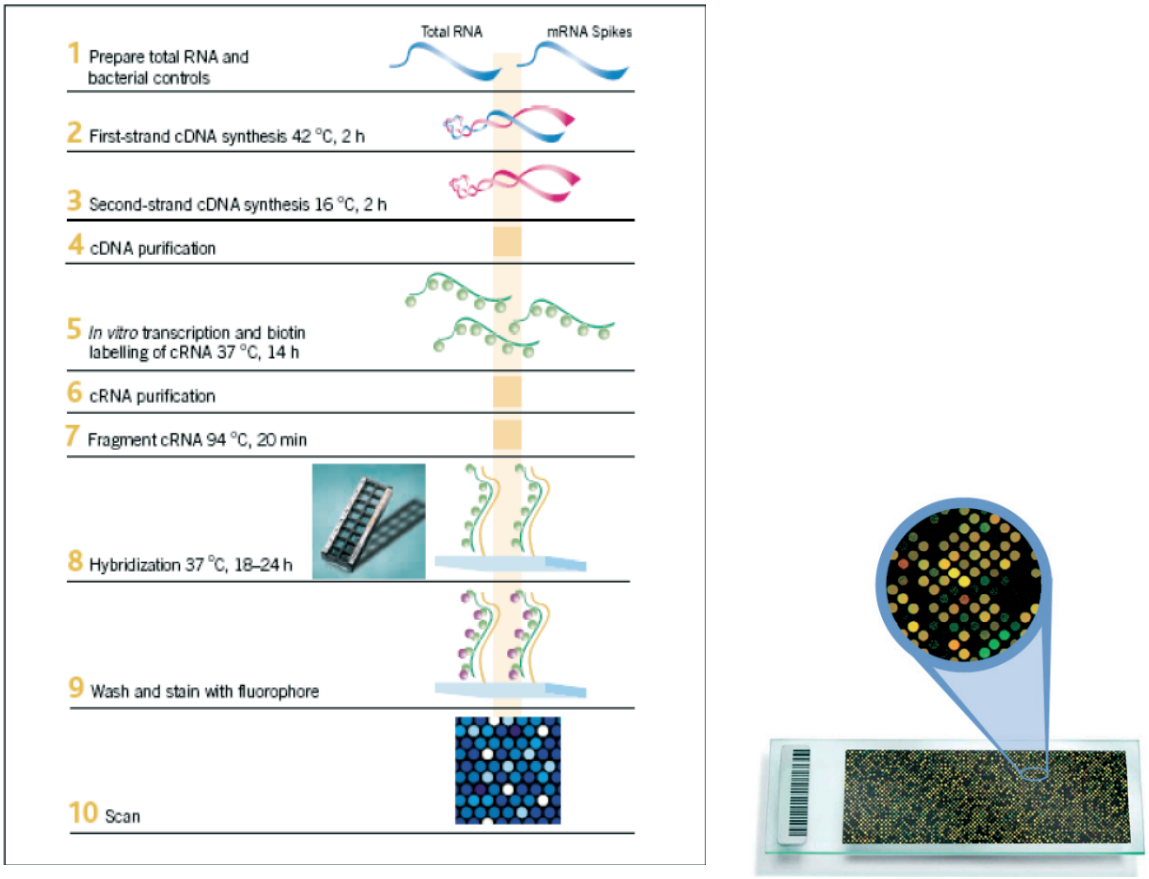

Figure 6: Principles of microarray hybridisation (on the left) and exemplary magnification of spots on an array (on the right) (from the Applied Microarray User Guie: Handbook CodeLink Gene Expression System: 16-Assay Bioarray Hybridization and Detection).

2.1.7 Spot quantification and CodeLink ImaGene Batch Automation software

We used the CodeLink ImaGene 5.5 software (BioDiscovery, Marina Del Ray, CA) to quantify the spot signals of the CodeLink bioarrays. For each probe, the local background comprises a circular area of pixels surrounding the segmented signal. For each spot, the mean intensity is taken and background corrected by subtracting the surrounding median local background intensity. If the mean spot signal is less than its

corresponding local background mean plus obe standard deviation of local background pixels, the spot is considered “absent”. Further information to the image segmentation and quantification process is outlined in the ImaGene 5.5 user’s manual. Shown below is a sample scanned image of the CodeLink bioarray after hybridization with a highlighted area showing the typical circles in *doughnut* form.

2.1.8 Description of the CodeLink data file

The CodeLink ImaGene 5.5 software allows exporting the data as Excel, Txt or a XML file. We used the Excel file format for later processing. Shown below is a sample from a CodeLink Excel file (Figure 7).

CodeLink™ Expression Analysis	4.1.0.29054							
Analysis Report Name:	Expression Report							
Image File Name:	T00340628_2008-3-17.tif							
Analysis Date and Time:	21.May.08 17:07:22							
GEN file name:	EXP287X160-957.22.GEN	Product:	Mouse Whole Genome					
Normalization Method:	Median-Normalization							
Computation Method for Median:	Spot Based							
Threshold Trim Percentage:	20							
Array	1							
Raw TrimMean Negative Control	20.97617939							
Normalized TrimMean Negative Control	0.245716779							
Median	85.36730576							
Sample Name	MOUSE M1 T1 LM1 1500 24H M6-1 2004-01-14							
Idx	Array	ACCN#	Probe_Name	Type	Raw_Intensity	Normalized_Intensity	Quality Flag	Description
1	1	NM_030598.2	GE102179	DISCOVERY	690.873413	8.09295089	G	Down syndro
2	1	NM_027248.1	GE102180	DISCOVERY	1886.96838	22.10411078	G	zinc finger pr
3	1	NM_019439.2	GE102182	DISCOVERY	73.8421021	0.864992767	G	gamma-amino
4	1	NM_011110.2	GE102183	DISCOVERY	66.5285721	0.779321445	G	phospholipas
5	1	AI390431.1	GE102184	DISCOVERY	142.844162	1.673288863	G	mv54h09y1 S
6	1	AI852334.1	GE102186	DISCOVERY	2475.15552	28.99418572	G	UI-M-BH0-ajo-
7	1	NM_009855.1	GE102187	DISCOVERY	40.6938782	0.476691607	G	CD80 antigen
8	1	NM_029702.2	GE102188	DISCOVERY	1223.97144	14.33770721	G	ADP-ribosylat
9	1	NM_021389.3	GE102189	DISCOVERY	215.133331	2.520090442	G	SH3-domain k
10	1	NM_008975.2	GE102190	DISCOVERY	673.494141	7.88936859	G	protein tyrosi
11	1	NM_020618.3	GE102191	DISCOVERY	1236.70837	14.48690881	G	SWI/SNF relat
12	1	NM_183171.1	GE102192	DISCOVERY	1.24705887	0.014608155	L	fasciculation
13	1	AV025990.2	GE102193	DISCOVERY	397.487793	4.656206371	G	adult C57BL/6
14	1	NM_175402.3	GE102194	DISCOVERY	286.20929	3.352680362	G	RNA binding r
15	1	AV116077.2	GE102195	DISCOVERY	1569.93542	18.39035929	G	C57BL/6J 10-
16	1	NM_175364.2	GE102196	DISCOVERY	905.645142	10.60880549	G	RIKEN cDNA
17	1	NM_134003.1	GE102198	DISCOVERY	1029.3595	12.05800614	G	zinc finger CC
18	1	AI481899.1	GE102199	DISCOVERY	635.285706	7.441791678	G	vh18b07x1 S
19	1	AK077048.1	GE102200	DISCOVERY	905.34613	10.60530284	G	adult male tes
20	1	NM_030265.2	GE102201	DISCOVERY	3.42424393	0.040111889	L	Kv channel in

Figure 7: Important details like time of analysis, array type, image file used to create the data, normalization used, thresholds for raw and normalized data and name of the array are provided. In addition, the file contains the probeset identifiers and the raw and intraslide normalized expression values. Each probeset identifier is associated with descriptive flags: *Number*: a numerical index; *Array*: the array number; *Accn*: Gene Bank accession number; *Probe name*: The name of the probe; *Type*: the type of probe (discovery, positive, negative, fiducial, other); *Raw intensity*: the mean spot intensity minus the median local background; *Normalized intensity*: the raw intensity divided by a normalization factor; *Threshold*: indicates whether the probe intensity is above the

threshold (True or False); *Quality Flag*: indicates spot quality (Good, Empty, Poor, Neg or MSR) and *Description*: Gene description.

2.1.8.1 Threshold and quality flag

The threshold is an array specific value which is calculated for each array by probe values of non-mouse, but bacterial or fungal gene probes. In accordance with the ideal, no cRNA binds to these probes. However, to a low degree, there is always unspecific ligation of cRNA to gene probes, which by this way may be quantified for each array. With the threshold value, it is possible to appraise, if the probe fluorescence signal is a true representation of specific cRNA binding or if the binding is unspecific. Expression values that are lower than the threshold are considered a unspecific binding and are excluded from the analysis in the following quality control pipeline. Thus, the threshold is an important quality marker for all expression values, but especially of gene probes with low intensities.

The CodeLink Expression software attributes a quality flag to each gene probe (good, empty, neg, poor or MSR). Ideally, the intensity of gene probes increases circularly and centripetally leading to the typical doughnut morphology. With respect to the probe morphology and symmetry, it is possible to attribute the probe quality and to identify probes with a low quality. According to the morphology and symmetry, gene probes are attributed GOOD, if the probe structure is circular and symmetric; EMPTY, if the intensity is lower than the local background intensity, POOR, if the probe is partially asymmetric and NEG, if the probe morphology is totally asymmetric. Furthermore, some probes are attributed MSR (Manufacturer Spot Removed), which are in general known to be of low quality. NEG, POOR and MSR attributed probes are deleted, so that in these lines no expression values occur. GOOD and EMPTY attributed gene probes, are implemented into the quality control pipeline.

2.1.9 Quality Control of the raw data

A typical microarray experiment has many different sources of variation which can be attributed to biological and technical causes. To generate high quality and reproducible microarray data, it is fundamental not only to confirm every step in the laboratory, but also to control every step the produced data. The quality control of microarray data is

essential, because low quality data are identified early and may be eliminated, before they have impact on the later biological interpretation of the processes. Two hierarchies of quality control may be distinguished: spotbased and arraybased quality control. Spotbased control means, that gene probes with low quality are identified. These spots are deleted, but may be imputed by statistical methods. Arraybased quality control may identify low quality microarrays by computing the correlation between the arrays. In contrast to low quality spots, there is possibility to reconstruct whole microarray data of deleted arrays and also not to use the qualitative good data of deleted microarrays. Therefore, we have developed a quality control pipeline to prevent the exclusion of whole arrays and prepare high quality data. The elements of the quality control pipeline include the cleantable, threshold, outlier filter module and the MVA plot module.

2.1.9.1 Cleantable module

Cleantable is a module developed by us, which verifies, how many empty field within a gene line occur. If the number of empty fields within a group is >50%, the gene is eliminated from analysis (Figure 8).

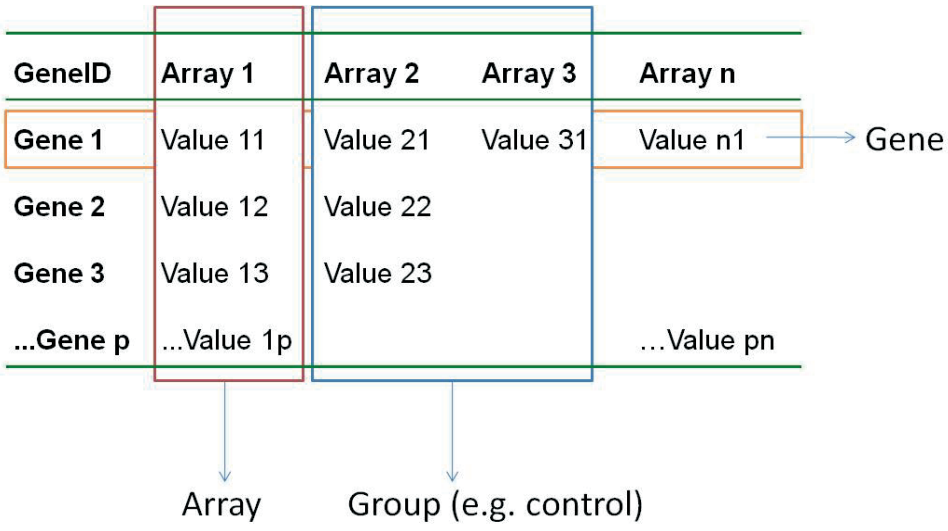

Figure 8: The cleantable module identifies empty fields in an excel spreadsheet that provides the displayed structure. The first column includes the unique gene identifiers. The following columns represent the expression of the particular gene on an single biochip. These arrays may be clustered in different groups, e.g. “control” and “4h p.i” etc. The clean table module identifies genes that have a missing value in >50% of cases in a given group of arrays. These genes are eliminated from further investigation.

2.1.9.2 Threshold module

The Threshold module compares each expression value within an array with the according threshold value reflecting the intrinsic background signal of this array. If more than 50% of the expression values within a gene line are higher than the threshold, it is assumed that these are unspecific bound to the probes and are eliminated from the analysis.

2.1.9.3 Imputation of empty fields

The imputation of missing values is necessary for the efficient use of the microarray data, because many clustering algorithms, some statistical analysis and the outlier filter require a complete data set. We used the sequential K nearest neighbour [197] based on the classical KNN. KNN selects gene lines, which share high similarity in expression profile to the gene line, in which an empty field occurs and which should be imputed. For example, if Gene line X contains an empty field, KNN searches for K similar neighbor gene lines. K means the number of neighbors that influence the mean value of the empty field. The neighbor impact on the imputation value of the empty field is thereby dependent on the similarity of the neighbor to the gene line with the empty field. This means, neighbors with high similarity do have a high impact on the value of the empty field, whereas only a little impact is made by neighbors with low similarity. However, KNN only overlooks information of gene lines without empty fields, leading to a lower accuracy compared to SKNN. SKNN initially sorts gene lines beginning with the gene line with the lowest number of empty fields and imputes empty fields as described for KNN. In contrast to KNN, SKNN then uses the gene lines that were filled with to impute the following empty fields. Thus, the permanently growing data set is used to impute empty fields and thereby exhibiting a higher accuracy of imputed empty fields.

2.1.9.4 Outlier filter module

The outlier filter module was newly developed tool to identify spot outliers. The tool calculates the median (MED) and the standard deviation of every gene line. Then, outliers are identified that are higher or lower than the +/- 2 MED within a group. Each

group represents an experiment of four to two biological replicates. If expression value is identified as outlier, it is deleted. In a further step, the whole process is repeated without respect to the group affiliation. Thus, overall outlier may be identified and eliminated as done in the prior step.

2.1.9.5 Quantile normalization and logarithm

The goal of the quantile method is to make the distribution of probe intensities for each array in a set of arrays the same. This motivates the following algorithm for normalizing a set of data vectors by giving them the same distribution [107]:

1. given n arrays of length p, form X of dimension $p \times n$ where each array is a column;
2. sort each column of X to give Xsort;
3. take the means across rows of Xsort and assign this mean to each element in the row to get $X_$sort;
4. get Xnormalized by rearranging each column of $X_$sort to have the same ordering as original X

We then calculated and proceeded with the LN of the quantile normalized data.

2.1.9.6 Correlation matrix and microarray outlier filter (MOF)

Microarrays measure the whole mouse genome in only one assay and there is variation within the biological experiments. However, a number of genes, such as housekeeping genes, are expressed to very similar amounts and there is only small variation within these. Thus, one would expect that interindividual intensities correspond to a high percentage. Therefore, outlier microarrays would differ in an extended manner comparing it with other microarrays. The microarray outlier filter calculates three attributes for a data set: a) percentage of outlier spots of every array compared to the whole collective; b) correlation of each array compared to the collective and c) correlation matrix, in which the correlation of each array compared to every single array. The correlation matrix is visualized as heatmap, in which the correlation between arrays is represented by a colored square. Each color is assigned a degree of correlation. The value of each color is visualized separately in the color bar, beginning with lowest up to the highest correlation value p=1.

2.1.9.7 Mean Versus Average Plot (MVA)

The MVA plot is a further way to characterize the data quality of a single array in the context of a collective of arrays. For each gene line of the normalized and log2data set the mean is calculated and gene lines are sorted by descending values and are assigned a rank. Following, each gene line mean is plotted against the according mean value of the other microarrays. In this plot, the horizontal axis represents the rank of the gene line mean and the vertical axis depicts the remainder (expression value minus mean value of the gene line).

Resulting dots on the MVA plot should be randomly scattered around a line on y = 0. If there is a systematic fault, the plot becomes deformed; in the case of better cRNA ligation in high expression value intervals the plot typically becomes trumpet formed.

2.1.9.8 Quality control algorithm

The above described elements of the quality control are executed serially beginning with the cleantable and threshold module. Result of this, is a data set X with empty fields. These are filled by the SKNN algorithm, before outliers are deleted by the outlier filter module. Appearing empty fields are again filled by the SKNN algorithm and the resulting dataset Y quantile normalized and logged to the basis 2. In the case of low array quality in the MVA plot and MOF, the array is excluded from analysis and the whole sequence is repeated without the outlier array (Figure 9). Quantile normalization, log2 and correlation matrices were created by AVADIS (Strand Genomics Pvt Ltd. 2003). SKNN and the MVA plot script were executed by the open source software R (www.r-project.org).

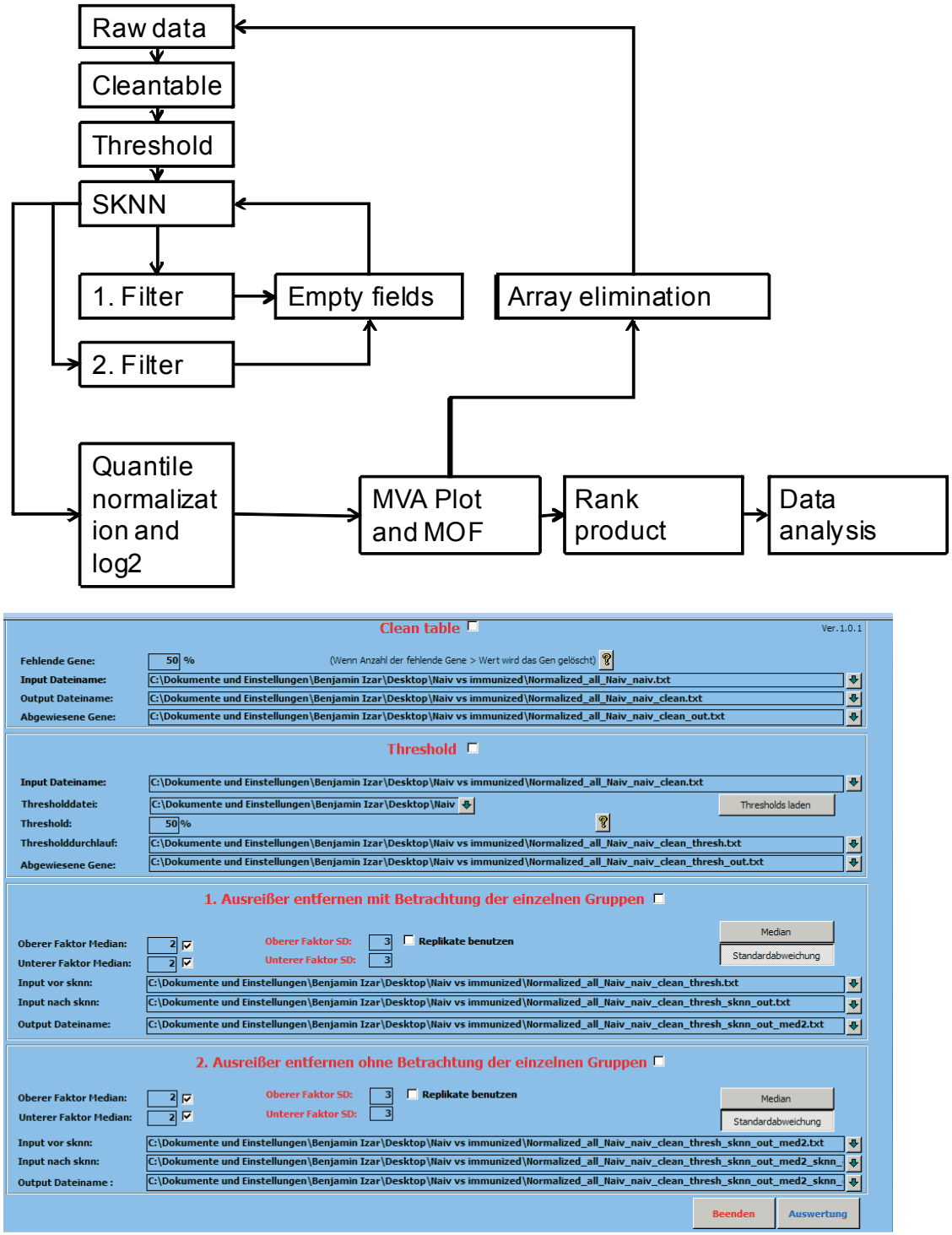

Figure 9: Quality control workflow and the mask of the in house quality control (QC) tool. Each array and each individual expression value undergo a strict quality control. In a first step, the cleantable module eliminates genes that miss a value in >50% in a single group of arrays, e.g. the "control" group or cluster of microarrays that represent a time point post infection (e.g. 4h p.i.). The threshold module identifies expression values that are below the background intensity of an individual microarray. If 50% of expression values of a gene in a single group are above this threshold value, the gene was kept in

the analysis. All genes that passed these two QC steps were kept in the analysis. A complete data set is needed to use the next step in the QC, the outlier module. In order to ensure that each gene had an expression value for all observation points, we used the SKNN model to fill in missing values. Values that were above/below twice the median within a group/among all groups were eliminated. Subsequently, all deleted values were imputed using SKNN. The values of the resulting data set were quantile normalized and the logarithm was taken for further calculation. Microarrays that met criteria and had a favorable MVA plot were kept in the analysis.

2.1.10 Analysis methodology

Enormous amounts of data pertaining to the nature of genes and proteins and their interactions in the cell are generated by microarrays. For the reason that it is impossible to evaluate these data manually, several tools were created that help to identify statistically significant genes, visualize gene/protein interaction networks, identify overrepresented biological categories and map genes to known pathways.

2.1.10.1 Identification of differentially expressed genes using the rank products (RP) tool

We used the rank products routine tool to discriminate the differential expression of genes between control and experimental settings. Result of RP is a fold change (FC) and a False Discovery Rate (FDR). The FC describes the x-fold change of gene expression in an experimental group compared to the control group. For the reason that we have biological replicates, it is necessary to estimate the group mean of each gene and build the quotient of experimental mean and the control mean to get the FC.

The FDR quantifies the probability of error associated with every FC. Thus, the FDR assesses, if a gene regulation occurs randomly or expresses an actual biological regulation. Small FDRs indicate a high probability that the observation is a true biological effect.

Simple permutation-based estimation is used to determine how likely a given RP value or better is observed in a fictive random experiment [178]

1. Sort the list by decreasing FC
2. Assign a rank to every FC. High FCs are located above and are assigned low ranks.
3. Generate p permutations of k rank lists of length n

4. Calculate the rank products of the n genes in the *p* permutations
5. Count how many times the rank products of the genes in the permutations are smaller or equal to the observed rank product. Set *c* to this value.
6. Calculate the average expected value for the rank product by $E = c / p$
7. Calculate the percentage of false positives as $pfp = E/ r$

ranklist *k*	replicates			
rank	*a*	*B*	*...z*	*Rank product*
1	value a1	value b1		rank*value ab_1
2	value a2	value b2		rank*value ab_2
3	value a3	value b3		rank*value ab_3
…n				rank*value ab_n

If a randomly permuted value y from the data set does not influence the rank product of the investigated FC, the investigated expression value is very robust and the probability that the according FC represents a true biological effect is higher and subsequently the according FDR is low.

Prior to executing the RP script, it is necessary to determine the count of permutations *k*. RP calculation of whole genome arrays with almost ~36 000 probes and at least 6 replicates per experiment as apparent in this study has high pretensions on computer recourses, which are limited.
For this reason, it is useful to determine the minimum number of permutation that still represents the biological gene regulation as the highest possible number of permutation does. Knowledge to this aspect is limited. For this reason, we have executed an exemplary experiment with three control and three experimental replicates based on whole mouse genome arrays with increasing number of permutation, beginning with 50 permutations up to 500. As first result, we determined the number of up-/downregulated genes within the different permutation settings. However, the number of differentially expressed genes makes no statement on biological effects of permutation variation. Therefore, we implemented the exemplary data into the Ingenuity Pathway analysis tool and compared the pathways and gene association networks of the different permutation settings. By doing so, we investigated the effect of permutation variation on quantity, but also its effect on *visible* biological processes.

For our study, we considered genes differentially regulated with a FDR < 0.05 to at least one of the observation points (Table S1, appendix) . Only those genes, which are assigned a GO function according to the gene ontology consortium, were included for further analysis, since this is a prerequisite for enrichment tools used during the downstream investigation. If a gene is assigned to more than one biological process according to the GO consortium, either the main function was used or in equivocal cases, the main function was assigned based on known literature to the gene.

2.1.10.2 Annotation of significantly deregulated genes

Significantly expressed genes were annotated by the open web-based tool SOURCE from the Stanford University, USA. Additionally, we used the Clone/Gene ID converter [108], if the gene was not found in the SOURCE data base. SOURCE and the ID converter together cover most public gene data bases, including UniGene, EntrezGene, GeneBank Accession, Locus Link ID, Swiss-Prot, Ensembl and UCSC. Furthermore, manual search was performed for genes that were not detected by any of the mentioned sources.

2.1.10.3 Enrichment of overrepresented categories

All known and validated genes are assigned with terms by the Gene Ontology Consortium that describes the molecular function, subcellular component and the biological process the gene and its product are involved. These GO terms are divided into three major categories

biological process: describes the biological process, in which the gene/gene product is involved e.g. Immune response or lipid metabolism

molecular function: the function that is allocated to the gene/gene product, such as transcription factor activity or enzyme

subcellular component: describes, where the gene product is located, e.g. nucleus or endoplasmic reticulum.

These parent terms do have several child terms, that are hierarchically subordinated, but may parallelly have more than one parent term. The GO terms provide a short description of the most important information to a gene and may admit investigators to overlook its relevance for the study.

DAVID (*database for annotation, visualization and integrated discovery*) is a free project of the *National Institute of Allergy and Infectious Diseases (*Bethesda, MD, USA), with the goal to identify biological processes that are significantly present in a study. To achieve this goal, DAVID uses the GO terms of each implemented gene, assigns it to the according category and calculates how probable a regulation of this category is. The probability is calculated by a simple term: $P = X(S)/ X(B)$;
X(S) = number of significantly expressed genes of the category X,
X(B) = number of all genes present in the category X (taken from the background list.
Before giving the list of significantly expressed genes into DAVID, it is important to provide a background list, including all genes that have passed the quality control procedure. The lower a calculated p-value is the higher the probability for a category to be overrepresented in the study. We used a cutoff p <= 0.05. The enrichment of differentially expressed genes within overrepresented categories provides the possibility to investigate more focused on relevant biological mechanisms. Since we explore biological processes in this study, we have focused on analyzing the GO category *Biological Processes All* and *Kyoto Encyclopedia of Genes and Genomes* (KEGG)-Pathways. KEGG is a pathway databank, in which genes are assigned to their functional localization in known biological signaling and metabolic pathways.

2.1.10.4 Literature search

The extensive internet wide literature search is crucial to find and combine information and search for meaningful biological interpretation. Since it is impossible to read all relevant publications to a molecule, some data bases provide the possibility to get the information of interest in a compact manner.
We used the PubMed.org search module to find relevant abstracts. These provide insight into the background, methods, results and a conclusion of a publication and if it is necessary read the whole publication.
Furthermore, we used iHop for literature search. IHop is a web-based gene search tool and provides summary information on more than 80,000 biological molecules by automatically extracting key sentences from millions of PubMed documents. Thereby, iHop provides a global perspective on information to a single gene from different recourses. Additionally, we used the integrated search function of the IPA tool, which supplementary to the other search tools provides information, such as the *role in cell*,

associated diseases and the *transcription factors* that regulate its expression, thereby connecting molecular function with clinically relevant studies and information.

2.1.10.5 Cluster analysis with *dCHIP* and *biolayout*

The analysis of microarray experiments is nontrivial because of large data size and many levels of variation introduced at different stages of the experiments. The analysis is further complicated by the large differences that may exist among different probes used to interrogate the same gene. In the case of this study, the complexity is further increased by observation of a time course with five time points.

Therefore, visualization of the large data set is an important step in the analysis of microarray data. In addition to the visualization, some tools provide information about gene clusters that exhibit similar expression profiles. We used biolayout and dChip for visualization, K-Means Clustering and hierarchical clustering, respectively.

Biolayout networks consist of nodes representing transcripts connected by their virtue of expression profile similarity across different conditions. Moreover, the tool clusters genes that exhibit similar expression profiles over the time. In our observation we used GO terms as condition of interest, thus genes that exhibit similar expression profiles in the same functional group are colored identically.

DChip hierarchical clustering arranges arrays and genes that show similar expression profiles regardless of their groups and is therefore called an *unsupervised* analysis. The clustering algorithm is based on the standard algorithm of dChip (version: *Build date: Mar 8 2006)* used with standard options.

The distance of two genes is defined as 1-r (r= Pearson correlation coefficient) between the standardized expression values (mean = 0, standard deviation =1) of two genes over all observed arrays. The two genes with the lowest distance are the first super gene and linked by lines representing the distance, and excluded from the further clustering. The so created super gene represents the mean of the two standardized expression values over all arrays, which is also called the centroid-linkage. According to the first super gene, the procedure is repeated n-1 times always taking the two genes with the nearest distance.

The result of the mathematical process is then visualized using a cluster dendogram that implicates the proximity of arrays and genes with comparable expression profiles. Furthermore, the cluster dendogram includes a color bar, indicating the relation of gene

expression to the mean of the gene over all observed arrays. Red highlighted genes are overexpressed in the corresponding gene line, green are lower expressed and black highlighted genes show no expression differences to the corresponding gene line mean.

2.1.10.6 Pathway and Network analysis by *Ingenuity Pathway Analysis (IPA)*

To determine the biological effects of the biostatistically gained information from gene expression, we investigated the association and relevancy of our result in context to recent knowledge about infectious diseases, immunology and host response by using special software. Ingenuity pathway analysis (IPA) (Ingenuity Systems®, www.ingenuity.com) is a commercially available tool that visualizes microarray data and illustrates interactions of genes involved in the same biological processes or diseases as networks and maps differentially expressed genes to metabolic, disease and further pathways. Biological associations between two factors are visualized as two-dimensional illustration. The connection is further characterized by using different symbols and lines indicating the quality of association, e.g. an activation, inactivation or phosphorylation. The base of the tool is an enormous data bank, which claims to be always updated to most recent literature findings (U.S. National Library of Medicine, 8600 Rockville Pike, Bethesda, MD 20894, USA). IPA was used to great extent by investigators elucidating the impact of drugs in organisms, but during the last years, IPA became the most frequently used pathway analysis tool in nearly all subjects of medicine and biology using microarrays.

Goal of the tool is to translate a large data sets into an easily to interpretate biological matrix. Furthermore, the time dependent illustration activation of intracellular signal cascades indicates the temporal significance of central biological functions. Thus, IPA may emphasize important pathways and networks and point to relevant biological processes that should be considered in the interpretation of microarray data.

2.1.11 cDNA synthesis for quantitative Real-Time Ploymerase Chain Reaction

Validation of Microarray data was performed by two-step Real-Time PCR (RT-PCR) for 12 target murine genes (that were highly regulated during microarray analysis and relevant for the question, namely lipid metabolism and immune response In the first step, complementary DNA (cDNA) was obtained from each mouse by reverese

transcription of RNA. RNA samples were digested with DNAse I (Promega) and purified again using the RNeasy Mini kit (Qiagen). Each sample to be synthesized was prepped at 0°C containing:

500 ng of total RNA

1 µl of a 20 pmol/µl dilution of T21 primer

1 µl of a 200 pmol/µl dilution of N9 primer

Nuclease-free water to 11 µl final volume.

Samples were centrifuged for 5 seconds and incubated 5 min at 70°C and placed on ice again. Then following substrated were added to the 11 µl RNA/primer mix to a final volume of 20 µl:

4 µl 5x First-strand buffer

2 µl DTT

1 µl RNase inhibitor (RNaseOut, Invitrogen)

1 µl 10mM dNTP mix

1 µl SS II reverse transcriptase (Invitrogen)

The reaction was incubated for 1h in 42°C thermo mixer at 300 rpm. The smaple was centrifuged for 5 seconds to collect samples at the bottom of the tube and were then heated at 70°C for 15 minutes to inactivate the enzyme. Resulting cDNA was used for RT-PCR or stored at -20°C if RT-PCR was performed to a later time point.

2.1.12 Quantitative Real-Time PCR and data analysis

Duplicates were made for each primer pair combination. Following primers were purchased from Qiagen (Quantitect Primer Assay) and diluted to 1 pmol/µl for further procedure and qRT-PCR was run (7900 HT Fast Real Time System, Applied Biosystems):

Acyl-CoA thioesterase 1 (ACOT1, catalog No QT00167734), acyl-CoA thioesterase 3 (ACOT3, QT00145439), activin A receptor type II-like 1 (ALK-1, QT00161434), baculoviral IAP repeat-containing 5 (BIRC5, QT00113379), chemokine (C-C motif) ligand 24 (CCL24, QT00126021), chemokine (C-C motif) ligand 5 (CCL5, QT01747165) ,CD5 molecule-like (SP-α, QT00113309), cyclin-dependent kinase 1 (CDK1, QT00167734), cathelicidin antimicrobial peptide (CRAMP, QT01195922), cytochrome P450, family 7, subfamily A, polypeptide 1 (CYP7A1, QT00121569).

Primer sequence of self-validated gene was as follows Glucose – 6 phosphate dehydrogenase (G6PD) G6PD-forward: 5'- AGCAGTGGGGTGAAAATAC-3', G6PD-reverse: 5'-CCTGACCTACGGCAACAGA-3'. Primer sequences of self-validated house-keeping genes were as follows beta-2 microglobulin (B2M) B2M-forward: 5'-TCTTTTTCAGTGGGGGTGA-3', B2M-reverse: 5'-TCCATCCGACATTGAAGTT-3'. Three housekeeping genes (B2M, PPIA and RPLP2) were used for normalization and calculation of relative expression.

Following substances were pipetted in the wells of a 96x0,2 Well Plate (Nerbe Plus):

12.5µl of Quantitect SYBR Green PCR Reaction Mix (Qiagen)

5 µl of diluted cDNA

7.5µl of 1 pmol/µl primer to a final volume 25 µl/well.

Wells were covered with PP cover strips (Nerbe Plus) and centrifuged at 300g/15s in a plate centrifuge. The qRT-PCR was performed in the TaqMan® by the following conditions: 95°C for 15 min, 40 cycles: 95°C x 15s, 55°C x 20s, 72°C x 25s and cooled down to terminate the reaction.

Threshold cycle values (CT) of the tested genes were determined and normalized expression of each target gene was given as the ΔCt between the log2 transformed CT of the target gene and the log2 transformed CT of the internal control (ACTB). Both log2 transformed microarray intensities and RT gene expression levels (ΔCt) of each target gene for each condition (4h, 1d, 2d, 3d, and 5d p.i.,) were expressed as log2differences from control (=log2 ΔΔCt method). Relative expressions obtained from qRT-PCR were plotted against relative expression values from microarrays and Pearson's correlation r^2 between both fold changes was indicated. Data was acquired and analyzed with the SDS 2.3 and RQ-Manager 1.2, respectively.

2.1.13 Electrophoresis of primer products

To ensure the specificity of primer products we conducted a gel electrophoresis for all primer pairs used in this study. cDNA applied to electrophoresis on agarose gel (1.2 % agarose; 0,5 g/l Ethidiumbromid in 1 x TAE-buffer), and voltage was applied (150 V) to the gel for 1 h. Detection and determination were obtained under ultraviolet light. Data were analyzed with Quantitiy One 4.6.3 (BioRad).

2.1.14 Preparation of cryosections

Cryosections of 12 µm thickness were cut from organs with a cryostate (LEICA CM 1900). Eight slides each were obtained from three individually harvested livers from controls and each experimental condition (control, 4h, 24h, 48h post infection). Preparation of cryosections was done by Eva Schneider, Institute for Anatomy, Giessen, Germany.

2.1.15 Lipid droplets staining with Oil Red O

Oil Red O solution was prepared as following: oil Red O was soluted in a ratio of 1% propan-2-ol (0.6g of oil Red O in 6ml propan-2-ol). The mixture is heated to 37°C for 30 min to dissolve the solution. 4ml of H_2O are added to the 6ml oil red O + propan-2-ol solution, resulting in a 0.6% oil red O solution. Precipitates are filtered through a 0.45um filter with a syringe; the filtrate is the final staining solution. Cryosections were rinsed with 60% of isopropanol. Cryosections were incubated with oil red O for 15 minutes and washed again with 60% isopropanol, rinsed with distilled water and mounted in glycerine. Stained lipid droplets appear red in light microscopy.

2.1.16 Cell Cultures, lipid droplets with BODIPY 493/503 and immunofluoresence staining

HepG2 (human hepatoma cells) (American Type Culture Collection HB-8065) were cultured as monolayers at 37°C in a humidified 95% air/5% CO2 incubator. The cells were cultured in Dulbecco's Modified Eagle's Medium (DMEM) supplemented with 10% (v/v) fetal bovine serum (Invitrogen). The cells were split every 3days in a 1:3 – 1:4 ratio when they reached 70–80% confluence. Cells were detached from wells using 0.05% trypsin-EDTA solution for 7 minutes. To deactivate trypsin an equal volume of full growth medium with 10% FBS was added. For infection and immunofluorescence experiments we used wells with cells that were 70-80% confluent. Lipid droplets in HepG2 cells were stained using BODIPY 493/503 (Sigma Aldreich). Cells were permeabilized with 0.2% Triton X 100 in PBS for 10 minutes and washed three times in 1xPBS for 5 minutes. We then blocked the cells with 1%BSA + 0.3% Triton X diluted in PBS by incubating them for 1h at 37°C. BODIPY 493/503 was diluted to a 50µM solution in 1%BSA + 0.3% Triton X and incubated at 37°C for 1h. Phallodin was used to stain the cytoskeleton and

was diluted in a ratio of 1:80 in the same solution with BODIPY 493/503. Cells were then fixed on glass plates using ProLong (Applied Biosystems). Lipid droplets stained by BODIPY 493/503 appear as green circles/globules. DAPI fluorescent was used to stain nuclei. Stained lipid droplets appear as green intracellular globules, the cytoskeleton appears gray/white and nuclei stain blue.

HuH-7 (human hepatocellular carcinoma) cells were were cultured as monolayers at 37°C in a humidified 95% air/5% CO2 incubator. The cells were cultured in Dulbecco's Modified Eagle's Medium (DMEM) supplemented with 10% (v/v) fetal bovine serum (Invitrogen). The cells were split every 3days in a 1:3 – 1:4 ratio when they reached 70–80% confluence. Cells were detached from wells using 0.05% trypsin-EDTA solution for 7 minutes. To deactivate trypsin an equal volume of full growth medium with 10% FBS was added. For infection and immunofluorescence experiments we used wells with cells that were 70-80% confluent. Cells were infected with a MOI 1:10 with *L. monocytogenes*. Infection was terminated by fixation of cells at 0h, 2h, 4h, 6h and 8h following infection. Every cell culture was assigned an uninfected cell culture of cells. Fixated HuH-7 cells were prepared for antibody hybridization. First, cells were treated with Triton X 0.2% for 2 minutes to increase permeability for the following antibody hybridization. Cells were washed three times with PBS consecutively in three independent bins. Cells were incubated with LXR-α antibody solution, which was produced according to the solution for the cryosections. After 1h incubation at 37°C cells were washed in PBS and incubated with the secondary antibody solution + Phalloidin ,prepared as described above, for 1h at 37°C. After washing cells with PBS cells were incubated with DAPI for 5 minutes, washed and fixed with ProLong at a glass slide. Primary antibodies against LXR-α (LXR-α (P-20): sc-1202; santa cruz biotechnology, inc.) or antibody against phosphorylated LXR-α (LXR-αP) (kindly provided by Dr. M. Garabedian, Department of Microbiology and Urology, NYU School of Medicine, New York, USA) and mouse serum diluted to 1:200 in 450µl PBS were incubated for 1 hour at 37°C. LXR-αP antibody targets LXR-α that is phosphorylated at S198 position (equivalent to residue 196 of mouse LXR-α). The probes were then incubated with 3% H2O2 and rinsed 3 times in PBS and upon incubation with 2% BSA probes were washed in again. Parallelly the secondary antibody was prepared. Anti- LXR-α -ab was soluted in a ratio 1:40 in 300µl PBS. Additionally, Phalloidin green was mixed with the secondary antibody in a ratio 1:40. The tube was incubated for 30 min at room temperature. The probes were incubated with the primary antibody for 1h at RT

and then rinsed in PBS. After washing, the probes were incubated with secondary Ab + phalloidin solution for 30 min at RT and subsequently washed in PBS three times. The probes were then incubated with DAPI for 5 minutes and washed again. Finally the plates were stippled with ProLong and enclosed with coverslips on a glass plate. After drying over night the specimens were given to fluorescence microscopy analysis.

2.1.17 Triascin C treatment

Monolayers of HepG2 were grown on glass plates cultured in DMEM supplemented with 10% FBS cells were incubated with 5 μM triacsin C (Sigma Aldreich) in DMSO (0.1%, v/v, final concentration) for 9h or 24h. Control cells received the vehicle alone. After 9h and 24h, respectively, the incubation was stopped by aspirating the medium. Residuals were removed by washing the cells three times with 1% PBS.

2.1.18 Measurement of liver and lipid serum parameters

Clinical biochemistry parameters were obtained from three naïve mice and three biological replicates at 4h, 1, 2 and 3d upon infection with *L. monocytogenes*. In the following serum 11 parameters were measured: sodium (mMol/l), potassium (mMol/l), calcium (mMol/l), chloride (mMol/l), glucose (mg/dl), lactate dehydrogenase (LDH) (U/l), glutamate-oxalacetic transaminase (GOT) (U/l), glutamate-pyruvate transaminase (GPT) (U/l), glutamyl-gamma transaminase (GGT) (U/l), cholinesterase (CHE) (U/l), cholesterol (mg/dl) and triglyceride (TAG) (mg/dl). For variables with changes $p>0.1$ (Bartlett's test) a one way ANOVA test was run for each parameter, with $p<0.05$ considered significant changes and box plots were created for these parameters. All serum parameters were obtained by Dr. Späth from the clinical biochemnistry, Uniklinikum Giessen Marburg, Giessen, Germany.

2.1.19 Workflow for analysis of data acquired by microarrays

A single microarray generates an enormous amount of data. In order to illustrate the workflow that was chosen for the interpretation and validation of the data discussed in this work, a summary of the methodology is given (Figure 10)

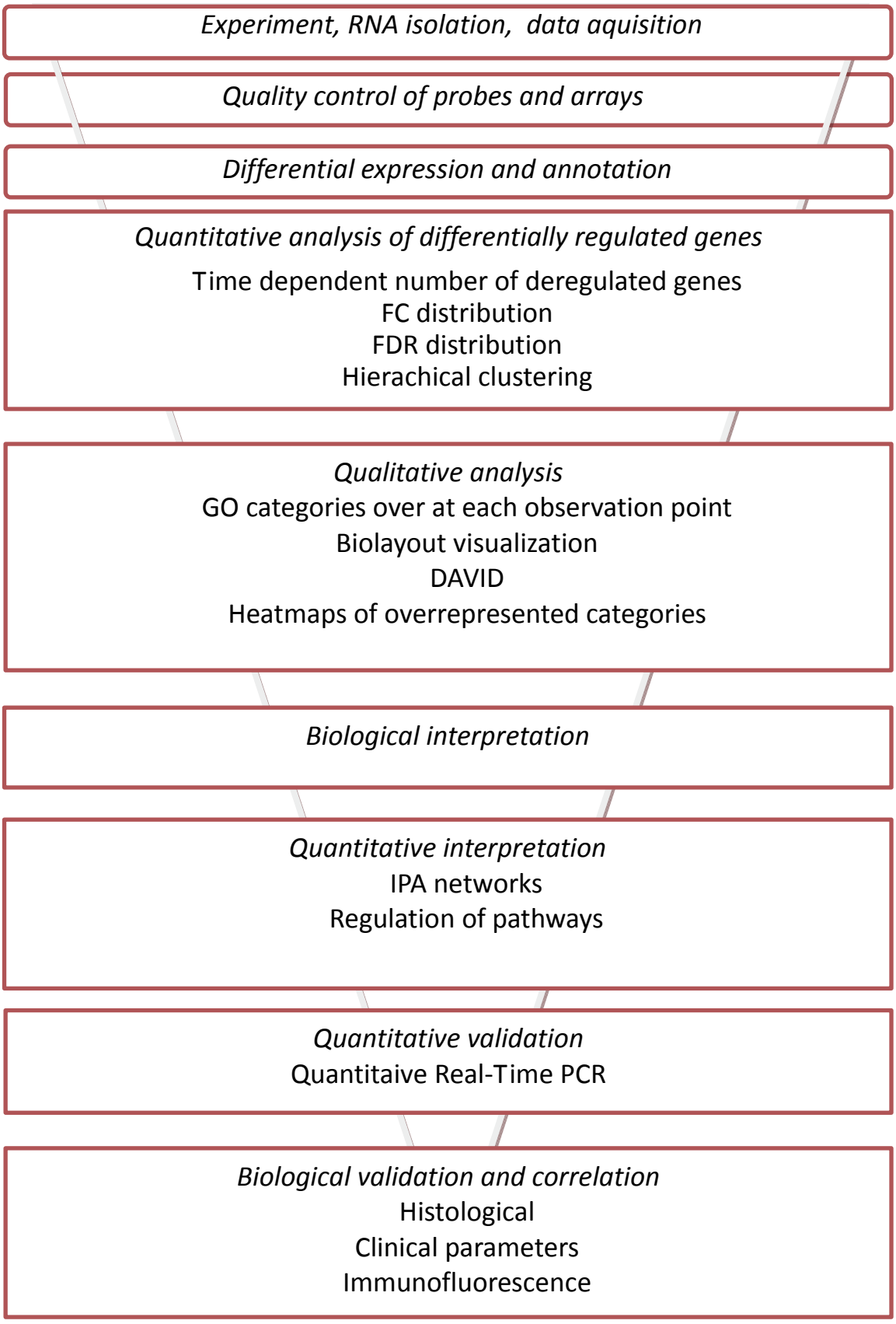

Figure 10: Workflow and analysis methodology applied in this study.

3. RESULTS

3.1 Quality control of microarrays

Quality control of microarrays is essential in order to ensure robust data that are used for biological interpretation. Messenger RNA samples that passed the Agilent Analyzer quality control were used for microarray analysis and intensities were measured for each setting. Each gene line assigned with the quality flag GOOD or EMPTY was applied to the quality control pipeline; POOR, NEG and MSR flagged gene lines were eliminated from analysis. Gene lines that were used for slide quality control and threshold calculation were also excluded from further analysis.

Each step and consequence in quality control progression for the investigated settings is displayed in Table 1.

The host response in the liver was elucidated by comparing the transcriptional response of non-infected control mice with mice infected with a sublethal dose of *Listeria*. We have investigated the temporal response for the intervals 4h, 1d, 2d, 3d and 5d upon infection, each depicted by three biological replicates from independently infected mice, excluding time point 5d p.i. with two biological replicates. In this experiment 18 microarrays were implemented into quality control. Only 0.943% (5789 fields) of the 613386 probes were flagged empty. By using the cleantable module 94 genes were eliminated and the empty field rate was reduced to 0.657%. 7640 gene lines were identified to be expressed below the array specific threshold and eliminated from analysis resulting in an empty field rate of 0.124%. 7399 expression values were excluded from analysis by the 1. Outlier filter, 7553 by the second outlier filter leaving 1.53% and 1.61% empty fields, respectively. Empty fields were imputed by using SKNN (K=5) following each step that resulted in empty field generation. Finally, the resulting gene lists were quantile normalized and log2 transformed. Detailed information about quality control steps for each investigated setting may be followed in Table 1.

Step in QC	*# of genes*	*#total probes*	*#empty fields*	*% empty/total probes*
raw data	34102	608047	5789	0.943
clean table	33908	606330	4014	0.657
threshold	26368	474035	589	0.124
SKNN 1	26368	474624	0	0.00
Filter 1	26368	467225	7399	1.53
SKNN 2	26368	474624	0	0.00
Filter 2	26368	467071	7553	1.61
SKNN 3	26368	474624	0	0.00

Table 1: Number of genes, total probes, empty fields and empty fields to total probe ratio after each step of the quality control (QC) workflow.

3.1.1 Correlation matrix and MVA plots

Following the spot-based quality control, the quality of the whole genome microarray was assessed by calculating the correlation coefficient of each slide (Table 2). The quality and consistency of each slide used in this study was very high as reflected by correlation coefficient values ranging from 0.9421 to 0.9911, which allowed us to keep all arrays in the study.

To further characterize the data quality of a single array in the context of a collective of arrays we applied the MVA plot function. As described above, the mean for each gene of the normalized and log2data set is calculated and genes are sorted by descending values and are assigned a rank. Then, each gene mean is plotted against the according mean value of the other microarrays. The horizontal axis represents the rank of the gene line mean and the vertical axis depicts the remainder (expression value minus mean value of the gene line). Good array quality is reflected by a horizontal line with dots scattered around y = 0. Spot-focused array quality control was high in this study as reflected by MVA plots. The vast majority of gene means was scattered around y = 2 to -2. No systemic faults were detectable and as such supporting above presented results (Figure 11).

Sample	K1	K3	K6	K7	M1	M2	M3	M4	M5	M6	M7	M8	M9	M10	M11	M12	M16	M18
K1	1,00	0,98	0,99	0,99	0,98	0,98	0,98	0,98	0,98	0,98	0,96	0,95	0,95	0,97	0,96	0,96	0,96	0,97
K3	0,98	1,00	0,99	0,99	0,98	0,97	0,97	0,98	0,97	0,97	0,96	0,96	0,95	0,96	0,97	0,96	0,96	0,97
K6	0,99	0,99	1,00	0,99	0,98	0,98	0,98	0,98	0,97	0,97	0,95	0,95	0,94	0,96	0,96	0,96	0,96	0,97
K7	0,99	0,99	0,99	1,00	0,98	0,98	0,98	0,98	0,98	0,98	0,96	0,95	0,95	0,96	0,96	0,96	0,96	0,97
4h M1	0,98	0,98	0,98	0,98	1,00	0,99	0,99	0,98	0,98	0,98	0,96	0,95	0,95	0,97	0,96	0,97	0,95	0,97
4h M2	0,98	0,97	0,98	0,98	0,99	1,00	0,99	0,98	0,98	0,98	0,96	0,95	0,95	0,97	0,96	0,97	0,95	0,97
4h M3	0,98	0,97	0,98	0,98	0,99	0,99	1,00	0,98	0,97	0,98	0,96	0,95	0,95	0,97	0,95	0,97	0,95	0,97
24h M4	0,98	0,98	0,98	0,98	0,98	0,98	0,98	1,00	0,99	0,99	0,97	0,97	0,96	0,97	0,97	0,97	0,96	0,97
24h M5	0,98	0,97	0,97	0,98	0,98	0,98	0,97	0,99	1,00	0,99	0,97	0,96	0,96	0,97	0,97	0,97	0,96	0,97
24h M6	0,98	0,97	0,97	0,98	0,98	0,98	0,98	0,99	0,99	1,00	0,97	0,96	0,96	0,97	0,96	0,97	0,96	0,97
48h M7	0,96	0,96	0,95	0,96	0,96	0,96	0,96	0,97	0,97	0,97	1,00	0,99	0,99	0,98	0,98	0,98	0,97	0,98
48h M8	0,95	0,96	0,95	0,95	0,95	0,95	0,95	0,97	0,96	0,96	0,99	1,00	0,99	0,98	0,98	0,98	0,98	0,98
48h M9	0,95	0,95	0,94	0,95	0,95	0,95	0,95	0,96	0,96	0,96	0,99	0,99	1,00	0,98	0,97	0,98	0,97	0,97
72h M10	0,97	0,96	0,96	0,96	0,97	0,97	0,97	0,97	0,97	0,97	0,98	0,98	0,98	1,00	0,98	0,99	0,98	0,98
72h M11	0,96	0,97	0,96	0,96	0,96	0,96	0,95	0,97	0,97	0,96	0,98	0,98	0,97	0,98	1,00	0,99	0,99	0,98
72h M12	0,96	0,96	0,96	0,96	0,97	0,97	0,97	0,97	0,97	0,97	0,98	0,98	0,98	0,99	0,99	1,00	0,98	0,99
M16 120h	0,96	0,96	0,96	0,96	0,95	0,95	0,95	0,96	0,96	0,96	0,97	0,98	0,97	0,98	0,99	0,98	1,00	0,99
M18 120h	0,97	0,97	0,97	0,97	0,97	0,97	0,97	0,97	0,97	0,97	0,98	0,98	0,97	0,98	0,98	0,99	0,99	1,00

Table 2: Correlation matrix. The first column indicates arrays of biological replicates of control mice (K1,K3,K6 and K7) and experimental mice, designated with "M" at each observation time point. The correlation matrix displays the Pearson correlation coefficient r^2 between each array with all arrays used in this experiment is displayed. R^2 ranged from 0.9421 to 0.9911 which reflects a very strong array quality and consistency of arrays used in this study.

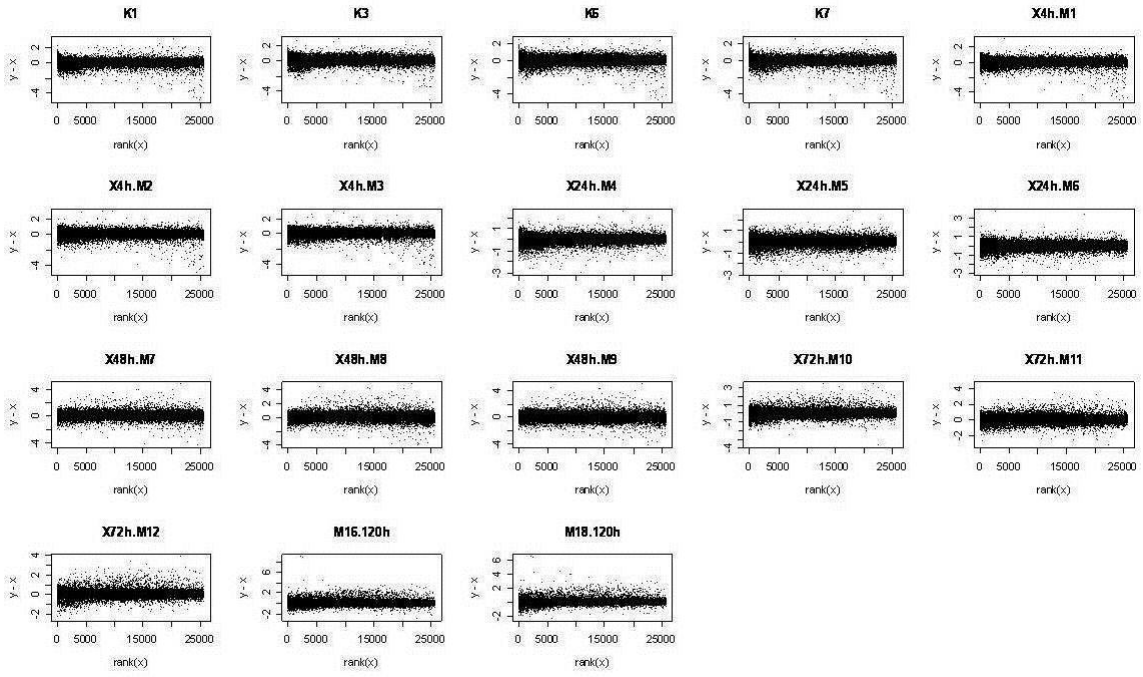

Figure 11: MVA plots of all microarrays used in this study.

3.1.2 Rank products

We used the rank products routine tool to identify differentially regulated genes. As described above, it is necessary to determine the number of permutation before starting the analysis. Due to the fact that high permutation number requires a large amount of computer recourses, which are limited, it is valuable to determine the minimal number of permutations that is necessary to gain the biological meaning of expression data. For this reason we tested

1. how permutation alteration influences the FDR and thus the number of differentially regulated genes 2. if the biological interpretation changes with different permutation numbers and

3. the minimal number of required permutation that still reflects the biological interpretation that is visible with the highest chosen permutation count.

Our results reveal a dependence of the number of differentially expressed genes that is determined by changing significance levels with changes in the permutation number chosen (Figure 12). The number of differentially expressed genes ranged from 295 to 302. The analysis revealed most prevalent differences in the number of differentially expressed genes between 100P and 200P and 300P, respectively. In particular, these alterations accounted for 2.3% of differentially expressed genes. There was, however, no difference between 350, 400 and 800 permutations. Both, the number of upregulated and downregulated were identical in these settings. Biological effects were estimated by conducting biological analysis using the IPA tool. These results (data not shown) indicate that differences in biological interpretation of the data occurred when using a number of permutations that is too low, indicating the importance of reassuring an appropriate individual number of permutations for each experiment.

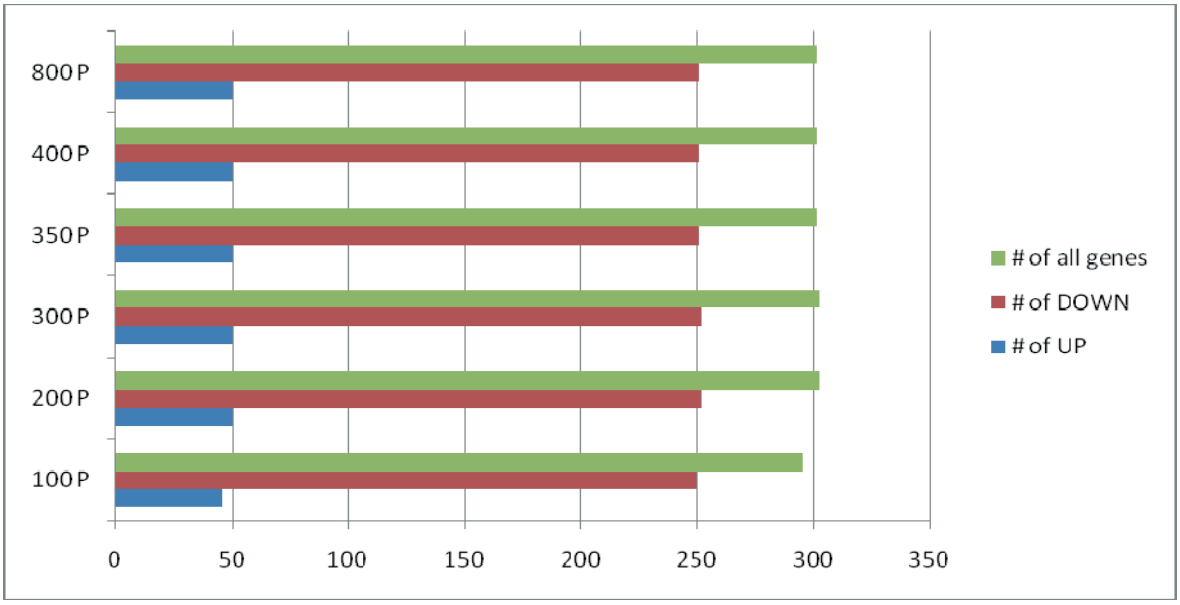

Figure 12: Effect of permutations on the number of differentially regulated genes. An increasing number of permutations was used, starting at 100 and up to 800 permutations. Numbers of all differentially regulated genes and a breakdown of up and downregulated genes are shown.

3.2 Hepatic response upon infection with *L. monocytogenes*

3.2.1 Global view of hepatic response to *L. monocytogenes*

We injected Balb/c mice intravenously with a sublethal dose (10^3 CFU) of *L. monocytogenes* and islolated the liver mRNA at various time points up to 5d post p.i. The mRNA samples were hybridized to oligonucleotides arrays containing ~36k probes that represent the whole mouse genome. The time course-experiment was replicated three times by using material from independently injected mice at each time point. 2661 probes displayed deregulation to at least one time point of observation. Of these, 2357 genes are mapped to common gene data banks and 1775 were scored as *L. monocytogenes*-responsive genes, corresponding to the criteria to be differentially regulated to almost one time point with a FDR < 0.05 and assigned to a GO category according to the Gene Ontology Consortium. Thus, approximately 9 % of the protein-coding genes of the whole mouse genome are mobilized upon listerial infection in liver in response to a single stimulus (Table S1, appendix, Figure 13 and 14).

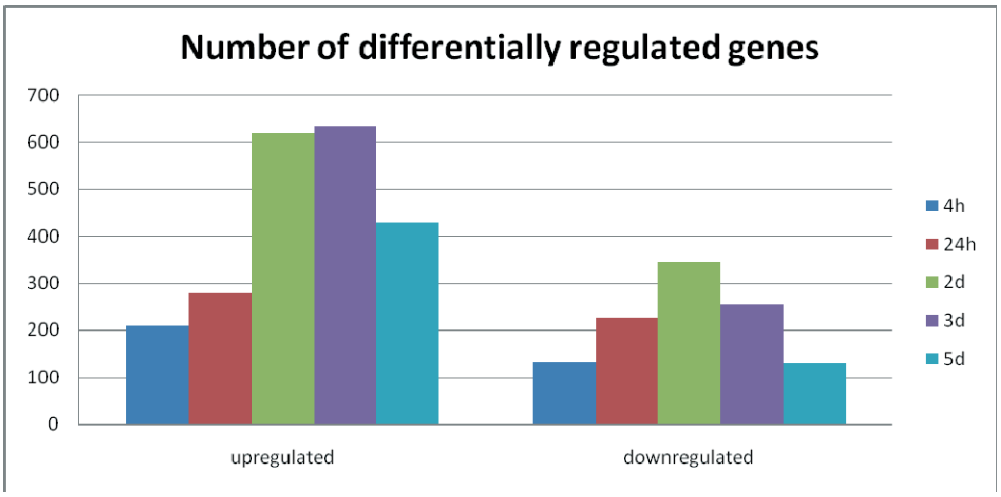

Figure 13: Distribution of number of upregulated and downregulated genes at each observation point. The number of upregulated genes outweighted the downregulated genes at each time point. There is an increasing number of deregulated genes peaking at 2 – 3d p.i. followed by a subsequent decay of deregulated genes.

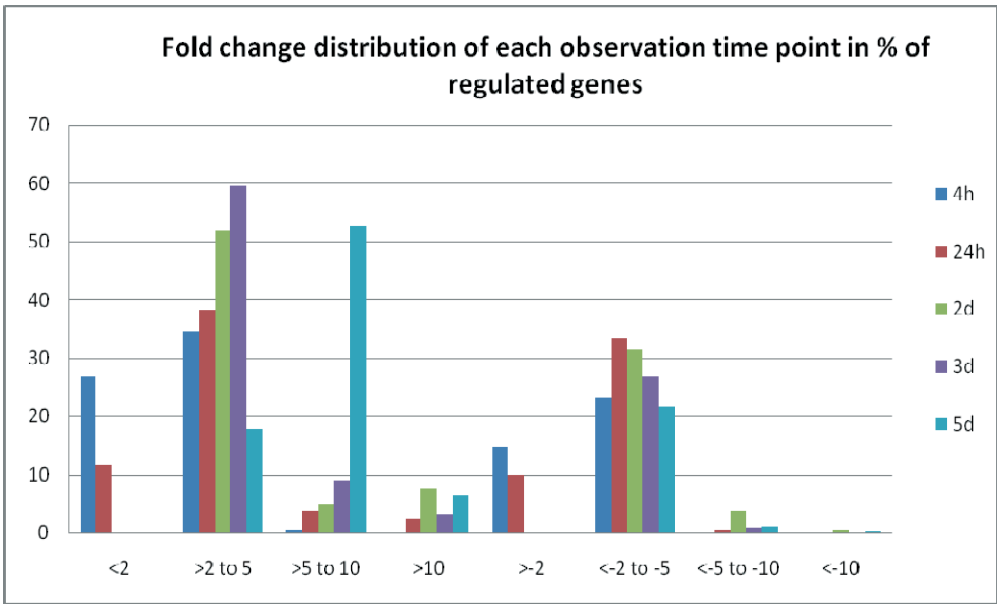

Figure 14: Distribution of the relative expression levels compared to controls at each observation point. Most deregulated genes had 2 to 5 fold higher and -2 to -5 fold lower mRNA levels. Highest deregulation levels were observed at day 2 p.i. where approximately 8% of genes displayed fold changes >10 as compared to control group and reflect a strong transcriptional response.

An enormous amount of data is generated in microarray experiments and analysis as well as biological interpretation is intricate. In this study, the complexity was further augmented by transcriptional dynamics that occurred over a time course at five observation points.

For these reasons, visualization of the large data set is an essential step in the analysis of microarray data. In order to acquire a global expression profile of each gene over the time course we used dChip for visualization, K-Means Clustering and hierarchical clustering, respectively. Results of this study is a so called “heatmap”, which either clusters arrays based on their similarity of their transcriptome or genes, which demonstrate a similar expression profile over the time course. Interestingly, as a result of this heatmap study, the vast majority of differentially expressed genes fitted to two major expression signatures (Figure 15)

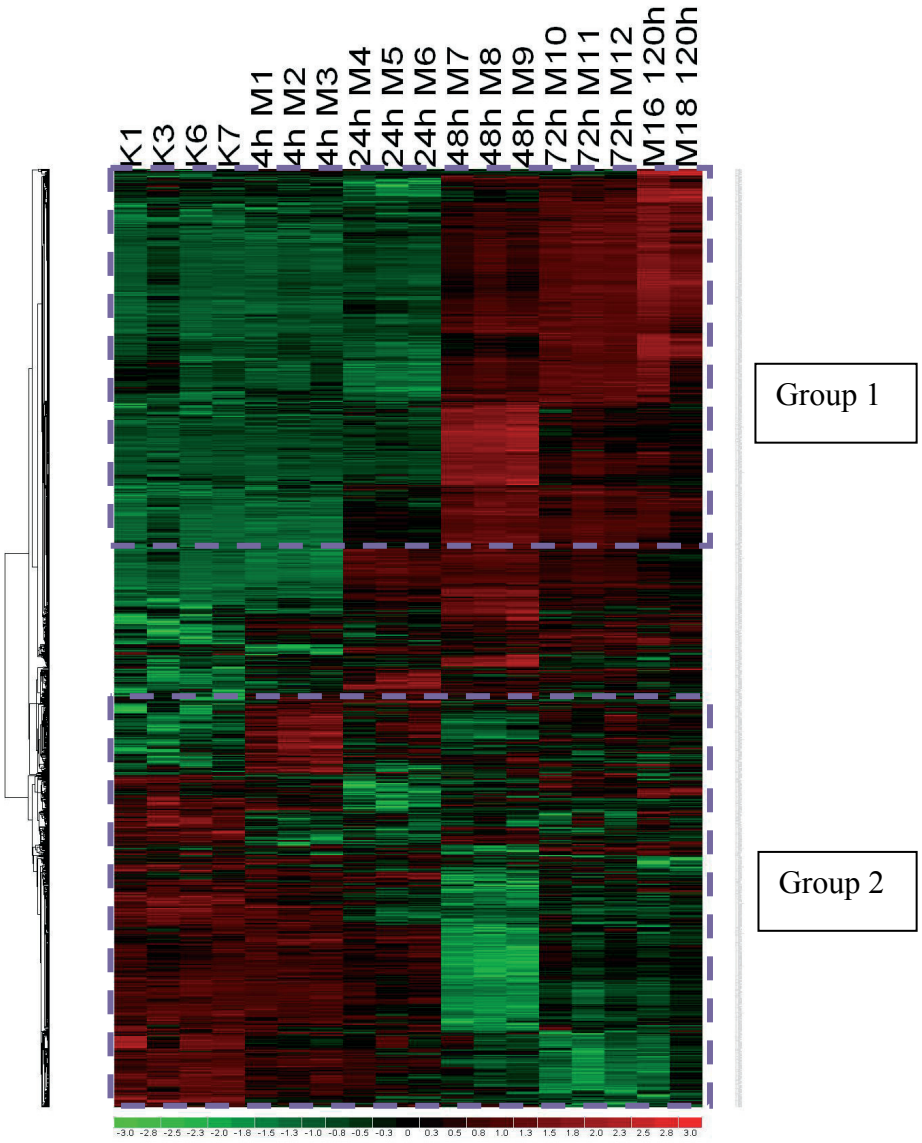

Figure 15: A global view on the transcriptional response in the liver upon listerial infection in mouse. Red highlighted genes are overexpressed in the corresponding gene mean. Accordingly, green are lower expressed and black highlighted genes show no expression differences to the corresponding gene mean. Two major groups with a biphasic response can be distinguished regarding their expression profiles over the time course. *L. monocytogenes* – responsive genes in group 1 show low expression during the early phase of infection (4 and 24 h post infection) and high expression of the same gene set during the later phase of infection (starting at 48h p.i.). An expression profile reciprocal to that of group 1 was observed for genes in clustered to group 2.

.

To gain insight into the biological function of deregulated genes and their products, genes were mapped to GO functional groups as defined by the Gene Ontology Consortium. As a result, the relative representation of each group over the whole study was visualized. Strikingly, two functional groups “immune response” and “metabolism” were heavily represented (Figure 16).

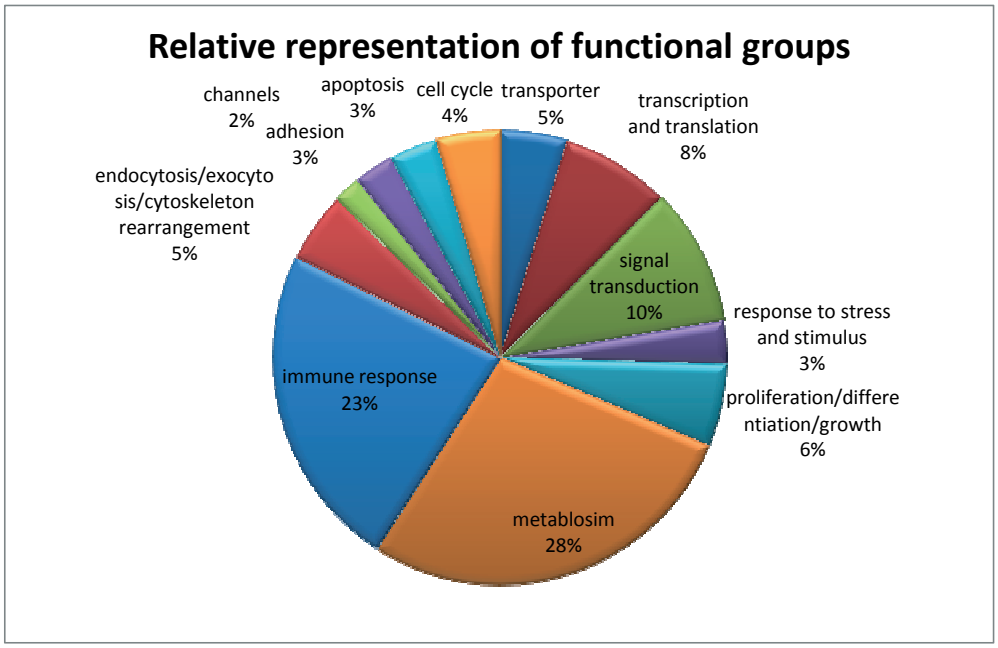

Figure 16: Genes were assigned to one of 13 functional GO groups as defined by the Gene Ontology Consortium. This graph displays the relative distribution of the functional groups over all time points. Genes assigned to “Immune response” or “metabolism” account for more than 50% of all deregulated genes.

However, this global representation does not reflect the quantitative deregulation of each functional group to a certain observation point.

For this reason, the relative number of genes within a functional group was assessed for each time point. allowing to gain insight into quantitative fluctuations of particular functional group over the time course (Figure 17).

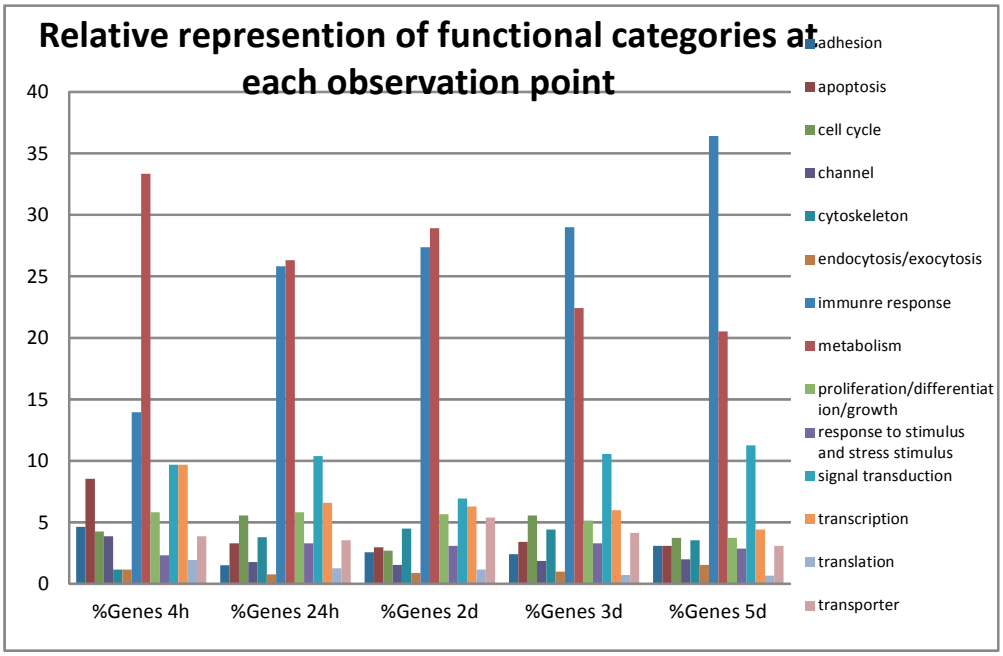

Figure 17: 1775 genes were clustered in functional groups according to GO terms. The genes were assigned to one of 13 functional categories, as defined by the Gene Ontology Consortium. Immune response and metabolic response represent the two major categories and are strongly deregulated at each observation point. While the relative number of genes involved in metabolism represents 33% of deregulated genes at 4h p.i., this number declines to 20% at day 5 p.i. In contrast, the ratio of genes that are involved in immune response increases from 14% to 37% over the time course, demonstrating a quantitative reciprocal relation between metabolic and immune response.

In a further step, we sought to cluster genes with a similar signature within a functional category of interest. Biolayout Express 3D is a helpful tool that helps to visualize a large number of genes with regard to 1) their expression profile at different time points,

2) their functional GO group and 3) shows interconnections of subgroups within one category and between different categories according to their expression patterns. This information is visualized by grouping genes with a similar expression profile in a node. Nodes that belong to the identical GO category are displayed in the same node color and are connected. Also, subgroups of genes within other categories may be connected according to the similarity of expression profile over the time course. *Biolayout* revealed that most genes exhibited a biphasic wave of expression over the time of observation. Biolayout networks consist of nodes representing transcripts connected by their virtue of expression profile similarity across different conditions. In our observation we used GO terms as condition of interest, thus genes that exhibit similar expression profiles in the same functional group are colored identically (Figure 18).

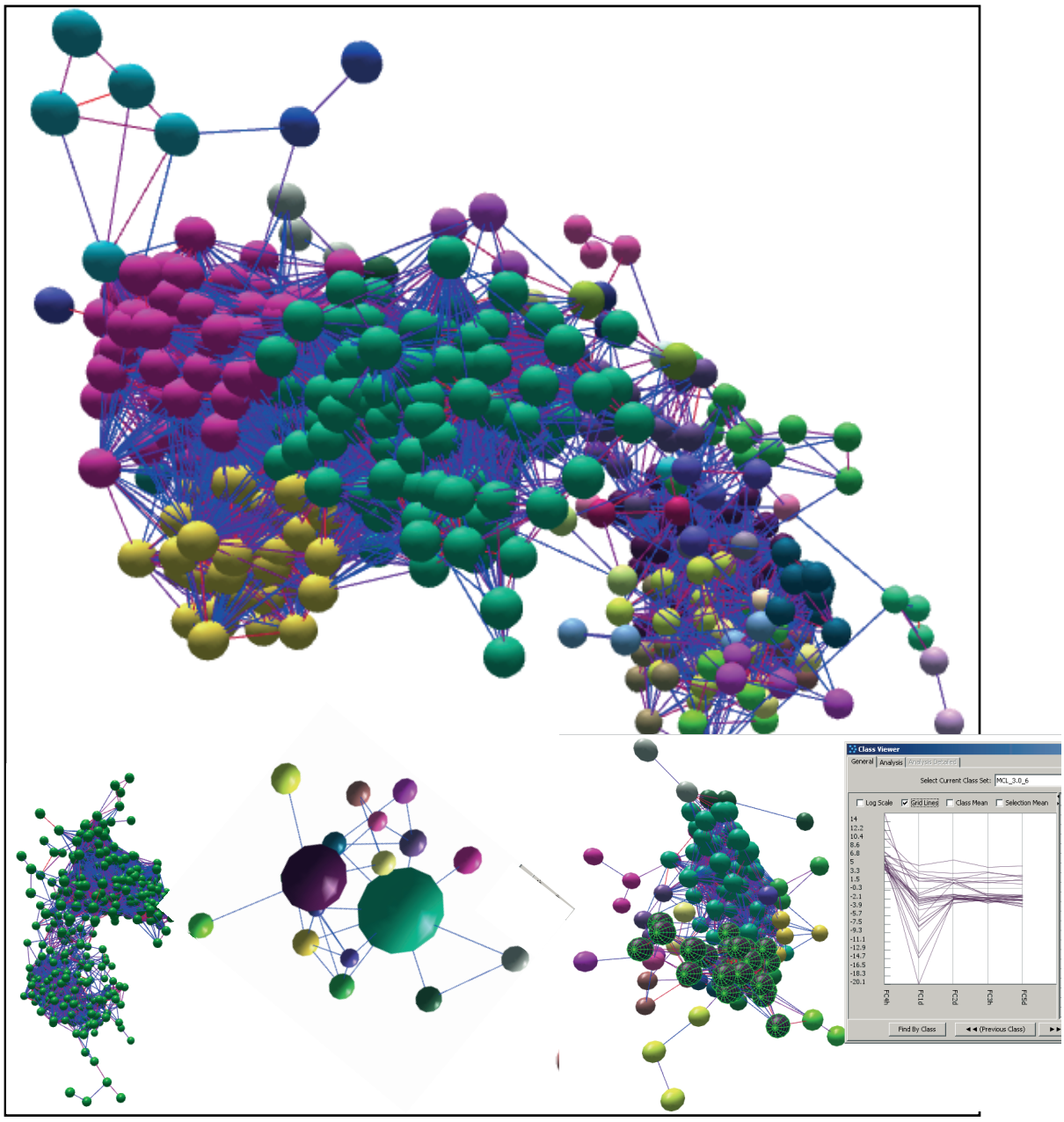

Figure 18: Hierachial clustering and visualization of differentially expressed genes using *biolayout.* Each sphere represents a group of genes, which belong to the same GO category, reflected by the same node color and exhibit a similar expression profile, which is reflected by interconnections of spheres. In this case, green spheres are clustered to the functional category metabolism; purple spheres include genes involved in the immune response. By collapsing spheres, the level of connections can be decreased leaving a more global connection pattern. The 3D – display allows changing the view permitting the user to display the expression pattern of selected spheres.

An important step in the analysis of significantly deregulated genes is the enrichment analysis, which provides information about overrepresented categories and the possibility to focus on more relevant biological mechanisms. To obtain a global view on significantly overrepresented functional GO groups, we used DAVID (*database for annotation, visualization and integrated discovery*) is a free project of the *National Institute of Allergy and Infectious Diseases (*Bethesda, MD, USA) [198]. This bioinformatics tool uses the GO terms of each implemented gene, assigns it to the according category and calculates how likely a non-random regulation of this category is. The probability is calculated by a simple term: $P = X(S)/ X(B)$; X(S) = number of significantly expressed genes of the category X,

X(B) = number of all genes present in the category X (taken from the background list). An essential part of this study is to upload a background list containing all gene identifiers that passed the quality control process and then provide the list of interest comprising all significantly deregulated genes.

The lower a calculated p-value is the higher the probability for a category to be overrepresented in the study and vice versa. We set a cutoff for significant overrepresentation at $p < 0.05$.

As a result of this, several overrepresented functional categories and pathways were identified (see supplemental material). Categories involved in immune response, such as “defense response”(GO:0006952), “chemotaxis” (GO:0006935) and ”antigen processing and presentation” (GO:0019882) “positive regulation of T cell activation” (GO:0050870) were overrepresented with p-values < 0.0001. Strikingly, several functional categories as well as pathways that are involved in the metabolism, particularly lipid metabolism were seen significantly overrepresented, including “cellular lipid catabolic process” (GO:0044242), “steroid metabolic process” (GO:0008202), ”acyl-CoA thioesterase activity” (GO:0016291) “mmu00591:Linoleic acid metabolism” and “mmu00590:Arachidonic acid metabolism”. Further important overrepresented categories were ”ligand-dependent nuclear receptor activity” (GO:0004879),”regulation of phosphorylation” (GO:0042325) “regulation of foam cell differentiation” (GO:0010743) “phagocytosis” (GO:0006909) and “anti-apoptosis” (GO:0006916) as well as “induction of apoptosis” (GO:0006917).

Combining this result with above presented data and with regard to the quantitative and qualitative involvement in this study, we separately investigated the expression pattern of genes involved in lipid metabolism and immune response.

This study displayed a reciprocal relationship between these groups on a global transcriptional view that was apparent over the entire infectious course. The majority of lipid metabolism regulating genes was seen highly expressed within 24h p.i. and a decay of expression was observed over the later time points. Strikingly, genes involved in immune response exhibited a reciprocal kinetic with respect to the directionality of response over the infectious course. This was visualized by using heatmaps of the particular functional groups (Figure 19)

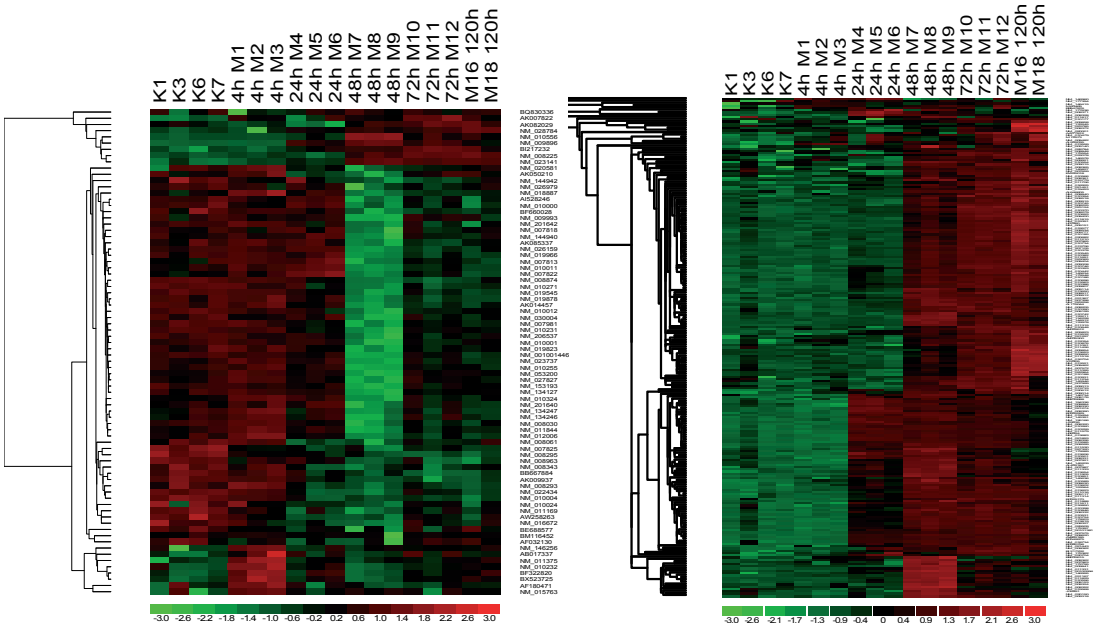

(A) (B)

Figure 19: (A) Hierachical clustering of genes that are mainly involved in lipid metabolism or (B) immune response is shown. A biphasic response with respect to the direction of gene expression is visible upon single injection of *L. monocytogenes*. While genes are mainly lower expressed in control mice and 4h/24h p.i., they exhibit higher expression during the other time points observed. Comparing both heat maps illustrates the reciprocal dependence of lipid metabolism and immune response on transcriptional level.

To determine the biological effects of the biostatistically gained information from gene expression, we investigated the association and relevancy of our result in context to most recent knowledge about infectious diseases, immunology and host response by using the Ingentuity Pathway Analysis tool (IPA). For each observation point this tool visualizes microarray data, illustrates gene interactions, generates networks of functionally related genes, and maps differentially expressed genes to metabolic,

disease and further pathways. Biological associations between two factors are visualized as two-dimensional illustrations, which also display the qualitative association of interacting genes, e.g. activation, inactivation or phosphorylation. A comparison analysis of all time points was also employed to clarify changes in biological and cellular functions as well as interconnection of generate networks. The base of the tool is an enormous data bank, which is broadly used and accepted by researchers in all biological fields. A p – value < 0.05 (Fisher's exact test) was considered significant for biological and cellular functions as well as networks and canonical pathway deregulation.

The top regulated cellular function was "lipid metabolism" (p = 0.0001); within the top 5 regulated functions the other metabolic categories "carbohydrate metabolism" (p = 0.0003) and "small molecules biochemistry" (p = 0.0001) were found 4h p.i. Furthermore, the top three gene interaction networks were dominated by molecules that regulate lipid metabolic processes (Table 3). Among the top 10 upregulated genes 4hp.i., several genes involved in lipid metabolism are seen, such as CYP3A14, FMO, SULT1E1 and Perilipin 4 (PLIN4), a protein that is bound to intracellular lipid collections called *lipid droplets*, while genes of the acute phase response, such as MMP3, A2M and MAPK14 were found among the top 10 downregulated transcripts.

ID	Molecules in Network	Score	Focus Molecules	Top Functions
1	ACADM, ↑**ACOT1 (includes EG:26897)**, ↓**ADAD1**, ↓**AQP8**, CCNT1, CYC5 (includes EG:13063), ↑CYP7A1, ↓**CYP7B1**, ↑**ESRRA**, FDFT1, GABPA, ↑**GCK**, ↑**GDE1**, ↑**HEXIM1**, ↑**HMGCR**, ↓**HMGCS1**, HNF4A, LEP, ↓**LOC100129193***, ↑**LPIN1***, ↓**MKI67**, PPARA, PPARG, PPARGC1A, SAT1, SCD, ↑**SLC2A4**, YBX2	14	14	Lipid Metabolism, Small Molecule Biochemistry, Carbohydrate Metabolism
2	↑**AK4**, ↑**BDNF**, ↑**C10RF51**, CEBPB, CREB1, CREM, ↓**CROT**, ↑**CYP4A14**, ↓**EGR2**, ELK4, FASN, ↑**FMO5***, FOS, ↑**GADD45B**, ↓**GAPDH (includes EG:14433)***, GPAM, ↓**GRIK2**, ↑**HMGCR**, HTT, ↑IL1B, ↓JUNB, LEP, ↓**MAPK14**, NCOA6, ↓**NR4A1**, PPARA, PPARG, SCP2, ↑**SIK1**, ↑**SREBF1***, SRF, ↑STAT3*, TCOF1, TNF	14	15	Lipid Metabolism, Molecular Transport, Small Molecule Biochemistry
3	↑**ARID5A**, CD3E, ↓**CDH1**, ↓**CLDN1**, CLDN6, ↑CYP7A1, ↑**ESR1**, FOXA2, ↓**FUS**, ↓**GADD45G**, GDF9, GJB1, ↑**GREM1**, HNF4A, ↑**HSD3B2**, ↓**IFI47**, ↓**IFIT1B**, IFNG, IL4, IL6, IL12 (complex), ↓**IL18R1**, ↑**KLF4**, LHCGR, NR1H4, NR5A2, ↑PTGS2, RARA, RNA polymerase II, STAR, ↓**TGTP1**, ↑TLR4, TNF, ↑**TNFRSF1B**, ↑**YWHAG**	13	15	Lipid Metabolism, Small Molecule Biochemistry, Vitamin and Mineral Metabolism
4	AEBP1, AGER, BCL2L1, ↑**CCL8**, ↑**CD36***, CEBPB, ↑**CRAT**, ↑**ETS2**, ↑**HSP90AA1**, IDH1, IFNG, IL4, IL6, IL21, IL11RA, ↓IL1A, ↑IL1B, ↑**IL6R**, ↓**ITGB6**, LEP, ↓**LPL**, ↓**MMP3**, MMP9, ↑**MMP12**, ↑**ODC1**, ↑**PLIN4**, PPARG, PRKCD, PRKCE, ↓**SAA2***, SAT1, TCR, TLR9, TNF, ↑**USP2**	12	14	Hematological System Development and Function, Inflammatory Response, Lymphoid Tissue Structure and Development
5	↑**ALAS1**, ALDH1A1, ALDH1A7, ↓AR, ↓ARNTL, BAG1, ↑**CD36***, CES6, CLOCK, CRY1, CRY2, CSNK1E, DMRT1, ↓**DYNC2LI1**, EZH2, ↑**FKBP5**, FOXA2, GLI1, GLI2, ↑GSTA5*, ↑**HSPA1A***, INSIG1, ↑**MAP2K6**, ↑**NR1I2**, NR1I3, ↓**PAX2**, PER1, ↑**PER2**, ↑**PER3**, ↑**POR**, SHH, ↓**SMAD3**, ↑**STRA8**, ↑**SULT1E1**, UGT1A1	12	14	Behavior, Nervous System Development and Function, Connective Tissue Development and Function

Table 3: This table was generated using IPA. It shows genes names and indicates upregulation (red arrow) or downregulation (green arrow) of each gene. Genes that are functionally connected are clustered in on network. Based on the number of connections, each network gets a score and is ranked in order starting with the network that was assigned the highest score. The very right column indicates the function of each network and reflects the GO categories of genes that are represented in that particular network. This exemplary table shows the top 5 scored networks at 4h p.i. The network with the highest score includes mainly genes that are involved in metabolism, particularly lipid and carbohydrate metabolism.

Pathways that were linked to both, lipid metabolism control and immune response, including “LXR/RXR activation” and “LPS/IL-1 mediated inhibition of RXR function” were among the top 10 upregulated canonical pathways (Figure 20). Further pathways involved in the synthesis and modification of lipids or lipid derivates, such as steroids, were strongly overrepresented. At the same time, several genes found in the inflammatory response by macrophages and fibroblasts pathway show significantly decreased expression levels, including ILR181, MAPK14, PRKD3, MMP3, PRSS41 and the nuclear factor of activated T cell NFATC4, which is critically involved in the transcriptional regulation of cytokines that are key players in the immune response, such as IL-2, IL-8 and TNF [109] (Figure 21 and 22).

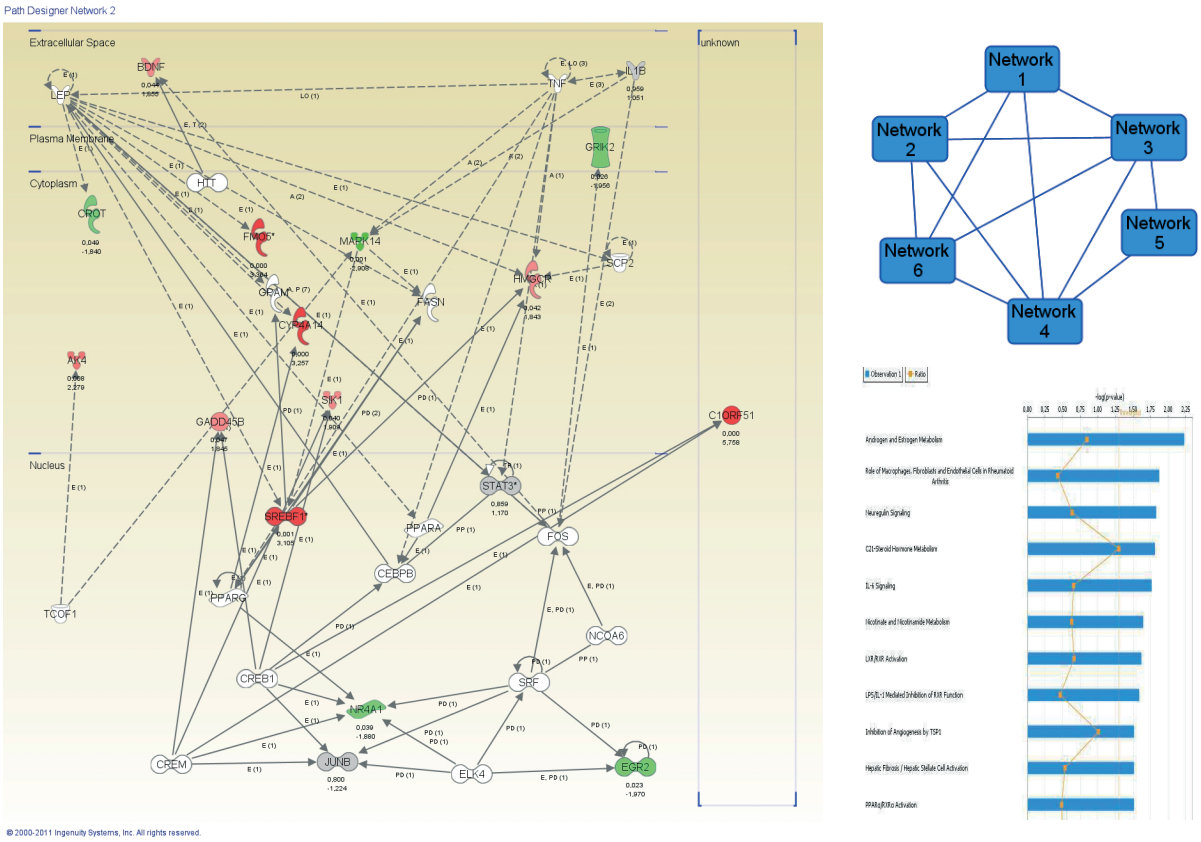

Figure 20: (Left) Connections between genes included in network 2 of the 4h experiment are displayed. In addition to the magnitude of gene deregulation, FDRs are indicated for each gene. This illustration also demonstrates the subcellular localization of the gene product, for example “extracellular“ or “nucleus”, thus allowing the user to gain several information from a single network visualization. In this network, SREBF1, a regulator of intracellular lipid modification and lipid droplet synthesis is seen strongly upregulated. NR4A1, a nuclear activator of the major inflammatory transcription factor NFkB and a potent inducer of programmed death is seen strongly downregulated [110].

(Right upper) Demonstrates how strong each network is connected to genes within other networks. (Right lower) Canonical pathways, which are strongly overrepresented in this experiment are shown here, including several lipid metabolism pathways present at 4h p.i.

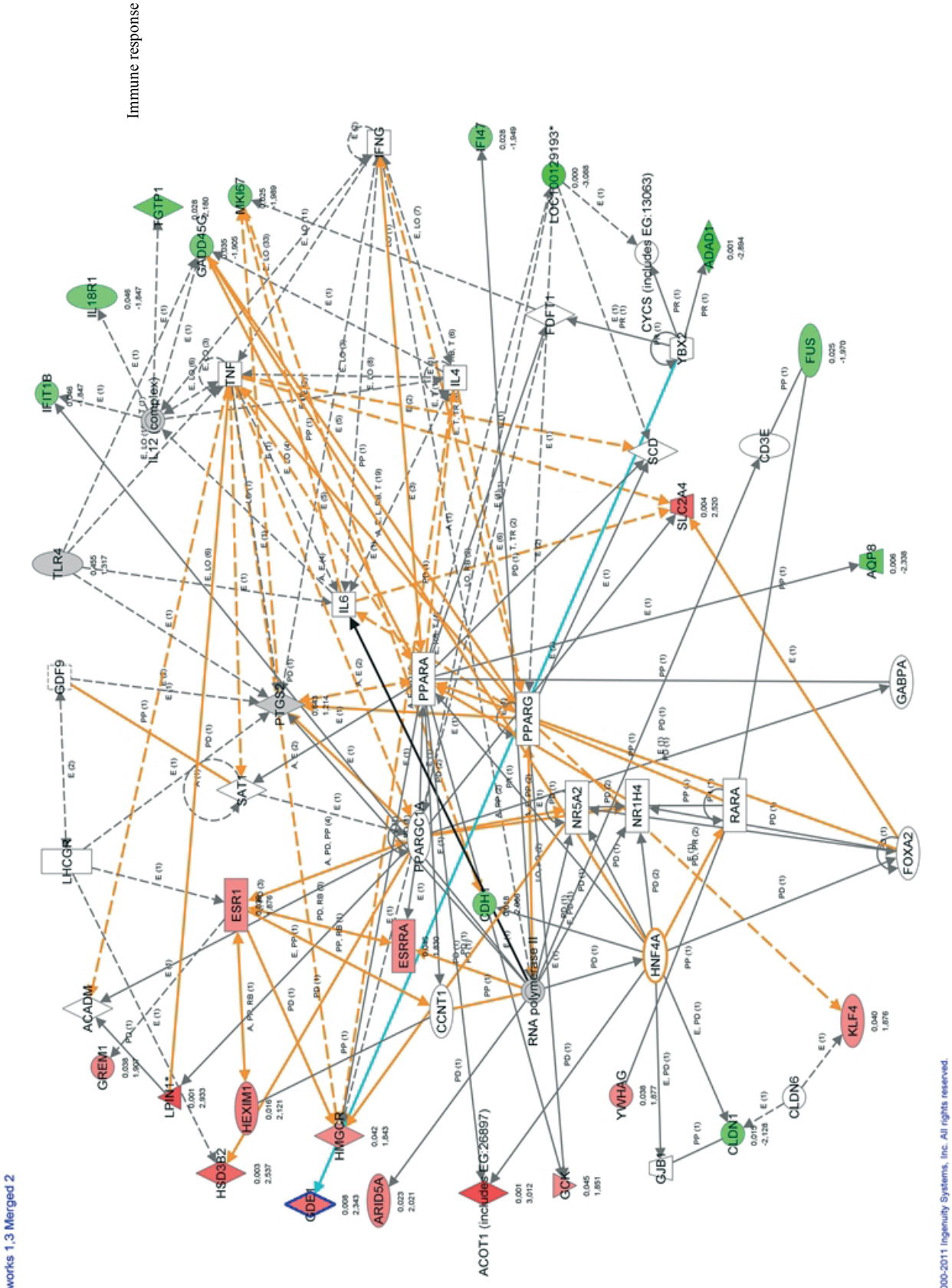
Immune response
Lipid metabolism
Networks 1,3 Merged 2
IFIT1B
IL18R1
IFGTP1
GADD45G
MK67
IFNG
IFI47
LOC100129193*
CYCS (includes EG:13063)
ADAD1
FDFT1
IL12 (complex)
TNF
IL4
BX2
FUS
SCD
CD3E
SLC2A4
TLR4
AQP8
IL6
PPARA
PPARG
GABPA
GDF9
PTGS2
SAT1
NR5A2
NR1H4
RARA
FOXA2
LHCGR
PPARGC1A
ESR1
GDH
ESRRA
HNF4A
CCNT1
RNA polymerase II
ACADM
GREM1
LPIN1*
HEXIM1
HMGCR
HSD3B2
GDF1
ARID5A
ACOT1 (includes EG:26897)
GCK
YWHAG
GJB1
CLDN1
CLDN6
KLF4
© 2000-2011 Ingenuity Systems, Inc. All rights reserved.

Figure 21: This network is the result of network 1 and network 3 obtained from the 4h experiment. As visible, genes of the immune response and lipid metabolism are heavily interconnected, indicating a strong functional dependence. This network translates the global impression of a reciprocal relationship of immune response and lipid metabolic response to a gene to gene level, thereby supporting the analysis flow that was approached. (Red highlighted genes are upregulated; green highlighted genes are downregulated; gray indicates genes that were in the analysis set, but not significantly deregulated; white indicates genes that were not in the analysis set).

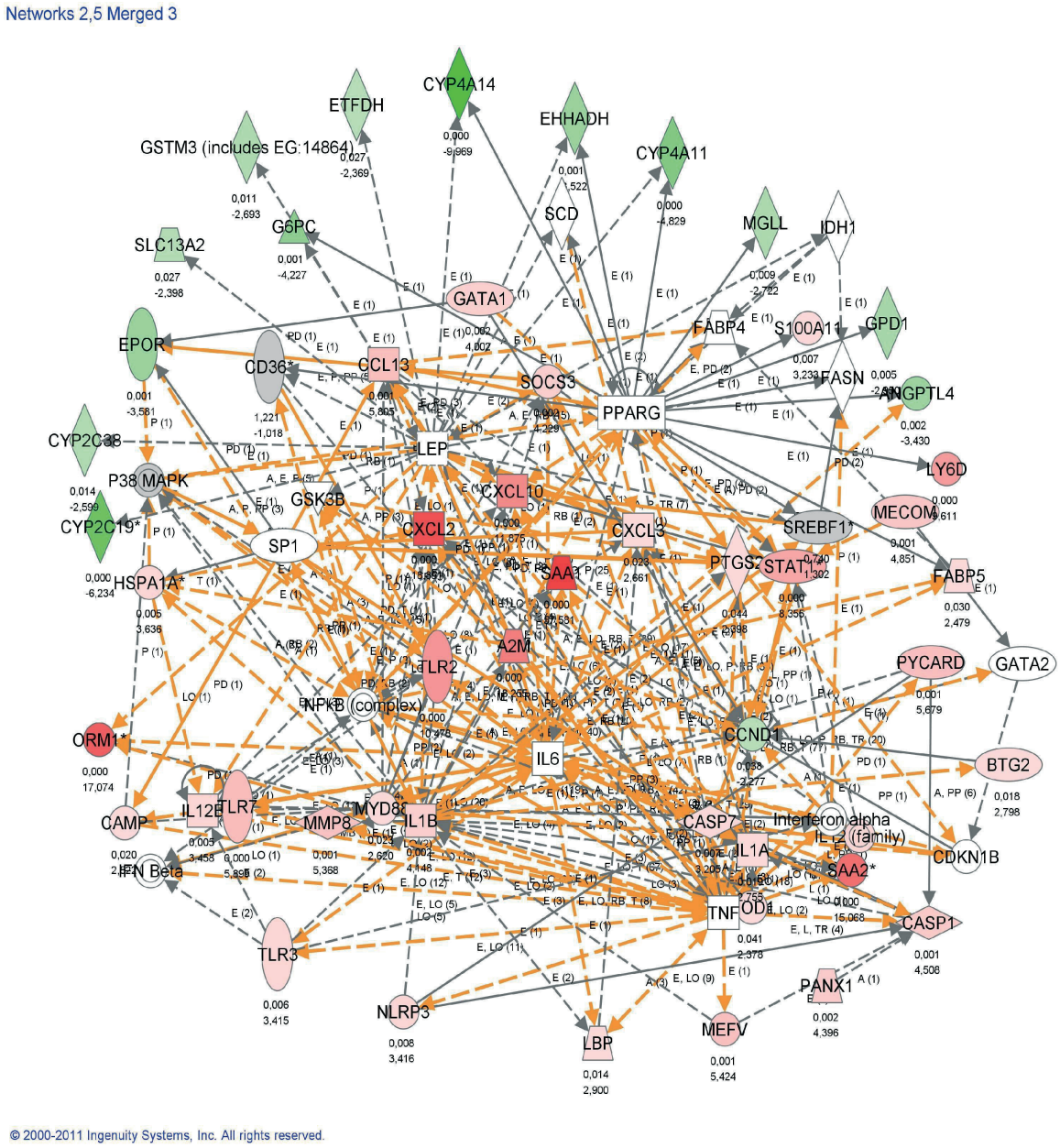

Figure 22: In contrast to the figure above, an interactome resulting of merging network 2 and 5 at day 2 p.i. uncovers an inversed reciprocal relation of immune response, reflected by upregulation of several genes involved in the pathogen recognition and acute phase response, such as, TLR2, SAA, IL1 and downregulation of genes involved in the regulation of fatty acids and cholesterol modification. Genes from both categories that were seen among the top 10 deregulated genes at 4 h p.i. are inversely regulated at day 2 p.i., such as A2M and CYP3A14. A deregulation of several regulators programmed cell death, such as CASP1, CASP7, CD5L and BIRC5, indicates a well-coordinated regulation of survival and apoptosis. (Red highlighted genes are upregulated; green highlighted genes are downregulated; gray indicates genes that were

in the analysis set, but not significantly deregulated; white indicates genes that were not in the analysis set)

Of the transcription factors essentially involved in regulation of lipid metabolism and possess regulatory function in the immune system, LXR gained much attention during the last years. As we show lipid metabolism regulated by LXR could be a central factor for immunoregulation during listeriosis and other infectious diseases in liver. Using the Ingenuity Pathway analysis tool concordantly revealed, that beside the immune response pathways the LXR pathway and LXR regulated genes are strongly deregulated during hepatic *Listeria* infection.

3.2.2 Innate and adaptive immune response intersect in a global view upon challenge with *L. monocytogenes*

We have identified about 319 genes with roles in host defense that showed significant alterations in expression in response to *L. monocytogenes*. Elevated expression of several marker genes for innate immunity, such as complement factors, serum amyloid protein (SAP), PRRs, antibacterial peptides (Figure 23) and pathogen recognition by TLR pathway were accompanied with higher expression of genes involved in adaptive immunity, such as MHC class I and class II molecules. Interestingly, most genes of innate immune response initially presents about 24h p.i. in our global evaluation. This is astonishing, since acute phase response upon endotoxin stimulus was shown on transcriptional level to occur as early as 3 hours after LPS injection [111]. Thus, we observe a substantial difference of hepatic APR dependent on the stimulus. Adaptive immunity intersected with innate immunity with respect to the temporal transcriptional regulation in this global view. This phenomenon was observed in 12k microarray analysis in mice challenged with intravenous LPS inoculation, but not for Gram-positive bacteria. Also, the hepatic transcriptional response upon LPS stimulation demonstrates a global expression pattern inversely directed with regard to gene deregulation when compared with our results.

Gene products, which act in concert to present endogenous and bacterial peptides by MHC class I and class II, respectively, were also seen higher expressed from 24h p.i. up to 5d p.i This group included MHC I molecules (H2-M, H2-Q, H2-T); MHC II molecules (H2B, H2A); the peptide transporters TAP1, TAP2 and Tapasin, which together promote loading of MHC molecules with antigens; Class II transactivator, a

transcription factor involved in induction of MHC II molecules and CD74, a class II antigen-associated invariant polypeptide of MHC, CD80 and CD86, which are important co-stimulatory proteins located on the surface of dendritic cells and initiate T – cell priming. We also observed an upregulation of all major constituents of the immunoproteasome PSMB10, PSMB8 and PSMB9, a machinery that promotes adaptive immunity by the degradation of listerial virulence factors [112], such as LLO and p60 found in host cytosol after vacuole disruption.

Genes of both compartments, innate and adaptive immunity exhibit low expression within the early phase of infection response and display a strong transcriptional response initiated 24h p.i. Several transcription factors and regulators are responsible for expression control of innate and adaptive immune system. Additionally, metabolic constituents, such as lipid derivates including modified cholesterol products and fatty acids gained increasing attention as regulators of several biological processes, e.g. defense response during the last years. In this context and with regard to results presented in this study, it is noticeable that genes of lipid metabolism have an inverse expression profile when compared to genes of defense response. We propose that in addition to the reversed temporal transcriptional response pattern there is a functional connection between both biological processes.

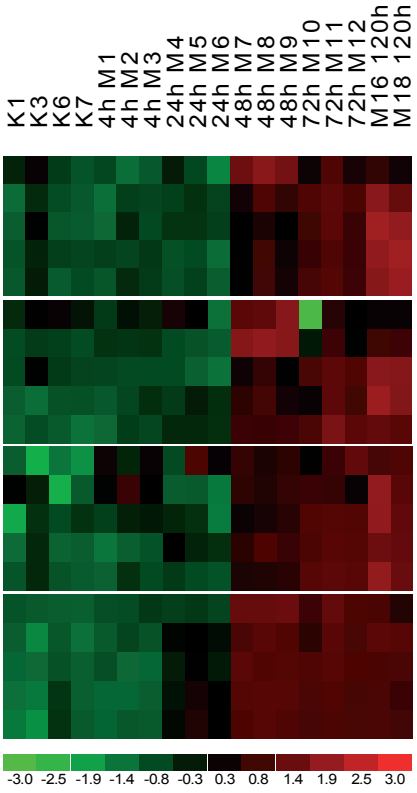

Figure 23: Differentially regulated genes of innate immunity. Several genes that are involved in APR exhibit the biphasic expression profile mentioned above. (A) Complement factors: C6, CFH, C1QBETA, C1ALPHA and complement factor properdin. (B) PRRs: MARCO, MSR1, CD5L, LBP, CD14. (C) Category response to bacterium: DEFB29, CARD12, FCGR1 and FCER1G. (D) SAA1, SAA2, SAA3, ORM2 and ORM3.

3.2.3 Hepatic lipid metabolic and immune response are reciprocally regulated in a global view

Investigation of *L. monocytogenes*-responsive genes provided insight into the drastic changes in lipid metabolism during hepatic APR. 381 genes involved in the metabolic processes or in the regulation are differentially regulated. Specifically, approximately 140 genes involved in the lipid metabolism undergo significant alterations in transcription intensity in our observation. Previous work revealed that different lipids are important for effects of listerial toxins, listerial adhesion to lipid membranes and influence microbial inactivation [113, 114]. Several genes of fatty acid and TAG synthesis, cholesterol modification to oxysterols, bile acid formation, linoleic and arachidonic acid metabolism and LXR/RXR signaling pathway were concordantly biphasic regulated (Figure 24).

During the early phase of infection, in particular 4h p.i. several genes of lipid metabolism are seen upregulated. Acyl-CoA thioesterase 1 (Acot1), Acot3 and Acot4 catalyze the hydrolysis of acyl-CoAs to the corresponding free fatty acid and CoA [115] show increased mRNA levels 4h and 1d p.i. but are lower expressed during the later phase of infection; ACSM2, a member of the acyl-CoA synthetase family and the carnitine O-octanoyltransferase (CROT) supply the beta-oxidation pathway with its substrates are seen downregulated 4h p.i. [111] In concert with the deregulation of ACOT enzymes, energy supply from the degradation of fatty acids is decreased during this early phase of infection. Furthermore, GDE1 [116] and ESR1 synthesize precursors for triacylglyceride (TAG) synthesis from degradation of phospholipids as well as AOAH [117], an enzyme with lipase activity that releases free fatty acids by hydrolysis of bacterial lipids are seen significantly upregulated 4h p.i.; at the same time, AGPAT1 and AGPAT6 [118], enzymes responsible for TAG precursors synthesis are upregulated at 4h and 24h p.i. Furthermore, the intake of TAG is increased by the upregulation of CD36 [119], a surface receptor for oxidized LDL particles containing TAG and cholesterol. SREBF1, a LXR – responsive gene, is a transcription factor regulation a subset of genes that promote the synthesis of fatty acids as well as TAG [120]. In line with this, SREBF1deregulation was linked to metabolic syndrome as well as cholestatic liver disease, because it prevents modification of several substrates, such as oxysterols to bile acids through inhibition of HNFA4 [121].

Recently, a study demonstrated a crucial role of lipin 1 (LPN1) in the buildup of cytoplasmic TAG storages in human hepatoma cells (HuH-7) that is mediated by SREBF-1 regulation [122]. Both, SREBF-1 and LPN1 are strongly upregulated within the first 24h p.i. and display lower mRNA levels in the later phase of infection. Interestingly, SREBF-1 activation leads to a transcription decay of lipoprotein lipase (LPL), a gene that promotes TAG hydrolase and is ligand/bridging factor for receptor-mediated lipoprotein uptake [123]. Consequently, LPL mRNA level alterations are seen over the time course with strong downregulation in the early phase and upregulation in the following period.

Expression of perilipin 4 and 5 (PLIN4 and PLIN5) increase stabilize intracellular accumulations of TAG deposited as lipid particles, also known as lipid droplets [124, 125]. Both genes were among the strongest upregulated genes 4h upon *L. monocytogenes* inoculation.

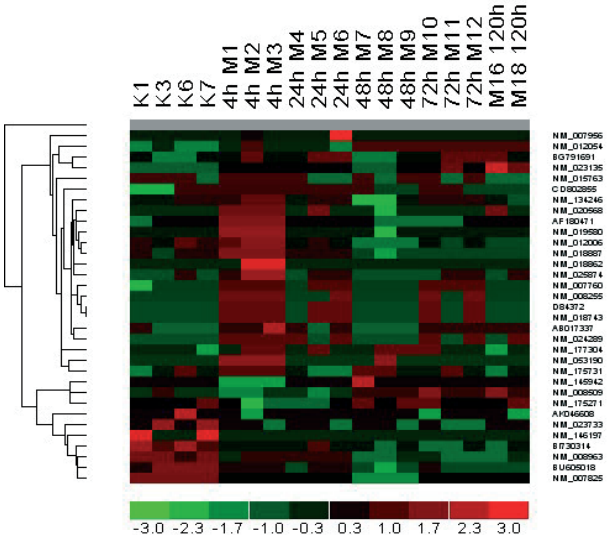

Figure 24: Intensities of above discussed genes assigned to the GO category "lipid metabolism" at 4h p.i. As visible, the majority of genes is seen highly upregulated in the early phase of infection.

3.2.4 Transient gene deregulation is associated with the accumulation of intracellular lipid droplets

As a consequence of this deregulation measured by microarrays, our analysis predicted a massive intracellular accumulation of fatty acids mediated by a concerted transcriptional alteration of genes involved in the uptake, synthesis and degradation of lipid metabolites. To address this hypothesis, cryosections of the livers harvested at 4h, 24h and 48h post injection were rinsed with oil red O, a dye that stains neutral fatty acids and cholesterolesters (Figure 25).

Astonishingly, we found the biological consequence predicted by microarray analysis to be accurate. A substantial number of intracellular lipid accumulations were apparent in stained cryosections over a period of 48h.

Although deregulation of metabolic genes was mainly found within 24h after *L. monocytogenes* injection, the quantity of lipid droplets clearly presents to the largest extent at 48h p.i. This relative delay in biological visibility of expected effects does not surprise since post-transcriptional and translation processes may take up to 6 hours to build the gene product and influence of these products occur with a certain deferment. However, the increasing concentration of lipid droplets over the time course indicates that a transient deregulation of involved genes may be sufficient to mediate a prolonged accumulation of these lipid droplets.

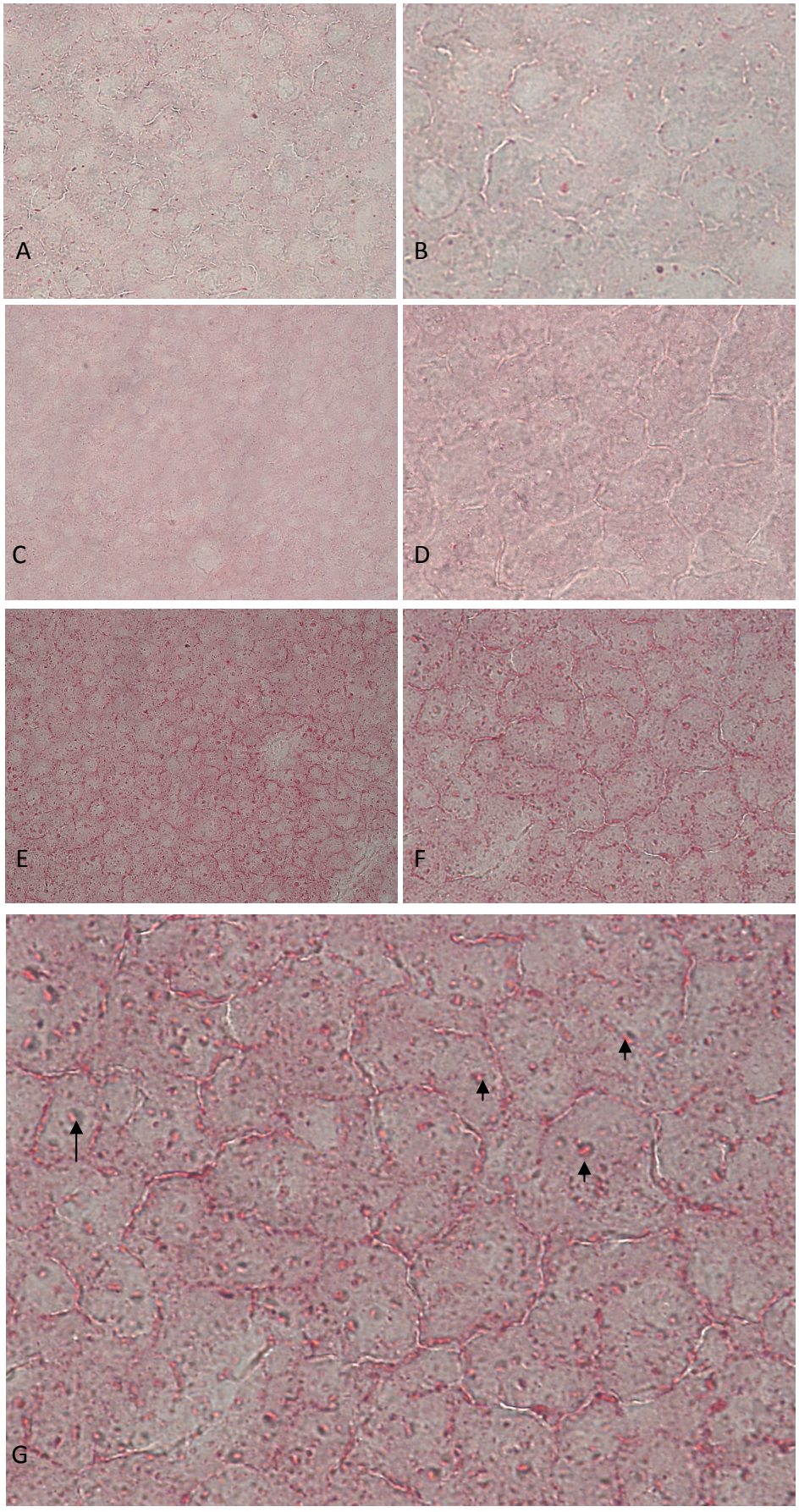
A
B
C
D
E
F
G

Figure 25: Cryosections of livers infected with *Listeria monocytogenes* and stained with Oil Red O. (A) Low power and (B) medium power magnificationof sections of a liver 4h post infection. Few red staining droplets are visible. (C) and (D) demonstrate a liver 24h post infection with increasing levels of lipid droplets. (E) to (G) show the same section in low, moderate and high power magnification field 48h following infection. Staining with Oil red O uncovers the appearance of lipid droplets. As visible, the number of lipid droplets increases from very few at time point 4h p.i.innumerablelipid droplets 48h p.i. (E)-(G). High power magnification (G) confirms the appearance of lipid droplets in all visible hepatocytes on the slide. Arrows indicate stained lipid droplets.

3.2.5 *L. monocytogenes* induces the formation of lipid droplets through an alternative pathway

Formation of lipid droplets depends on enzymes that control the cellular lipid metabolism. Acyl-CoA synthetase (ACSL) and its homologues play a crucial role in the synthesis of fatty acids and cholesterylesters, the main constituents of lipid droplets. Specific inhibition of a subset of ACSLs was shown to disrupt lipid droplet synthesis in a dose-dependent manner [199]. In cultured human hepatoma cells, induction of lipid droplets was achieved by adding long-chain fatty acids, the main substrate of ACLS [200]. A human hepatocellular carcinoma cell line (HepG2) promotes an endogenous storage of lipid droplets [201] mediated by acyl-CoA synthetases [202]. HepG2 cells have been used as a model cell line for the characterization of lipid droplets and the investigation of hepatic steatotic liver disease [203] and obesity [202].
Furthermore, the formation of lipid droplets is associated with several factors and biological processes, including viral infections, oxidative stress and autophagy [204].
Induction of lipid droplets has been observed for intracellular pathogens, such as *Mycobacterium tuberculosis* and *Trypanosoma cruzi* [205]. Although TLR2-dependent pathway activation seems to induce lipid droplet formation during *M. tuberculosis* infection, it is unclear if this involves activation of ACLS. In order to confirm our *in vivo* results and to determine if *L. monocytogenes* induces lipid droplet formation through the classical pathway, we used a HepG2 infection model. Cells were infected

with a MOI:20 and LD immunofluorescence was performed for different time points (Figure 26).

As previously reported, we support the observation of endogenous LD presence in HepG2 cells. There was a distinct accumulation of cytosolic LD in infected cells. The increase in quantity appeared within 1h post infection and was most apparent at 4h p.i., while no differences were seen between control and infected cells at 24hp.i. At this point, however, the impact of endogenous LD synthesis biased the observations found in infected cells. For this reason, we performed a further infection experiment with HepG2 cells that were incubated with Trisacsin C for 9 and 24h, respectively. Endogenous LD synthesis diasappeared entirely when incubated with Triascin C. Incubation with TC resulted in prolonged inhibition of LD that lasted for the whole time period of observation. We found no difference in the potency of TC to inhibit LD formation between cells incubated for 9 or 24h, respectively. Since TC may have cytotoxic effects, we subsequently incubated HepG2 cells for 9 instead of 24h.

Infection of TC preincubated cells resulted in a drastic induction of LD synthesis (Figure 27). Quantity as well as temporal characteristics of LD induction was comparable to non-preincubated cells, indicating, that above described results were independent from the endogenous LD synthesis. These results indicate the endogenous synthesis of LD in HepG2 follow the classical pathway that is inhibited by TC incubation. However, induction of LD synthesis by *L. monocytogenes* is independent from this classical pathway and follows an alternative unknown pathway.

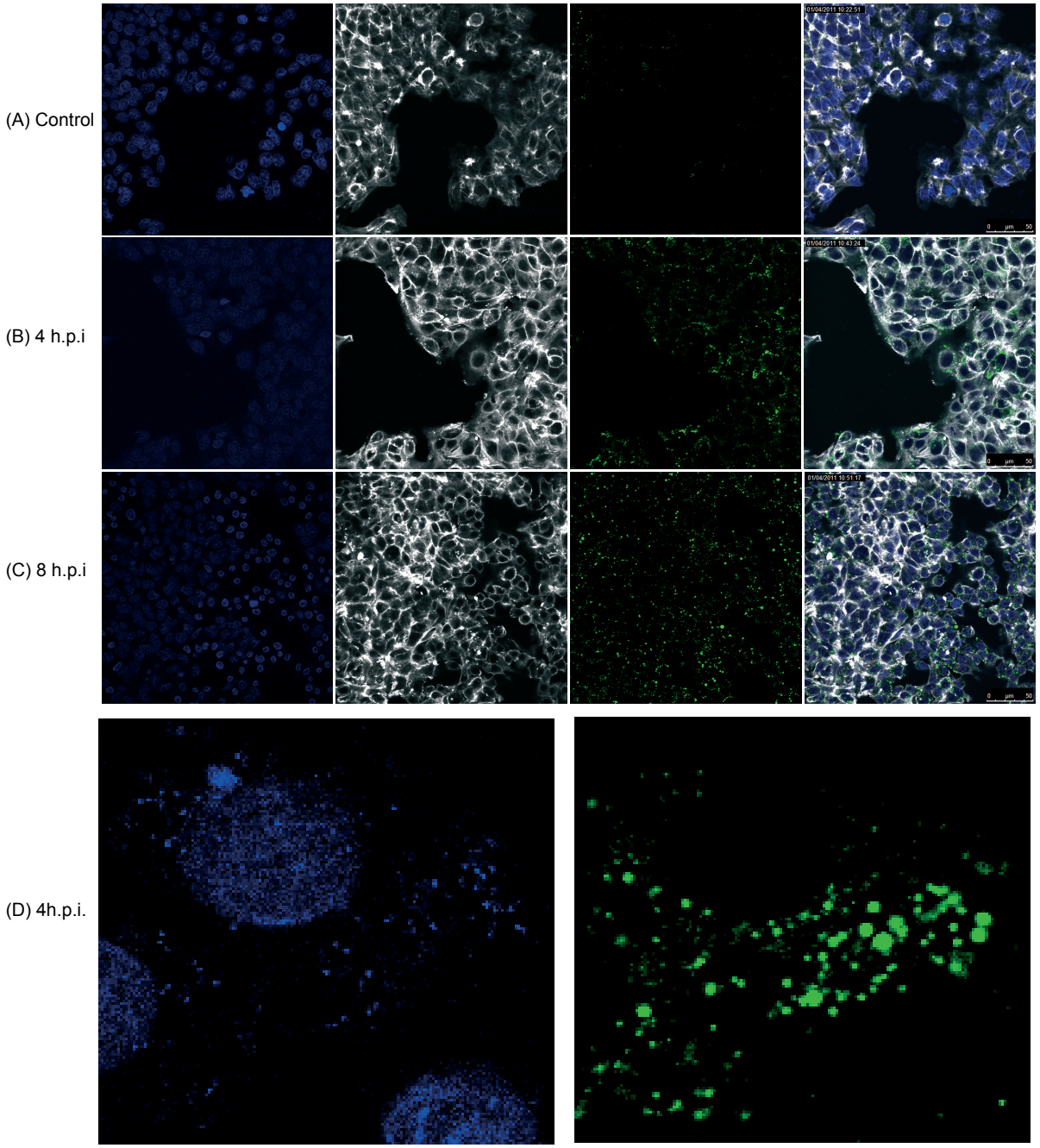

Figure 26: Lipid droplets accumulate within HepG2 cells infected with *L. monocytogenes*. The upper row (A) indicates control cells, middle (B) and lower (C) row show stains of HepG2 cells 4h and 8h following infection, respectively. The first column demonstrates staining of the nuclei with DAPI, second column shows staining of the cytoskeleton with phalloidin, the third column indicates stained lipid droplets and the fourth column is an overlay of each row. Cells were fixed in 4% formaldehyde and stained with the neutral lipid dye BODIPY493/503. The lowest row demonstrates a high power field magnification of the 4h experiment showing stained nuclei and bacteria

(left) and lipid droplets (right). (A) Control cells display a low baseline synthesis of lipid droplets. (B) Accumulation of intracellular neutral lipids 4h and 8h post infection (C). The close up (D) demonstrates a close spatial association of lipid droplets and intracellularly localized bacteria.

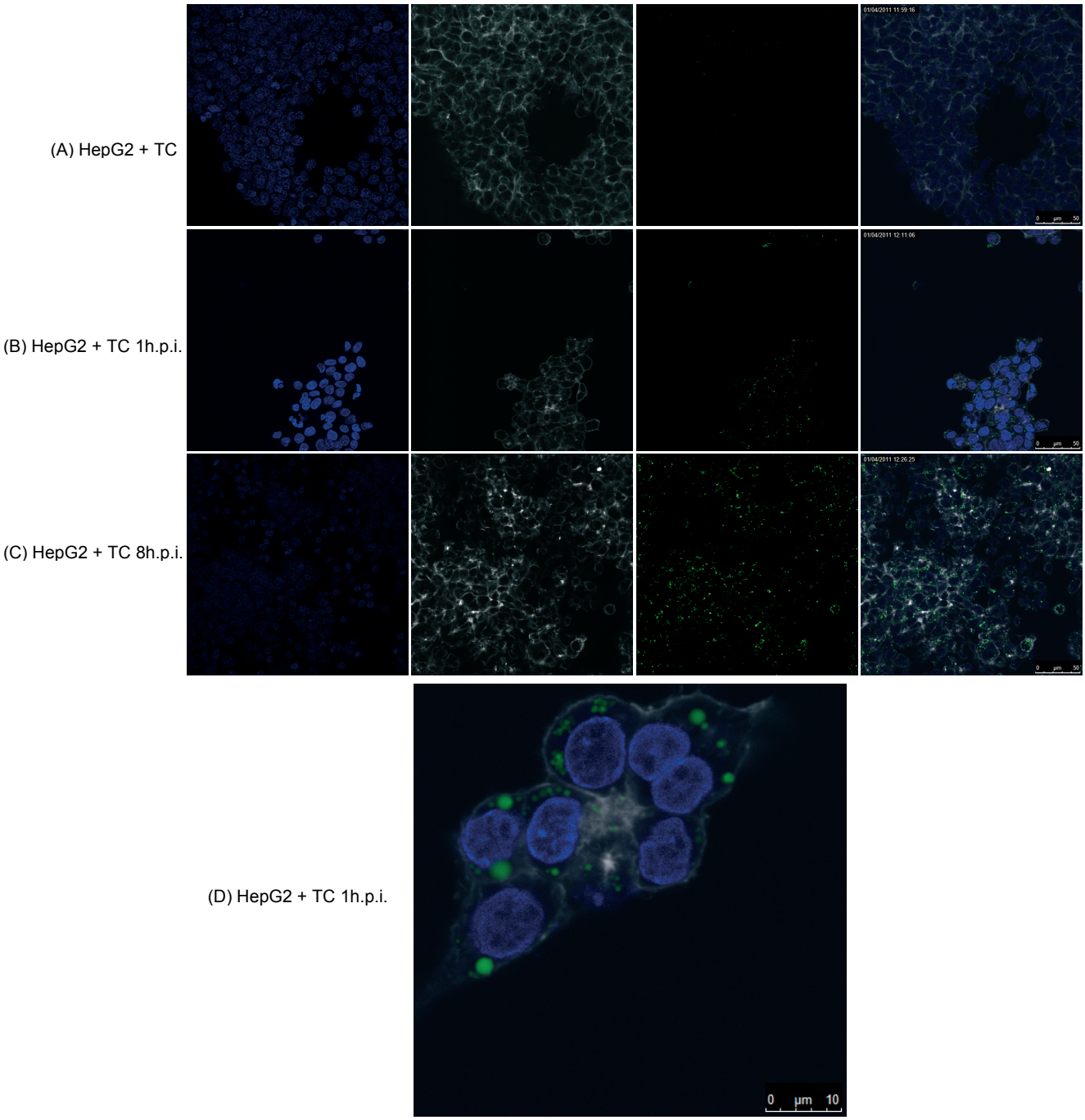

Figure 27: Induction of lipid droplets by *L. monocytogenes* through an alternative pathway. The upper row (A) indicates control cells that were incubated with Triascin C,

middle (B) and lower (C) row show stains of HepG2 cells that were incubated with Triascin C and 4h and 8h following infection, respectively. The first column demonstrates staining of the nuclei with DAPI, second column shows staining of the cytoskeleton with phalloidin, the third column indicates stained lipid droplets and the fourth column is an overlay of each row. (A) Control cells incubated with 5mM Triascin C for 9h show total inability to synthesize lipid droplets through the *classical* pathway. This effected lasted for 24h (not shown). (B) and (C) Triascin C incubated cells that were subsequently infected with *L. monocytogenes* accumulate lipid droplets 1h and 8h post infection, indicating that *Listeria*e induced lipid droplet synthesis through an *alternative* pathway. (D) Higher magnification of HepG2 following prior incubation with Triscin , but able to synthesize intracellular lipid droplets 1h after infection.

3.2.5.1 *L. monocytogenes* induces LXR dependent gene expression mediated by increasing levels of oxysterols

L. monocytogenes is phagocyted by macrophages and dendritic cells and promotes its own endocytosis into non-phagocytotic cells by Internalins. In invaded cells, *L. monocytogenes* prompts lysis of vacuoles due to LLO, the pore-forming listerial toxin [1]. Upon perforation of vacuoles, cholesterol is released into cytosol of infected cells. Also, some of these vacuoles may fuse with lysosomes leading to accumulation of cholesterol, a major product of lysosomal actions. In a previous work, we showed that a single LLO-application induced maintaining upregulation of Cholesterol-25-hydroxylase (CH25H) in bone-marrow derived macrophages [206]. This enzyme mediates the conversion of cholesterol to 25-oxysterol is seen differentially upregulated over several time points. Furthermore, CYP7A1, a LXR – responsive gene, mediates the hydroxylation of free cholesterol to 7-oxysterol [129] is seen significantly upregulated 4h p.i., but in contrast to CH25H expression displays significant downregulation over the time course. This observation may be associated with its function in bile acid homeostasis or altered transcription regulation by LXR. In line with this, CYP2R1, CYP8B1 and CYP7B1, which promote the modification and clearance of 7-oxysterol and 25-oxysterol to bile acid [129, 130]. Subsequently, synthesis and decreased clearance lead to increasing oxysterol concentration within hepatic cells. When occurring in abundance, intracellular oxysterols are bound to oxysterol binding proteins (OSB) or OSB – like (OSBL) proteins. Presumably as a consequence of increasing

oxysterols levels OSBPL5 and OSBPL9 are higher expressed at 4h and 24h p.i., respectively.

Both, 7-oxysterol and 25-oxysterol are known to affect a wide range of biological processes, including inflammatory response in macrophages, cell calcium levels, cell proliferation and differentiation and disruption of migration. Importantly, several of the immune modulatory effects of oxysterols are mediated by binding and activating the liver X receptor alpha (LXR-α) [131, 132]. Two transcription factors, LXR-α and LXR-β, form a subfamily of the nuclear receptor superfamily and are key regulators of macrophage function, controlling transcriptional programs involved in lipid homeostasis and inflammation. The inducible LXR-α is highly expressed in liver, adrenal gland, intestine, adipose tissue, macrophages, lung, and kidney, whereas LXR-β is ubiquitously expressed. Ligand-activated LXRs form heterodimers with retinoid X receptors (RXRs) and regulate expression of target genes containing LXR response elements [133]. Several LXR-α – responsive genes are seen differentially regulated upon infection with *L. monocytogenes* which reflects activation LXR, presumably mediated by accumulating oxysterols. In 1996, Janowski et al. first reported that oxysterols, including 7-oxysterol and 25-oxysterol, activate transcription via the LXR [132]. Using DNA microarrays further studies showed that LXR activation with the synthetic agonist GW3965 leads to inhibition of genes that are involved in immune response and survival in mouse macrophages. Subsequent investigations revealed that LXR antagonizes NFkB transcription, which is crucial for promoting inflammation in response to bacteria [134]. Consistent with these observations, Crestani et al. found reciprocal interference between LXR and the NF-kB pathways by transient transfection assays with NF-kB- and LXR-driven reporter genes [131].

3.2.5.2 LXR responsive genes involved in immune response or apoptosis are distinctly regulated from the genes of metabolism

The expression pattern of genes that are dependent on LXR induction showed a biphasic response and can be divided into three groups: (1) LXR responsive genes of metabolism (CD36, CYP7A1, CYP39A1, SREBF1, S14, TGM2, GLK, GLUT4) that were seen highly expressed during the early phase of infection, but downregulated or expressed to reduced extend during the later phase of infection with the exception of ABCG1, which is seen higher expressed; (2) LXR responsive genes involved in lipid metabolism that

are not differentially regulated early but downregulated during the latter phase of infection (ABCG5, ABCG8, ACSL1) and (3) genes involved in apoptosis and/or immune response, (SP-α, CCL24, TRIM34, CCL5, CCL7, CD80, TLR4, IL12B) which are seen low expressed during the early and heavily upregulated in the later phase of infection. Thus, LXR - responsive genes of lipid homeostasis display a reciprocal regulation compared to genes involved in immune response.

3.2.5.3 Role of LXR – regulated genes

SP-α, CCL24, CCL5, CCL7, IL12B, and TRIM34 are LXR responsive genes in macrophages. SP-α, also known as apoptosis-inhibitor, was shown to protect macrophages from apoptosis upon *in vitro* infection with *L. monocytogenes* [135]. CCL24 induces recruitment of eosinophils, basophils, neutrophils, and macrophages to the site of infection and thereby is involved in effective clearance of *L. monocytogenes* [136]. TRIM34 contains the TRIM motif that includes three zinc-binding domains, a RING, a B-box type 1 and a B-box type 2, and a coiled-coil region. Expression of this gene is up-regulated by interferon, indicating its involvement in immune response. [135]. Several chemotactic cytokines as well as cytokine receptors are under direct or indirect control of LXR. Among these, IL12B, CCL24, CCL5 and CCL7 are seen upregulated in the late phase of infection. CD80, TLR4 and TRIM34have important roles in pathogen recognition, initiation of cell mediated immunity and Interferon-γ response.

Furthermore, CYP39A1, a gene involved in the bile acid homeostasis is seen upregulated 4h p.i. but is seen lower expressed during the later phase of infection. SREBF1 (also known as SREBP-1c) is the best characterized and investigated LXR – responsive gene involved in biological pathways, including lipid metabolism and insulin signaling [137]. SREBF1 was also implicated in the execution of an apoptosis program that appears early in apoptotic cells [138]. Another study investigating HIV infection revealed higher expression of SREBF1 in apoptotic cells and involved in foam cell formation in macrophages. Thus, apart from its role in regulating lipid metabolism, SREBF1 upregulation induces a pro-survival signal. In concert, the upregulation of GLK [139] and GLUT4 [140] lead to a higher transmembranous uptake of glucose from blood and accumulation within liver cells. S14 stimulates aberrant hepatic de novo lipid synthesis and was identified as potential factor in the development of fatty lliver disease

and insulin resistance [141]. Members of the ATP-binding cassette (ABC) family represent a group of membrane spanning transporters. ABCG1, ABCG5 and ABCG8 are important for the efflux of intracellular sterols and cholesterol; ACSL1, a member of the acyl CoA synthetase family displays a very similar expression pattern. In contrast, ABCG1 is seen strongly upregulated during the late phase. ABCG1 was shown to be induced by oxysterols, especially by 25 – oxysterols [142]. A more recent study revealed that ABCG1 enhances efflux of 7-oxysterol and related oxysterols from macrophages and thus protect macrophages from oxysterol-induced apoptosis [143].

3.2.5.4 Posttranslational modification of LXR potentially controls the gene expression panel of LXR responsive genes

Posttranslational modifications, such as SUMOylation [144] or phosphorylation [145] alter the gene subset that is transcribed by LXR. Recent studies revealed that phosphorylation of LXR-α selectively regulates the expression of and CCL24 [107, 145, 146] and SREBF1, which is transcribed to lower extent when LXR is phosphorylated [107, 146]. Thus, modification may be responsible for a distinct panel of genes regulated by LXR. Two kinases, PKA/PKC and ALK-1 were also shown to phosphorylate LXR [146, 147]. ALK-1 was originally found to be a cell-surface receptor for the TGF-beta superfamily of ligands. In this study, PKA/PKC and ALK-1 are seen differentially upregulated during the late phase of infection and could contribute in a distinct gene regulation by LXR.

3.2.5.5 LXR-α accumulates in the nucleus in an *in vitro* infection model with *L. monocytogenes*

Transcriptional response to *L. monocytogenes* strongly indicates an important role of LXR in the host response. Previous work has revealed that LXR dependent gene regulation is important apoptosis control in macrophages infected with *L. monocytogenes* [135]. A recent study revealed increased protection of LXR deficient mice against *Leishmania* [148] indicating the importance of LXR in response to intracellular pathogen. To support the *in vivo* observations of LXR dependent gene regulation in *Listeria* infection we further characterized the localization of LXR in HuH-7 cells at several time points. HuH-7 is mammalian hepatic cell line that has been

broadly used to investigate metabolic liver diseases, infections and in cancer research. These cells preferentially express LXR-α over LXR-β [149].

Immunofluorescence indicates an alteration of the subcellular localization of LXR-α in response to *L. monocytogenes* (Figure 28). While the cytoplasmic fraction of LXR-α dominates early upon inoculation with *L. monocytogenes*, translocation of LXR-α into the nucleus occurs resulting in a strong nuclear fluorescence signal. Thereby, the ratio of nuclear: cytoplasmic fraction increases during the observation, indicating a dynamic change of LXR-α location upon *Listeria* challenge.

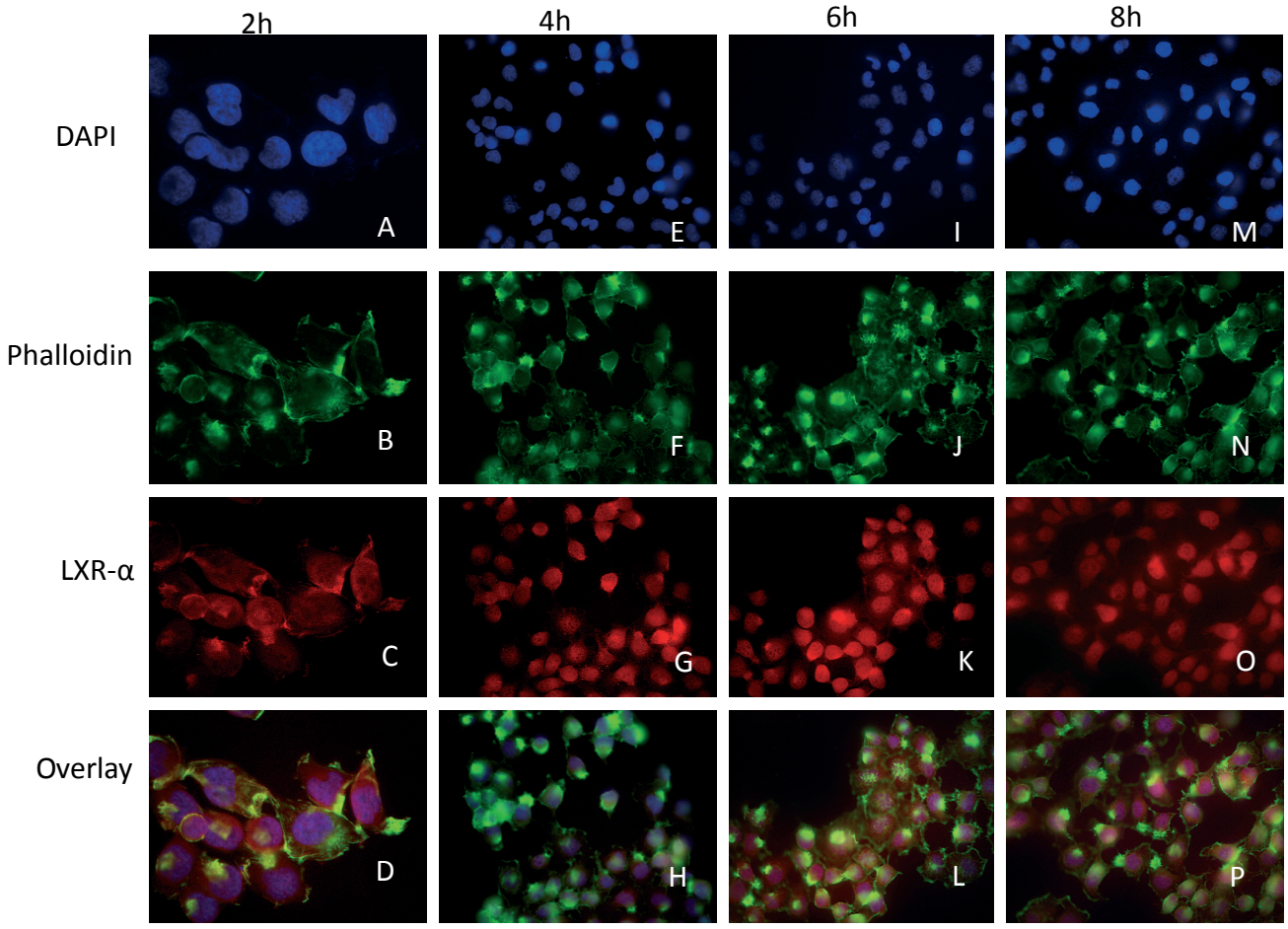

Figure 28: Subcellular localization of LXR-αin HuH-7 cells following infection with *L. monocytogenes*. Cytoplasmic localization of LXR-α is seen at 4h p.i. The nuclear intensity of LXR-α increases over the course of the infection.

3.2.5.6 Dynamic delocalization of LXR that is phosphorylated at S198

Phosphorylation of LXR controls its transcription activity, but may also lead to its delocalization from the nucleus to the cytoplasmic compartment [147]. Although, this was initially shown for LXR-β, further studies revealed the potential importance of nucleo-cytoplasmic trafficking of nuclear receptors, including LXR-α [150]. However, another study, indicating that phosphorylation of LXR-α is present under basal conditions could not identify changes in localization of modified LXR. However, the phosphorylation of LXR-α abrogates its function as repressor of proinflammatory genes, such as CCL24 [145]. Other modifications, such as ligand-induced SUMOylation of LXR-α was also shown to prevent the removal of proinflammatory complexes, such as NCoR [151, 152]. Thus, posttranscriptional modification of LXR-α is suggested to be a way to alter the expression of its gene repertoire.

We used an antibody that specifically binds to phosphorylated LXR-α, but not to its dephosphorylated form (created and provided to us by Dr. MJ Garabedian, Department of Microbiology and Urology, New York School of Medicine; also see [145]). Immunofluorescence indicates that phosphorylated LXR-α (LXR-αP) is present under basal conditions and is located adjacent to the nucleus (Figure 29). At the first observation point, barely any LXR-αP is visible within the nucleus or cytoplasm. Fluorescent intensity within the nucleus increases at 6h p.i. and is seen within as well as adjacent to the nucleus 8h p.i.

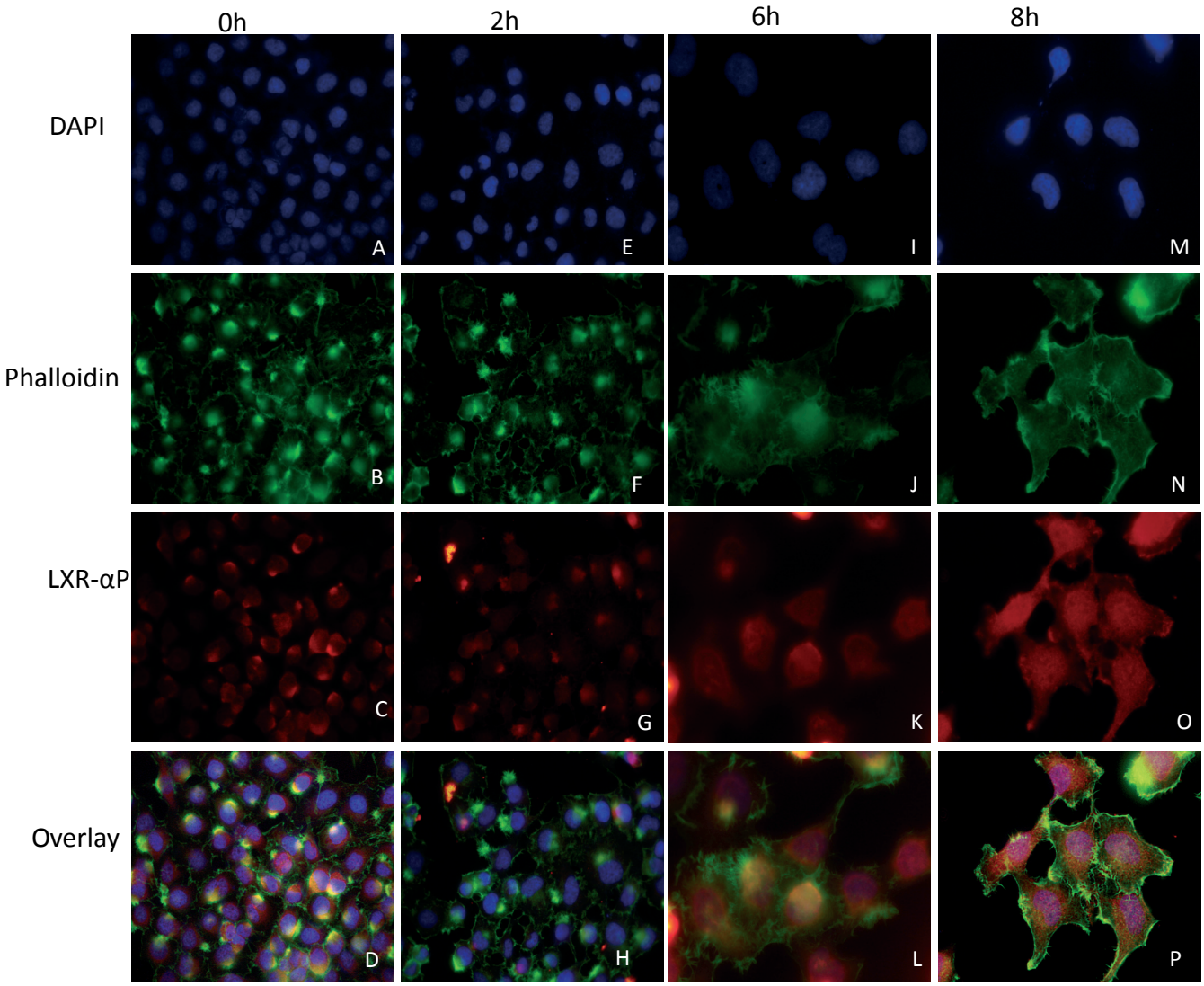

Figure 29: Subcellular of LXR-α that is phosphorylated at S198 (LXR-αP). Under basal conditions, LXR-αP is seen adjacent to the nuclei of HuH-7 cells. This perinuclear "cap" appears to exist on one pole of the nucles. At 2h p.i. no perinuclear LXR-αP is identified, while increased LXR-αP intensity is visible within the nucleusat 4h and 8h p.i., respectively. Interestingly, perinuclear LXR-αPseems to rebuild at 8h p.i. and is present in both, the cytoplasmic and nuclear compartment. These observations demonstrate a dynamic change of LXR-αP localization upon infection with *L. monocytogenes*.

This indicates that LXR-αP undergoes a dynamic delocalization upon infection with *L. monocytogenes* and a possible role of LXR-α and LXR-αP in the observed deregulation of genes of lipid metabolism and immune response.

Although it has been reported that LXR-α reciprocally regulates inflammation and lipid metabolism [134], the underlying mechanism has not been identified. We propose a potential role of phosphorylation at S198 in this inverse gene regulation. Furthermore, *L. monocytogenes* possibly induces this pathway to improve its own survival within the host cell in order to escape from the early inflammatory response in the liver (Figure 30).

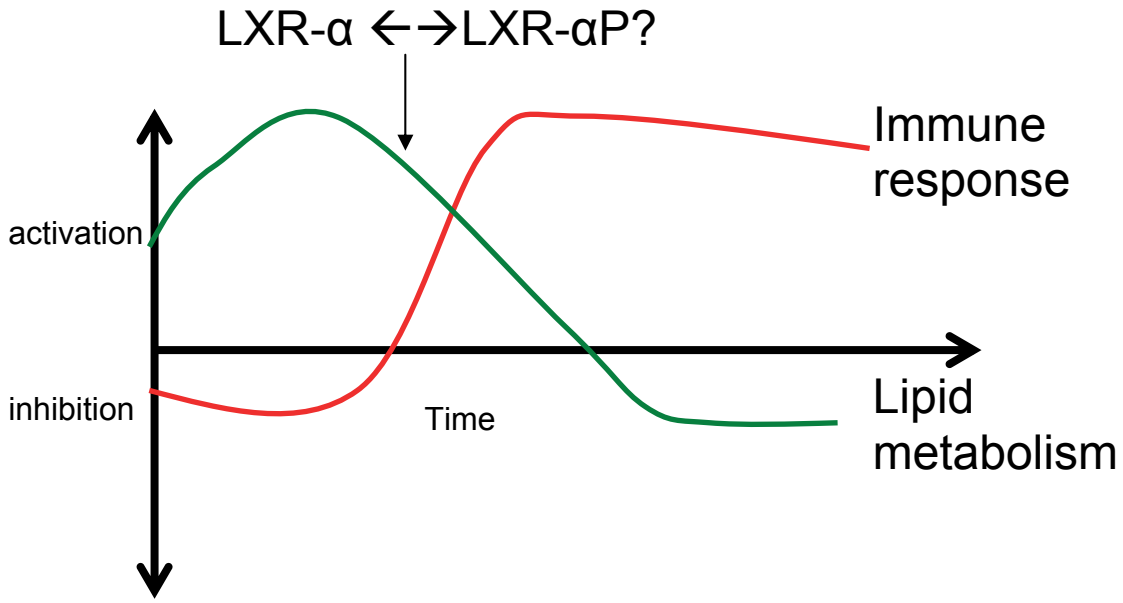

Figure 30: Based on the results described above, we hypothesized that transcriptional changes observed in this global view may be associated with transcriptional regulation of LXR-α and its modified forms, such as LXR-αP. The X-axis indicates the time after infection, Y-axis indicates the directionality of expression of genes in the biologic categories "immune response" and "lipid metabolism", while the area above the X-axis indicates upregulation and below the X-axis indicates downregulation of genes in the particular category.

3.2.6 Infection with *L. monocytogenes* leads to altered serum lipid profile and transiently impaired liver function

The liver is the most important organ in the regulation of serum lipid parameters. To elucidate the liver function and possible changes in we obtained a serum cholesterol and triglycerides as well as liver function parameters (GOT, GPT, CHE) from three control mice and three infected mice for each observation points 4h, 1d, 2d and 3d upon RESULTSinfection with *L. monocytogenes*.

Protein synthesis function in the liver was clearly impaired at the first observation point reflected by a significantly decreased activity ($p < 0.05$) of CHE. CHE levels are within normal range after this period and even higher at 3d p.i. Furthermore, triglyceride levels were significantly ($p<0.05$) altered at two observations. A decay of serum TAG levels is seen 4h p.i., which is consistent with the intracellular accumulation of TAGs starting in this phase of infection. A strong increase is seen at day 1 p.i. before normal ranges of TAG levels are seen in the later phase of observation (Figure 31). No changes in serum levels were observed for GPT, GOT or cholesterol (Table S2, appendix).

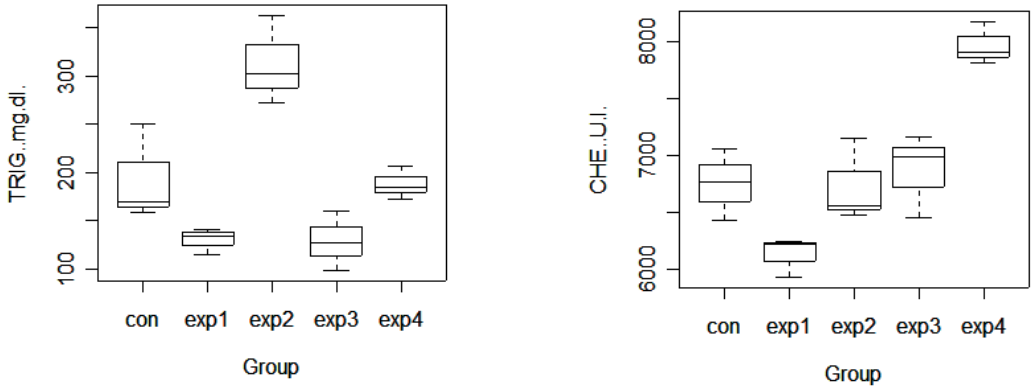

Figure 31: Changes of serum TAGs in mg/dl (left) and cholinesterase (CHE) in U.I. (right) are shown for control mice and at different time points following infection. Exp1 summarizes values for mice 4h p.i, exp2 24h p.i., exp3 2d p.i. and exp4 3d p.i. There is significant decrease in serum levels of TAGs 4h p.i. followed by and transient increase and normalization over at the last observation point. Early decrease of TAGs was associated with increased expression of genes that promote translocation of TAGs from the blood into cells as well as upregulation of enzymes that promote synthesis of fatty acids and inhibit their degradation. CHE represents a global marker that surrogates the synthetic function of the liver. The CHE level was markedly decreased at the initial observation point post infection, indicating an decreased liver function at this time point. While CHE levels return to a baseline level thereafter, we observed an significantly elevated CHE serum level 3d p.i indicating a “hyperactive” liver function at this point.

3.2.7 Innate immune response by interacting Kupffer cells and neutrophils by Calgranulins

The ability of T cell depleted mice to counteract *L. monocytogenes* during the first days after infection reveals the importance of innate defense mechanisms [153]. Kupffer cells are important for trapping *L. monocytogenes* in the liver, but do not show intrinsic antibacterial or phagocytic activity. Clearance of *L. monocytogenes* by Kupffer cells was suggested to be due to interactions with pathogen surface sugar and lectin residues by binding the pathogen by unknown receptors. Because they physically interact with neutrophils it was further suggested that neutrophils are involved in killing of trapped bacteria [49].

Microarray data revealed that intercellular adhesion molecules necessary for neutrophil-Kupffer interaction ICAM-1, MAC-1 and the C-type lectin receptors CLEC1A, CLEC1B, CLEC2D and CLEC9A are seen differentially upregulated upon *L. monocytogenes* infection in liver. A recent study revealed that CLEC9A is expressed on the surface of immune cells, including macrophages [154]. Among others CLECs, it was shown that CLEC9A binds to lectins and induces an intracellular cascade resulting in local inflammation and chemotaxis of neutrophils [155] (Figure 32).

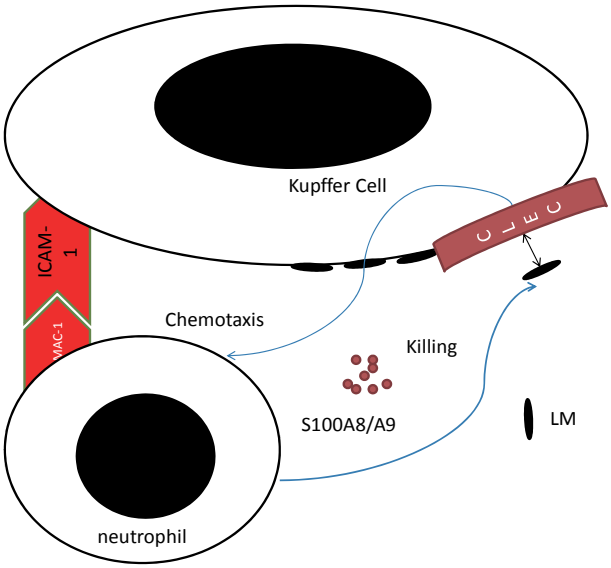

Figure 32: Among other effector peptides like CRAMP or defensins, further anti-microbial peptides were shown to be effective against extracellular localized bacteria including calgranulins S100A8 and S100A9. S100A8/A9 form extracellular complexes

and display cytostatic and bactericidal activity against bacteria trapped on the surface of Kupffer cells. Also, they are potent chemotactic agents for leukocytes [156]. Both, S100A8 and S100A9 are seen upregulated upon infection with *L. monocytogenes* with a peaking fold change 2d p.i. As we reported previously, S100 proteins are a potent target to aim for *Listeria monocytogenes* to impair antibacterial activity of host cells (Izar B, Hossain H, Chakraborty T. The organ specific host response upon challange with *Listeria monocytogenes*. November 2007. 5th Nationales Genom Forschugsnetz (NGFN) Symposium; Heidelberg, Germany).

3.2.8 *L. monocytogenes* modulates the early innate response by inhibition of antimicrobial peptides

Antimicrobial peptides play an important role in the innate immune response against Gram-positive and –negative bacteria. Cathelecidin-related antimicrobial peptide (CRAMP) and its human orthologue LL-37 were shown to possess potent ability to kill bacteria *in vitro* and *in vivo and* exhibit chemotactic effects [157, 158]. A recent study revealed that expression of murine CRAMP inhibits the intracellular proliferation of *Salmonella typhimurium* [159]. The defensin family consists of oligonucleotide peptides implicated in innate response in different tissues and cells, including macrophages. In mammals, defensins have evolved to have a central function in the host defense properties of granulocytic leukocytes, mucosal surfaces, skin and other epithelia [160]. Although most effects were shown for human defensins, mouse defensins share high homology and it was shown that antimicrobial activity against bacteria by defensins from different species occurred to similar extent [161, 162]. However, in contrast to CRAMP these results are based on *in vitro* experiments.

To our knowledge, this is the first report of defensin deregulation by *L. monocytogenes in vivo*. Interestingly, DEF23A is seen downregulated at the earliest observation points. DEF7 and DEF37 are seen differentially upregulated during the following phase of infection, while mRNA levels of DEF29 are clearly increased at all observations. Gene expression of CRAMP is significantly inhibited during the early period, but strongly induced during the later phase of infection. This expression pattern was also confirmed by qRT-PCR (Figure 33).

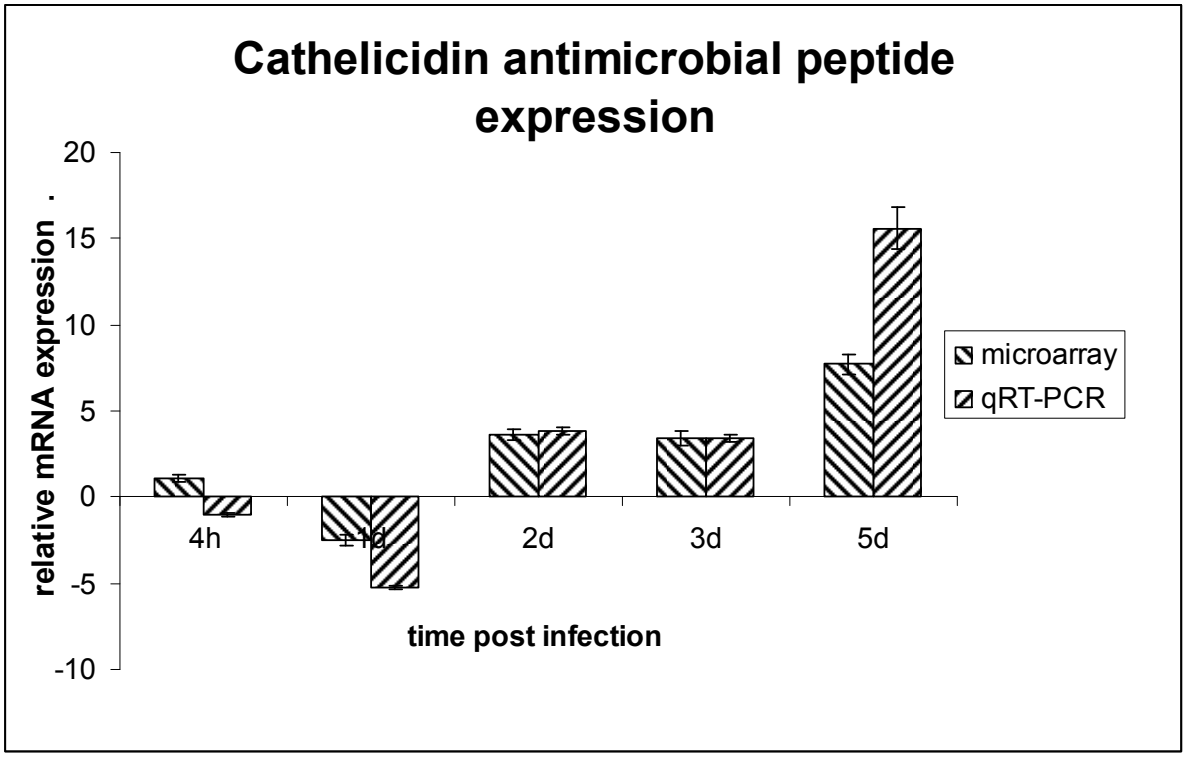

Figure 33: Relative mRNA levels of CRAMP obtained by microarray and validated by qRT-PCR. Decreased levels of CRAMP, a potent antimicrobial peptide contributes to improved survival of *L. monocytogenes*.

3.2.9 Intersection of classical and non-classical MHC-Ib antigen presentation pathways following listerial infection

Antigen presentation by major histocompatibility (MHC) class I and class II is the crucial step in cognation of CD8+ and CD4+ positive T lymphocytes, respectively and thereby links innate and adaptive immunity. Development of a long-term T cell system is dependent on MHC-Ia presentation, whereas MHC-Ib restricted T cells display more rapid responders to stimuli, including infections with *Mycobacterium tuberculosis* and *Salmonella enterica* [163] [164]. Microarray data analysis revealed strong induction of MHC-class Ib molecules in the liver following infection with *L. monocytogenes* (Figure 34).

These molecules are associated with N-formylated methionine (*f-peptides*) that are released by *L. monocytogenes* and presented on the cell as well as proteins degraded by the immunoproteasome [165]. With the exception of H2-T22 and H2-T23 these

peptides are not delivered by the proteasome. Consistent with this observation, *in vivo* studies showed that H2-M3 restricted T cells proliferation occurs 24h p.i. and peak at day 5d p.i.[166]. However, this is the first study to show the temporal expression profile of the MHC-Ib gene subset upon listerial infection. Several *f-peptides* are recognized to be presented by the MHC – class Ib molecule H2-M3, including FR38 (f-MIVIL) Lem 1-7 (f-MIVIL) and Attm 1-6 (f-MIVTLF) [167, 168]. Furthermore, we reveal strong upregulation of H2-M3 related MHC molecules, including, H2-M1 and H2-M9 that share high similarity with H2-M3; however, ligands and exact function are unknown.

3.2.9.1 Induction of H2-M3 independent MHC-Ib antigen presentation

In addition to the classical H2-M3 family, members of the non-classical MHC-Ib pathway, including H2-T and –Q family are upregulated. H2-T proteins are expressed on the surface of hepatocytes and cytotoxic cells were shown to induce apoptosis through antigens bound to these MHC-Ib molecules. Furthermore, H2-T22/T23 bound peptides are also recognized by NK-cell receptor NKG2B which is seen upregulated, indicating involvement of NK-cell mediated killing of intracellular *L. monocytogenes* [169-171].

Two further MHC-class Ib molecules, H2-QA2 and H2-Q8 are seen higher expressed. H2-QA2 is known to bind short peptides similar to H2-M3 [172] and stimulate unknown NK-cell receptors. Recent investigations show, that H2-QA2 expressing tumor cells were efficiently killed by CTLs [173] and in addition, H2-QA2 presented antigens were involved in promoting protective immunity [174].

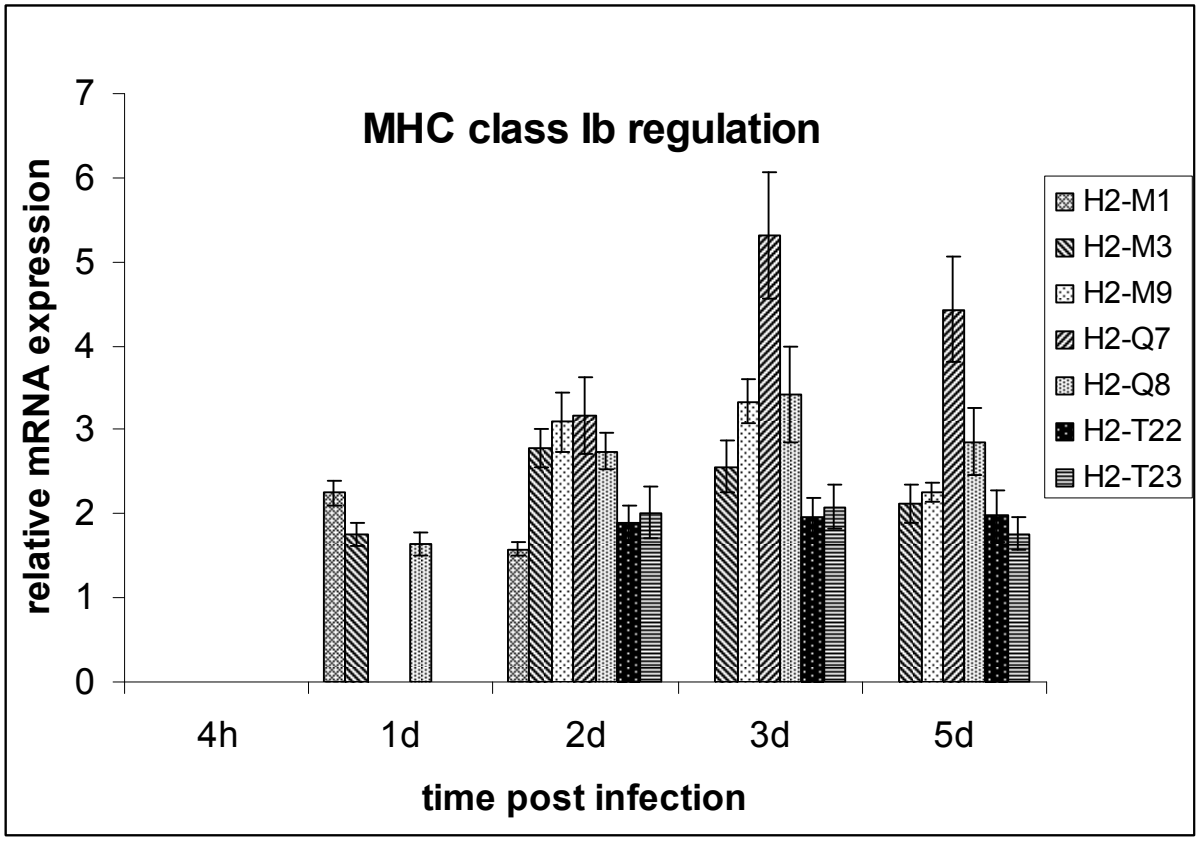

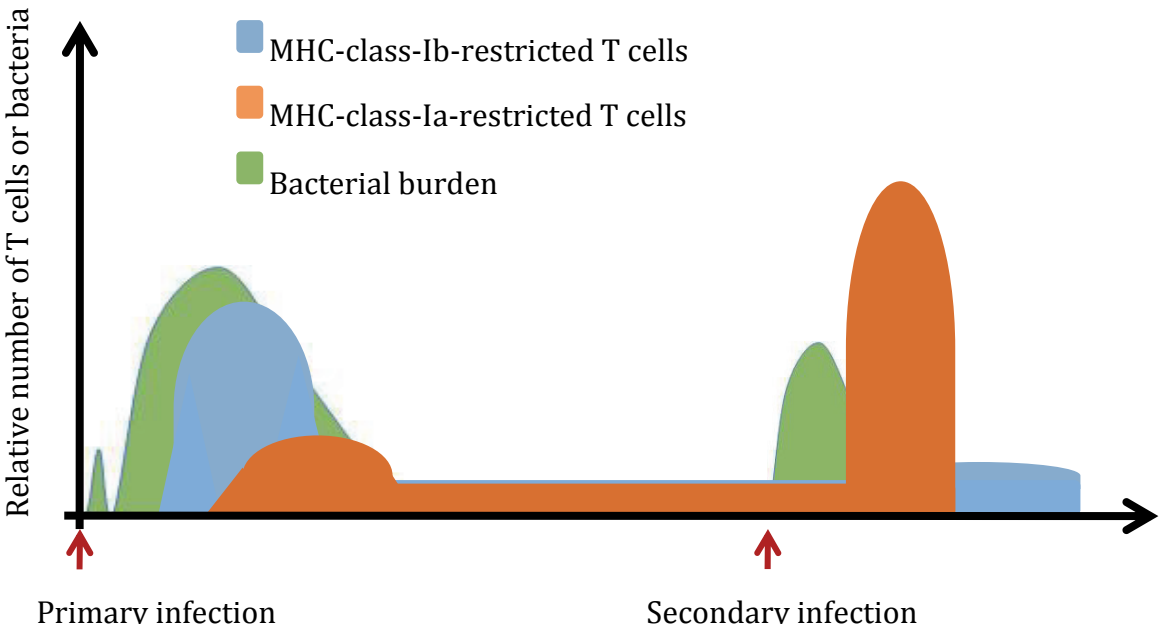

Figure 34: (Upper graph) Relative mRNA levels for MHC-Ib associated HLA genes and time dependent distribution of MHC-class-Ia and MHC-class-Ib restricted T cells during primary and secondary infection with *L. monocytogenes* (lower illustration). A significant number of MHC-Ib genes are significantly upregulated. The majority of

these genes is markedly upregulated by 2 days after infection, which is consistent with prior observations of MHC-class-Ib-restricted T cell dependent activity. This graph also demonstrates that classical and non-classical MHC-Ib gene deregulation intersects in a global view. This concordant regulation is likely linked to presentation of cytosolic pathogen peptides as well as proteins degraded by the immunoproteasome (see below). While proliferating Class-Ib restricted T cells clear the pathogen during the primary infection primary infection, these genes play a minor role during secondary infection. Class-Ia-restricted T cells mediated the elimination of *L. monocytogenes* during secondary infection.

3.2.9.2 Induction of the immunoproteasome and potential role for p60 in the activation of NK cells

While MHC-Ib restricted T cells are mainly responsible for rapid killing of bacteria during primary infection, MHC-Ia restricted cells contribute to protective long-term immunity. Class Ia associated peptides are dependent on cleavage by the proteasome. The peptides are then pumped into the ER by TAP1/TAP2 and associated with the MHC-Ia, such as H2-K1, which is seen significantly upregulated **(Figure 35 and 36)**. As mentioned before the proteasome is critically involved in the production of MHC class I-restricted T cell epitopes. As part of the MHC class I pathway the immune system has developed the ability to modify proteasome activity in inflammatory sites through the cytokine-mediated induction and replacement of proteasome active site subunits consisting of LMP-7, MECL-1 and LMP2 forming the immunoproteasome that degrades exogenous proteins [174, 175]. MECL1 and LMP7 are seen upregulated upon listerial infection in liver, indicating an effective change from proteasome to immunoproteasome and cleavage of listerial proteins, such as LLO or p60.

In line with these result, effector proteins secreted by cytotoxic T cells, including perforin 1, granzyme a and granzyme b, that act in concert in the pathogen elimination are seen highly expressed during the late phase of infection from day 2 to 5.

A recent study by Humann et al. found a depence of NK cell response to p60. However, since direct application of p60 did not provoke NK cell activation, an indirect way was proposed by the authors. Here we present a potential role of H2-K1 – mediated antigen presentation in NK cell activation. It is known that p60 is secreted into the cytosol and processed by the immunoproteasome. Furthermore, H2-K1 was identified as MHC

protein that binds processed p60 fragments. Thus, presentation of p60 peptides by MHC-H2-K1 could be the link for this observation, since H2-K1 associated p60 – antigen is presented to T cells as well as to NK – cell receptors, which are seen higher expressed in this study [176, 177].

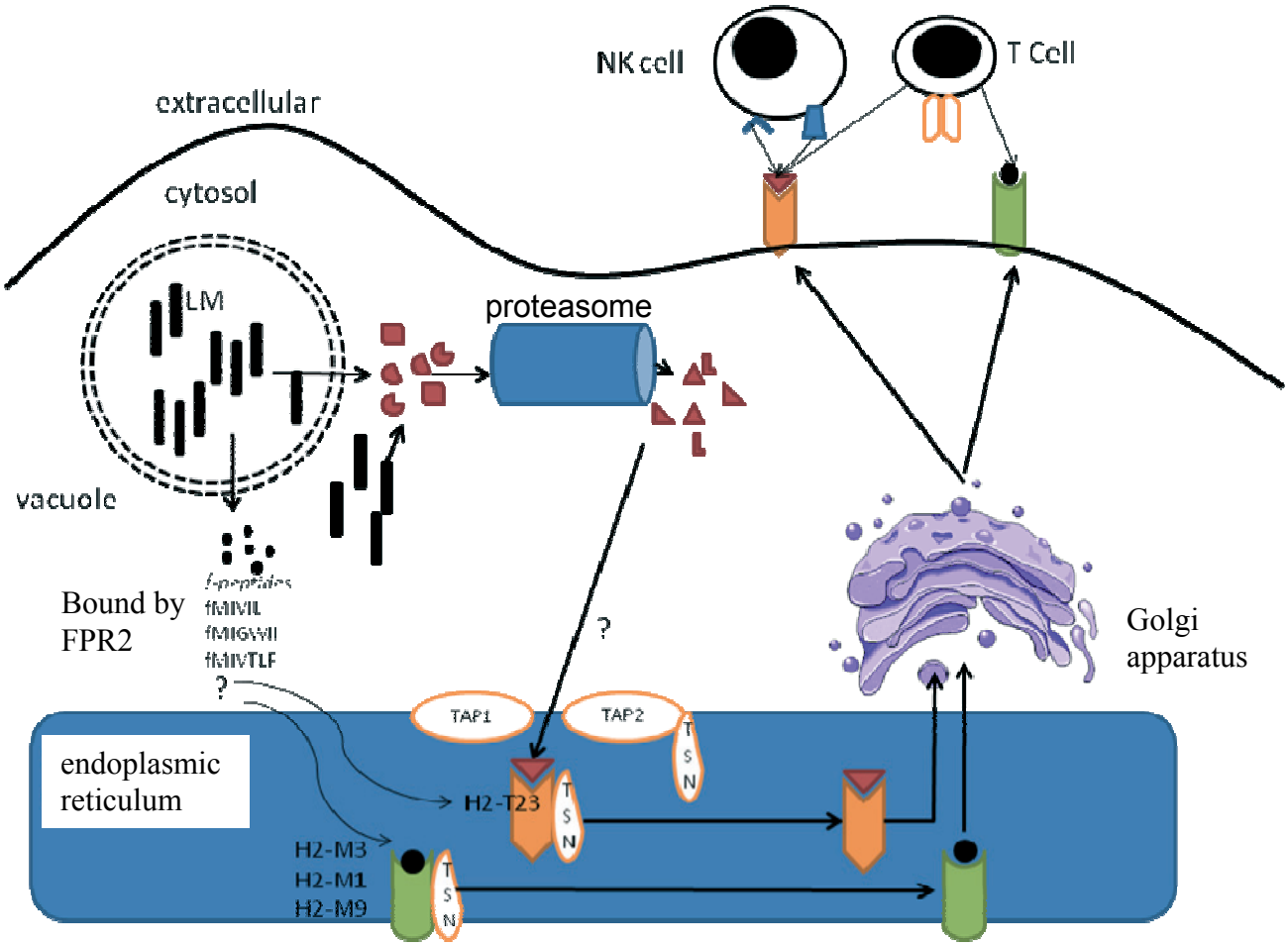

Figure 35: Several genes that are involved in the classical MHC-Ib pathway are activated during infection with *L. monocytogenes*. N-formylated methionine peptides (*f-peptides*) are secreted into the cytosol by *Listeria* and recognized by the FPR2. Once transported into the endoplasmic reticulum, H2-M3 and other classical MHC-Ib molecules (here H2-M1 and H2-M9) are loaded with *f-peptides* and associated to TSN, before TSN dissociates from the loaded MHC molecule which is then relocated to the cell surface through the Golgi apparatus. The loaded antigens are presented to T cells. Through a different pathway, cytosolic LM secrete virulence factors that are processed by the proteasome and through an TAP1/TAP2 dependent mechanism loaded to H2-T23, which similar to classical MHC-Ib molecules is initially associated to TSN before

directed to the cell surface through the Golgi apparatus. Antigens bound by this MHC-Ib molecule are presented to NK cells as well as to T cells. NK cells bind to these antigens via different receptors, that are seen upregulated as well. Both pathways represent a cell mediated immunity pathway that lead to cell mediated defence against *L. monocytogens*. (Abbreviations: LM = *L. monocytogenes,* FPR2 = formyl peptide receptor 2, *f-peptides* = N-formylated peptides, NK cell = natural killer cell, TAP1 = transporter 1, ATP-binding cassette, sub-family B (MDR/TAP), TAP2 = transporter 2, ATP-binding cassette, sub-family B (MDR/TAP), TSN = tapasin).

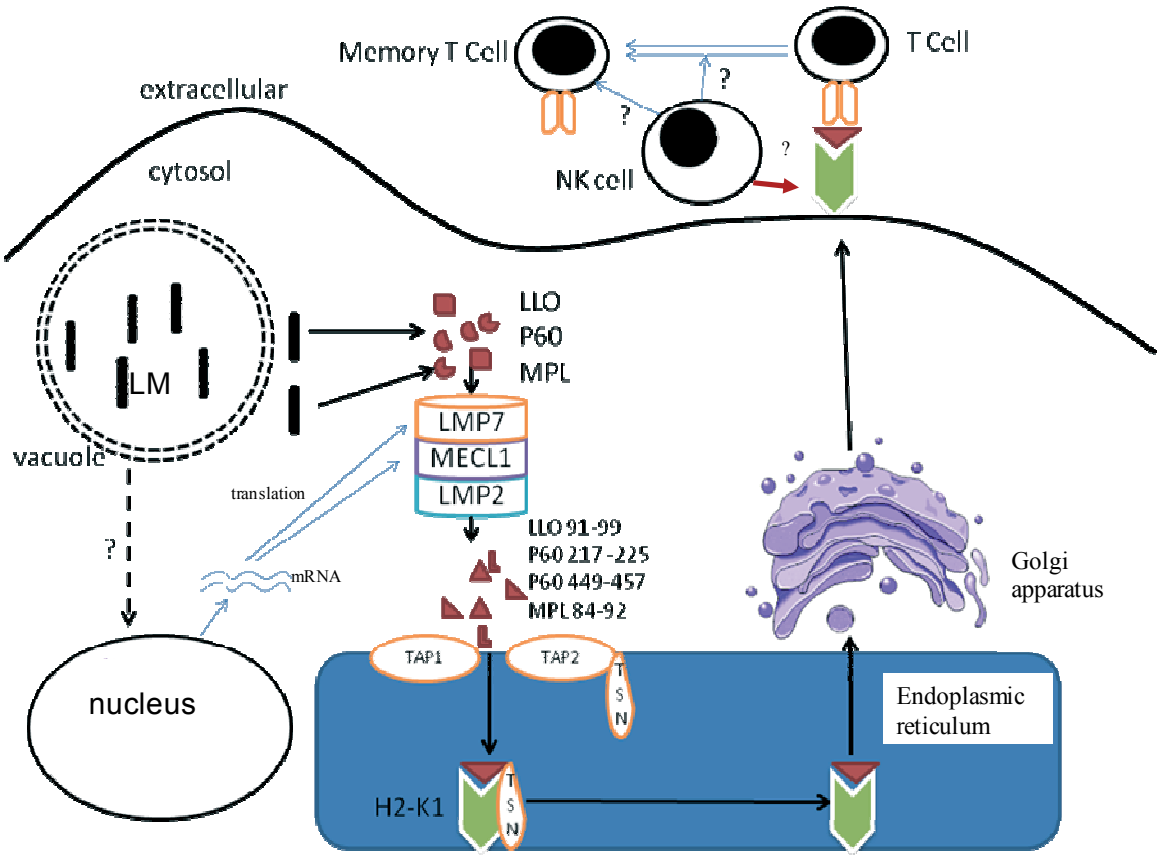

Figure 36: Several genes that are essential for the activation of the non – classical MHC-Ib pathway are upregulated following infection with *L. monocytenges*. This figure demonstrates a potential mechanism of antigen derivation from secreted listerial virulence factors. The pathogen escapes from the vacuole by secreting LLO and secretes further virulence factors, including MPL and p60. Through an unknown mechanism, *Listeria* leads to induction of the subunits of the immunoproteasome, which assembles

in the cytosol to a functional unit. These subunits are seen upregulated on transcriptional level. Secreted virulence factors are processed to short (known) antigens that are 8 amino acids in length. These include LLO 91-99, p60 217-225, p60 339-457 and MPL 84-92. Through TAP1/TAP2 and TSN dependent processing, the non-classical MHC-Ib molecule H2-K1 is loaded with these antigens before TSN dissociates from H2-K1, which is then directed to the cell surface. H2-K1 associated antigens are presented to T cell, which then mature to memory T cells. In addition, these antigens are also presented to NK cells. Derived peptides are bound to H2-K1 and presented to T cells and possibly to NK cells. (Abbreviations: LM = *L. monocytogenes,* LLO = listeriolysin, p60 = protein 60 (product of the *iap* gene), mpl = metalloprotease, LMP7 = proteasome (prosome, macropain) subunit, beta type 8 (large multifunctional peptidase 7), LMP2 = proteasome (prosome, macropain) subunit, beta type 9 (large multifunctional peptidase 2), MECL1 = proteasome (prosome, macropain) subunit, beta type 10 NK cell = natural killer cell, TAP1 = transporter 1, ATP- binding cassette, sub-family B (MDR/TAP), TAP2 = transporter 2, ATP-binding cassette, sub-family B (MDR/TAP), TSN = tapasin).

3.2.10 Validation of microarrays by qRT-PCR

Primer specificity was determined by electrophoresis of each primer pair and revealed that no unspecific DNA products were present with any of the used primers (Figure S1, appendix). We validated relative gene expression of 10 representative genes discussed in this study. The horizontal axis reflects relative expression levels obtained by microarrays and the vertical axis shows correlating fold changes determined by qRT-PCR. Pearson's correlation coefficient (R^2) is given for each graph representing one observation point (Figure 37).

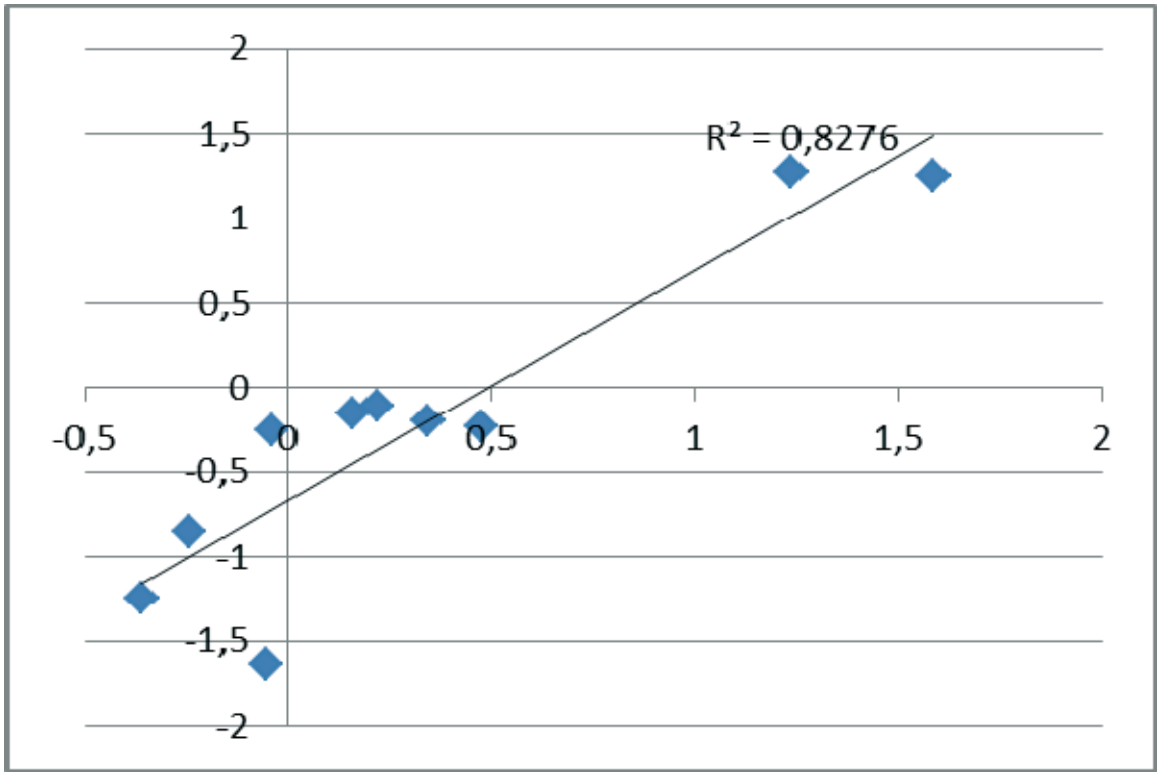
R² = 0,8276
2
1,5
1
0,5
0
-0,5
-1
-1,5
-2
-0,5
0
0,5
1
1,5
2

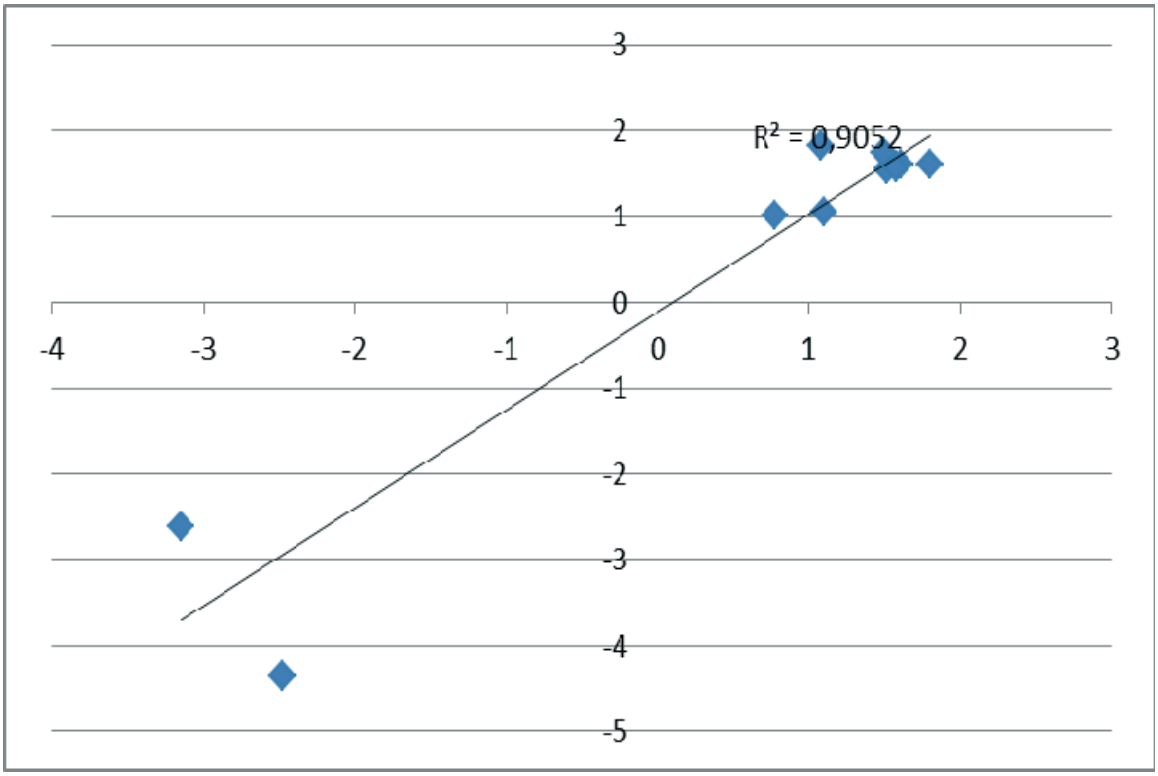
R² = 0,9052
3
2
1
0
-1
-2
-3
-4
-5
-4
-3
-2
-1
0
1
2
3

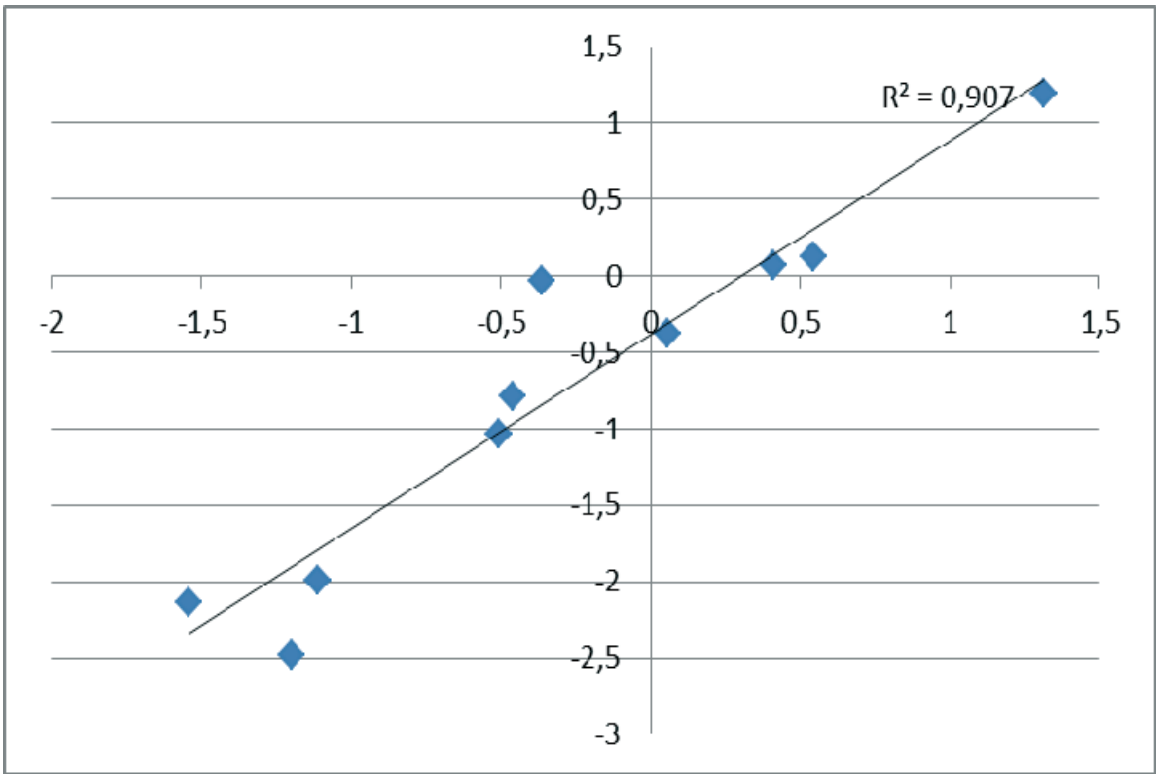
R² = 0,907
1,5
1
0,5
0
-0,5
-1
-1,5
-2
-2,5
-3
-2
-1,5
-1
-0,5
0
0,5
1
1,5

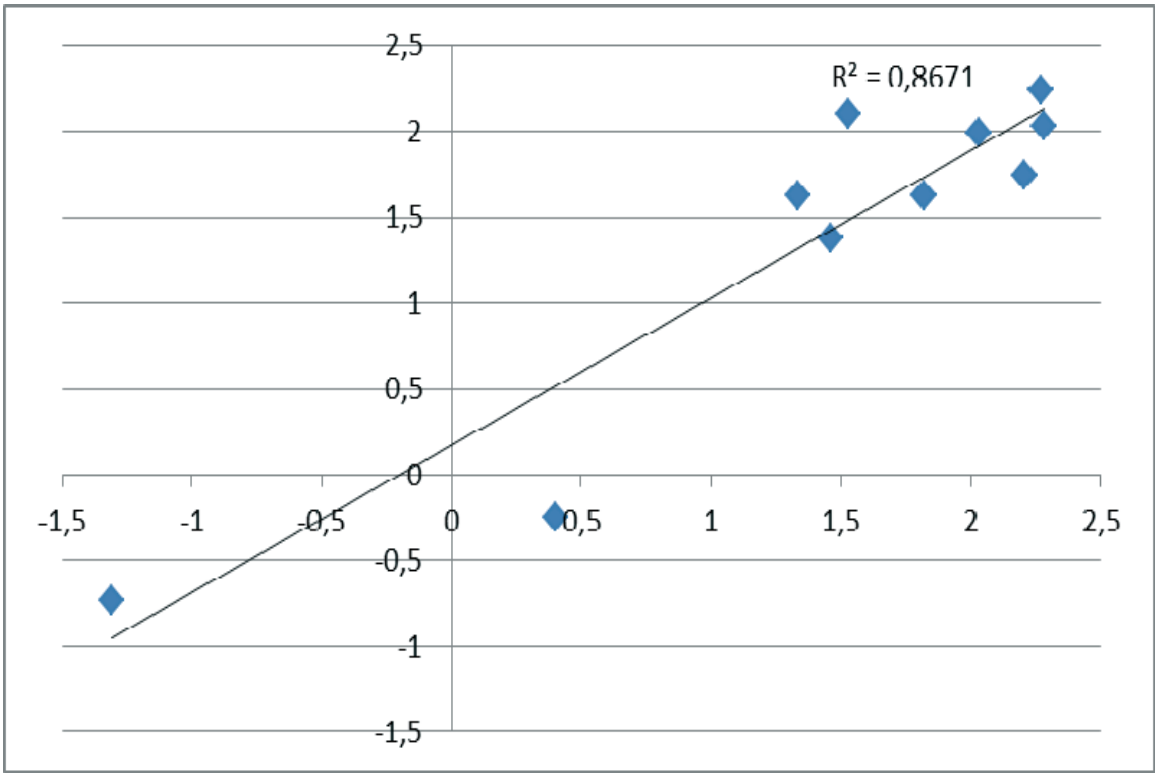
R² = 0,8671
2,5
2
1,5
1
0,5
0
-0,5
-1
-1,5
-1,5
-1
-0,5
0
0,5
1
1,5
2
2,5

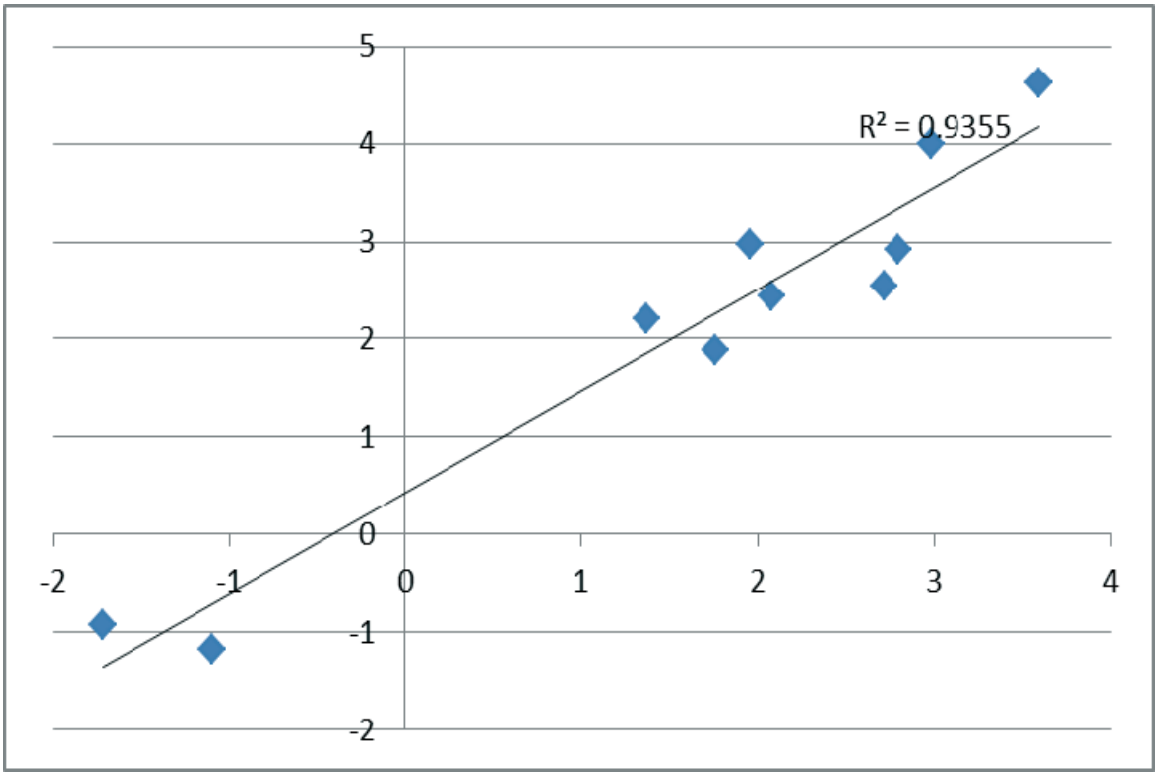

Figure 37: Correlation of relative mRNA levels measured by microarrays and qRT-PCR. The X axis shows log fold changes of genes measured by microarrays and the Y axis shows log fold changes measured by qRT-PCR. Ten significantly regulated and relevant genes from different functional categories were chosen to validate fold changes measured by microarrays. These include ACOT1 (Acyl-CoA thioesterase 1), acyl-CoA thioesterase 3 (ACOT3), activin A receptor type II-like 1 (ALK-1), baculoviral IAP repeat-containing 5 (BIRC5), chemokine (C-C motif) ligand 24 (CCL24), chemokine (C-C motif) ligand 5 (CCL5), CD5 molecule-like (SP-α), cyclin-dependent kinase 1 (CDK1), cathelicidin antimicrobial peptide (CRAMP), cytochrome P450, family 7, subfamily A, polypeptide 1 (CYP7A1). Each blue square represents one gene. Each of the graphs represents the correlation of these genes at a particular observation point, starting with 4h p.i. (upper) to 5d p.i. (lowest). The correlation (R^2) of fold changes measured by both techniques is indicated for each time point. The correlation R^2 ranged from 0.8276 to 0.9355, all of which indicate a very strong corrleation between both techniques, thus validating fold changes measured by microarrys.

4. DISCUSSION

In this study we examined the temporal transcriptional response in the liver of mice following intravenous infection with a sublethal burden of *L. monocytogenes* using whole genome microarrays. Microarrays are a powerful high-throughput tool to determine profiles of thousands of transcripts in a single run. The massive amount of data acquired by a single array requires a robust and rigorous quality control to ensure the possibility to make meaningful biological interpretations. In order to provide highly reliably array data, we present a quality control workflow that was developed at our institution. Within this, spot-based and array-based quality is tested, detects and eliminates outlier probes as well as outlier arrays. As a part of this continuous development and optimization process, the number of required permutations using the rank product (RP) function was investigated in this study. RP is a widely used tool in the detection of differentially expressed genes and the calculation of the false-discovery rate (FDR) of microarray experiments [178], which is based on the robustness of a tested value as compared to the effect on this value due to randomly permutated values. However, there are no guidelines for the number of permutations that should be used. Furthermore, this tool requires a significant amount of computer memory, which is limited. To address the effect of different permutation cycles on the number of differentially expressed genes based on changes of the FDR and subsequent changes of the biological interpretation of acquired data, we tested an exemplary data set at different permutations rates - 100, 200, 300, 350, 400 and 800 (Figure 8). We sought to determine the minimum number of permutations required to reflect differential expression gained by highest permutation numbers and thereby minimize required computer resources. As results show, choosing a permutation number that is too low will effect on the number of differentially expressed genes. Moreover, these differences impact the biological interpretation when using these results for to obtain a global view on investigated processes. It is therefore of importance to determine an appropriate number of permutations for each experiment by testing different values. Based on these results, we choose to use 400 permutations in the determination of differentially expressed genes.

L. monocytogenes is a Gram-positive, facultative intracellular living bacterium that causes foodborne infections in immunocompromised, pregnants, infants and elderly [1]. Apart from its global clinical importance, *L. monocytogenes* is a model pathogen for the

investigation of the host response upon infection with Gram-positive, intracellular as well as extracellular pathogens. The variety of virulence factors produced by the pathogenic *Listeria* strains allow the investigation of phsyiologcial processes, such as actin-polymerization, but also pathogenic processes, including the cholesterol-dependent pore-forming ability of LLO, which is closely related to perfringolysin, streptolysin and pneumoysin [179]. Due to the reliability and reproducibility of listerial infections in mice, *Listeria* became one of the most commonly used model stimulant in the investigation of innate and adaptive immune system *in vivo.* From our experience and results from other studies, we learned that the systemic response upon listerial infection does not reflect the organ specific immune processes. Thus, it is important to elucidate the local mechanisms triggered by infection with *Listeria* to make conclusions about the pathophysiology and contributions of each organ to systemic observations. Since the liver is the major organ in the clearance of *L. monocytogenes*, but also represents an important localization of listerial proliferation, we examined the global organ specific response in a time dependent manner. In order to determine important processes from the large data set obtained, we followed a strict analysis and validation procedure (Figure 9 and 10).

Approximately 9% of the protein-coding portion of the mouse genome is mobilized in the liver in response to a single intravenous inoculation of *L. monocytogenes* (Figure 13). This is comparable to an estimation that was made for a comparable experiment using LPS injection, a model for Gram-negative infection [111]. In our global evaluation, more than 50% of deregulated genes are appendent to the categories “metabolism” and “immune response” (Figure 16 and 17). Overrepresentation of these categories was also reflected by several canonical pathways and functions, including LXR/FXR activation pathway, lipid metabolism and antigen presentation. Surprisingly, analysis of the category “immune response” revealed that innate and adaptive immunity intersect in this global evaluation. Several genes of the hepatic acute phase reaction and MHC genes were concomitantly expressed at the same observation points. While similar observations were described for the hepatic acute phase response after LPS injection [111], this is the first study reporting similar events for Gram-positive bacteria. Strikingly, the time dependent gene expression pattern reported by Yoo et al. mirrors an inverse regulation of immunity with respect to the directionality of response. They showed that several genes are highly expressed as early as 3h and within 12h p.i., but downregulated at 24 – 48h p.i. In the present study, the majority of genes of immune

response are weakly expressed during the first 24h, but significantly upregulated at 48h p.i. This delayed activation of immunity compared to a rapid induction by LPS may in part explain the early pathophysiology of *Listeria* infection in liver. Although only a very small portion of injected organisms survives after hours of inoculation, these are able to proliferate exponentially within 48h of infection in the liver, before effective clearance occurs [44]. In line with this, we report for the first time that mRNA levels of genes of anti-microbial peptides, such as CRAMP and DEF23A are differentially downregulated within the early phase of infection (Figure 23 and 33). CRAMP is effective against a number of bacteria, *including P. aeruginosa, S. typhimurium, E. coli, L. monocytogenes, S. epidermidis, S.aureus* and *vancomycin-resistant enterococci* [157-162, 180], making it a potent target to aim in order to escape from early elimination. During the late phase of our observation, several defensins as well as CRAMP were upregulated and presumably contribute to effective killing of bacteria (Figure 33). Although the precise mechanism of immunomodulation is unclear, a recent study reports that *Listeria* impairs innate response by targeting the regulation of NFkB, a transcription factor essential to inflammatory pathways [181] that is also responsible for CRAMP transcription control [182]. However, the complex regulatory network leading to a permissive environment allowing the pathogen to proliferate remained unclear.

Interestingly, our results display a reciprocal regulation of lipid metabolism and immune response (Figure 17, 21 and 22). While genes of the lipid metabolism were seen higher expressed during the first 24h p.i., we observed strong downregulation in the concluding phase. Yoo and Desiderio made a similar observation upon intravenous LPS inoculation, but again, the temporal relationship of both functional categories was conversed as compared to our results. Although, the authors have not used a whole genome chip, but a mouse array containing 12,488 probes (U74A v2; Affymetrix), which may limit a comparison, we may conclude the following: (i) there is a substantial difference between hepatic gene expression in response to LPS as compared to Gram-positive *Listeria*, (ii) liver specific transcriptional response shows a reciprocal regulation of lipid metabolism and inflammation and (iii) this reciprocal regulation is reversed in LPS and *Listeria* infection.

As a result of this deregulation in the early hepatic response, we show for the first time that intracellular lipid droplets (LDs) accumulate within hepatocytes after infection with *L. monocytogenes* (Figure 25). Cytoplasmic lipid droplets consist of a core of TAGs and cholesterol esters surrounded by a phospholipid monolayer comprising a complex with

perilipin proteins which participate in the formation of a protective coat that limits lipolysis by lipases [134, 183]. Although the precise function of LDs is not yet clear, there is evidence for a role in the pathogenesis of intracellular pathogens, including *Mycobacterium* [184] and *Chlamydia trachomatis* [185]. Several studies linked the synthesis of LD to inflammatory pathways. TLR-2deficiency for example, impaires LD biogenesis and cytokines as well as chemokines were able to induce LD formation *in vitro*, but failed to provoke LD accumulation *in vivo* [186]. Further studies suggested a role as energy source, concluded from the close relation and interaction with LDs by some intracellular pathogens [185]. LDs may also present a protected compartment for pathogens to escape from host defense mechanisms and proliferate within [186]. This is indicated in the immunofluorescence studies presented here. Furthermore, the origin of neutral lipids accumulating to LDs during infection is unclear. Physiologically, neutral lipids are synthesized from fatty acids and cholesterol by ER enzymes and deposited in the cytoplasm between 2 leaflets of the ER [186]. Biogenesis of LDs during infection however is not well described.

We show that *L. monocytogenes* induces lipid droplets *in vivo* and in a subsequent *in vitro* model using HepG2 (Figure 26). Clasically, the LD biogenesis pathway is driven by enzymes that control the lipid metabolism and can be blocked by incubation with Triascin C. Our results indicate that LD biogenesis occurs in HepG2 cells at baseline, but is dramatically increased following infection with *L. monocytogenes*. Furthremore, we show that *L. monocytogenes* is capable of inducing the synthesis of LD through an alternative pathway (Figure 27). In HepG2 cells that were incubated with Triascin C and lack endogenous LD synthesis, *L. monocytogenes* induced the formation of LD to a similar extent compared to infected HepG2 cells without prior Triascin C treatment. Based on these *in vivo* and *in vitro* results, we suggest that intracellular neutral lipids synthesis and plasma lipids incorporated during the phagocytic process and released into the cytoplasm may contribute to LD formation following infection with *L. monocytogenes*. This idea is supported by the deregulation of genes that in concert lead to increasing levels of fatty acids and by significantly decreased TAG levels measured in the serum of infected mice (Figure 31). In line with this, LDs were shown to be inducible by extracellular fatty acids, but also in the absence of exogenous lipids [187, 188]. We observed a close spatial relationship of bacterial and induced lipid droplets indicating that *Listeriae* potentially use lipid droplets as energy source or to evade from intracellular defence mechanisms. The exact role of LDs in the pathogenesis of *Listeria*

infection, possible protein candidates that could mediate association to LDs and the link to inflammatory pathways are subject of further investigation.

As mentioned above, LXR-α triggers a reciprocal regulation of lipid metabolism and immune response. In this study, several LXR target genes were seen differentially deregulated at different time points. Strikingly, genes involved in lipid metabolism are distinctly regulated from LXR-responsive genes with implications in immune response and apoptosis regulation. While regulators of the lipid metabolism were seen highly expressed during the early period but significantly lower expressed in the following observation, genes of the immune response displayed an inverse expression pattern. Deregulation of important LXR-α reporter genes, such as SREBF1 and overrepresentation of the LXR pathway lead to the conclusion that there is significant LXR-α activation in this infection model. We further confirmed this observation in the *in vitro* infection model using HuH-7 cells by showing increased signal intensity within of LXR-α within the nuclei of infected cells (Figure 28). In line with dynamic LXR-α dependent gene expression found in the microarray experiments, we also observed a time dependent LXR-α accumulation within the nucleus, thus demonstrating a dynamic change of activity of this transcription factor.

Based on the expression profile of LXR-α-responsive genes we hypotheized that LXR-α undergoes posttranslational modifications leading to a change of the transcribed gene repertoire regulated by LXR. It was shown that modification of LXR-α by SUMOylation or phosphorylation results in an altered expression profile. Furthermore, reporter genes such as SREBF1 and CCL24 exhibit an inversed directionality of expression dependent on the native or modified state of LXR-α [144-146]. Based on these observations we hypothesized that LXR-α becomes phosphorylated during infection with *L. monocytogenes.* We confirmed this hypothesis by showing that phosphorylation occurs in HuH-7 cells when infected with *L. monocytogenes* and furthermore show that there is also a time dependent change in localization of this modified form of LXR-α (Figure 29). Possible kinases that mediate phosphorylation during infection with *L. monocytogenes* are ALK-1 and PKA/PKC. Both were shown to mediate phosphorylation of LXR-α and were seen upregulated in *in vivo.* Interestingly, we observed that the phosphorylated form of this transcription factor is present at baseline, but the signal is mainly found in the perinuclear region. This further led us to the hypothesis that modified LXR-α is present at a baseline and a stimulus, such as

infection with *L. monocytogenes* may trigger dephosphorylation and translocation of LXR-α.

Furthermore, it is important to consider degradation of LXR-α as a cause for altered expression of its target genes. A recent study demonstrated that LXR-α ligands, such as T0901317 prevented LXR-α ubiquitination and subsequent degradation, which was promoted by BARD1 (BRCA1-associated RING domain 1)/BRCA1 (breast and ovarian cancer susceptibility 1) [189]. Provided that endogenous ligands such as 25-oxysterol or 7-oxysterol have similar effects, LXR-α degradation could be prevented by increasing intracellular oxysterol levels in early infection with *Listeria*. Then, due to efflux of oxysterols through ABCG1 as observed on here this inhibition abrogates and eventually leads to an altered gene expression. The impact of LXR-α modification and resulting consequences for the response against pathogens such as *L. monocytogenes* may represent an important biological switch that has strong impact on the course of infection and represents an interesting intersection between the metabolic and immune regulation in the liver that warrants further investigation.

As presented in this study, the transcription regulation by LXR-α may alter in a time dependent manner. This observation emphasizes the necessity to consider that gene expression controlled by LXR-α alters over the time course due to above discussed mechanisms. Two studies investigating the inflammatory response upon LPS challenge after pre-treatment using identical LXR agonists *in vivo* and *in vitro*, respectively illustrate the complexity of interpretation of these data. Fontaine et al. pre-treated human macrophages with the same concentration of either T0901317 or GW3965 for 0, 6, 12, 24 or 48h, then challenged these cells with LPS and measured secretion levels of MCP-1 and TNFα 8h after stimulation. As a result they saw a strong inhibition of chemokine as well as cytokine secretion in cells that were incubated for up to 12h. However, cells pre-incubated for 24 and especially 48h demonstrated an enormous increase in MCP-1 and TNFα secretion. Although, the authors focused on the late potentiated LPS response, short-term pretreatment clearly indicated an anti-inflammatory signal. Change in secretion could be due to ligand-induced modifications of LXR and consequent alteration in gene expression [190]. In a rat model of endotoxemia, GW3965 was shown to protect against liver injury and dysfunction by exerting an anti-inflammatory effect [191]. Wang and colleges nicely illustrated that intravenous administration of GW3965 30 minutes before LPS injection was able to limit liver injury by LXR-mediated inhibition of TNFα. Thus, this study demonstrated

how LXR activation was able to reverse early inflammatory effects shown by Yoo and Desiderio in a LPS endotoxemia [111]. Considering its enormous effects in the hepatic inflammatory response to LPS and Gram-positive bacteria, LXR is positioned to be a central biological switch in the integration and regulation of the metabolic and immune system. LXR dependent immune suppression could therefore contribute to the observation that *L. monocytogenes* is capable to survive in the early phase of infection. Although oxysterols represents endogenous ligands for LXR activation during *Listeria* infection, it is an potent target to aim and direct interaction of listerial virulence factors with transcription factor or its regulators occurs and represent a pathogen driven mechanism of host immunomodulation [181].

The most important endogenous ligands of LXR are oxysterols, representing hydroxylated cholesterol. Enzymes promoting hydroxylation of cholesterol to oxysterol include CH25H and CYP7A1, which are seen differentially upregulated in this study. Recently, a study revealed a relationship between upregulation of CH25H and survival of macrophages that were challenged with *L. monocytogenes* [192]. Pro-survival signals were also associated with SP-α, also known as CD5L, a LXR-responsive gene, which has been previously reported [135]. Survival of host cells permits *Listeria* to proliferate within the cytoplasm, thus, upregulation of CH25H could contribute to pro-pathogen environment through different pathways, including LXR activation. In this study, SP-α was seen upregulated in the late phase of infection, indicating a pro-survival signal in host cells. However, since cell mediated anti-listerial effects occur in this phase of infection, it is not clear how upregulation could contribute to listerial survival *in vivo*. Possibly, pro-survival signals induced by SP-α are present, but more superior mechanisms of cell mediated immune response could overcome these effects.

Due to upregulation of CH25H and CYP7A1 in the early phase of infection, it appears likely that converted cholesterol is the ligand of LXR in this study. In accordance with this, oxysterol binding – like proteins are seen highly expressed, indicating an accumulation of their ligands. However, the origin of cholesterol that is modified to oxysterols is unclear. Possibly, cholesterol from the blood is incorporated during phagocytosis that is then released upon vacuole disruption. However, clinical parameters obtained in this study do not support this idea, because cholesterol levels in the blood remained unchanged. Another source could be the vacuole membrane itself, which contains high levels of cholesterol that are released upon vacuole disruption by listerial virulence factors and subsequently converted to oxysterols by CYP7A1 and

CH25H. Furthermore, de novo synthesis of cholesterol within the cell could contribute to increasing intracellular concentrations. A schematic summary of the potential cellular LXR dependent response following listerial infection is demonstrated in Figure 38.

Although an early permissive environment allows *Listeria* to survive and proliferate within the liver, effective immune response eliminates the pathogen during the following phase. Several mechanisms are involved in the final clearance of *Listeria*, including neutrophils, macrophages and ultimately T cell mediated response [1].

The ability of T cell depleted mice to effectively clear bacteria during the first days of infection emphasizes the importance of neutrophils and macrophages, including the resident liver macrophages Kupffer cells [153]. Although Kupffer cells were shown to be important for the clearance and trapping of *Listeria* from bloodstream, they lack phagocytic activity. Rather they were suggested to bind *Listeria* organisms on their surface and by interaction with neutrophils they subsequently contributed to bacterial killing [49]. Adhesion between both cell types was mediated by ICAM-1 MAC-1, both of which are upregulated in this study. Furthermore, S100 proteins were shown to be important for the adhesion of neutrophils through the same intercellular adhesion molecules [193].

However, the receptors responsible for adhesion to Kupffer cell surface have not been identified. Our study revealed upregulation of several members of the C-type lectin receptors a family member, including CLEC1A, CLEC1B, CLEC2D and CLEC9A that could account for this function. CLEC9A was shown to bind pathogen antigens without triggering a phagocytic cascade and instead leads to an intracellular signal cascade that results in the release of peptides that are chemotactic to neutrophils [154]. Thus, CLEC9A is a potential candidate for binding of pathogens by Kupffer cells (Figure 32).

In addition to their function in activation the intercellular adhesion, two members of the S100 molecules, S100A8 and S100A9 are major cytosolic constitutes in neutrophils and monocytes, representing about 40% of the total protein content [194]. When secreted, S100A8 and A9 form extracellular complexes that possess antimicrobial activity [195, 196]. As recently shown bacteria may decrease expression or inactivate the S100A8/A9 complex [194] and thereby improve survival in the infected host. In conclusion, the interaction between neutrophils and Kupffer cells, could result in killing of trapped bacteria bound to CLECs by S100A8/A9 secretion starting 2d p.i.and thereby contribute to T cell independent clearance of *L. monocytogenes* from the liver.

Antigen presentation by professional macrophages represents the link between innate and adaptive immune response. Antigens bound to MHC class II (MHCII) proteins are presented to CD4 – positive T cells, while MHC class I (MHCI) present exogenous as well as endogenous peptides to CD8 – positive T cells and Natural Killer cells (NKC) [74, 112, 153, 176]. Two families within the MCHI proteins, class Ia and Ib possess distinct functions and answer by T cells activated by these MHC molecules is temporally restricted. MHC-Ia presented peptides mediate the differentiation of T cells to memory cells, which drive a rapid and effective cell mediated immune response upon secondary infection. In contrast, MHC-Ib restricted T cells expand within few days during a primary infection, but play a minor role in secondary infection [74, 112, 153, 166]. Although MHC-Ib restricted T cells were shown to play an important role in listerial clearance, the temporal transcriptional changes of MHC-Ib genes has not been revealed. In this study, we observed a time-dependent deregulation of several MHC-Ib genes, all of which were upregulated. Gene expression was increased starting mainly 2d p.i., which is in accordance with known literature describing an expansion of MHC-Ib restricted T cells 2 – 3d p.i. [74, 74, 165, 172]. In this global evaluation, the classical MHC-Ib – pathway which describes the immunoproteasome independent acquisition of exogenous peptides and the non – classical pathway intersect with respect to the temporal expression and directionality of deregulation (Figure 34). Classical MHC-Ib proteins are loaded with N-formylated methionine (*f-peptides*), which are actively secreted by *L. monocytogenes*. The most important intracellular receptor for these peptide FPR2 is also seen significantly upregulated, thus supporting the conclusion of antigen presentation by members of the H2-M3 family. Apart from H2-M3, the best characterized MHC-Ib gene, we saw several H2-M family member upregulated that share high similarity with H2-M3 and could contribute to activation MHC-Ib restriceted T cells during listeriosis. Non-classical MHC-Ib genes, such as H2-K1 and H2-T23 are seen upregulated during the same phase of infection, indicating a temporal overlap with classical MHC-Ib mechanisms despite their distinct function. These MHC-Ib proteins are ligated to short peptides (8 amino acids) derived from degradation of listerial virulence factors, including LLO and p60 by the immunoproteasome. The immunoproteasome contains three major proteins, LMP7, MECL1 and LMP2, which replace the physiological proteasome upon appropriate stimulus such as infection [175]. LMP7 and MECL1 as well as TAP1 and TAP2, which are necessary for associating peptides with MHCI proteins are seen significantly higher expressed. In a recent study,

a group showed a dependence of NKC activity by p60, which was not due to direct interaction, since application of p60 did not provoke NKC activation and the authors suggested an indirect way of stimulation [207]. Combining our results with this observation offers the possibility that antigen presentation by MHC-Ib protein H2-K1, which is seen highly expressed, could be responsible for indirect enhancement of NKC activation. H2-K1 was identified as p60 – fragment binding protein that presents antigen to T cells as well as to NKC expressing certain receptors - NKG2A or NKG2D [176, 177]. Both receptors are seen highly expressed indicating an enhanced potency to recognize immunoproteasome derived p60 peptides presented by H2-K1. In conclusion, we show that both MHC-Ib pathways are stimulated upon listerial infection and peptides secreted into the cytosol as well as protein fragments derived from an activated immunoproteasome are involved in activation of MHC-Ib restricted T cells and NKC, thus mediating an early occurring cell driven clearance of *L. monocytogenes* (Figure 35 and 36). In accordance, effector proteins secreted by activated T cells, such as perforin 1 and granzymes which possess a high toxicity towards infected cells are highly upregulated during this period of infection.

Microarray studies are generally limited by isolated measurement of mRNA levels. It was shown that mRNAs are regulated by non coding RNAs, such as microRNAs on a postransciptional level during infection with *L. monocytogenes* in intestinal cells [208]. Furthermore, *L. monocytogens* produces a number of small non-coding RNAs [209] and it can not be excluded that these are secreted and interfere with host mRNAs. However, in this study we were able to confirm conclusions that were drawn from transcriptional data in functional and serologic experiments. This demonstrates that generation of robust transcriptional data using a rigorous quality control and analysis workflow can indicate the expected phenotype. This became most apparaent in this study in the investigation of lipid droplets.

In conclusion, we present the liver specific transcriptional response to *L. monocytogenes*. We uncovered substantial differences to LPS infection models and hypothesize that the nuclear factor LXR-α plays an essential role in the integration of metabolic and inflammatory response to *L. monocytogenes*, which presents a model pathogen for Gram-positive bacteria. We have indication that oxysterols are strongly involved in the pathogenesis of *L. monocytogenes* by activating LXR. We display that innate and adaptive immunity intersect in a global evaluation and importantly both are reciprocally deregulated to genes of the lipid metabolism. Furthermore, we were able to

detect a modified form of LXR-α in an *in vitro* infection model that could account for these *in vivo* findings. We further demonstrated for the first time that *Listeria* induces the formation of lipid droplets within hepatocytes and changes in measured serum lipids could account for this accumulation. Furthermore, we report a downregulation of potent antimicrobial peptides such as CRAMP by two independent techniques. We hypothesize that *Listeria* actively leads to CRAMP downregulation in order to improve its own survival. Microarray finding were validated by qRT-PCR which showed a high correlation to relative mRNA levels measured by microarray (Figure 37).

Overall, a permissive environment allows *L. monocytogenes* to proliferate during the first 24h p.i. before cellular response is enhanced. We propose a role of surface receptors of Kupffer cells to be involved in the clearance and eventually, by interacting with neutrophils killing of *Listeria* organisms. Finally, cell mediated response is driven by MHC-Ib restricted T cells and NK cells, which lead to an effective killing of bacteria during the late phase of infection.

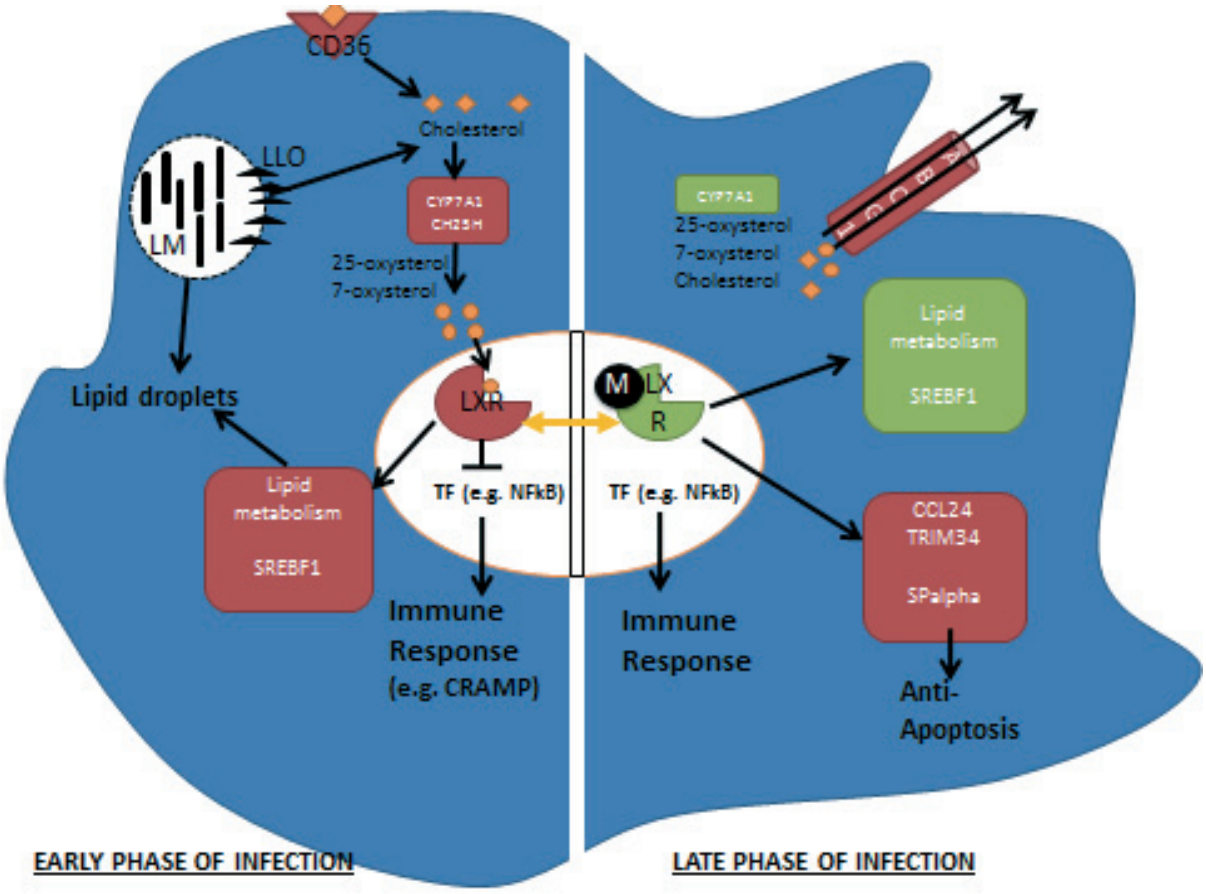

Figure 38: LXR dependent response during infection with *L. monocytogenes*. Red highlighted genes and biological processes are seen higher expressed compared to control, green are seen lower expressed. Early phase of infection represents the first 24h p.i., the late phase of infection represent the later time points that we have observed. During the early phase of infection, LLO leads to vacuole disruption and mediates an increase of cholesterol which either originates from the vacuole membrane or is released from the inside of the phagosome. Intracellular enzymes mediate conversion of cholesterol to oxysterols which bind to LXR. LXR translocates into the nucleus and induces the expression of genes, involved in the lipid metabolism, such as SREBF1. At the same time, LXR activation leads to a suppression of transcription factors (TFs) that drive inflammatory response, for example NFkB, which may also be the reason for decreased transcription of cathelecidin-related anti-microbial peptide (CRAMP) observed in the early phase of infection. Activation of the lipid metabolism leads to synthesis of fatty acids that accumulate to lipid droplets (LDs). In addition, neutral lipids from the blood may be released from the phagosome upon disruption due to LLO and contribute to increasing levels of fatty acids and LDs. During the late phase of

infection, LXR targets change possibly due to modifications (M), such as phosphorylation or sumoylation. TFs driving immune response are subsequently disinhibited by conformational changes of LXR and lead to increased transcription of chemokines (CCL24) and anti-apoptotic proteins (SP-α). This change is accompanied with a decrease of transcription of genes involved in lipid metabolism. Oxysterols and cholesterol are transported to the extracellular space via ABCG1, which is higher expressed in this phase, thus, in conjunction with other mechanisms described in this work allow a sufficient bacterial clearance by the host. LXR and its modified forms may play an essential role and function as a biological switch in the immune response/ lipid metabolism axis observed in this study.

5. REFERENCES

1. Vazquez-Boland JA, Kuhn M, Berche P, et al. *Listeria* pathogenesis and molecular virulence determinants. Clin Microbiol Rev 2001;14:584-640.

2. Schuchat A, Swaminathan B, Broome CV. *Listeria monocytogenes* CAMP reaction. Clin Microbiol Rev 1991;4:396.

4. Junttila JR, Niemela SI, Hirn J. Minimum growth temperatures of *Listeria monocytogenes* and non-haemolytic *Listeria*. J Appl Bacteriol 1988;65:321-7.

5. Swaminathan B, Barrett TJ, Hunter SB, Tauxe RV. PulseNet: the molecular subtyping network for foodborne bacterial disease surveillance, United States. Emerg Infect Dis 2001;7:382-9.

6. Lety MA, Frehel C, Berche P, Charbit A. Critical role of the N-terminal residues of listeriolysin O in phagosomal escape and virulence of *Listeria monocytogenes*. Mol Microbiol 2002;46:367-79.

7. Glomski IJ, Gedde MM, Tsang AW, Swanson JA, Portnoy DA. The *Listeria monocytogenes* hemolysin has an acidic pH optimum to compartmentalize activity and prevent damage to infected host cells. J Cell Biol 2002;156:1029-38.

8. Tweten RK, Parker MW, Johnson AE. The cholesterol-dependent cytolysins. Curr Top Microbiol Immunol 2001;257:15-33.

9. Gedde MM, Higgins DE, Tilney LG, Portnoy DA. Role of listeriolysin O in cell-to-cell spread of *Listeria monocytogenes*. Infect Immun 2000;68:999-1003.

10. Schuerch DW, Wilson-Kubalek EM, Tweten RK. Molecular basis of listeriolysin O pH dependence. Proc Natl Acad Sci U S A 2005;102:12537-42.

11. Decatur AL, Portnoy DA. A PEST-like sequence in listeriolysin O essential for *Listeria monocytogenes* pathogenicity. Science 2000;290:992-5.

12. Rechsteiner M, Rogers SW. PEST sequences and regulation by proteolysis. Trends Biochem Sci 1996;21:267-71.

13. Lety MA, Frehel C, Dubail I, et al. Identification of a PEST-like motif in listeriolysin O required for phagosomal escape and for virulence in *Listeria monocytogenes*. Mol Microbiol 2001;39:1124-39.

14. Coconnier MH, Lorrot M, Barbat A, Laboisse C, Servin AL. Listeriolysin O-induced stimulation of mucin exocytosis in polarized intestinal mucin-secreting cells: evidence for toxin recognition of membrane-associated lipids and subsequent toxin internalization through caveolae. Cell Microbiol 2000;2:487-504.

15. Yoshikawa H, Kawamura I, Fujita M, Tsukada H, Arakawa M, Mitsuyama M. Membrane damage and interleukin-1 production in murine macrophages exposed to listeriolysin O. Infect Immun 1993;61:1334-9.

16. Carrero JA, Calderon B, Unanue ER. Type I interferon sensitizes lymphocytes to apoptosis and reduces resistance to *Listeria* infection. J Exp Med 2004;200:535-40.

17. Repp H, Pamukci Z, Koschinski A, et al. Listeriolysin of *Listeria monocytogenes* forms Ca2+-permeable pores leading to intracellular Ca2+ oscillations. Cell Microbiol 2002;4:483-91.

18. Portnoy DA, Jacks PS, Hinrichs DJ. Role of hemolysin for the intracellular growth of *Listeria monocytogenes*. J Exp Med 1988;167:1459-71.

19. Raveneau J, Geoffroy C, Beretti JL, Gaillard JL, Alouf JE, Berche P. Reduced virulence of a *Listeria monocytogenes* phospholipase-deficient mutant obtained by transposon insertion into the zinc metalloprotease gene. Infect Immun 1992;60:916-21.

20. Greiffenberg L, Sokolovic Z, Schnittler HJ, et al. *Listeria monocytogenes*-infected human umbilical vein endothelial cells: internalin-independent invasion, intracellular growth, movement, and host cell responses. FEMS Microbiol Lett 1997;157:163-70.

21. Kolesnick RN, Kronke M. Regulation of ceramide production and apoptosis. Annu Rev Physiol 1998;60:643-65.

22. Kocks C, Gouin E, Tabouret M, Berche P, Ohayon H, Cossart P. *L. monocytogenes*-induced actin assembly requires the actA gene product, a surface protein. Cell 1992;68:521-31.

23. Domann E, Wehland J, Rohde M, et al. A novel bacterial virulence gene in *Listeria monocytogenes* required for host cell microfilament interaction with homology to the proline-rich region of vinculin. EMBO J 1992;11:1981-90.

24. Chakraborty T. The molecular mechanisms of actin-based intracellular motility by *Listeria monocytogenes*. Microbiologia 1996;12:237-44.

25. Welch MD, Iwamatsu A, Mitchison TJ. Actin polymerization is induced by Arp2/3 protein complex at the surface of *Listeria monocytogenes*. Nature 1997;385:265-9.

26. Machesky LM, Insall RH. Scar1 and the related Wiskott-Aldrich syndrome protein, WASP, regulate the actin cytoskeleton through the Arp2/3 complex. Curr Biol 1998;8:1347-56.

27. Gaillard JL, Berche P, Frehel C, Gouin E, Cossart P. Entry of *L. monocytogenes* into cells is mediated by internalin, a repeat protein reminiscent of surface antigens from Gram-positive cocci. Cell 1991;65:1127-41.

28. Cossart P, Jonquieres R. Sortase, a universal target for therapeutic agents against Gram-positive bacteria? Proc Natl Acad Sci U S A 2000;97:5013-5.

29. Braun L, Cossart P. Interactions between *Listeria monocytogenes* and host mammalian cells. Microbes Infect 2000;2:803-11.

30. Lecuit M, Dramsi S, Gottardi C, Fedor-Chaiken M, Gumbiner B, Cossart P. A single amino acid in E-cadherin responsible for host specificity towards the human pathogen *Listeria monocytogenes*. EMBO J 1999;18:3956-63.

31. Schubert WD, Urbanke C, Ziehm T, et al. Structure of internalin, a major invasion protein of *Listeria monocytogenes*, in complex with its human receptor E-cadherin. Cell 2002;111:825-36.

32. Geginat G, Nichterlein T, Kretschmar M, et al. Enhancement of the *Listeria monocytogenes* p60-specific CD4 and CD8 T cell memory by nonpathogenic *Listeria* innocua. J Immunol 1999;162:4781-9.

33. Gaillard JL, Berche P, Mounier J, Richard S, Sansonetti P. *In vitro* model of penetration and intracellular growth of *Listeria monocytogenes* in the human enterocyte-like cell line Caco-2. Infect Immun 1987;55:2822-9.

34. Dramsi S, Biswas I, Maguin E, Braun L, Mastroeni P, Cossart P. Entry of *Listeria monocytogenes* into hepatocytes requires expression of inIB, a surface protein of the internalin multigene family. Mol Microbiol 1995;16:251-61.

35. Dramsi S, Levi S, Triller A, Cossart P. Entry of *Listeria monocytogenes* into neurons occurs by cell-to-cell spread: an *in vitro* study. Infect Immun 1998;66:4461-8.

36. Drevets DA, Leenen PJ, Greenfield RA. Invasion of the central nervous system by intracellular bacteria. Clin Microbiol Rev 2004;17:323-47.

37. Kuhn M, Goebel W. Internalization of *Listeria monocytogenes* by nonprofessional and professional phagocytes. Subcell Biochem 2000;33:411-36.

38. Mengaud J, Ohayon H, Gounon P, Mege R-M, Cossart P. E-cadherin is the receptor for internalin, a surface protein required for entry of *L. monocytogenes* into epithelial cells. Cell 1996;84:923-32.

39. Braun L, Ghebrehiwet B, Cossart P. gC1q-R/p32, a C1q-binding protein, is a receptor for the InlB invasion protein of *Listeria monocytogenes*. EMBO J 2000;19:1458-66.

40. Shen H, Tato CM, Fan X. *Listeria monocytogenes* as a probe to study cell-mediated immunity. Curr Opin Immunol 1998;10:450-8.

41. varez-Dominguez C, Vazquez-Boland JA, Carrasco-Marin E, Lopez-Mato P, Leyva-Cobian F. Host cell heparan sulfate proteoglycans mediate attachment and entry of *Listeria monocytogenes*, and the listerial surface protein ActA is involved in heparan sulfate receptor recognition. Infect Immun 1997;65:78-88.

42. Gilot P, Andre P, Content J. *Listeria monocytogenes* possesses adhesins for fibronectin. Infect Immun 1999;67:6698-701.

43. MACKANESS GB. Cellular resistance to infection. J Exp Med 1962;116:381-406.

44. Conlan JW, North RJ. Early pathogenesis of infection in the liver with the facultative intracellular bacteria *Listeria monocytogenes*, Francisella tularensis, and Salmonella typhimurium involves lysis of infected hepatocytes by leukocytes. Infect Immun 1992;60:5164-71.

45. North RJ, Spitalny G. Inflammatory lymphocyte in cell-mediated antibacterial immunity: factors governing the accumulation of mediator T cells in peritoneal exudates. Infect Immun 1974;10:489-98.

46. Medzhitov R, Janeway CA, Jr. Decoding the patterns of self and nonself by the innate immune system. Science 2002;296:298-300.

47. Dempsey PW, Vaidya SA, Cheng G. The art of war: Innate and adaptive immune responses. Cell Mol Life Sci 2003;60:2604-21.

48. Drevets DA. *Listeria monocytogenes* infection of cultured endothelial cells stimulates neutrophil adhesion and adhesion molecule expression. J Immunol 1997;158:5305-13.

49. Gregory SH, Cousens LP, van RN, Dopp EA, Carlos TM, Wing EJ. Complementary adhesion molecules promote neutrophil-Kupffer cell interaction and the elimination of bacteria taken up by the liver. J Immunol 2002;168:308-15.

50. Hsieh CS, Macatonia SE, Tripp CS, Wolf SF, O'Garra A, Murphy KM. Development of TH1 CD4+ T cells through IL-12 produced by *Listeria*-induced macrophages. Science 1993;260:547-9.

51. Endres R, Luz A, Schulze H, et al. Listeriosis in p47(phox-/-) and TRp55-/- mice: protection despite absence of ROI and susceptibility despite presence of RNI. Immunity 1997;7:419-32.

52. varez-Dominguez C, Roberts R, Stahl PD. Internalized *Listeria monocytogenes* modulates intracellular trafficking and delays maturation of the phagosome. J Cell Sci 1997;110 (Pt 6):731-43.

53. Carrero JA, Calderon B, Unanue ER. Lymphocytes are detrimental during the early innate immune response against *Listeria monocytogenes*. J Exp Med 2006;203:933-40.

54. Fox ES, Thomas P, Broitman SA. Comparative studies of endotoxin uptake by isolated rat Kupffer and peritoneal cells. Infect Immun 1987;55:2962-6.

55. Gregory SH, Wing EJ, Danowski KL, van RN, Dyer KF, Tweardy DJ. IL-6 produced by Kupffer cells induces STAT protein activation in hepatocytes early during the course of systemic listerial infections. J Immunol 1998;160:6056-61.

56. Cousens LP, Wing EJ. Innate defenses in the liver during *Listeria* infection. Immunol Rev 2000;174:150-9.

57. Hoffmann JA, Reichhart JM. Drosophila innate immunity: an evolutionary perspective. Nat Immunol 2002;3:121-6.

58. Machata S, Tchatalbachev S, Mohamed W, Jansch L, Hain T, Chakraborty T. Lipoproteins of *Listeria monocytogenes* are critical for virulence and TLR2-mediated immune activation. J Immunol 2008;181:2028-35.

59. Ozoren N, Masumoto J, Franchi L, et al. Distinct roles of TLR2 and the adaptor ASC in IL-1beta/IL-18 secretion in response to *Listeria monocytogenes*. J Immunol 2006;176:4337-42.

60. Edelson BT, Unanue ER. MyD88-dependent but Toll-like receptor 2-independent innate immunity to *Listeria*: no role for either in macrophage listericidal activity. J Immunol 2002;169:3869-75.

61. Ting JP, Davis BK. CATERPILLER: a novel gene family important in immunity, cell death, and diseases. Annu Rev Immunol 2005;23:387-414.

62. Muraille E, Giannino R, Guirnalda P, et al. Distinct *in vivo* dendritic cell activation by live versus killed *Listeria monocytogenes*. Eur J Immunol 2005;35:1463-71.

63. Cooper AM, Adams LB, Dalton DK, Appelberg R, Ehlers S. IFN-gamma and NO in mycobacterial disease: new jobs for old hands. Trends Microbiol 2002;10:221-6.

64. Chang SR, Wang KJ, Lu YF, et al. Characterization of early gamma interferon (IFN-gamma) expression during murine listeriosis: identification of NK1.1+ CD11c+ cells as the primary IFN-gamma-expressing cells. Infect Immun 2007;75:1167-76.

65. Harty JT, Bevan MJ. Specific immunity to *Listeria monocytogenes* in the absence of IFN gamma. Immunity 1995;3:109-17.

66. Aderem A, Ulevitch RJ. Toll-like receptors in the induction of the innate immune response. Nature 2000;406:782-7.

67. McCaffrey RL, Fawcett P, O'Riordan M, et al. A specific gene expression program triggered by Gram-positive bacteria in the cytosol. Proc Natl Acad Sci U S A 2004;101:11386-91.

68. Mariathasan S, Monack DM. Inflammasome adaptors and sensors: intracellular regulators of infection and inflammation. Nat Rev Immunol 2007;7:31-40.

69. Kobayashi KS, Chamaillard M, Ogura Y, et al. Nod2-dependent regulation of innate and adaptive immunity in the intestinal tract. Science 2005;307:731-4.

70. Mizushima N, Levine B, Cuervo AM, Klionsky DJ. Autophagy fights disease through cellular self-digestion. Nature 2008;451:1069-75.

71. Rich KA, Burkett C, Webster P. Cytoplasmic bacteria can be targets for autophagy. Cell Microbiol 2003;5:455-68.

72. Yano T, Kurata S. Induction of autophagy via innate bacterial recognition. Autophagy 2008;4:958-60.

73. Ding WX, Li M, Chen X, et al. Autophagy reduces acute ethanol-induced hepatotoxicity and steatosis in mice. Gastroenterology 2010;139:1740-52.

74. Finelli A, Kerksiek KM, Allen SE, et al. MHC class I restricted T cell responses to *Listeria monocytogenes*, an intracellular bacterial pathogen. Immunol Res 1999;19:211-23.

75. Kaufmann SH, Hug E, De LG. *Listeria monocytogenes*-reactive T lymphocyte clones with cytolytic activity against infected target cells. J Exp Med 1986;164:363-8.

76. Shedlock DJ, Shen H. Requirement for CD4 T cell help in generating functional CD8 T cell memory. Science 2003;300:337-9.

77. Wong P, Pamer EG. Cutting edge: antigen-independent CD8 T cell proliferation. J Immunol 2001;166:5864-8.

78. Harty JT, Badovinac VP. Influence of effector molecules on the CD8(+) T cell response to infection. Curr Opin Immunol 2002;14:360-5.

79. Jiang J, Zenewicz LA, San Mateo LR, Lau LL, Shen H. Activation of antigen-specific CD8 T cells results in minimal killing of bystander bacteria. J Immunol 2003;171:6032-8.

80. Ho JL, Shands KN, Friedland G, Eckind P, Fraser DW. An outbreak of type 4b *Listeria monocytogenes* infection involving patients from eight Boston hospitals. Arch Intern Med 1986;146:520-4.

81. Jensen VB, Harty JT, Jones BD. Interactions of the invasive pathogens Salmonella typhimurium, *Listeria monocytogenes*, and Shigella flexneri with M cells and murine Peyer's patches. Infect Immun 1998;66:3758-66.

82. Marco AJ, Prats N, Ramos JA, et al. A microbiological, histopathological and immunohistological study of the intragastric inoculation of *Listeria monocytogenes* in mice. J Comp Pathol 1992;107:1-9.

83. Pron B, Boumaila C, Jaubert F, et al. Comprehensive study of the intestinal stage of listeriosis in a rat ligated ileal loop system. Infect Immun 1998;66:747-55.

84. Yoshikai Y. The interaction of intestinal epithelial cells and intraepithelial lymphocytes in host defense. Immunol Res 1999;20:219-35.

85. Dunne DW, Resnick D, Greenberg J, Krieger M, Joiner KA. The type I macrophage scavenger receptor binds to Gram-positive bacteria and recognizes lipoteichoic acid. Proc Natl Acad Sci U S A 1994;91:1863-7.

86. Gregory SH, Wing EJ. IFN-gamma inhibits the replication of *Listeria monocytogenes* in hepatocytes. J Immunol 1993;151:1401-9.

87. Ebe Y, Hasegawa G, Takatsuka H, et al. The role of Kupffer cells and regulation of neutrophil migration into the liver by macrophage inflammatory protein-2 in primary listeriosis in mice. Pathol Int 1999;49:519-32.

88. Lecuit M. Human listeriosis and animal models. Microbes Infect 2007;9:1216-25.

89. Conlan JW. Early pathogenesis of *Listeria monocytogenes* infection in the mouse spleen. J Med Microbiol 1996;44:295-302.

90. Aichele P, Zinke J, Grode L, Schwendener RA, Kaufmann SH, Seiler P. Macrophages of the splenic marginal zone are essential for trapping of blood-borne particulate antigen but dispensable for induction of specific T cell responses. J Immunol 2003;171:1148-55.

91. Stockinger S, Materna T, Stoiber D, et al. Production of type I IFN sensitizes macrophages to cell death induced by *Listeria monocytogenes*. J Immunol 2002;169:6522-9.

92. Parkash V, Morotti RA, Joshi V, Cartun R, Rauch CA, West AB. Immunohistochemical detection of *Listeria* antigens in the placenta in perinatal listeriosis. Int J Gynecol Pathol 1998;17:343-50.

93. Farber JM, Peterkin PI. *Listeria monocytogenes*, a food-borne pathogen. Microbiol Rev 1991;55:476-511.

94. Lavi O, Louzoun Y, Klement E. Listeriosis: a model for the fine balance between immunity and morbidity. Epidemiology 2008;19:581-7.

95. Jurado RL, Farley MM, Pereira E, et al. Increased risk of meningitis and bacteremia due to *Listeria monocytogenes* in patients with human immunodeficiency virus infection. Clin Infect Dis 1993;17:224-7.

96. Ewert DP, Lieb L, Hayes PS, Reeves MW, Mascola L. *Listeria monocytogenes* infection and serotype distribution among HIV-infected persons in Los Angeles County, 1985-1992. J Acquir Immune Defic Syndr Hum Retrovirol 1995;8:461-5.

97. Southwick FS, Purich DL. Intracellular pathogenesis of listeriosis. N Engl J Med 1996;334:770-6.

98. Maijala R, Lyytikainen O, Autio T, Aalto T, Haavisto L, Honkanen-Buzalski T. Exposure of *Listeria monocytogenes* within an epidemic caused by butter in Finland. Int J Food Microbiol 2001;70:97-109.

99. Gray ML, Killinger AH. *Listeria monocytogenes* and listeric infections. Bacteriol Rev 1966;30:309-82.

100. Doganay M. Listeriosis: clinical presentation. FEMS Immunol Med Microbiol 2003;35:173-5.

101. Goulet V, Marchetti P. Listeriosis in 225 non-pregnant patients in 1992: clinical aspects and outcome in relation to predisposing conditions. Scand J Infect Dis 1996;28:367-74.

102. Dalton CB, Austin CC, Sobel J, et al. An outbreak of gastroenteritis and fever due to *Listeria monocytogenes* in milk. N Engl J Med 1997;336:100-5.

103. Aureli P, Fiorucci GC, Caroli D, et al. An outbreak of febrile gastroenteritis associated with corn contaminated by *Listeria monocytogenes*. N Engl J Med 2000;342:1236-41.

104. Schlech WF, III. *Listeria* gastroenteritis--old syndrome, new pathogen. N Engl J Med 1997;336:130-2.

105. Stelma GN, Jr., Reyes AL, Peeler JT, et al. Pathogenicity test for *Listeria monocytogenes* using immunocompromised mice. J Clin Microbiol 1987;25:2085-9.

106. Glaser P, Frangeul L, Buchrieser C, et al. Comparative genomics of *Listeria* species. Science 2001;294:849-52.

107. Bolstad BM, Irizarry RA, Astrand M, Speed TP. A comparison of normalization methods for high density oligonucleotide array data based on variance and bias. Bioinformatics 2003;19:185-93.

108. Alibes A, Yankilevich P, Canada A, az-Uriarte R. IDconverter and IDClight: conversion and annotation of gene and protein IDs. BMC Bioinformatics 2007;8:9.

109. Minami T, Miura M, Aird WC, Kodama T. Thrombin-induced autoinhibitory factor, Down syndrome critical region-1, attenuates NFAT-dependent vascular cell adhesion molecule-1 expression and inflammation in the endothelium. J Biol Chem 2006;281:20503-20.

110. You B, Jiang YY, Chen S, Yan G, Sun J. The orphan nuclear receptor Nur77 suppresses endothelial cell activation through induction of IkappaBalpha expression. Circ Res 2009;104:742-9.

111. Yoo JY, Desiderio S. Innate and acquired immunity intersect in a global view of the acute-phase response. Proc Natl Acad Sci U S A 2003;100:1157-62.

112. Kloetzel PM, Ossendorp F. Proteasome and peptidase function in MHC-class-I-mediated antigen presentation. Curr Opin Immunol 2004;16:76-81.

113. Gianotti A, Serrazanetti D, Sado KS, Guerzoni ME. Involvement of cell fatty acid composition and lipid metabolism in adhesion mechanism of *Listeria monocytogenes*. Int J Food Microbiol 2008;123:9-17.

114. Kim SR, Park HJ, Yim dS, Kim HT, Choi IG, Kim KH. Analysis of survival rates and cellular fatty acid profiles of *Listeria monocytogenes* treated with supercritical carbon dioxide under the influence of cosolvents. J Microbiol Methods 2008;75:47-54.

115. Hunt MC, Lindquist PJ, Peters JM, Gonzalez FJ, Diczfalusy U, Alexson SE. Involvement of the peroxisome proliferator-activated receptor alpha in regulating long-chain acyl-CoA thioesterases. J Lipid Res 2000;41:814-23.

116. Zheng B, Chen D, Farquhar MG. MIR16, a putative membrane glycerophosphodiester phosphodiesterase, interacts with RGS16. Proc Natl Acad Sci U S A 2000;97:3999-4004.

117. Hagen FS, Grant FJ, Kuijper JL, et al. Expression and characterization of recombinant human acyloxyacyl hydrolase, a leukocyte enzyme that deacylates bacterial lipopolysaccharides. Biochemistry 1991;30:8415-23.

118. Aguado B, Campbell RD. Characterization of a human lysophosphatidic acid acyltransferase that is encoded by a gene located in the class III region of the human major histocompatibility complex. J Biol Chem 1998;273:4096-105.

119. Calvo D, Gomez-Coronado D, Suarez Y, Lasuncion MA, Vega MA. Human CD36 is a high affinity receptor for the native lipoproteins HDL, LDL, and VLDL. J Lipid Res 1998;39:777-88.

120. Lehr S, Kotzka J, Avci H, et al. Effect of sterol regulatory element binding protein-1a on the mitochondrial protein pattern in human liver cells detected by 2D-DIGE. Biochemistry 2005;44:5117-28.

121. Li T, Kong X, Owsley E, Ellis E, Strom S, Chiang JY. Insulin regulation of cholesterol 7alpha-hydroxylase expression in human hepatocytes: roles of forkhead box O1 and sterol regulatory element-binding protein 1c. J Biol Chem 2006;281:28745-54.

122. Ishimoto K, Nakamura H, Tachibana K, et al. Sterol-mediated regulation of human lipin 1 gene expression in hepatoblastoma cells. J Biol Chem 2009;284:22195-205.

123. Kim JB, Spiegelman BM. ADD1/SREBP1 promotes adipocyte differentiation and gene expression linked to fatty acid metabolism. Genes Dev 1996;10:1096-107.

124. Wolins NE, Quaynor BK, Skinner JR, Schoenfish MJ, Tzekov A, Bickel PE. S3-12, Adipophilin, and TIP47 package lipid in adipocytes. J Biol Chem 2005;280:19146-55.

125. Granneman JG, Moore HP, Mottillo EP, Zhu Z. Functional interactions between Mldp (LSDP5) and Abhd5 in the control of intracellular lipid accumulation. J Biol Chem 2009;284:3049-57.

126. Zhu K, Ding X, Julotok M, Wilkinson BJ. Exogenous isoleucine and fatty acid shortening ensure the high content of anteiso-C15:0 fatty acid required for low-temperature growth of *Listeria monocytogenes*. Appl Environ Microbiol 2005;71:8002-7.

127. Hong C, Tontonoz P. Coordination of inflammation and metabolism by PPAR and LXR nuclear receptors. Curr Opin Genet Dev 2008.

128. Morales JR, Ballesteros I, Deniz JM, et al. Activation of liver X receptors promotes neuroprotection and reduces brain inflammation in experimental stroke. Circulation 2008;118:1450-9.

129. Gupta S, Pandak WM, Hylemon PB. LXR alpha is the dominant regulator of CYP7A1 transcription. Biochem Biophys Res Commun 2002;293:338-43.

130. Pandak WM, Hylemon PB, Ren S, et al. Regulation of oxysterol 7alpha-hydroxylase (CYP7B1) in primary cultures of rat hepatocytes. Hepatology 2002;35:1400-8.

131. Crestani M, De FE, Caruso D, et al. LXR (liver X receptor) and HNF-4 (hepatocyte nuclear factor-4): key regulators in reverse cholesterol transport. Biochem Soc Trans 2004;32:92-6.

132. Janowski BA, Willy PJ, Devi TR, Falck JR, Mangelsdorf DJ. An oxysterol signalling pathway mediated by the nuclear receptor LXR alpha. Nature 1996;383:728-31.

133. Korf H, Vander BS, Romano M, et al. Liver X receptors contribute to the protective immune response against Mycobacterium tuberculosis in mice. J Clin Invest 2009;119:1626-37.

134. Joseph SB, Castrillo A, Laffitte BA, Mangelsdorf DJ, Tontonoz P. Reciprocal regulation of inflammation and lipid metabolism by liver X receptors. Nat Med 2003;9:213-9.

135. Joseph SB, Bradley MN, Castrillo A, et al. LXR-dependent gene expression is important for macrophage survival and the innate immune response. Cell 2004;119:299-309.

136. Menzies-Gow A, Ying S, Sabroe I, et al. Eotaxin (CCL11) and eotaxin-2 (CCL24) induce recruitment of eosinophils, basophils, neutrophils, and macrophages as well as features of early- and late-phase allergic reactions following cutaneous injection in human atopic and nonatopic volunteers. J Immunol 2002;169:2712-8.

137. Reed BD, Charos AE, Szekely AM, Weissman SM, Snyder M. Genome-wide occupancy of SREBP1 and its partners NFY and SP1 reveals novel functional roles and combinatorial regulation of distinct classes of genes. PLoS Genet 2008;4:e1000133.

138. Higgins ME, Ioannou YA. Apoptosis-induced release of mature sterol regulatory element-binding proteins activates sterol-responsive genes. J Lipid Res 2001;42:1939-46.

139. Kim TH, Kim H, Park JM, et al. Interrelationship between liver X receptor alpha, sterol regulatory element-binding protein-1c, peroxisome proliferator-activated receptor gamma, and small heterodimer partner in the transcriptional regulation of glucokinase gene expression in liver. J Biol Chem 2009;284:15071-83.

140. Laffitte BA, Chao LC, Li J, et al. Activation of liver X receptor improves glucose tolerance through coordinate regulation of glucose metabolism in liver and adipose tissue. Proc Natl Acad Sci U S A 2003;100:5419-24.

141. Hummasti S, Laffitte BA, Watson MA, et al. Liver X receptors are regulators of adipocyte gene expression but not differentiation: identification of apoD as a direct target. J Lipid Res 2004;45:616-25.

142. Venkateswaran A, Laffitte BA, Joseph SB, et al. Control of cellular cholesterol efflux by the nuclear oxysterol receptor LXR alpha. Proc Natl Acad Sci U S A 2000;97:12097-102.

143. Terasaka N, Wang N, Yvan-Charvet L, Tall AR. High-density lipoprotein protects macrophages from oxidized low-density lipoprotein-induced apoptosis by promoting efflux of 7-ketocholesterol via ABCG1. Proc Natl Acad Sci U S A 2007;104:15093-8.

144. Ghisletti S, Huang W, Ogawa S, et al. Parallel SUMOylation-dependent pathways mediate gene- and signal-specific transrepression by LXRs and PPARgamma. Mol Cell 2007;25:57-70.

145. Torra IP, Ismaili N, Feig JE, et al. Phosphorylation of liver X receptor alpha selectively regulates target gene expression in macrophages. Mol Cell Biol 2008;28:2626-36.

146. Yamamoto T, Shimano H, Inoue N, et al. Protein kinase A suppresses sterol regulatory element-binding protein-1C expression via phosphorylation of liver X receptor in the liver. J Biol Chem 2007;282:11687-95.

147. Mo J, Fang SJ, Chen W, Blobe GC. Regulation of ALK-1 signaling by the nuclear receptor LXRbeta. J Biol Chem 2002;277:50788-94.

148. Bruhn KW, Marathe C, Maretti-Mira AC, et al. LXR deficiency confers increased protection against visceral Leishmania infection in mice. PLoS Negl Trop Dis 2010;4:e886.

149. Jakobsson T, Osman W, Gustafsson JA, Zilliacus J, Warnmark A. Molecular basis for repression of liver X receptor-mediated gene transcription by receptor-interacting protein 140. Biochem J 2007;405:31-9.

150. Prufer K, Boudreaux J. Nuclear localization of liver X receptor alpha and beta is differentially regulated. J Cell Biochem 2007;100:69-85.

151. Ghisletti S, Huang W, Jepsen K, et al. Cooperative NCoR/SMRT interactions establish a corepressor-based strategy for integration of inflammatory and anti-inflammatory signaling pathways. Genes Dev 2009;23:681-93.

152. Ghisletti S, Huang W, Ogawa S, et al. Parallel SUMOylation-dependent pathways mediate gene- and signal-specific transrepression by LXRs and PPARgamma. Mol Cell 2007;25:57-70.

153. Kaufmann SH. Immunity to intracellular bacteria. Annu Rev Immunol 1993;11:129-63.

154. Huysamen C, Willment JA, Dennehy KM, Brown GD. CLEC9A is a novel activation C-type lectin-like receptor expressed on BDCA3+ dendritic cells and a subset of monocytes. J Biol Chem 2008;283:16693-701.

155. Robinson MJ, Sancho D, Slack EC, LeibundGut-Landmann S, Reis e Sousa. Myeloid C-type lectins in innate immunity. Nat Immunol 2006;7:1258-65.

156. Lackmann M, Rajasekariah P, Iismaa SE, et al. Identification of a chemotactic domain of the pro-inflammatory S100 protein CP-10. J Immunol 1993;150:2981-91.

157. Nizet V, Ohtake T, Lauth X, et al. Innate antimicrobial peptide protects the skin from invasive bacterial infection. Nature 2001;414:454-7.

158. Kurosaka K, Chen Q, Yarovinsky F, Oppenheim JJ, Yang D. Mouse cathelin-related antimicrobial peptide chemoattracts leukocytes using formyl peptide receptor-like 1/mouse formyl peptide receptor-like 2 as the receptor and acts as an immune adjuvant. J Immunol 2005;174:6257-65.

159. Rosenberger CM, Gallo RL, Finlay BB. Interplay between antibacterial effectors: a macrophage antimicrobial peptide impairs intracellular Salmonella replication. Proc Natl Acad Sci U S A 2004;101:2422-7.

160. Selsted ME, Ouellette AJ. Mammalian defensins in the antimicrobial immune response. Nat Immunol 2005;6:551-7.

161. Lopez-Solanilla E, Gonzalez-Zorn B, Novella S, Vazquez-Boland JA, Rodriguez-Palenzuela P. Susceptibility of *Listeria monocytogenes* to antimicrobial peptides. FEMS Microbiol Lett 2003;226:101-5.

162. Arnett E, Lehrer RI, Pratikhya P, Lu W, Seveau S. Defensins enable macrophages to inhibit the intracellular proliferation of *Listeria monocytogenes*. Cell Microbiol 2010.

163. Skold M, Behar SM. The role of group 1 and group 2 CD1-restricted T cells in microbial immunity. Microbes Infect 2005;7:544-51.

164. Ugrinovic S, Brooks CG, Robson J, Blacklaws BA, Hormaeche CE, Robinson JH. H2-M3 major histocompatibility complex class Ib-restricted CD8 T cells induced by Salmonella enterica serovar Typhimurium infection recognize proteins released by Salmonella serovar Typhimurium. Infect Immun 2005;73:8002-8.

165. Kurlander RJ, Shawar SM, Brown ML, Rich RR. Specialized role for a murine class I-b MHC molecule in prokaryotic host defenses. Science 1992;257:678-9.

166. Kerksiek KM, Busch DH, Pilip IM, Allen SE, Pamer EG. H2-M3-restricted T cells in bacterial infection: rapid primary but diminished memory responses. J Exp Med 1999;190:195-204.

167. Gulden PH, Fischer P, III, Sherman NE, et al. A *Listeria monocytogenes* pentapeptide is presented to cytolytic T lymphocytes by the H2-M3 MHC class Ib molecule. Immunity 1996;5:73-9.

168. Lenz LL, Bevan MJ. H2-M3 restricted presentation of *Listeria monocytogenes* antigens. Immunol Rev 1996;151:107-21.

169. Comiskey M, Goldstein CY, De F, Sr., Mammolenti M, Newmark JA, Warner CM. Evidence that HLA-G is the functional homolog of mouse Qa-2, the Ped gene product. Hum Immunol 2003;64:999-1004.

170. Horuzsko A, Lenfant F, Munn DH, Mellor AL. Maturation of antigen-presenting cells is compromised in HLA-G transgenic mice. Int Immunol 2001;13:385-94.

171. Nicolae D, Cox NJ, Lester LA, et al. Fine mapping and positional candidate studies identify HLA-G as an asthma susceptibility gene on chromosome 6p21. Am J Hum Genet 2005;76:349-57.

172. Rodgers JR, Cook RG. MHC class Ib molecules bridge innate and acquired immunity. Nat Rev Immunol 2005;5:459-71.

173. Stroynowski I, Forman J. Novel molecules related to MHC antigens. Curr Opin Immunol 1995;7:97-102.

174. Cook RG, Leone B, Leone JW, Widacki SM, Zavell PJ. Characterization of T cell proliferative responses induced by anti-Qa-2 monoclonal antibodies. Cell Immunol 1992;144:367-81.

175. Driscoll J, Brown MG, Finley D, Monaco JJ. MHC-linked LMP gene products specifically alter peptidase activities of the proteasome. Nature 1993;365:262-4.

176. Sundback J, Achour A, Michaelsson J, Lindstrom H, Karre K. NK cell inhibitory receptor Ly-49C residues involved in MHC class I binding. J Immunol 2002;168:793-800.

177. Lowin-Kropf B, Held W. Positive impact of inhibitory Ly49 receptor-MHC class I interaction on NK cell development. J Immunol 2000;165:91-5.

178. Breitling R, Armengaud P, Amtmann A, Herzyk P. Rank products: a simple, yet powerful, new method to detect differentially regulated genes in replicated microarray experiments. FEBS Lett 2004;573:83-92.

179. Gilbert RJ. Cholesterol-dependent cytolysins. Adv Exp Med Biol 2010;677:56-66.

180. Turner J, Cho Y, Dinh NN, Waring AJ, Lehrer RI. Activities of LL-37, a cathelin-associated antimicrobial peptide of human neutrophils. Antimicrob Agents Chemother 1998;42:2206-14.

181. Gouin E, dib-Conquy M, Balestrino D, et al. The *Listeria monocytogenes* InlC protein interferes with innate immune responses by targeting the I{kappa}B kinase subunit IKK{alpha}. Proc Natl Acad Sci U S A 2010;107:17333-8.

182. Li G, Domenico J, Jia Y, Lucas JJ, Gelfand EW. NF-kappaB-dependent induction of cathelicidin-related antimicrobial peptide in murine mast cells by lipopolysaccharide. Int Arch Allergy Immunol 2009;150:122-32.

183. Martin S, Parton RG. Lipid droplets: a unified view of a dynamic organelle. Nat Rev Mol Cell Biol 2006;7:373-8.

184. Almeida PE, Silva AR, Maya-Monteiro CM, et al. Mycobacterium bovis bacillus Calmette-Guerin infection induces TLR2-dependent peroxisome proliferator-activated receptor gamma expression and activation: functions in inflammation, lipid metabolism, and pathogenesis. J Immunol 2009;183:1337-45.

185. Kumar Y, Cocchiaro J, Valdivia RH. The obligate intracellular pathogen Chlamydia trachomatis targets host lipid droplets. Curr Biol 2006;16:1646-51.

186. Bozza PT, Melo RC, Bandeira-Melo C. Leukocyte lipid bodies regulation and function: contribution to allergy and host defense. Pharmacol Ther 2007;113:30-49.

187. Bozza PT, Yu W, Cassara J, Weller PF. Pathways for eosinophil lipid body induction: differing signal transduction in cells from normal and hypereosinophilic subjects. J Leukoc Biol 1998;64:563-9.

188. Bozza PT, Weller PF. Arachidonyl trifluoromethyl ketone induces lipid body formation in leukocytes. Prostaglandins Leukot Essent Fatty Acids 2001;64:227-30.

189. Kim KH, Yoon JM, Choi AH, Kim WS, Lee GY, Kim JB. Liver X receptor ligands suppress ubiquitination and degradation of LXRalpha by displacing BARD1/BRCA1. Mol Endocrinol 2009;23:466-74.

190. Fontaine C, Rigamonti E, Nohara A, et al. Liver X receptor activation potentiates the lipopolysaccharide response in human macrophages. Circ Res 2007;101:40-9.

191. Wang YY, Dahle MK, Steffensen KR, et al. Liver X receptor agonist GW3965dose-dependently regulates lps-mediated liver injury and modulates posttranscriptional TNF-alpha production and p38 mitogen-activated protein kinase activation in liver macrophages. Shock 2009;32:548-53.

192. Zou T, Garifulin O, Berland R, Boyartchuk VL. *Listeria monocytogenes* infection induces pro-survival metabolic signaling in macrophages. Infect Immun 2011.

193. Anceriz N, Vandal K, Tessier PA. S100A9 mediates neutrophil adhesion to fibronectin through activation of beta2 integrins. Biochem Biophys Res Commun 2007;354:84-9.

194. Akerstrom B, Bjorck L. Bacterial surface protein L binds and inactivates neutrophil proteins S100A8/A9. J Immunol 2009;183:4583-92.

195. Sohnle PG, Hunter MJ, Hahn B, Chazin WJ. Zinc-reversible antimicrobial activity of recombinant calprotectin (migration inhibitory factor-related proteins 8 and 14). J Infect Dis 2000;182:1272-5.

196. Steinbakk M, Naess-Andresen CF, Lingaas E, Dale I, Brandtzaeg P, Fagerhol MK. Antimicrobial actions of calcium binding leucocyte L1 protein, calprotectin. Lancet 1990;336:763-5.

197. Kim KY, Kim BJ, YI GS. Reuse of imputed data in microarry analysis increases imputation efficiency. BMC Bioinformatics 2004;26:5-160.

198. Huang da W, Sherman BY, Lempicki RA. Systematic and integrative analysis of large gene list using DAVID bionformatics resources. Nature Protoc 2009;4:44-57.

199. Igal RA, Wang P, Coleman RA. Triacsin C blocks de novo synthesis of glycerolipids and cholesterol esters but not recycling of fatty acid into phospholipid: evidence for functionally separate pools of acyl-CoA. Biochem J. 1997;324:529-34.

200. Fujimoto Y, Itabe H, Kinoshita T, Homma KJ, Onoduka J, Mori M, Yamaguchi S, Makita M, Higashi Y, Yamashita A, Takano T. Involvement of ACSL in local synthesis of neutral lipids in cytoplasmic lipid droplets in human hepatocyte HuH-7. J Lipid Res. 2007;48:1280-92.

201. Furth EE, Sprecher H, Fisher EA, Fleishman HD, Laposata M. An in vitro model for essential fatty acid deficiency: HepG2 cells permanently maintained in lipid-free medium. J lipid Res. 1992;33:1719-26.

202. Parkes HA, Preston E, Wilks D, Ballesteros M, Carpenter L, Wood L, Kraegen EW, Furler SM, Cooney GJ. Overexpression of acyl-CoA synthetase-1 increases lipid deposition in hepatic (HepG2) cells and rodent liver in vivo. Am J Physiol Endocrinol Metab. 2006;291:E737-44.

203. Dixon JL, Ginsberg HN. Regulation of hepatic secretion of apolipoprotein B-containinglipoproteins: information obtained from cultured liver cells. J Lipid Res. 1993;34:167-79.

204. Bozza PT, Viola JP. Lipid droplets in inflammation and cancer. Prostaglandins Leukot Essent Fatty Acids. 2010;82:243-50.

205. Melo RC, D'Avila H, Fabrino DL, Almeida PE, Bozza TE. Macrophage lipid body induction by Chagas disease in vivo: putative intracellular domains for eicosanoid formation during infection. Tissue Cell. 2003;35:59-67.

206. Zou T, Garifulin O, Berland R, Boyartchuk VL. Listeria monocytogenes infection induces prosurvival metabolic signaling in macrophages. Infect Immun. 2011;79:1526-35.

207. Humann J, Bjordahl R, Andreasen K, Lenz LL. Expression of the p60 autolysin enhancesNK cell activation and is required for Listeria monocytogenes expansion in IFN-gamm-responsive mice. J Immunol. 2007;178:2401-14.

208. Izar B, Mannala GK, Mraheil MA, Chakraborty T, Hain T. microRNA Response to Listeria monocytogenes Infection in Epithelial Cells. Int J Mol Sci. 2012;13:1173-85.

209. Izar B, Mraheil MA, Hain T. Identification and role of regulatory non-coding RNAs in Listeria monocytogens. Int J Mol Sci. 2011;12:5070-9.

6. FIGURE AND TABLE LEGENDS

7. SUMMARY

In the present study, we investigated the liver specific response upon infection with *L. monocytogenes*, a model pathogen for Gram-positive infections over a period of 5days. We used whole genome microarray chips to determine the temporal transcriptome at five observation points. Relative mRNA levels were validated for a representative subset of genes by quantitative Real-Time PCR. In the analysis of these data we followed a strict methodology. The quality of microarray data was ensured by several measures, including quality control tools developed and optimized at our institution. The biological effects of differentially expressed genes were investigated and interpretation of these results was followed by confirmatory experiments.

Our global evaluation revealed a reciprocal regulation of lipid metabolism and inflammatory response. Lipogenic effects were present in the early phase of infection, which was temporally restricted to the first 24h post infection. A delayed inflammatory response appeared in the later phase of infection. Strikingly, a previous study investigating the hepatic acute phase reaction after LPS stimulation, which is a model for Gram-negative infection, revealed a converse dependence of lipid metabolism and immune response. Thus, we show for the first time the acute phase response in the liver is substantially different in Gram-positive versus Gram-negative bacteria.. A transcription factor, liver X receptor alpha (LXR-α) has been identified in previous studies as a key player in the integration of inflammatory response and lipid metabolism. We show that LXR-α-dependent transcription is distinctly regulated in *Listeria* infection. While LXR-α-controlled genes of lipid metabolism were upregulated early and a decay of mRNA levels was observed in the following phase of infection, inflammatory cytokines regulated by LXR-α displayed an inverse regulation, thus reflecting the global hepatic response. Selective gene regulation by LXR-α was shown to be due to posttranslational modifications, such as phosphorylation. Thus, we hypothesized, that distinct gene regulation by LXR-α in listerial but also in Gram—negative infections is mediated by these mechanisms. In order to investigate the role of LXR-α and modifications post infection, we used an *in vitro* model for hepatic infection by *Listeria* and hybridized cells with antibodies specific to LXR-α and to its phosphorylated form LXR-αP. Immunofluorescence revealed an accumulation of LXR-α in the nucleus, thus providing evidence for a role in hepatic infection. Furthermore, we showed that LXR-αP was present under basal conditions, which is consistent with

previous reports. LXR-αP displayed a transient changes in subcellular localization, indicating dynamic changes in the gene regulation by LXR-α/LXR-αP. Furthermore, lipogenic signals observed in the early phase of infection lead us to the conclusion that accumulation of neutral lipids occurs in infected cells. To confirm this hypothesis, we conducted a further study, staining cryosections of livers from infected mice with Oil Red O. In accordance with microarray results, we revealed for the first time that a strong accumulation of intracellular lipid droplets (LDs) occurs upon infection with a Gram-positive bacterium. LDs have been implicated in a number of biological effects, including inflammatory response and intracellular signaling pathways and thus contributing to host response. We were further interested in the origin of neutral lipids. For this purpose we measured the serum lipid profile of infected mice which revealed significant changes in triacylglycerol (TAG) concentrations and decreased cholinesterase (CHE) activity, a general marker for liver function. Decrease of TAG during the early phase of infection indicated that extracellular neutral lipids contributed to increased intracellular lipid levels and subsequently LD formation. In addition, enzymes that promote the synthesis of fatty acids were upregulated while enzymes for the degradation of lipids had lower mRNA levels. We concluded that both, intracellular as well as extracellular TAG contributed to the formation of LDs. However, the precise role of LDs in *Listeria* infection is subject of further investigation. In a subsequent *in vitro* infection model using HepG2 cells, we demonstrate that induction of LDs occurs in these cells. We also uncovered that LD synthesis following infection is induced thorugh an alternative pathway as HepG2 cells that were unable to synthesize through the classical pathway were shown to accumulate LDs in response to *L. monocytogenes*.
Furthermore, we show an intersection of innate and adaptive immunity in a global evaluation. Although this was observed in LPS models, again a reversed expression pattern was exhibited, supporting the conclusion of essential differences in hepatic response. Cell mediated immunity was present two days after infection and included neutrophil-Kupffer cell interaction, classical and non-classical MHC-Ib response by T cells and NK cells. Interestingly, the expression of anti-microbial effectors of the innate immune response, such as cathelecidine-related antimicrobial peptide (CRAMP) were seen significantly downregulated during the early infection phase. Decreased levels of CRAMP were also validated by qRT-PCR and possibly illustrate a listerial immunomodulatory effect in the host resulting in improved survival of the pathogen.

Although a possible association with LXR activity appeared likely based on known literature, this immunosuppressive effect by LXR is subject of investigation.

In conclusion, this work allows a unique insight into regulatory networks of several biological processes and interconnections following an infection with *L. monocytogenes*. Based on our results and by integration of known literature, LXR-α and related transcription factors are proposed to be fundamental for the regulation of hepatic and subsequently systemic response to pathogens.

8. ZUSAMMENFASSUNG

In der vorliegenden Studie untersuchten wir die Leber-spezifische Antwort nach Infektion mit *L. monocytogenes*, ein Gram-positives Modell-Bakterium über einen Zeitraum von 5 Tagen hinweg. Dabei machten wir Gebrauch von *whole genome microarrays,* mit dessen Hilfe das transiente Transkriptom zu fünf verschiedenen Zeitpunkten bestimmt wurde. Relative mRNA-Veränderungen wurden anhand einer repräsentativen Auswahl von Genen mittels quantitativer Echtzeit-PCR validiert. Die Analyse gewonnener Daten folgte einer strikten Methodologie. Die Qualität der microarray Daten wurde durch bioinformatische Programme, die an unserem Institut enwickelt und optimiert wurden, gesichert. Basierend auf dem Expressionsmuster differenziell regulierter Gene wurden biologische Rückschlüsse gezogen, die in subsequenten Experimenten untersucht und validiert wurden.

In der globalen Untersuchung der Leber-Antwort stellte sich ein reziprokes Verhältnis zwischen Fettstoffwechsel und inflammatorischer Antwort dar. Während lipogene Effekte innerhalb eines begrenzten Zeitraums deutlich wurden, schloss sich eine effektive Immunantwort mit einer gewissen Verzögerung der frühen Infektionsphase an. Interessanterweise wurde ein ähnliches Verhältnis der Genexpression zwischen beiden biologischen Prozess nach LPS – Stimulation, welches ein Modell für Infektionen mit Gram-negativen Erregern darstellt, beobachtet. Allerdings stellte sich dieses Verhältnis im Vergleich zu unseren Resultaten invers dar. Eine zentrale Rolle bei der Integration metabolischer und inflammatorischer Signale wurde für einen Transkriptionsfaktor, liver x receptor alpha (LXR-α), belegt. Wie in dieser Studie gezeigt wird, ändert sich Expression LXR-abhängiger Gene während des Experiments in einer feinregulierten Art und Weise. Während LXR-kontrollierte Gene des Metabolismus in der frühen Phase vermehrt exprimiert wurden und im Anschluss daran ein Abfall der mRNA Menge beobachtet wurde, verhielt es sich mit LXR-abhängigen Genen der Immunantwort reziprok, spiegelte somit das globale Expressionsmuster in der Leber wieder. Ein selektives Genexpressionsmuster durch LXR wurde in Versuchen beobachtet, in dessen Rahmen posttranslationelle Modifikationen, wie z.B. Phosphorylierung und führte uns zur Hypothese das solche Mechanismen in der Genregulation bei Listerien-Infektion, aber auch bei Gram-negativen Infektion eine Rolle spielen könnte. Um diese Hypothese zu untersuchen, führten wir eine *in vitro* Infektion, die als Modell für die Leberantwort dient, durch. Durch Antikörper-Hybridisierung und subsequente Immunfluoreszenz-

Analyse konnten wir nachweisen, dass LXR-α im Zellkern akkumuliert und somit Evidenz für eine Rolle in der hepatischen Immunantwort besteht. Weiterhin war LXR-αP unter Normalbedingungen nachweisebar und zeigte während des Infektionsgeschehens dynamische Veränderungen in der subzellulären Lokalisation. Somit wurde die Schlussfolgerung über die Beteiligung modifizierten LXR-α zu LXR-αP bestätigt.

Weiterhin beobachteten wir während des frühen Infektionsgeschehens die vermehrte Expression lipogener Gene. Wir folgerten, dass dieses Signal in der Akkumulation von Fetten in den Zellen stattfinden musste. Um dies zu bestätigen, wurden Kältegefrierschnitte infizierter Lebern mit Oil Red O gefärbt und im Einklang mit den microarray Daten konnten wir erstmals nachweisen, dass eine Infektion durch *L. moncoytogenes* zur Akkumulation von Fett-Tröpfchen, sogenannter lipid droplets (LDs) führt. LDs sind in einer Reihe biologischer Prozesse, wie z.B. bei der Regulation intrazellulärer Signalkaskaden und der inflammatorischen Antwort beteiligt. Wir waren weiterhin daran interessiert, den Herkunftsort der Fette zu bestimmen. Für diesen Zweck wurden Lipid-Profile im Serum infizierter Mäuse bestimmt, die folglich Konzentrationsänderungen der Serum-Triazylglyzeride (TAG) und der Cholinesterase (CHE), welche ein allgemeiner Parameter für die Synthesefunktion der Leber darstellt nachwiesen. Die verminderte TAG Serumkonzentration weist darauf hin, dass LDs durch extrazelluläre Neutralfette gespeist wurden. Zusätzlich beobachteten wir eine Hochregulation von Enzymen, die Fettsäuren synthetisieren und gleichzeitig eine Herunterregulation Fett-abbauender Enzyme. Wir zogen daher die Schlussfolgerung, dass TAGs des intra- und extrazellulären Kompartiments zur Bildung der LDs führten. Die genaue Rolle von LDs in der Pathogenese von *L. monocytogenes* wird währenddessen weiterhin von uns erforscht. In einem weiteren Experiment mit humanen HepG2 Zellen konnten wir die *in vivo* bestätigen und zeigen, dass *L. monocytogenes* auch in diesem Leberzellmodell LDs induziert. Wir zeigen weiterhin, dass die LD induction in Folge der Infektion einem alternativen pathway folgt, da HepG2 Zellen, in welchen der klassiche LD Syntheseweg blockiert wurde, eine LD Synthese - Induktion durch *L. monocytogenes* beobachtet wurde.

Zusätzliche Ergebnisse zeigten, dass sich innate und adaptive Immunantwort in dieser globalen Evaluation stark überschneiden. Obwohl Ähnliches bereits bei LPS-Modellen beobachtet wurde, handelte es sich dabei wiederum um ein reziprokes Expressionsmuster. Diese Beobachtung verdeutlicht wieder die substantiellen

Unterschiede zwischen Gram-positiven und –negativen Bakterien in der hepatischen Immunantwort. Die zellgesteuerte Immunantwort beginnt 2 Tage nach Infektion und beinhalten unter anderem Abwehrmechanismen durch Neutrophilen-Kupffer-Zell Interaktionen, Aktivierung von T- und NK-Zellen durch den klassischen und alternativen MHC-Ib – Signalweg. Interessanterweise wurden anti-mikrobielle Peptide, wie cathelecidine-related antimicrobial peptide (CRAMP) signifikant herunterregulliert. Verminderte CRAMP – mRNA Mengen wurden zusätzlich durch qRT-PCR bestätigt und könnten Hinweis auf die immunmodulatorische Fähigkeit von *L. monocytogenes* geben, die das eigene Überleben verbessern. Obwohl uns eine Assoziation mit LXR basierend auf bekannter Literatur wahrscheinlich ist, besteht kein nachgewiesener Zusammenhang und wird der zeitlich von uns in weiteren Experimenten untersucht.

Zusammenfassend bietet diese Arbeit einen einzigartigen Einblick in regulatorische Netzwerke verschiedenster biologischer Funktionen und Interaktionen nach Infektion mit *L. monocytogenes*. Basierend auf diesen Resultaten und eingebettet in bekannte Literatur, stellt sich eine herausragende Rolle für LXR und verwandte Transkriptionsfaktoren bei der hepatischen und subsequent auch systemischen Immunantwort dar.

9. LIST OF OWN PUBLICATIONS AND POSTERS

PUBLICATIONS

1. Izar B, Mraheil MA, Hain T. "Identification and Role of Regulatory Non-Coding RNAs in *Listeria monocytogenes*." *Int J Mol Sci*. 2011; 12(8):5070-5079.

This publication was supported by the open access publication fonds of the Justus Liebig University Giessen

2. Izar B, Mannala GK, Mraheil MA, Chakraborty T, Hain T. "microRNA Response to *Listeria monocytogenes* Infection in Epithelial Cells." *Int J Mol Sci*. 2012;13(1):1173-85.

This publication was supported by the open access publication fonds of the Justus Liebig University Giessen.

3. Seifart Gomes C*, **Izar B***, Pazan F*, Mohamed W, Mraheil MA, Mukherjee K, Billion A, Aharonowitz Y, Chakraborty T, Hain T. "Universal Stress Proteins Are Important for Oxidative and Acid Stress Resistance and Growth of *Listeria monocytogenes* EGD-e *In vitro* and *In vivo*. " *PLoS ONE* 2011 6(9): e24965. doi:10.1371/journal.pone.0024965.

***equally contributing author**

This publication was supported by the open access publication fonds of the Justus Liebig University Giessen.

4. Izar B, Rai A, Raghuram K, Rotruck J, Carpenter J. "Comparison of Devices Used for Stent-Assisted Coiling of Intracranial Aneurysms." *PLoS ONE* 2011 6(9): e24875. doi:10.1371/journal.pone.0024875

5. Hain T, Ghai R, Billion A, Kuenne CT, Steinweg C, **Izar B**, Mohamed W, Mraheil M, Domann E, Schaffrath S, Kärst U, Goesmann A, Oehm S, Pühler A, Merkl R, Vorwerk S, Glaser P, Garrido P, Rusniok C, Buchrieser C, Goebel W, Chakraborty T**.** "Comparative genomics and transcriptomics of lineages I, II, and III strains of *Listeria monocytogenes*." *BMC Genomics*. 2012 Apr 24;13(1):144

6. Theruvath TP, **Izar B,** McGillicuddy J, Stewar E, Reuben A, Chavin KD. "Hepatocellular adenoma in men: a rare cause for liver resection. " *Am Surg*. 2011 Mar;77(3):373-6

7. Izar B, Tchatalbachev S, Mohamed W, Parzan F, Chakraborty T, Hossain H. "Transient reciprocal alteration of metabolic system and immune defense during hepatic APR upon listerial infection" (manuscript in preperation)

8. Hilgendorff A, Tchatalbachev S, Gortner L, Kreuder J, Klein M, Billon A, **Izar B**, Maier M, Adelhelm J, Chakraborty T, Hossain H. "Deciphering the pathophysiology of early onset infection in preterm infants by whole blood gene expression profiling. " (under review *PLoS Medicine*)

POSTERS

1. **Izar B**, Hossain H., Chakraborty T. (2007, November). ”The organ specific host response upon challange with *Listeria monocytogenes.*” 5th Nationales Genom Forschugsnetz (NGFN) Symposium; Heidelberg, Germany.

2. **Izar B**, Rai A, Carpenter J, Raghuram K (2010, July). ”Progressive occlusion in aneurysms treated with stent assisted coiling. Flow diversion? ” Society of NeuroInterventional Surgery 7th Annual Meeting; Carlsbad, CA.

3. **Izar B**, Mueller vom Hagen J, Mei M, Hazen-Martin D, Vela M (2010, October) ”Evaluation of inter-observer agreement shows that intercellular space distance is a reliable marker of GERD.” American College of Gastroenterology; San Antonio, TX.

4. Rai A, Hobbs G., Meadows J, **Izar B**, Carpenter J, Raghuram K. (2010, July). ”Collateral blood supply as predictor of good clinical outcome in patients undergoing endovascular treatment for acute ischemic stroke.” Society of NeuroInterventional Surgery 7th Annual Meeting; Carlsbad, CA.

5. Theruvath TP, **Izar B**, Stewart E, Reuben A, Chavin KD. (2010, February). ”Hepatocellular adenoma in men: a rare cause for liver resection.” Surgical Annual Congress; Savannah, GA.

6. Giese S, Hossain H, **Izar B**, Chakraborty T, Chatalbachev S, Willecke K,Guillou F,Cavalcanti M, Bergmann M, Brehm R. ”The effect of a Sertoli cell-specific knockout of connexin 43 on testicular gene expression in prepubertal mice.” Presented at

1. XXVIIIth EAVA Congress – Paris, France (2010), Foreword. Anatomia, Histologia, Embryologia, 39: 243–259

2. Reproduction in Domestic Animals (43rd Annual Conference of Physiology and Pathology of Reproduction and 35th Mutual Conference on Veterinary and Human Reproductive Medicine. 24-26 February 2010, Munich) 45 Supplement 1, Abstract 35 p:14

3. 105th Society of Anatomy Congress, Hamburg, Germany.

10. ERKLÄRUNG

Erklärung zur Dissertation

„Hiermit erkläre ich, dass ich die vorliegende Arbeit selbständig und ohne unzulässige Hilfe oder Benutzung anderer als der angegebenen Hilfsmittel angefertigt habe. Alle Textstellen, die wörtlich oder sinngemäß aus veröffentlichten oder nichtveröffentlichten Schriften entnommen sind, und alle Angaben, die auf mündlichen Auskünften beruhen, sind als solche kenntlich gemacht. Bei den von mir durchgeführten und in der Dissertation erwähnten Untersuchungen habe ich die Grundsätze guter wissenschaftlicher Praxis, wie sie in der „Satzung der Justus-Liebig-Universität Gießen zur Sicherung guter wissenschaftlicher Praxis“ niedergelegt sind, eingehalten sowie ethische, datenschutzrechtliche und tierschutzrechtliche Grundsätze befolgt. Ich versichere, dass Dritte von mir weder unmittelbar noch mittelbar geldwerte Leistungen für Arbeiten erhalten haben, die im Zusammenhang mit dem Inhalt der vorgelegten Dissertation stehen, oder habe diese nachstehend spezifiziert. Die vorgelegte Arbeit wurde weder im Inland noch im Ausland in gleicher oder ähnlicher Form einer anderen Prüfungsbehörde zum Zweck einer Promotion oder eines anderen Prüfungsverfahrens vorgelegt. Alles aus anderen Quellen und von anderen Personen übernommene Material, das in der Arbeit verwendet wurde oder auf das direkt Bezug genommen wird, wurde als solches kenntlich gemacht. Insbesondere wurden alle Personen genannt, die direkt und indirekt an der Entstehung der vorliegenden Arbeit beteiligt waren. Mit der Überprüfung meiner Arbeit durch eine Plagiatserkennungssoftware bzw. ein internetbasiertes Softwareprogramm erkläre ich mich einverstanden.“

_____ _____

Ort, Datum Unterschrift

11. ACKNOWLEDGEMENTS

I would like to thank my mentor Prof. Dr. Trinad Chakraborty for having given me the chance to work on this project, for his continous support and scientific guidance when I was “meandering”. I also thank him for his advices regarding my career plans and for always taking the time to discuss my thoughts despite his busy appointment calendar.

I sincerely want to thank my supervisor Dr. Hamid Hossain for all the daily help he provided throughout the years. I thank him for constructive scientific and personal words of advice.

I would like to thank Svetlin and Walid for techniqcal support and for performing the mouse infection experiments which are the back bone of this work. I thank Juri, Farhad, Martin and Rafed for technical support. I would like to thank Prof. Dr. Andreas Meinhardt and Eva Schneider for their help with the cryosections and Dr. Späth for support with the clinical biochemistry.

Thanks to all team members at the Gaffkystraße, especially Dr. Torsten Hain for advice and interesting collaborations, Andre Billon for great coffee and Irene Ruocco for help with administrative issues.

I thank my parents for making medical school possible, for support in all my plans and I would like to dedicate this work to them. My warm thanks go to my brothers Piyer and Robert and my sister Nicme for supporting my plans.

12. APPENDIX

Table S1: List of genes that were significantly deregulated on at least 1 time point. Significant regulation was defined as a deregulation with an FDR <0.05. The table shows the unique gene ID, the official gene symbol and name. FDR and FC are given for each gene for each time point.

Gene ID	Symbol	Gene Name	4h p.i.		1d p.i.		2d p.i.		3d p.i.		5d p.i.	
			FDR	FC	FDR	FC	FDR	FC	FDR	FC	FDR	FC
NM_175628	A2m	Alpha-2-macroglobulin	0.00	-3.83	0.98	0.37	1.23	-0.92	0.79	-1.25	1.11	-0.98
NM_153145	Abca8a	ATP-binding cassette, sub-family A (ABC1), member 8a	0.81	1.18	0.83	-1.22	0.00	-3.14	0.31	-1.55	0.06	-2.17
NM_019552	Abcb10	ATP-binding cassette, sub-family B (MDR/TAP), member 10	0.41	1.36	0.02	2.20	0.01	3.41	0.01	2.89	0.14	2.10
NM_008830	Abcb4	ATP-binding cassette, sub-family B (MDR/TAP), member 4	1.17	-1.04	1.09	-1.10	0.03	-2.40	0.34	-1.53	0.59	-1.46
NM_008576	Abcc1	ATP-binding cassette, sub-family C (CFTR/MRP), member 1	1.19	-0.95	0.98	1.13	0.42	1.53	0.02	2.43	0.04	2.89
AK030123	Abcc12	ATP-binding cassette, sub-family C (CFTR/MRP), member 12	1.16	-0.93	0.76	1.24	0.01	3.49	0.11	1.86	0.32	1.67
NM_011994	Abcd2	ATP-binding cassette, sub-family D (ALD), member 2	0.90	-1.12	0.16	-1.61	0.00	-5.42	0.10	-1.84	0.30	-1.66
NM_009593	Abcg1	ATP-binding cassette, sub-family G (WHITE), member 1	1.19	-0.98	1.20	-0.96	0.05	2.28	0.00	3.28	0.01	4.52
NM_030239	Abcg3	ATP-binding cassette, sub-family G (WHITE), member 3	1.18	-0.96	0.17	-1.60	0.31	1.61	0.02	2.60	0.06	2.61
NM_138955	Abcg4	ATP-binding cassette, sub-family G (WHITE), member 4	0.81	1.20	0.84	1.20	0.02	2.59	0.56	1.37	0.48	1.51
NM_031884	Abcg5	ATP-binding cassette, sub-family G (WHITE), member 5	1.14	-1.05	0.79	-1.21	0.05	-2.02	0.90	-1.21	1.11	-1.05
NM_026180	Abcg8	ATP-binding cassette, sub-family G (WHITE), member 8	0.95	-1.13	0.42	-1.38	0.04	-2.11	0.40	-1.48	1.04	-1.13
NM_198018	Abr	Active BCR-related gene	1.16	-1.07	0.93	1.16	0.05	2.30	0.01	3.07	0.01	3.84
BE630391	Acacb	Acetyl-Coenzyme A carboxylase beta	0.60	1.28	0.01	2.30	0.01	3.16	0.00	4.14	0.03	3.27
NM_012006	Acot1	Acyl-CoA thioesterase 1	0.00	3.01	0.52	-1.29	0.43	-1.49	0.13	-1.77	0.73	-1.28
NM_134246	Acot3	Acyl-CoA thioesterase 3	0.01	2.36	0.46	1.33	0.00	-4.17	0.00	-4.52	0.00	-7.53
NM_134247	Acot4	Acyl-CoA thioesterase 4	0.13	1.62	1.09	-1.01	0.02	-2.54	0.87	-1.18	0.40	-1.59
NM_153807	Acsf2	Acyl-CoA synthetase family member 2	1.19	-1.00	1.18	-0.91	0.00	-6.17	0.04	-2.10	0.22	-1.76
NM_007981	Acsl1	Acyl-CoA synthetase long-chain family member 1	1.17	-1.04	0.29	-1.47	0.00	-3.20	0.36	-1.52	0.27	-1.71
NM_146197	Acsm2	Acyl-CoA synthetase medium-chain family member 2	0.02	-2.10	0.00	-2.72	0.03	2.51	0.02	2.50	0.05	2.72
NM_031404	Actl6b	Actin-like 6B	1.02	-1.04	0.45	1.36	0.93	1.18	0.04	2.23	1.09	-0.92
NM_009612	Acvrl1	Activin A receptor, type II-like 1	0.61	1.27	0.29	1.46	0.02	2.87	0.00	4.08	0.00	6.59
NM_007398	Ada	Adenosine deaminase	1.17	-0.95	0.95	1.16	0.01	3.09	0.01	2.91	0.09	2.40

NM_009350	Adad1	Adenosine deaminase domain containing 1 (testis specific)	0.00	-2.89	0.00	-2.63	0.00	7.68	0.00	8.27	0.01	4.54
NM_019655	Adar	Adenosine deaminase, RNA-specific	0.31	-1.41	0.01	2.31	0.02	2.62	0.26	1.60	0.38	1.60
W09272	Add3	Adducin 3 (gamma)	1.19	-0.98	0.01	-2.18	0.01	3.18	0.04	2.28	0.19	1.99
NM_009633	Adra2b	Adrenergic receptor, alpha 2b	0.50	-1.31	0.06	-1.82	0.02	-2.51	0.35	-1.51	0.78	-1.34
NM_027373	Afap1	Actin filament associated protein 1	0.22	1.44	0.23	1.48	0.04	2.41	0.15	1.80	0.25	1.88
NM_027827	Afmid	Arylformamidase	0.49	1.33	1.14	-1.06	0.00	-3.20	1.20	-1.02	0.85	-1.28
NM_018862	Agpat1	1-acylglycerol-3-phosphate O-acyltransferase 1 (lysophosphatidic acid acyltransferase, alpha)	0.02	2.03	1.19	-0.93	0.00	-9.28	0.00	-17.70	0.00	-17.07
NM_018743	Agpat6	1-acylglycerol-3-phosphate O-acyltransferase 6 (lysophosphatidic acid acyltransferase, zeta)	0.02	2.03	0.06	1.80	0.00	-6.12	0.00	-3.40	0.00	-4.88
NM_027907	Agxt2l1	Alanine-glyoxylate aminotransferase 2-like 1	1.18	-0.93	0.90	-1.16	0.00	-11.50	0.09	-1.86	0.13	-1.94
AV252993	Ahctf1	AT hook containing transcription factor 1	1.09	-1.10	0.42	-1.39	0.04	-2.23	0.68	-1.30	0.89	-1.25
AI115981	AI132487	Expressed sequence AI132487	0.52	-1.32	0.46	-1.38	0.38	-1.56	0.02	-2.34	0.32	-1.67
AI430742	AI430742	Membrane-associated ring finger (C3HC4) 8	0.05	1.85	0.50	1.34	0.35	1.58	0.61	1.32	1.01	-1.08
NM_019467	Aif1	Allograft inflammatory factor 1	1.03	-1.12	0.35	1.41	0.00	4.37	0.00	5.72	0.00	7.05
NM_153779	Aifm2	Apoptosis-inducing factor, mitochondrion-associated 2	0.03	1.96	0.13	1.64	1.24	-0.87	0.22	1.63	0.80	1.29
NM_009647	Ak3l1	Adenylate kinase 3-like 1	0.01	2.28	0.16	1.62	0.04	2.44	0.19	1.72	0.60	1.45
BB546359	Ak5	Adenylate kinase 5	0.04	-1.88	0.10	-1.70	0.01	3.55	0.00	4.25	0.00	6.93
AK029555	Ak7	Adenylate kinase 7	1.17	-1.01	0.01	2.23	0.00	29.35	0.00	29.79	0.00	27.64
NM_009731	Akr1b7	Aldo-keto reductase family 1, member B7	0.15	1.57	0.92	1.16	0.17	-1.77	0.00	3.93	0.04	2.96
AF124142	Akt3	Thymoma viral proto-oncogene 3	0.91	-1.14	0.16	1.62	0.09	2.11	0.02	2.47	0.12	2.25
NM_020559	Alas1	Aminolevulinic acid synthase 1	0.04	1.86	1.17	-0.96	0.01	2.96	0.03	2.37	0.02	3.40
AK007822	Aldh1l1	Aldehyde dehydrogenase 1 family, member L1	0.09	1.67	0.60	1.30	0.30	1.60	0.03	2.34	0.34	1.66
NM_007437	Aldh3a2	Aldehyde dehydrogenase family 3, subfamily A2	0.37	1.39	1.17	-1.03	0.01	-2.65	1.21	-0.93	0.79	-1.32
NM_026316	Aldh3b1	Aldehyde dehydrogenase 3 family, member B1	1.14	-1.09	1.19	-1.01	0.03	2.56	0.01	2.76	0.08	2.51
AK016920	Aldoart2	Aldolase 1, A isoform, retrogene 2	0.12	-1.58	0.40	-1.31	0.06	-2.06	0.00	-2.93	0.09	-2.06
NM_009663	Alox5ap	Arachidonate 5-lipoxygenase activating protein	0.79	1.20	1.18	-1.01	0.03	2.53	0.01	2.93	0.00	5.08
AK018401	Alpk1	Alpha-kinase 1	0.39	1.38	1.00	1.09	0.00	3.51	0.04	2.20	0.10	2.25
NM_007431	Alpl	Alkaline phosphatase, liver/bone/kidney	0.03	1.95	0.16	1.60	0.05	-2.17	0.01	-2.69	0.01	-2.79
NM_007442	Alx4	Aristaless-like homeobox 4	1.19	-1.00	1.05	-1.12	0.47	-1.47	0.03	-2.13	0.44	-1.56
NM_172669	Ambra1	Autophagy/beclin 1 regulator 1	1.16	-1.06	0.38	-1.43	0.41	-1.52	0.04	-2.10	0.59	-1.45

NM_033603	Amn	Amnionless	1.19	-0.96	0.41	-1.35	0.50	-1.45	0.05	-2.01	1.06	-1.14
NM_011923	Angptl2	Angiopoietin-like 2	0.98	1.12	0.44	-1.39	0.05	-2.18	0.02	-2.24	0.27	-1.71
NM_020581	Angptl4	Angiopoietin-like 4	0.63	1.27	0.05	-1.87	0.00	-3.43	0.08	-1.93	0.59	-1.45
BC023373	Angptl7	Angiopoietin-like 7	0.69	1.16	0.02	-2.07	0.67	1.31	0.44	1.48	0.45	1.58
NM_172922	Ankk1	Ankyrin repeat and kinase domain containing 1	1.14	-1.06	0.96	-1.15	0.03	-2.33	0.08	-1.91	0.01	-2.83
BB313429	Anln	Anillin, actin binding protein	0.02	2.03	0.26	1.50	0.00	-3.72	0.00	-4.08	0.02	-2.56
BI730314	Anxa5	Annexin A5	0.01	-2.36	0.01	-2.25	0.38	-1.55	0.50	-1.42	0.86	-1.29
NM_012054	Aoah	Acyloxyacyl hydrolase	0.01	2.36	0.47	1.28	0.02	2.63	0.01	2.82	0.03	3.13
NM_007461	Apba2	Amyloid beta (A4) precursor protein-binding, family A, member 2	0.57	1.30	1.18	-0.96	0.05	-2.20	0.54	1.38	1.00	-1.15
AF020313	Apbb1ip	Amyloid beta (A4) precursor protein-binding, family B, member 1 interacting protein	0.41	-1.39	0.46	-1.39	0.19	1.81	0.01	2.80	0.02	3.38
NM_146104	Aph1a	Anterior pharynx defective 1a homolog (C. elegans)	0.90	1.17	1.19	-1.02	0.03	-2.36	0.58	-1.37	0.84	-1.30
NM_009691	Aplp2	Amyloid beta (A4) precursor-like protein 2	1.17	-1.06	1.20	-0.98	0.03	-2.38	0.66	-1.34	0.81	-1.32
NM_007468	Apoa4	Apolipoprotein A-IV	0.94	-1.16	0.53	-1.33	0.26	-1.66	0.02	-2.29	0.11	-2.03
NM_138310	Apob48r	Apolipoprotein B48 receptor	0.81	-1.22	0.82	-1.23	0.68	1.34	0.03	2.34	0.06	2.71
NM_030255	Apobec3	Apolipoprotein B mRNA editing enzyme, catalytic polypeptide 3	1.19	-0.95	0.13	1.65	0.01	3.29	0.00	3.44	0.05	2.76
NM_175087	Aqp6	Aquaporin 6	0.35	-1.35	1.16	-0.96	0.00	4.35	0.04	2.23	0.07	2.47
NM_007474	Aqp8	Aquaporin 8	0.01	-2.34	0.10	-1.71	0.01	-2.88	0.00	-4.15	0.00	-3.16
NM_009705	Arg2	Arginase type II	0.17	1.56	0.00	-2.89	0.01	-2.59	0.16	-1.71	0.88	-1.20
NM_181416	Arhgap11a	Rho GTPase activating protein 11A	0.98	-1.10	0.82	-1.21	0.07	2.13	0.00	3.30	0.03	3.37
AW213816	Arhgap19	Rho GTPase activating protein 19	0.57	-1.32	0.00	-2.64	0.26	1.71	0.55	1.40	1.06	-1.10
NM_029270	Arhgap24	Rho GTPase activating protein 24	0.25	-1.47	0.57	-1.29	0.02	-2.50	0.52	-1.39	0.24	-1.74
CB527909	Arhgap26	Rho GTPase activating protein 26	0.48	-1.32	0.30	-1.44	0.02	-2.59	0.11	-1.79	0.02	-2.54
AW060237	Arhgef17	Rho guanine nucleotide exchange factor (GEF) 17	1.19	-0.97	0.82	1.21	0.01	3.05	0.33	1.53	0.48	1.50
AK016806	Arhgef7	Rho guanine nucleotide exchange factor (GEF7)	0.00	-2.46	0.03	-1.99	0.05	-2.13	0.56	-1.38	0.60	-1.44
BC027152	Arid5a	AT rich interactive domain 5A (MRF1-like)	0.02	2.02	0.00	6.68	1.18	-1.07	1.15	-1.09	0.52	-1.49
NM_177337	Arl11	ADP-ribosylation factor-like 11	1.02	-1.15	0.24	-1.50	1.25	-0.89	0.02	2.52	0.02	3.38
NM_007489	Arntl	Aryl hydrocarbon receptor nuclear translocator-like	0.07	-1.74	0.01	-2.37	0.47	1.47	1.16	-0.94	1.08	-0.97
NM_029690	Arpm1	Actin related protein M1	1.18	-0.97	1.16	-0.91	0.02	2.76	0.67	1.32	0.40	1.58
NM_028710	Arsg	Arylsulfatase G	0.92	-1.19	0.04	-1.96	0.03	-2.37	0.24	-1.63	0.47	-1.52

NM_007490	Art2a	ADP-ribosyltransferase 2a	1.16	-1.06	1.19	-0.99	0.64	1.36	0.22	1.65	0.03	3.17
NM_175731	Asah3	Alkaline ceramidase 1	0.04	1.91	0.15	-1.62	0.17	1.91	0.05	2.25	0.21	2.04
BB153889	Ascl1	Achaete-scute complex homolog 1 (Drosophila)	1.19	-0.98	1.20	-0.92	0.01	2.94	1.21	-1.00	1.10	-1.06
NM_024184	Asf1b	ASF1 anti-silencing function 1 homolog B (S. cerevisiae)	0.66	1.18	0.09	-1.76	0.00	4.51	0.00	4.74	0.04	3.17
NM_012055	Asns	Asparagine synthetase	1.12	-1.08	0.76	1.23	0.00	7.41	0.05	2.18	0.09	2.38
NM_009791	Aspm	Asp (abnormal spindle)-like, microcephaly associated (Drosophila)	0.87	-1.08	1.00	1.06	0.04	2.50	0.01	2.90	0.03	3.26
NM_027435	Atad2	ATPase family, AAA domain containing 2	1.19	-0.94	0.65	-1.26	0.10	2.03	0.02	2.47	0.17	2.05
NM_007498	Atf3	Activating transcription factor 3	0.43	1.36	0.04	1.92	0.20	-1.75	0.06	-1.98	0.04	-2.24
BC018510	Atf7ip2	Activating transcription factor 7 interacting protein 2	0.03	2.01	0.05	1.89	0.02	2.72	0.01	3.20	0.03	3.31
NM_015804	Atp11a	ATPase, class VI, type 11A	1.17	-1.02	0.55	1.31	0.03	2.47	0.33	1.53	0.35	1.65
NM_009723	Atp2b2	ATPase, Ca++ transporting, plasma membrane 2	1.17	-0.92	0.46	-1.30	0.01	-2.73	1.06	-1.11	0.51	-1.50
NM_011596	Atp6v0a2	ATPase, H+ transporting, lysosomal V0 subunit A2	0.00	-2.46	0.04	-1.88	1.18	-1.02	1.18	-1.05	1.12	-0.90
AY517482	Atp6v0d2	ATPase, H+ transporting, lysosomal V0 subunit D2	0.70	1.21	0.57	-1.31	0.02	-2.41	0.88	-1.22	1.08	-1.02
NM_133699	Atp6v1c2	ATPase, H+ transporting, lysosomal V1 subunit C2	0.18	1.53	0.02	2.12	0.10	2.01	0.18	1.71	0.42	1.60
NM_009727	Atp8a1	ATPase, aminophospholipid transporter (APLT), class I, type 8A, member 1	0.66	1.13	0.02	2.21	0.00	10.48	0.00	3.87	0.01	4.17
NM_177809	AU042651	Expressed sequence AU042651	0.67	1.25	0.08	1.74	0.06	2.21	0.03	2.38	1.13	-0.91
NM_011497	Aurka	Aurora kinase A	0.70	-1.15	0.02	-2.15	1.28	-0.94	0.25	1.61	0.44	1.55
NM_009465	Axl	AXL receptor tyrosine kinase	1.18	-1.02	0.99	-1.16	0.11	1.99	0.04	2.23	0.05	2.77
NM_145229	AY074887	CDNA sequence AY074887	0.63	-1.28	0.05	-1.88	0.05	-2.17	0.00	-3.08	0.10	-2.00
NM_025874	AY919875	Perilipin 5	0.01	2.32	0.91	1.15	0.00	14.54	0.00	15.98	0.00	19.96
NM_020283	B3galt1	UDP-Gal:betaGlcNAc beta 1,3-galactosyltransferase, polypeptide 1	0.96	-1.09	0.95	1.07	0.01	3.10	0.38	1.53	0.10	2.31
R74827	B4galnt4	Beta-1,4-N-acetyl-galactosaminyl transferase 4	1.17	-0.94	1.16	-0.91	0.00	5.54	0.00	3.93	0.06	2.67
NM_146045	B4galt7	Xylosylprotein beta1,4-galactosyltransferase, polypeptide 7 (galactosyltransferase I)	1.15	-0.91	0.70	1.26	0.00	10.41	0.00	4.42	0.03	3.07
NM_130862	Baiap2	Brain-specific angiogenesis inhibitor 1-associated protein 2	0.24	-1.51	0.04	-1.93	0.53	-1.43	0.01	-2.54	0.14	-1.90
NM_025833	Baiap2l1	BAI1-associated protein 2-like 1	0.01	2.46	0.04	1.94	0.00	-8.67	0.01	-2.65	0.00	-3.97
NM_007523	Bak1	BCL2-antagonist/killer 1	1.14	-1.08	0.15	1.59	0.04	2.37	0.03	2.29	0.20	1.91
CF581094	Banp	BTG3 associated nuclear protein	0.36	1.40	0.02	-2.11	0.09	2.06	0.07	2.06	0.42	1.62
NM_016767	Batf	Basic leucine zipper transcription factor, ATF-like	0.03	1.79	0.08	1.72	0.01	-2.63	0.00	-4.29	0.00	-3.32

NM_028967	Batf2	Basic leucine zipper transcription factor, ATF-like 2	1.15	-1.06	0.00	11.05	0.01	-2.80	0.03	-2.13	0.02	-2.64
NM_030060	Batf3	Basic leucine zipper transcription factor, ATF-like 3	0.98	-1.17	0.00	2.66	0.00	-3.25	0.03	-2.20	0.05	-2.22
AA612185	Baz1a	Bromodomain adjacent to zinc finger domain 1A	0.10	1.66	0.93	1.11	0.00	3.66	0.00	3.28	0.02	3.49
NM_181857	BC023882	DNA polymerase N	0.06	-1.79	0.14	-1.64	0.00	-3.56	0.02	-2.24	0.04	-2.27
AK173168	BC067047	Phosphatidylinositol-3,4,5-trisphosphate-dependent Rac exchange factor 1	1.07	-1.12	1.19	-0.96	0.13	1.91	0.01	2.95	0.01	4.45
NM_153172	BC107230	Protease, serine, 45	0.06	-1.76	0.32	-1.39	0.18	-1.75	0.01	-2.49	0.14	-1.92
NM_016707	Bcl11a	B-cell CLL/lymphoma 11A (zinc finger protein)	1.02	-1.09	0.48	1.35	0.15	1.93	0.45	1.47	0.04	3.01
NM_027208	Bdh2	3-hydroxybutyrate dehydrogenase, type 2	0.89	1.16	0.90	1.14	0.04	-2.23	0.81	-1.20	0.19	-1.81
X55573	Bdnf	Brain derived neurotrophic factor	0.04	1.86	0.36	1.40	0.06	2.18	0.04	2.26	0.31	1.70
NM_007544	Bid	BH3 interacting domain death agonist	0.95	1.15	0.01	2.18	0.05	2.33	0.23	1.70	1.10	-1.03
NM_009668	Bin1	Bridging integrator 1	0.56	1.30	0.75	-1.23	0.03	-2.33	0.54	-1.39	0.59	-1.45
NM_009689	Birc5	Baculoviral IAP repeat-containing 5	0.45	-1.28	0.02	-2.16	0.47	1.47	0.24	1.62	0.58	1.43
NM_008528	Blnk	B-cell linker	0.54	-1.29	0.02	-2.07	0.03	2.58	0.01	2.85	0.05	2.75
NM_007559	Bmp8b	Bone morphogenetic protein 8b	0.77	1.23	0.01	2.22	0.01	3.19	0.01	3.11	0.04	3.04
BU605018	Bpi	Bactericidal permeablility increasing protein	0.04	-1.89	0.01	-2.27	0.51	1.44	0.17	1.71	0.33	1.66
AK033205	Brip1	BRCA1 interacting protein C-terminal helicase 1	0.89	-1.16	0.04	1.92	0.00	58.24	0.00	43.10	0.00	58.89
NM_007567	Bsn	Bassoon	0.18	-1.53	0.00	-2.99	0.00	20.54	0.00	17.87	0.00	15.34
NM_009763	Bst1	Bone marrow stromal cell antigen 1	0.73	1.16	0.41	1.35	0.02	2.75	0.05	2.22	0.15	2.13
BU709551	Btbd9	BTB (POZ) domain containing 9	0.19	1.54	0.66	1.27	0.04	-2.25	0.72	-1.29	0.72	-1.37
NM_007570	Btg2	B-cell translocation gene 2, anti-proliferative	0.21	1.51	0.09	1.76	0.02	2.80	0.40	1.51	0.32	1.71
NM_013482	Btk	Bruton agammaglobulinemia tyrosine kinase	0.25	-1.45	0.64	1.21	0.02	2.92	0.00	4.01	0.01	4.01
NM_007572	C1qa	Complement component 1, q subcomponent, alpha polypeptide	1.18	-1.00	1.00	1.09	0.45	1.50	0.08	2.03	0.03	3.19
NM_009777	C1qb	Complement component 1, q subcomponent, beta polypeptide	1.18	-1.01	0.98	1.12	0.08	2.11	0.02	2.52	0.03	3.23
NM_007574	C1qc	Complement component 1, q subcomponent, C chain	0.99	-1.16	1.17	-1.05	0.22	1.76	0.03	2.35	0.04	2.92
NM_026979	C1qtnf2	C1q and tumor necrosis factor related protein 2	0.45	-1.35	0.96	-1.16	0.05	-2.19	0.15	-1.74	0.75	-1.36
NM_013484	C2	Complement component 2 (within H-2S)	0.75	1.22	1.11	-1.05	0.04	2.36	0.07	2.04	0.61	1.44
BY741494	C2cd3	C2 calcium-dependent domain containing 3	1.18	-0.94	0.92	-1.18	0.03	-2.37	0.11	-1.83	0.17	-1.84
NM_009779	C3ar1	Complement component 3a receptor 1	0.50	1.32	0.14	-1.64	0.01	-2.83	0.38	-1.49	0.55	1.47
NM_016704	C6	Complement component 6	1.19	-0.99	0.84	-1.23	0.09	2.06	0.02	2.64	0.00	5.68
NM_172578	C79407	Expressed sequence C79407	0.13	-1.63	0.03	-2.00	0.00	7.87	0.01	2.79	0.05	2.64

U31629	Cabc1	Chaperone, ABC1 activity of bc1 complex like (S. pombe)	0.18	-1.55	0.35	-1.43	0.01	-2.67	0.33	-1.54	0.21	-1.78
NM_178721	Cadm2	Cell adhesion molecule 2	0.00	-2.60	0.20	-1.56	0.19	1.76	0.33	1.55	0.23	1.81
BB027891	Calcoco1	Calcium binding and coiled coil domain 1	1.14	-1.08	0.53	-1.34	0.04	-2.24	0.06	-1.96	0.11	-1.99
NM_018782	Calcrl	Calcitonin receptor-like	0.53	-1.33	0.02	-2.09	0.00	3.77	0.00	3.39	0.05	2.83
NM_028500	Calr3	Calreticulin 3	0.98	1.07	0.28	-1.46	0.01	-2.92	0.22	-1.64	0.05	-2.26
NM_023813	Camk2d	Calcium/calmodulin-dependent protein kinase II, delta	0.88	1.17	0.37	1.40	0.06	2.22	0.02	2.42	0.15	2.07
AK013788	Camk2n2	Calcium/calmodulin-dependent protein kinase II inhibitor 2	0.10	1.69	0.42	1.40	0.04	2.40	0.89	-1.03	0.60	1.45
NM_145358	Camkk2	Calcium/calmodulin-dependent protein kinase kinase 2, beta	0.42	-1.36	0.01	-2.30	0.02	2.81	0.01	2.79	0.09	2.38
NM_009921	Camp	Cathelicidin antimicrobial peptide	0.40	1.39	0.01	-2.30	0.62	-1.37	0.26	-1.61	0.14	-1.92
BC025636	Caprin2	Caprin family member 2	0.03	-1.94	0.05	-1.89	0.33	1.63	0.42	1.50	0.92	1.25
NM_009799	Car1	Carbonic anhydrase 1	0.82	1.21	1.10	-1.03	0.00	-3.41	0.03	-2.14	0.23	-1.74
NM_009800	Car11	Carbonic anhydrase 11	0.96	1.07	1.12	-1.04	0.04	-2.27	0.00	-2.79	0.45	-1.54
NM_178396	Car12	Carbonic anyhydrase 12	0.59	1.26	0.71	1.25	0.01	3.27	0.42	1.48	0.78	1.33
NM_024495	Car13	Carbonic anhydrase 13	1.15	-1.07	0.60	1.28	0.00	3.94	0.00	3.99	0.02	3.67
NM_011797	Car14	Carbonic anhydrase 14	0.79	1.20	0.72	1.25	0.00	-8.30	0.52	-1.38	0.45	-1.54
NM_007606	Car3	Carbonic anhydrase 3	1.18	-0.96	0.74	-1.23	0.00	-6.16	0.77	-1.27	0.45	-1.54
NM_175362	Card11	Caspase recruitment domain family, member 11	0.54	1.29	0.02	2.09	0.01	-2.94	0.27	-1.57	0.29	-1.69
AK009937	Cars2	Cysteinyl-tRNA synthetase 2 (mitochondrial)(putative)	1.08	-1.13	0.13	-1.67	0.01	-2.65	0.00	-2.96	0.02	-2.51
NM_009807	Casp1	Caspase 1	1.18	-0.95	0.04	1.95	0.00	-4.67	1.17	-0.92	0.96	-1.03
NM_007609	Casp4	Caspase 4, apoptosis-related cysteine peptidase	0.94	1.16	0.00	2.63	0.00	10.48	0.00	6.98	0.05	2.84
BB680906	Casp6	Caspase 6	0.91	1.16	0.99	1.13	0.03	-2.33	0.21	-1.65	0.44	-1.55
AI415274	Casp7	Caspase 7	0.11	1.62	0.12	1.65	0.01	3.21	0.03	2.31	0.23	1.81
NM_173023	Catsperb	Cation channel, sperm-associated, beta	0.88	1.18	0.74	1.25	0.02	2.75	0.50	1.42	1.12	-0.84
NM_016900	Cav2	Caveolin 2	0.89	1.16	0.05	-1.89	0.35	1.61	0.18	1.77	0.32	1.75
AK082029	Ccdc88a	Coiled coil domain containing 88A	0.45	-1.34	0.01	-2.21	0.00	4.50	0.01	3.34	0.08	2.61
NM_027411	Ccdc99	Coiled-coil domain containing 99	0.08	-1.73	0.11	-1.70	0.11	2.07	0.03	2.55	0.25	1.92
NM_011331	Ccl12	Chemokine (C-C motif) ligand 12	1.13	-0.90	0.05	1.84	0.00	5.26	0.01	2.78	0.63	1.39
NM_011888	Ccl19	Chemokine (C-C motif) ligand 19	1.02	-1.15	0.06	1.82	0.00	4.36	0.00	3.24	0.06	2.69
NM_011333	Ccl2	Chemokine (C-C motif) ligand 2	0.94	-1.16	0.00	3.00	0.81	-1.27	0.84	1.23	0.70	-1.36
NM_019577	Ccl24	Chemokine (C-C motif) ligand 24	1.14	-0.89	1.20	-0.96	0.01	3.05	0.00	4.62	0.00	6.97

NM_013653	Ccl5	Chemokine (C-C motif) ligand 5	1.18	-1.03	0.46	-1.38	0.08	2.14	0.00	4.82	0.00	12.10
NM_013654	Ccl7	Chemokine (C-C motif) ligand 7	0.30	-1.22	0.00	5.22	0.00	4.13	0.00	5.13	0.02	3.68
NM_021443	Ccl8	Chemokine (C-C motif) ligand 8	0.00	3.74	0.00	6.52	0.59	1.39	0.08	1.96	0.38	1.71
AV259618	Ccna1	Cyclin A1	0.05	1.89	0.13	1.71	1.05	-1.15	0.39	1.48	0.87	1.27
NM_009828	Ccna2	Cyclin A2	0.12	-1.61	0.00	-3.01	0.00	3.63	0.00	3.23	0.13	2.15
NM_172301	Ccnb1	Cyclin B1	0.70	-1.23	0.02	-2.08	1.17	-1.09	0.19	-1.69	0.79	-1.32
NM_007630	Ccnb2	Cyclin B2	0.07	-1.76	0.00	-4.48	0.00	11.69	0.00	8.55	0.00	5.78
NM_007631	Ccnd1	Cyclin D1	0.76	-1.16	0.02	-2.18	0.01	3.21	0.04	2.23	0.52	1.52
NM_009830	Ccne2	Cyclin E2	0.01	2.37	0.79	1.06	0.50	1.41	0.50	1.41	0.23	2.03
NM_009912	Ccr1	Chemokine (C-C motif) receptor 1	1.19	-0.93	0.45	1.38	0.00	3.73	0.00	3.21	0.03	3.15
NM_009915	Ccr2	Chemokine (C-C motif) receptor 2	0.88	-1.16	0.82	-1.21	0.02	2.73	0.00	3.57	0.00	5.42
NM_009914	Ccr3	Chemokine (C-C motif) receptor 3	1.11	-1.04	0.00	-4.31	0.39	-1.55	1.04	-1.09	0.59	-1.46
NM_145700	Ccrl1	Chemokine (C-C motif) receptor-like 1	0.88	1.18	0.00	-2.72	0.12	-1.90	0.99	-1.13	0.08	-2.06
NM_017466	Ccrl2	Chemokine (C-C motif) receptor-like 2	1.01	-1.13	0.00	3.18	0.27	1.68	0.66	1.28	0.00	5.66
NM_009841	Cd14	CD14 antigen	0.65	1.25	0.88	-1.21	0.00	14.68	0.01	2.97	0.00	5.18
AK036455	Cd226	CD226 antigen	1.17	-0.91	1.12	-0.88	1.26	-0.90	1.18	-0.87	0.00	15.05
NM_021893	Cd274	CD274 antigen	0.14	-1.60	0.00	24.39	0.28	1.63	0.99	1.18	1.13	-0.98
NM_199225	Cd300c	CD300C antigen	1.18	-1.01	1.15	-1.05	1.27	-0.92	0.27	1.59	0.04	2.88
NM_172050	Cd300e	CD300e antigen	1.16	-1.05	0.88	1.17	0.04	2.41	0.00	4.68	0.00	7.19
NM_145634	Cd300lf	CD300 antigen like family member F	1.11	-1.10	0.59	1.30	0.04	2.35	0.01	2.70	0.03	3.32
NM_007643	Cd36	CD36 antigen	1.01	-1.13	0.03	-2.00	0.77	1.30	0.75	1.27	1.12	-0.90
L11332	Cd38	CD38 antigen	0.26	1.45	1.19	-0.95	0.00	3.99	0.00	3.76	0.02	3.77
NM_009850	Cd3g	CD3 antigen, gamma polypeptide	1.16	-1.04	1.10	-1.10	0.22	1.75	0.02	2.59	0.01	3.92
NM_011611	Cd40	CD40 antigen	0.46	-1.30	0.00	3.70	0.07	2.22	0.10	1.99	0.13	2.20
NM_007649	Cd48	CD48 antigen	1.02	-1.16	1.20	-0.97	0.02	2.65	0.00	4.03	0.01	4.95
NM_010016	Cd55	CD55 antigen	0.73	1.24	1.15	-1.07	0.12	1.93	0.04	2.24	0.19	1.93
NM_009690	Cd5l	CD5 antigen-like	0.97	-1.18	0.43	-1.42	0.25	1.71	0.02	2.53	0.01	3.89
NM_009854	Cd7	CD7 antigen	1.19	-0.97	1.09	-1.09	0.71	1.33	0.02	2.55	0.01	4.70
NM_010545	Cd74	CD74 antigen (invariant polypeptide of major histocompatibility complex, class II antigen-associated)	1.04	-1.12	0.60	1.30	0.00	6.98	0.00	9.64	0.00	12.82
NM_008339	Cd79b	CD79B antigen	0.64	-1.26	0.02	2.07	0.55	-1.37	0.58	-1.30	0.40	-1.58

NM_009855	Cd80	CD80 antigen	0.11	1.69	0.34	1.47	0.22	1.78	0.03	2.34	0.05	2.75
NM_013489	Cd84	CD84 antigen	1.11	-1.09	0.02	-2.16	1.07	-1.18	0.65	1.33	0.19	1.92
NM_009858	Cd8b1	CD8 antigen, beta chain 1	0.76	1.10	0.85	-1.15	0.58	1.41	0.12	1.91	0.01	4.48
NM_023223	Cdc20	Cell division cycle 20 homolog (S. cerevisiae)	0.06	-1.79	0.00	-3.72	0.23	1.76	0.18	1.76	0.30	1.76
NM_178347	Cdc23	CDC23 (cell division cycle 23, yeast, homolog)	0.29	-1.43	0.48	-1.33	1.04	-1.09	0.03	-2.23	0.14	-1.92
NM_009860	Cdc25c	Cell division cycle 25 homolog C (S. pombe)	0.97	-1.16	0.00	-3.86	0.77	1.31	0.13	1.81	0.17	1.97
NM_007659	Cdc2a	Cell division cycle 2 homolog A (S. pombe)	1.10	-1.04	0.00	-2.91	0.56	-1.42	0.01	-2.72	0.01	-3.12
NM_026772	Cdc42ep2	CDC42 effector protein (Rho GTPase binding) 2	0.79	1.22	0.04	1.92	0.21	1.76	0.09	1.93	0.40	1.59
NM_009862	Cdc45l	Cell division cycle 45 homolog (S. cerevisiae)-like	0.47	1.34	1.19	-1.00	0.16	1.84	0.03	2.39	0.31	1.79
NM_011799	Cdc6	Cell division cycle 6 homolog (S. cerevisiae)	1.05	-1.06	0.63	-1.28	0.01	3.05	0.00	4.29	0.03	3.34
NM_013538	Cdca3	Cell division cycle associated 3	0.23	-1.48	0.01	-2.24	0.00	3.62	0.03	2.35	1.12	-0.93
NM_026410	Cdca5	Cell division cycle associated 5	1.02	-1.04	0.75	-1.19	0.09	2.10	0.02	2.67	0.16	2.16
NM_146040	Cdca7l	Cell division cycle associated 7 like	1.19	-0.95	1.20	-0.93	0.22	1.76	0.01	2.91	0.02	3.80
NM_009864	Cdh1	Cadherin 1	0.02	-2.07	0.72	-1.24	1.22	-1.10	0.12	1.84	0.35	1.64
NM_019707	Cdh13	Cadherin 13	1.10	-1.07	0.19	-1.59	0.01	-2.81	0.19	-1.70	0.20	-1.80
NM_007662	Cdh15	Cadherin 15	1.19	-0.93	0.04	1.89	0.00	4.20	0.01	2.86	0.25	1.82
NM_007665	Cdh3	Cadherin 3	0.01	-2.20	1.04	-1.04	0.57	1.37	0.64	1.30	1.12	-0.90
NM_172853	Cdh7	Cadherin 7, type 2	1.16	-1.04	0.08	-1.78	0.01	-2.82	0.49	-1.42	0.02	-2.64
BY183267	Cdk6	Cyclin-dependent kinase 6	0.76	1.23	0.55	-1.28	0.68	1.34	0.04	2.26	0.03	3.00
NM_007669	Cdkn1a	Cyclin-dependent kinase inhibitor 1A (P21)	0.10	1.61	0.65	-1.15	0.00	4.93	0.14	1.89	0.00	5.46
NM_009877	Cdkn2a	Cyclin-dependent kinase inhibitor 2A	0.05	1.86	0.19	1.58	0.25	-1.58	0.67	-1.17	0.95	1.16
U19596	Cdkn2c	Cyclin-dependent kinase inhibitor 2C (p18, inhibits CDK4)	0.42	-1.39	0.01	-2.24	0.11	1.98	0.11	1.91	0.39	1.64
AK033341	Cdkn3	Cyclin-dependent kinase inhibitor 3	0.15	-1.59	0.00	-2.65	0.00	5.68	0.00	5.17	0.01	4.41
NM_026014	Cdt1	Chromatin licensing and DNA replication factor 1	1.17	-0.94	0.02	-2.06	0.01	2.97	0.12	1.88	0.26	1.79
NM_001014996	Cenpj	Centromere protein J	1.00	-1.16	0.01	2.39	0.00	4.03	0.00	3.52	0.06	2.70
AV271338	Cep250	Centrosomal protein 250	0.53	1.26	0.04	2.00	1.09	-1.02	0.11	1.89	0.58	1.48
NM_028760	Cep55	Centrosomal protein 55	0.23	-1.49	0.00	4.91	0.04	-2.28	1.21	-0.90	1.13	-0.88
NM_021456	Ces1	Carboxylesterase 1	1.18	-1.03	0.83	-1.21	0.00	-6.41	0.26	-1.59	0.85	-1.29
NM_145603	Ces2	Carboxylesterase 2	0.83	-1.06	0.57	-1.24	0.02	-2.38	1.04	-1.05	0.68	-1.35
NM_053200	Ces3	Carboxylesterase 3	0.37	1.39	1.18	-1.02	0.00	-4.46	1.16	-1.07	1.01	-1.17

NM_133960	Ces6	Carboxylesterase 6	1.19	-0.95	1.17	-0.99	0.05	-2.20	0.83	-1.22	1.10	-1.05
NM_007685	Cfc1	Cripto, FRL-1, cryptic family 1	1.19	-0.96	0.84	1.20	0.00	3.50	0.81	1.25	0.73	1.34
AI613807	Cfh	Complement component factor h	0.31	-1.45	0.26	-1.50	0.05	2.37	0.37	1.53	0.33	1.76
X12905	Cfp	Complement factor properdin	1.18	-0.94	1.17	-1.06	0.17	1.85	0.03	2.34	0.01	3.79
BC023116	Cgref1	Cell growth regulator with EF hand domain 1	0.15	1.57	1.02	-1.04	0.01	3.45	0.97	1.17	1.13	-0.86
NM_009890	Ch25h	Cholesterol 25-hydroxylase	0.15	1.62	0.05	2.18	0.00	7.92	0.00	6.49	0.01	4.51
NM_013733	Chaf1a	Chromatin assembly factor 1, subunit A (p150)	1.18	-0.95	0.71	-1.25	0.10	2.01	0.02	2.50	0.11	2.35
NM_029716	Chn1	Chimerin (chimaerin) 1	0.30	1.41	0.86	1.14	0.01	3.05	0.03	2.37	0.65	1.46
NM_144803	Chrna2	Cholinergic receptor, nicotinic, alpha polypeptide 2 (neuronal)	0.01	2.28	0.87	1.13	0.00	4.37	0.00	4.21	0.03	3.36
NM_178373	Cidec	Cell death-inducing DFFA-like effector c	1.17	-1.05	1.18	-1.05	1.23	-1.06	0.19	1.70	0.04	2.82
NM_007575	Ciita	Class II transactivator	1.06	-1.12	0.00	7.32	1.20	-1.05	1.21	-0.93	0.17	1.98
NM_007709	Cited1	Cbp/p300-interacting transactivator with Glu/Asp-rich carboxy-terminal domain 1	0.92	1.14	1.05	-1.10	0.79	-1.30	0.00	-3.62	0.12	-2.01
NM_016674	Cldn1	Claudin 1	0.02	-2.13	0.01	-2.42	1.22	-1.04	0.00	6.66	0.01	3.98
NM_019985	Clec1b	C-type lectin domain family 1, member b	0.96	1.09	0.43	-1.41	0.16	1.89	0.02	2.48	0.02	3.48
NM_053109	Clec2d	C-type lectin domain family 2, member d	0.75	1.20	0.44	1.36	0.05	2.27	0.03	2.33	0.70	1.38
NM_016751	Clec4f	C-type lectin domain family 4, member f	1.19	-1.00	1.07	-1.11	0.96	1.18	0.08	2.02	0.03	3.12
NM_020001	Clec4n	C-type lectin domain family 4, member n	1.19	-1.01	0.25	-1.53	1.28	-0.99	0.51	1.40	0.03	3.11
AW318446	Clec9a	C-type lectin domain family 9, member a	0.03	1.97	0.14	1.66	0.00	-12.95	0.00	-9.22	0.00	-4.03
NM_033444	Clic1	Chloride intracellular channel 1	0.89	-1.18	0.78	1.23	0.02	2.73	0.02	2.50	0.08	2.48
NM_175554	Clspn	Claspin homolog (Xenopus laevis)	0.41	1.24	0.08	-1.70	0.03	2.68	0.00	4.01	0.06	2.87
NM_016760	Clta	Clathrin, light polypeptide (Lca)	0.00	-3.20	0.00	-2.65	0.91	-1.14	0.93	1.11	0.21	1.90
NM_008153	Cmklr1	Chemokine-like receptor 1	1.18	-0.97	0.05	1.89	0.00	11.09	0.00	3.32	0.01	3.77
NM_053097	Cml3	Camello-like 3	0.24	1.48	0.01	-2.36	0.16	-1.80	0.06	-1.95	0.47	-1.50
NM_133978	Cmtm7	CKLF-like MARVEL transmembrane domain containing 7	1.18	-1.03	1.15	-0.92	0.00	3.67	0.02	2.63	0.05	2.82
NM_016877	Cnot4	CCR4-NOT transcription complex, subunit 4	0.94	1.13	1.08	-1.07	0.01	-2.76	0.58	-1.34	0.78	-1.32
NM_016673	Cntfr	Ciliary neurotrophic factor receptor	0.01	2.30	0.73	-1.16	0.83	-1.28	0.09	-1.86	0.10	-2.02
NM_009930	Col3a1	Collagen, type III, alpha 1	0.13	-1.62	0.04	-1.99	0.47	1.50	0.40	1.53	1.03	-1.03
NM_009931	Col4a1	Collagen, type IV, alpha 1	0.47	-1.34	0.95	-1.18	0.04	2.44	0.65	1.34	1.13	-0.85
NM_199473	Col8a2	Collagen, type VIII, alpha 2	0.02	2.07	0.47	1.34	0.02	2.71	0.06	2.06	0.12	2.16
NM_173422	Colec10	Collectin sub-family member 10	1.17	-1.04	1.19	-1.03	0.01	-2.79	0.12	-1.78	1.13	-1.02

AK038221	Colq	Collagen-like tail subunit (single strand of homotrimer) of asymmetric acetylcholinesterase	0.98	-1.06	1.10	-0.97	0.00	-5.99	0.82	-1.18	0.21	-1.79
NM_009898	Coro1a	Coronin, actin binding protein 1A	1.15	-1.07	0.86	1.20	0.02	2.65	0.00	3.39	0.01	3.87
BE992497	Cox10	COX10 homolog, cytochrome c oxidase assembly protein, heme A: farnesyltransferase (yeast)	0.08	1.73	0.01	2.34	0.47	-1.48	1.00	-1.13	0.10	-2.13
NM_053091	Cox4i2	Cytochrome c oxidase subunit IV isoform 2	0.27	1.46	0.32	1.49	0.06	2.27	0.01	3.21	0.44	1.65
NM_009943	Cox6a2	Cytochrome c oxidase, subunit VI a, polypeptide 2	0.58	-1.29	0.13	-1.66	0.05	-2.19	0.00	-3.41	0.02	-2.49
NM_009944	Cox7a1	Cytochrome c oxidase, subunit VIIa 1	0.12	1.62	0.02	2.16	0.54	-1.42	1.22	-0.94	1.12	-0.89
NM_007760	Crat	Carnitine acetyltransferase	0.03	1.95	0.25	1.52	1.26	-0.93	0.07	2.03	0.78	1.33
X90648	Crkl	V-crk sarcoma virus CT10 oncogene homolog (avian)-like	0.03	1.97	0.50	1.33	0.71	1.33	0.84	1.25	0.69	1.41
BB272988	Crmp1	Collapsin response mediator protein 1	0.37	1.36	0.76	-1.20	0.16	-1.82	0.01	-2.53	0.05	-2.21
NM_023733	Crot	Carnitine O-octanoyltransferase	0.05	-1.84	0.03	-1.99	0.30	1.65	0.24	1.65	0.88	1.29
AW258263	Cryl1	Crystallin, lambda 1	0.14	-1.59	0.00	-2.44	1.22	-1.06	0.60	1.34	1.13	-0.90
NM_144942	Csad	Cysteine sulfinic acid decarboxylase	0.03	-1.94	0.01	-2.21	0.11	2.03	0.02	2.64	0.03	3.24
NM_007781	Csf2rb2	Colony stimulating factor 2 receptor, beta 2, low-affinity (granulocyte-macrophage)	1.18	-0.98	0.39	1.40	0.01	3.42	0.01	3.18	0.00	5.02
NM_007784	Csn1s1	Casein alpha s1	0.48	-1.34	0.03	-1.97	1.09	-1.12	0.68	1.30	0.89	1.24
NM_009973	Csn1s2b	Casein alpha s2-like B	1.19	-0.96	0.73	-1.24	0.00	-3.20	0.01	-2.44	0.09	-2.04
NM_007791	Csrp1	Cysteine and glycine-rich protein 1	1.19	-0.97	0.72	1.23	0.01	3.25	0.01	2.92	0.10	2.33
NM_028836	Ctbs	Chitobiase, di-N-acetyl-	0.99	1.12	0.25	1.50	0.02	2.66	0.12	1.87	0.28	1.76
NM_007796	Ctla2a	Cytotoxic T lymphocyte-associated protein 2 alpha	0.71	1.24	1.18	-1.03	0.01	3.24	0.00	3.43	0.01	4.43
NM_009843	Ctla4	Cytotoxic T-lymphocyte-associated protein 4	0.09	1.69	0.03	2.04	0.04	-2.19	0.48	-1.34	0.97	-1.11
NM_026906	Cts3	Cathepsin 3	0.64	-1.26	0.87	-1.18	0.61	-1.40	0.04	-2.05	0.20	-1.81
NM_009982	Ctsc	Cathepsin C	0.28	-1.46	0.83	-1.23	0.28	1.65	0.05	2.18	0.13	2.13
NM_007799	Ctse	Cathepsin E	0.86	1.15	0.89	1.16	0.00	-3.56	0.02	-2.30	0.29	-1.70
NM_019861	Ctsf	Cathepsin F	0.95	1.16	1.19	-1.01	0.02	-2.48	0.45	-1.45	1.03	-1.18
NM_021281	Ctss	Cathepsin S	1.05	-1.14	1.02	-1.16	0.11	2.01	0.02	2.50	0.01	3.86
NM_008411	Cuzd1	CUB and zona pellucida-like domains 1	0.03	2.02	0.05	1.97	0.40	-1.54	0.05	2.15	0.26	1.82
BY651162	Cx3cr1	Chemokine (C-X3-C) receptor 1	0.04	-1.89	0.00	-4.00	0.06	2.21	0.08	1.98	0.50	1.53
NM_008176	Cxcl1	Chemokine (C-X-C motif) ligand 1	0.23	1.48	0.00	15.69	0.18	-1.77	0.13	-1.78	0.07	-2.12
NM_021274	Cxcl10	Chemokine (C-X-C motif) ligand 10	0.59	-1.26	0.00	21.25	1.21	-1.05	0.19	1.72	0.02	3.47

NM_019494	Cxcl11	Chemokine (C-X-C motif) ligand 11	0.75	-1.22	0.00	7.41	0.12	1.97	0.02	2.44	0.05	2.80
NM_018866	Cxcl13	Chemokine (C-X-C motif) ligand 13	0.91	1.16	0.35	-1.42	0.29	-1.64	0.25	-1.62	0.05	2.81
NM_019568	Cxcl14	Chemokine (C-X-C motif) ligand 14	0.01	-2.38	0.14	-1.67	0.01	3.11	0.05	2.19	0.05	2.76
NM_009140	Cxcl2	Chemokine (C-X-C motif) ligand 2	0.97	-1.15	0.48	1.34	0.02	2.66	0.10	1.94	0.16	2.06
NM_008599	Cxcl9	Chemokine (C-X-C motif) ligand 9	1.18	-0.97	0.00	9.55	0.01	3.23	0.08	1.98	0.55	1.47
NM_009911	Cxcr4	Chemokine (C-X-C motif) receptor 4	0.61	1.25	0.25	-1.49	0.61	1.40	0.42	1.49	0.03	3.04
NM_030712	Cxcr6	Chemokine (C-X-C motif) receptor 6	1.18	-0.97	1.20	-0.99	0.02	2.64	0.01	3.18	0.06	2.66
NM_007805	Cyb561	Cytochrome b-561	1.18	-1.01	1.13	-0.88	0.00	8.46	0.03	2.33	0.06	2.71
NM_007806	Cyba	Cytochrome b-245, alpha polypeptide	1.16	-0.93	0.52	1.32	0.01	3.48	0.00	4.41	0.00	5.60
NM_009993	Cyp1a2	Cytochrome P450, family 1, subfamily a, polypeptide 2	1.17	-1.00	1.18	-0.99	0.02	-2.38	1.21	-0.97	0.90	-1.20
AK020848	Cyp20a1	Cytochrome P450, family 20, subfamily A, polypeptide 1	0.73	-1.24	0.05	-1.88	0.00	-4.39	0.00	-3.77	0.03	-2.44
NM_007811	Cyp26a1	Cytochrome P450, family 26, subfamily a, polypeptide 1	0.00	3.08	0.00	2.75	0.83	-1.29	0.31	-1.56	0.48	-1.53
CR521972	Cyp2a22	Cytochrome P450, family 2, subfamily a, polypeptide 22	0.15	1.58	0.33	1.45	0.00	-3.48	0.09	-1.87	0.23	-1.75
AI528246	Cyp2b13	Cytochrome P450, family 2, subfamily b, polypeptide 9	0.70	-1.23	1.20	-0.97	0.00	-3.60	0.27	-1.58	0.03	-2.42
NM_010000	Cyp2b9	Cytochrome P450, family 2, subfamily b, polypeptide 9	0.37	-1.38	1.20	-0.96	0.01	-2.84	0.17	-1.71	0.04	-2.35
NM_007815	Cyp2c29	Cytochrome P450, family 2, subfamily c, polypeptide 29	1.17	-0.93	1.18	-1.02	0.04	-2.26	0.47	-1.42	0.94	-1.23
NM_010001	Cyp2c37	Cytochrome P450, family 2, subfamily c, polypeptide 50	1.11	-1.07	1.09	-1.09	0.00	-5.53	0.13	-1.79	0.51	-1.50
BF660028	Cyp2c38	Cytochrome P450, family 2, subfamily c, polypeptide 38	0.98	-1.09	0.78	-1.18	0.01	-2.60	0.14	-1.74	0.26	-1.71
NM_001001446	Cyp2c44	Cytochrome P450, family 2, subfamily c, polypeptide 44	1.17	-1.05	0.94	-1.17	0.01	-2.63	0.86	-1.24	0.37	-1.61
NM_206537	Cyp2c54	Cytochrome P450, family 2, subfamily c, polypeptide 54	0.71	-1.22	0.54	-1.31	0.00	-6.23	0.07	-1.95	0.26	-1.72
NM_001024719	Cyp2c67	Cytochrome P450, family 2, subfamily c, polypeptide 67	0.15	-1.58	0.10	-1.70	0.50	-1.44	0.28	-1.59	0.01	-2.66
NM_019823	Cyp2d22	Cytochrome P450, family 2, subfamily d, polypeptide 22	1.17	-0.93	0.92	-1.17	0.02	-2.40	0.66	-1.33	0.83	-1.30
BI246674	Cyp2d9	Cytochrome P450, family 2, subfamily d, polypeptide 9	0.75	1.16	0.60	-1.24	0.22	-1.66	0.05	-2.06	0.72	-1.35
NM_028979	Cyp2j9	Cytochrome P450, family 2, subfamily j, polypeptide 9	0.97	-1.15	0.56	1.29	0.01	-2.73	0.39	-1.48	1.08	-1.13
BB667884	Cyp2r1	Cytochrome P450, family 2, subfamily r, polypeptide 1	0.92	-1.16	0.06	-1.86	0.02	-2.56	0.00	-3.58	0.01	-2.79
NM_018887	Cyp39a1	Cytochrome P450, family 39, subfamily a, polypeptide 1	0.02	2.15	0.64	1.28	0.09	2.11	0.17	1.79	0.11	2.25
NM_007818	Cyp3a11	Cytochrome P450, family 3, subfamily a, polypeptide 11	1.10	-1.05	0.94	1.11	0.00	-3.46	0.51	-1.38	1.03	-1.16
AI787320	Cyp3a13	Cytochrome P450, family 3, subfamily a, polypeptide 13	0.04	1.86	0.01	2.37	0.14	-1.83	1.15	-1.05	0.71	-1.38
NM_007820	Cyp3a16	Cytochrome P450, family 3, subfamily a, polypeptide 16	0.26	1.46	0.00	-3.37	1.24	-0.85	0.68	1.31	1.09	-1.09

NM_017396	Cyp3a41a	Cytochrome P450, family 3, subfamily a, polypeptide 41A	1.07	-1.06	0.01	-2.28	0.07	-2.04	0.04	-2.04	1.02	-1.15
NM_010011	Cyp4a10	Cytochrome P450, family 4, subfamily a, polypeptide 10	0.22	1.50	0.03	1.96	1.22	-1.02	0.42	1.48	0.44	1.61
NM_172306	Cyp4a12b	Cytochrome P450, family 4, subfamily a, polypeptide 12B	0.23	-1.46	1.19	-0.91	0.89	-1.19	1.21	-0.92	0.98	-1.16
NM_007822	Cyp4a14	Cytochrome P450, family 4, subfamily a, polypeptide 14	0.00	3.26	0.00	8.06	0.46	1.47	1.00	1.17	1.13	-1.02
NM_201640	Cyp4a31	Cytochrome P450, family 4, subfamily a, polypeptide 10	0.11	1.65	0.23	1.52	0.00	-6.11	1.17	-0.99	0.09	-2.02
NM_022434	Cyp4f14	Cytochrome P450, family 4, subfamily f, polypeptide 14	0.87	-1.18	0.02	-2.12	0.17	1.85	0.12	1.89	0.12	2.27
NM_134127	Cyp4f15	Cytochrome P450, family 4, subfamily f, polypeptide 15	1.17	-0.92	1.11	-1.07	0.00	-3.41	0.57	-1.37	0.87	-1.27
AK050210	Cyp7a1	Cytochrome P450, family 7, subfamily a, polypeptide 1	0.07	1.75	0.01	-2.30	0.00	7.46	0.00	5.32	0.00	5.41
NM_007825	Cyp7b1	Cytochrome P450, family 7, subfamily b, polypeptide 1	0.02	-2.09	0.00	-2.49	0.00	5.46	0.00	4.39	0.04	2.97
NM_010012	Cyp8b1	Cytochrome P450, family 8, subfamily b, polypeptide 1	0.46	-1.35	0.08	-1.78	0.00	-14.83	0.00	-3.31	0.01	-2.76
NM_010516	Cyr61	Cysteine rich protein 61	0.08	-1.73	0.02	-2.13	1.26	-0.99	0.10	-1.84	0.18	-1.86
NM_021476	Cysltr1	Cysteinyl leukotriene receptor 1	0.18	-1.55	0.03	-2.01	1.17	-1.10	0.58	1.37	0.21	1.88
NM_133720	Cysltr2	Cysteinyl leukotriene receptor 2	0.03	1.99	0.01	2.22	0.35	1.57	0.20	1.66	0.24	1.80
NM_053078	D0H4S114	DNA segment, human D4S114	1.14	-0.99	0.00	-3.69	0.14	1.89	0.41	1.48	0.07	2.55
BU515177	D2hgdh	D-2-hydroxyglutarate dehydrogenase	0.64	1.27	0.64	1.29	0.03	2.52	0.20	1.69	0.28	1.72
AK046608	D5Wsu178e	DNA segment, Chr 5, Wayne State University 178, expressed	0.01	-2.34	0.22	-1.53	0.36	1.58	0.21	1.75	0.17	2.17
NM_007829	Daxx	Fas death domain-associated protein	1.10	-1.11	0.04	1.95	0.16	1.91	0.67	1.32	0.92	-1.14
NM_016974	Dbp	D site albumin promoter binding protein	0.50	1.31	0.04	1.97	0.14	-1.86	0.49	-1.42	0.23	-1.76
BQ442821	Dclre1b	DNA cross-link repair 1B, PSO2 homolog (S. cerevisiae)	1.19	-0.97	1.14	-0.88	0.00	3.80	0.10	1.88	0.46	1.52
NM_010024	Dct	Dopachrome tautomerase	0.06	-1.82	0.00	-2.50	0.62	-1.40	0.55	-1.39	0.37	-1.64
NM_016672	Ddc	Dopa decarboxylase	0.26	-1.46	0.03	-2.05	0.13	-1.85	0.75	-1.29	1.09	-0.97
NM_010029	Ddx4	DEAD (Asp-Glu-Ala-Asp) box polypeptide 4	0.68	1.21	0.66	1.27	0.01	3.39	0.14	1.77	0.46	1.51
NM_172689	Ddx58	DEAD (Asp-Glu-Ala-Asp) box polypeptide 58	0.58	-1.30	0.05	1.85	0.03	2.50	0.20	1.70	1.13	-0.97
AI552035	Defb29	Defensin beta 29	0.02	2.10	0.02	2.15	0.02	-2.45	0.02	-2.28	0.06	-2.15
NM_181683	Defb37	Defensin beta 37	0.13	-1.60	1.13	-1.05	0.04	2.41	0.44	-1.47	1.13	-0.92
NM_139220	Defb7	Defensin beta 7	0.86	1.19	0.86	1.20	0.00	3.61	0.08	1.95	0.62	1.40
NM_007848	Defcr-rs7	Defensin, alpha, 23	0.02	-2.00	0.75	-1.21	0.09	-1.97	0.00	-2.90	0.06	-2.23
AK037415	Dennd1a	DENN/MADD domain containing 1A	0.37	-1.40	0.76	-1.25	0.01	-2.62	0.30	-1.57	0.87	-1.25
NM_029523	Depdc1a	DEP domain containing 1a	0.01	-2.22	0.00	-2.68	0.24	1.69	0.41	1.48	0.74	1.35
AK042743	Depdc2	Phosphatidylinositol-3,4,5-trisphosphate-dependent Rac exchange factor 2	0.78	1.18	1.19	-0.93	0.75	-1.31	1.21	-0.87	0.02	-2.59

NM_027903	Dhdh	Dihydrodiol dehydrogenase (dimeric)	0.91	-1.18	0.08	-1.75	0.03	-2.32	0.26	-1.61	0.44	-1.56
NM_030150	Dhx58	DEXH (Asp-Glu-X-His) box polypeptide 58	0.21	-1.52	1.14	-0.99	0.01	3.29	0.17	1.81	1.12	-0.92
NM_010050	Dio2	Deiodinase, iodothyronine, type II	0.52	1.32	0.64	1.29	0.04	2.33	1.18	-0.86	1.12	-0.90
AF178078	Dlc1	Deleted in liver cancer 1	0.53	-1.33	0.03	-2.02	0.00	-3.98	0.20	-1.63	0.01	-2.70
NM_144553	Dlgap5	Discs, large (Drosophila) homolog-associated protein 5	0.52	-1.31	0.06	-1.84	0.06	2.26	0.00	3.63	0.07	2.67
NM_010053	Dlx1	Distal-less homeobox 1	1.15	-1.06	1.19	-0.94	0.20	-1.74	0.04	-2.12	0.25	-1.74
AK039839	Dnahc17	Dynein, axonemal, heavy chain 17	0.05	-1.81	0.04	-1.97	0.62	1.37	0.01	2.72	0.00	5.48
AK051796	Dnahc2	Dynein, axonemal, heavy chain 2	1.15	-1.07	0.38	-1.42	0.01	-2.63	0.01	-2.49	0.07	-2.11
NM_021422	Dnaja4	DnaJ (Hsp40) homolog, subfamily A, member 4	0.04	1.84	0.55	1.33	0.11	-1.95	0.03	-2.16	0.02	-2.48
NM_153527	Dnajb13	DnaJ (Hsp40) related, subfamily B, member 13	0.57	1.30	0.04	2.57	0.77	1.29	0.57	1.37	1.13	-0.97
NM_013888	Dnajc12	DnaJ (Hsp40) homolog, subfamily C, member 12	1.19	-1.00	0.02	2.10	0.48	1.47	0.28	1.58	0.55	1.47
AK017170	Dock11	Dedicator of cytokinesis 11	1.19	-0.94	0.77	1.22	0.06	2.23	0.00	4.35	0.00	5.20
NM_028785	Dock8	Dedicator of cytokinesis 8	1.02	-1.11	0.86	-1.16	0.03	-2.37	0.40	-1.47	0.86	-1.28
NM_199021	Dpp10	Dipeptidylpeptidase 10	0.04	1.91	0.01	2.24	0.00	4.51	0.00	4.51	0.01	3.99
NM_019759	Dpt	Dermatopontin	0.95	-1.13	0.33	-1.44	0.03	-2.34	0.01	-2.58	0.36	-1.62
NM_022722	Dpys	Dihydropyrimidinase	1.19	-0.97	0.24	-1.51	0.01	-2.80	0.39	-1.50	0.24	-1.76
AK034104	Dsg1c	Desmoglein 1 gamma	0.02	2.03	0.27	1.49	0.66	1.32	0.12	-1.58	0.02	3.60
NM_028002	Dus4l	Dihydrouridine synthase 4-like (S. cerevisiae)	0.19	1.53	0.05	1.88	0.00	-7.90	0.01	-2.69	0.00	-3.61
NM_007889	Dvl3	Dishevelled 3, dsh homolog (Drosophila)	1.12	-0.89	0.43	1.38	0.00	7.63	0.00	3.35	0.08	2.45
AK008822	Dync2li1	Dynein cytoplasmic 2 light intermediate chain 1	0.01	-2.32	0.05	-1.87	0.01	3.06	0.04	2.23	0.08	2.41
NM_019682	Dynll1	Dynein light chain LC8-type 1	0.82	1.20	1.14	-0.89	0.04	2.33	0.18	1.69	0.25	1.76
NM_178609	E2f7	E2F transcription factor 7	0.97	-1.06	0.57	1.22	0.09	2.17	0.03	2.48	0.06	2.90
NM_007894	Ear1	Eosinophil-associated, ribonuclease A family, member 1	1.04	-1.08	1.19	-0.99	0.02	2.75	0.01	3.05	0.01	4.30
NM_053111	Ear6	Eosinophil-associated, ribonuclease A family, member 6	0.48	1.34	0.07	1.77	0.00	4.27	0.00	5.87	0.00	8.57
BG968652	Eef1a1	Eukaryotic translation elongation factor 1 alpha 1	0.49	1.33	0.23	1.54	0.00	3.67	0.13	1.87	0.07	2.52
NM_007906	Eef1a2	Eukaryotic translation elongation factor 1 alpha 2	0.12	1.61	0.68	1.26	0.02	-2.44	1.10	-1.08	0.89	-1.26
CA875530	Eftud2	Elongation factor Tu GTP binding domain containing 2	0.05	-1.85	0.46	-1.37	0.01	-2.79	0.00	-3.82	0.01	-3.05
NM_001013762	EG240549	Predicted gene 4952	0.04	-1.89	0.21	-1.54	0.46	-1.46	0.03	-2.17	0.08	-2.07
NM_203660	EG368203	Predicted gene 5136	0.10	-1.64	0.10	-1.68	0.07	-2.06	0.01	-2.53	0.05	-2.26
AK049201	EG435337	Predicted gene 5662	0.62	1.26	0.29	1.47	0.04	2.36	0.22	1.70	0.21	1.91

AK033431	Egfr	Epidermal growth factor receptor	0.08	-1.72	0.15	-1.61	0.86	-1.20	0.04	-2.10	0.77	-1.31
BC022961	Egln3	EGL nine homolog 3 (C. elegans)	0.01	-2.21	0.00	-2.70	0.00	4.07	0.02	2.63	0.25	1.87
NM_010118	Egr2	Early growth response 2	0.02	-1.97	0.36	1.44	0.01	-2.67	0.00	-3.88	0.01	-2.82
NM_023737	Ehhadh	Enoyl-Coenzyme A, hydratase/3-hydroxyacyl Coenzyme A dehydrogenase	0.57	1.29	1.20	-0.97	0.00	-3.52	0.88	-1.21	0.30	-1.67
M65029	Eif2ak2	Eukaryotic translation initiation factor 2-alpha kinase 2	0.42	-1.35	0.04	1.95	0.00	-3.84	0.03	-2.22	0.01	-2.66
NM_026114	Eif2s1	Eukaryotic translation initiation factor 2, subunit 1 alpha	0.86	1.19	1.15	-0.89	0.02	-2.51	0.12	-1.78	0.43	-1.56
BQ563769	Eif3k	Eukaryotic translation initiation factor 3, subunit K	0.95	-1.16	0.97	1.14	0.01	3.45	0.53	1.41	0.27	1.74
NM_013506	Eif4a2	Eukaryotic translation initiation factor 4A2	1.06	-1.13	0.04	-1.91	0.06	2.26	0.02	2.54	0.41	1.69
NM_025829	Eif4e3	Eukaryotic translation initiation factor 4E member 3	1.17	-1.03	0.24	1.50	0.00	5.63	0.00	5.15	0.01	4.37
NM_015779	Ela2	Elastase, neutrophil expressed	0.85	-1.17	0.91	1.17	0.02	2.88	0.12	1.89	0.07	2.51
NM_007921	Elf3	E74-like factor 3	0.16	-1.58	0.05	1.86	0.00	4.79	0.01	3.02	0.13	2.19
NM_145973	Ell3	Elongation factor RNA polymerase II-like 3	0.92	-1.08	0.28	-1.42	0.00	-7.07	0.31	-1.49	0.05	-2.24
U66889	Emr1	EGF-like module containing, mucin-like, hormone receptor-like sequence 1	0.73	1.19	0.02	-2.14	0.01	-3.00	0.00	-5.62	0.00	-3.76
NM_139138	Emr4	EGF-like module containing, mucin-like, hormone receptor-like sequence 4	1.19	-0.97	0.04	-1.96	0.00	-6.61	0.71	-1.29	0.13	2.27
NM_010135	Enah	Enabled homolog (Drosophila)	0.79	1.22	0.83	1.21	0.03	2.45	0.36	1.50	0.51	1.47
NM_015744	Enpp2	Ectonucleotide pyrophosphatase/phosphodiesterase 2	1.17	-1.02	1.18	-1.03	0.03	-2.30	0.52	-1.41	0.88	-1.22
BC005527	Enpp3	Ectonucleotide pyrophosphatase/phosphodiesterase 3	0.11	-1.68	0.05	-1.93	0.01	-2.64	0.00	-2.80	0.03	-2.40
AK173048	Enpp4	Ectonucleotide pyrophosphatase/phosphodiesterase 4	0.52	1.32	0.01	2.43	0.01	2.92	0.02	2.59	0.13	2.18
NM_177304	Enpp6	Ectonucleotide pyrophosphatase/phosphodiesterase 6	0.02	2.13	0.24	1.54	0.00	13.26	0.07	-1.86	0.02	3.44
AI326494	ENSMUSG00000074179	Glutathione S-transferase, alpha 1 (Ya)	0.85	1.09	0.45	1.37	0.00	-8.54	0.51	-1.39	0.64	-1.41
AK029512	Entpd1	Ectonucleoside triphosphate diphosphohydrolase 1	0.38	1.38	1.19	-0.97	0.05	2.24	0.01	3.02	0.03	3.29
NM_010136	Eomes	Eomesodermin homolog (Xenopus laevis)	1.18	-1.02	0.93	1.17	0.00	8.83	0.00	4.42	0.02	3.33
NM_013813	Epb4.1l3	Erythrocyte protein band 4.1-like 3	0.81	1.21	1.20	-0.97	0.03	2.47	0.00	3.50	0.01	4.17
NM_010145	Ephx1	Epoxide hydrolase 1, microsomal	0.80	-1.23	1.19	-1.01	0.01	-2.82	0.61	-1.36	1.08	-1.11
NM_010149	Epor	Erythropoietin receptor	1.17	-0.93	0.07	-1.80	0.00	-3.58	0.18	-1.70	0.80	-1.32
NM_144848	Eppk1	Epiplakin 1	0.76	-1.23	0.53	1.33	0.04	2.42	0.13	1.84	0.57	1.46
NM_007944	Eps15l1	Epidermal growth factor receptor pathway substrate 15-like 1	1.14	-1.07	0.77	-1.23	0.00	-5.42	0.00	-3.10	0.04	-2.29
NM_133191	Eps8l2	EPS8-like 2	0.00	-2.74	0.10	-1.75	0.01	-2.95	0.03	-2.15	0.06	-2.17

NM_133245	Eraf	Alpha hemoglobin stabilizing protein	0.78	1.22	0.72	1.25	1.24	-0.86	0.99	1.17	0.03	3.15
NM_146235	Ercc6l	Excision repair cross-complementing rodent repair deficiency complementation group 6 - like	0.83	1.06	0.74	1.17	0.01	3.27	0.00	4.81	0.05	3.03
NM_133660	Es22	Esterase 22	0.96	1.14	1.19	-0.99	0.00	-4.08	0.03	-2.12	0.09	-2.04
NM_007956	Esr1	Estrogen receptor 1 (alpha)	0.04	1.88	0.97	1.13	0.59	1.39	0.01	2.81	0.02	3.51
NM_007953	Esrra	Estrogen related receptor, alpha	0.05	1.83	0.67	1.28	0.30	-1.59	0.00	-3.63	0.00	-3.46
NM_011934	Esrrb	Estrogen related receptor, beta	0.92	1.15	0.01	2.44	0.84	1.26	0.02	2.51	0.03	3.25
BB502375	Esrrg	Estrogen-related receptor gamma	0.16	1.56	0.12	1.69	0.05	-2.16	0.28	1.61	1.09	-1.03
NM_025794	Etfdh	Electron transferring flavoprotein, dehydrogenase	1.17	-1.05	0.85	-1.20	0.03	-2.37	0.17	-1.70	0.24	-1.74
BB032615	Ets1	E26 avian leukemia oncogene 1, 5' domain	0.85	1.14	0.52	1.33	0.02	2.68	1.19	-0.87	0.65	1.39
J04103	Ets2	E26 avian leukemia oncogene 2, 3' domain	0.03	2.00	0.58	-1.28	0.32	-1.58	0.70	1.29	0.50	1.50
NM_007963	Evi1	MDS1 and EVI1 complex locus	0.27	1.46	0.94	1.17	0.00	4.85	0.05	2.13	0.47	1.53
NM_007965	Evl	Ena-vasodilator stimulated phosphoprotein	1.03	-1.15	1.20	-1.00	0.02	2.61	0.01	2.92	0.01	4.53
NM_025276	Evpl	Envoplakin	0.21	1.55	0.04	2.00	0.06	2.27	0.10	1.98	0.38	1.76
NM_028784	F13a1	Coagulation factor XIII, A1 subunit	0.03	1.96	0.00	2.86	0.84	-1.28	0.98	-1.19	0.98	-1.22
NM_010173	Faah	Fatty acid amide hydrolase	1.18	-0.97	0.84	-1.20	0.03	-2.29	0.32	-1.54	0.22	-1.77
NM_010634	Fabp5	Fatty acid binding protein 5, epidermal	0.26	-1.45	0.74	-1.24	0.03	2.48	0.55	1.37	1.12	-0.89
NM_021272	Fabp7	Fatty acid binding protein 7, brain	0.87	-1.16	0.46	-1.37	0.20	1.79	0.00	3.32	0.08	2.45
BY766215	Faim2	Fas apoptotic inhibitory molecule 2	0.82	1.21	1.19	-0.92	0.03	-2.28	1.21	-0.91	0.71	-1.31
NM_016925	Fanca	Fanconi anemia, complementation group A	0.28	-1.46	0.61	1.27	0.03	2.49	0.00	3.27	0.05	2.74
NM_145946	Fanci	Fanconi anemia, complementation group I	0.19	1.41	0.30	-1.31	0.01	3.32	0.00	4.45	0.04	3.11
NM_027379	Far1	Fatty acyl CoA reductase 1	0.38	-1.37	0.75	1.22	0.52	1.44	0.04	2.22	0.39	1.65
NM_007987	Fas	Fas (TNF receptor superfamily member 6)	1.19	-0.99	0.10	1.72	0.03	2.58	0.13	1.84	0.51	1.53
NM_010177	Fasl	Fas ligand (TNF superfamily, member 6)	1.19	-0.96	0.15	1.63	0.02	2.75	0.00	4.39	0.01	4.18
CA750482	Fat3	FAT tumor suppressor homolog 3 (Drosophila)	0.67	1.26	1.20	-1.01	0.02	-2.42	0.00	-2.95	0.04	-2.34
AF112151	Fbln5	Fibulin 5	0.45	-1.33	0.11	-1.72	0.00	-5.06	0.01	-2.43	0.40	-1.60
BF139521	Fbxl11	Lysine (K)-specific demethylase 2A	1.03	-1.12	0.78	-1.22	0.01	-2.72	0.10	-1.84	0.28	-1.73
NM_177076	Fbxl13	F-box and leucine-rich repeat protein 13	0.47	-1.31	0.83	-1.14	0.03	-2.35	1.07	-1.10	1.06	-1.05
AK012109	Fbxl20	F-box and leucine-rich repeat protein 20	1.08	-1.04	0.03	-2.01	0.61	-1.39	0.07	-1.94	0.92	-1.08
BU057149	Fbxo28	F-box protein 28	1.15	-0.92	0.67	1.26	0.04	2.35	0.72	1.29	1.11	-0.84
NM_133765	Fbxo31	F-box protein 31	0.04	1.85	0.21	1.51	0.41	1.52	0.53	1.41	0.28	1.78

NM_025995	Fbxo5	F-box protein 5	0.61	-1.29	0.53	-1.34	0.05	2.29	0.00	3.29	0.16	2.14
NM_010185	Fcer1g	Fc receptor, IgE, high affinity I, gamma polypeptide	1.18	-0.99	1.20	-0.98	0.04	2.40	0.00	3.66	0.00	5.08
NM_010186	Fcgr1	Fc receptor, IgG, high affinity I	0.94	-1.15	0.08	1.79	0.00	4.09	0.00	5.13	0.00	6.64
NM_010188	Fcgr3	Fc receptor, IgG, low affinity III	0.90	1.15	0.61	-1.32	0.22	1.72	0.01	2.67	0.01	4.29
NM_144559	Fcgr4	Fc receptor, IgG, low affinity IV	1.15	-0.91	0.00	2.54	0.00	7.17	0.00	12.45	0.00	13.96
NM_007999	Fen1	Flap structure specific endonuclease 1	0.96	1.12	1.18	-1.00	0.06	2.18	0.01	2.86	0.11	2.31
NM_153795	Fermt3	Fermitin family homolog 3 (Drosophila)	1.19	-1.00	1.10	-1.11	0.22	1.73	0.02	2.55	0.02	3.40
NM_013710	Fgd2	FYVE, RhoGEF and PH domain containing 2	1.03	-1.13	1.20	-0.96	0.13	1.93	0.02	2.52	0.02	3.50
BE949453	Fgd3	FYVE, RhoGEF and PH domain containing 3	1.03	-1.07	0.19	-1.55	1.24	-0.85	0.10	1.92	0.02	3.51
NM_008005	Fgf18	Fibroblast growth factor 18	0.77	1.10	0.00	-2.48	0.07	2.15	0.24	1.63	0.61	1.42
NM_020013	Fgf21	Fibroblast growth factor 21	0.00	-2.62	0.00	-6.31	0.06	2.20	0.08	1.99	0.40	1.61
NM_013518	Fgf9	Fibroblast growth factor 9	0.55	1.24	0.89	1.16	0.55	1.42	1.18	-1.03	0.02	-2.54
BC028893	Fgl2	Fibrinogen-like protein 2	0.91	1.06	0.30	1.48	0.00	4.79	0.00	6.79	0.00	7.56
NM_010208	Fgr	Gardner-Rasheed feline sarcoma viral (Fgr) oncogene homolog	0.84	-1.21	0.32	1.44	0.02	2.87	0.02	2.66	0.01	4.62
NM_024169	Fkbp11	FK506 binding protein 11	0.65	-1.24	0.35	-1.40	0.01	3.19	1.21	-0.96	1.05	-1.16
NM_010220	Fkbp5	FK506 binding protein 5	0.00	2.94	0.65	1.17	0.13	-1.85	0.00	-2.98	0.01	-2.87
AI503986	Flvcr1	Major facilitator superfamily domain containing 7B	0.27	1.48	0.90	1.12	0.00	-4.24	1.05	-1.00	1.03	-1.01
NM_010231	Fmo1	Flavin containing monooxygenase 1	1.17	-1.06	0.20	-1.55	0.00	-3.57	0.50	-1.42	0.43	-1.56
NM_008030	Fmo3	Flavin containing monooxygenase 3	0.10	1.65	0.13	-1.66	0.00	-12.20	0.01	-2.39	0.00	-3.64
BF322820	Fmo5	Flavin containing monooxygenase 5	0.00	3.36	0.11	1.71	0.16	-1.80	1.00	-1.10	0.57	-1.45
NM_022014	Fn3k	Fructosamine 3 kinase	1.19	-1.00	1.09	-1.07	0.01	-2.59	0.99	-1.18	0.56	-1.47
NM_173182	Fndc3b	Fibronectin type III domain containing 3B	1.18	-0.96	1.19	-1.01	0.05	2.33	0.65	1.33	0.49	1.54
NM_008034	Folr1	Folate receptor 1 (adult)	1.11	-0.88	1.16	-0.93	0.41	-1.54	0.04	-2.11	0.28	-1.69
X83971	Fosl2	Fos-like antigen 2	0.14	1.60	0.04	1.95	0.00	-4.83	0.28	-1.57	0.05	-2.20
NM_008592	Foxc1	Forkhead box C1	0.04	1.91	0.37	1.39	0.86	1.21	0.21	1.73	0.15	2.12
NM_019740	Foxo3a	Forkhead box O3	0.40	1.33	0.05	1.97	0.02	2.71	0.00	3.76	0.02	3.37
NM_194060	Foxo6	Forkhead box O6	0.03	-1.96	0.02	-2.13	0.01	3.07	0.16	1.74	0.46	1.52
NM_013521	Fpr1	Formyl peptide receptor 1	0.63	1.22	1.11	-1.09	0.11	2.01	0.00	3.41	0.00	6.45
NM_008039	Fpr2	Formyl peptide receptor 2	1.07	-1.10	0.03	2.08	0.07	2.12	0.01	2.88	0.06	2.58
NM_139149	Fus	Fusion, derived from t(12;16) malignant liposarcoma (human)	0.02	-1.97	0.99	-1.15	0.03	-2.32	0.00	-3.06	0.03	-2.50

NM_013524	Fut7	Fucosyltransferase 7	0.26	-1.41	0.98	-1.03	0.06	2.25	0.00	3.60	0.00	5.59
NM_008761	Fxyd5	FXYD domain-containing ion transport regulator 5	1.10	-1.10	1.15	-1.06	0.01	3.25	0.00	3.22	0.01	3.82
NM_011815	Fyb	FYN binding protein	1.03	-1.15	0.80	-1.25	0.05	2.38	0.00	4.48	0.00	6.45
M27266	Fyn	Fyn proto-oncogene	0.59	1.28	0.67	-1.26	0.14	1.87	0.05	2.18	0.16	2.02
AF272146	Fzd5	Frizzled homolog 5 (Drosophila)	0.01	2.45	0.05	1.98	0.82	1.25	0.04	2.26	0.41	1.61
NM_008058	Fzd8	Frizzled homolog 8 (Drosophila)	0.55	-1.28	0.48	-1.33	0.03	-2.27	0.19	-1.67	0.07	-2.12
NM_008059	G0s2	G0/G1 switch gene 2	0.00	3.44	0.86	1.03	0.30	1.65	0.69	1.21	0.25	1.92
NM_008061	G6pc	Glucose-6-phosphatase, catalytic	1.05	-1.10	0.00	-4.97	0.29	1.62	0.84	1.25	1.10	-1.06
NM_008062	G6pdx	Glucose-6-phosphate dehydrogenase X-linked	0.92	1.16	0.01	2.49	0.02	2.85	0.07	2.17	0.23	2.01
NM_010248	Gab2	Growth factor receptor bound protein 2-associated protein 2	0.74	1.24	0.66	-1.25	0.13	-1.89	0.01	-2.57	0.04	-2.37
NM_146017	Gabrp	Gamma-aminobutyric acid (GABA) A receptor, pi	0.38	-1.33	0.08	-1.79	0.04	-2.31	0.11	-1.82	0.02	-2.51
BY561866	Gabrq	Gamma-aminobutyric acid (GABA) A receptor, subunit theta	0.83	-1.14	0.83	-1.16	0.94	-1.19	0.01	-2.40	0.21	-1.77
NM_007836	Gadd45a	Growth arrest and DNA-damage-inducible 45 alpha	0.48	1.30	0.00	2.93	0.00	4.09	0.10	1.94	0.21	1.89
NM_008655	Gadd45b	Growth arrest and DNA-damage-inducible 45 beta	0.05	1.84	0.04	1.96	0.01	3.42	0.04	2.60	0.12	2.32
NM_011817	Gadd45g	Growth arrest and DNA-damage-inducible 45 gamma	0.04	-1.90	0.36	1.46	1.22	-1.02	1.16	-1.00	0.38	1.66
NM_178389	Gale	Galactose-4-epimerase, UDP	0.36	-1.35	0.36	1.45	0.04	2.34	0.52	1.41	1.03	-1.06
NM_015736	Galnt3	UDP-N-acetyl-alpha-D-galactosamine:polypeptide. N-acetylgalactosaminyltransferase 3	1.08	-1.08	1.20	-0.96	0.13	1.94	0.01	3.22	0.06	2.67
NM_010254	Galr2	Galanin receptor 2	0.63	1.20	0.74	-1.18	0.02	-2.57	1.20	-0.91	0.32	-1.65
NM_010255	Gamt	Guanidinoacetate methyltransferase	0.96	1.15	1.05	-1.09	0.00	-3.02	0.81	-1.26	0.65	-1.40
AI837470	Gapdh	Glyceraldehyde-3-phosphate dehydrogenase	0.02	-2.06	0.96	1.11	1.22	-1.09	0.99	-1.19	0.83	1.27
NM_008086	Gas1	Growth arrest specific 1	0.95	1.15	0.97	-1.10	0.01	-2.72	0.34	-1.51	0.15	-1.94
NM_008087	Gas2	Growth arrest specific 2	0.90	-1.14	0.89	-1.17	0.01	-2.88	1.21	-0.91	0.88	-1.24
NM_019521	Gas6	Growth arrest specific 6	1.14	-1.04	0.35	1.45	0.01	3.54	0.04	2.32	0.09	2.38
NM_008089	Gata1	GATA binding protein 1	1.14	-1.06	1.19	-0.97	0.00	4.00	0.33	1.52	0.61	1.40
NM_010292	Gck	Glucokinase	0.04	1.85	0.34	1.39	0.05	2.28	0.03	2.35	0.08	2.36
NM_010267	Gdap1	Ganglioside-induced differentiation-associated-protein 1	0.05	1.85	0.03	2.05	0.11	2.02	0.12	1.92	0.58	1.51
NM_019580	Gde1	Glycerophosphodiester phosphodiesterase 1	0.01	2.34	0.72	1.25	1.17	-1.10	0.32	-1.55	0.31	-1.70
NM_011819	Gdf15	Growth differentiation factor 15	1.17	-0.99	0.03	-2.05	0.97	1.16	0.40	-1.47	1.03	-1.07
NM_008114	Gfi1b	Growth factor independent 1B	0.86	1.17	0.62	1.29	0.39	1.52	0.01	2.69	0.01	4.01
NM_013528	Gfpt1	Glutamine fructose-6-phosphate transaminase 1	1.10	-1.07	0.53	1.33	0.04	2.34	0.56	1.38	0.65	1.38

AI846599	Gfra2	Glial cell line derived neurotrophic factor family receptor alpha 2	1.16	-0.94	0.02	-2.09	0.04	2.39	0.02	2.58	0.25	1.81
NM_027819	Ggt6	Gamma-glutamyltransferase 6	0.33	1.41	0.32	1.43	0.13	1.91	0.01	2.70	0.51	1.49
BY107228	Ghr	Growth hormone receptor	1.16	-0.94	0.43	-1.38	0.01	-2.58	0.31	-1.56	0.53	-1.48
NM_031184	Glis2	GLIS family zinc finger 2	1.15	-0.91	0.84	1.20	0.01	3.35	0.05	2.13	0.25	1.77
BM119314	Glrx	Glutaredoxin	0.52	-1.33	0.05	-1.91	0.02	2.59	1.21	-0.96	1.10	-0.96
NM_019821	Gltp	Glycolipid transfer protein	1.16	-1.06	0.46	-1.38	0.11	2.01	0.02	2.60	0.05	2.84
NM_146041	Gmds	GDP-mannose 4, 6-dehydratase	0.92	-1.13	1.19	-0.98	0.04	2.43	0.78	1.28	1.12	-0.89
NM_020567	Gmnn	Geminin	0.36	1.39	1.16	-1.00	0.38	1.54	0.05	2.16	0.35	1.64
NM_010304	Gna15	Guanine nucleotide binding protein, alpha 15	0.76	-1.24	1.20	-0.99	0.03	2.54	0.00	3.82	0.00	5.41
NM_008140	Gnat1	Guanine nucleotide binding protein, alpha transducing 1	0.83	1.19	0.44	1.34	0.00	3.57	0.32	1.56	0.36	1.68
NM_008141	Gnat2	Guanine nucleotide binding protein, alpha transducing 2	1.11	-1.04	0.96	-1.12	0.01	2.99	0.66	-1.31	0.61	-1.41
NM_013531	Gnb4	Guanine nucleotide binding protein (G protein), beta 4	1.16	-0.95	0.13	1.62	0.04	2.32	0.02	2.57	0.27	1.77
NM_010314	Gngt1	Guanine nucleotide binding protein (G protein), gamma transducing activity polypeptide 1	0.04	-1.89	0.57	1.29	0.79	-1.20	1.17	-0.89	0.06	-2.14
NM_010324	Got1	Glutamate oxaloacetate transaminase 1, soluble	0.13	1.59	0.65	1.27	0.02	-2.41	1.13	-1.08	1.06	-1.16
NM_018762	Gp9	Glycoprotein 9 (platelet)	0.05	1.86	0.71	1.22	0.96	1.16	0.24	1.65	0.23	1.85
NM_016697	Gpc3	Glypican 3	0.01	2.25	0.02	2.29	0.01	3.28	0.01	3.02	0.13	2.16
BB466704	Gpc5	Glypican 5	0.45	1.36	1.15	-0.98	0.00	-3.76	0.08	-1.87	0.46	-1.52
NM_011821	Gpc6	Glypican 6	1.19	-0.97	0.03	-2.05	1.13	-1.12	1.19	-1.03	0.99	1.20
NM_010271	Gpd1	Glycerol-3-phosphate dehydrogenase 1 (soluble)	0.93	-1.16	0.28	-1.48	0.01	-2.95	0.06	-1.99	0.16	-1.85
AJ251685	Gpnmb	Glycoprotein (transmembrane) nmb	0.28	1.38	0.29	1.43	0.04	2.42	0.32	1.54	0.08	2.51
NM_133776	Gpr110	G protein-coupled receptor 110	0.89	-1.17	0.53	-1.34	0.19	-1.76	0.01	-2.37	0.07	-2.11
BI150848	Gpr114	G protein-coupled receptor 114	0.61	-1.22	0.25	1.51	0.01	3.34	0.00	3.70	0.01	4.81
NM_175495	Gpr150	G protein-coupled receptor 150	0.04	-1.88	0.36	-1.37	1.22	-0.97	1.06	-1.00	1.09	-0.99
AK006330	Gpr160	G protein-coupled receptor 160	1.12	-1.01	0.98	1.15	0.05	2.25	0.03	2.40	0.09	2.39
NM_173398	Gpr171	G protein-coupled receptor 171	0.64	1.23	1.19	-0.96	0.05	2.25	0.01	2.88	0.02	3.73
NM_182806	Gpr18	G protein-coupled receptor 18	0.35	-1.42	0.54	1.32	0.03	2.53	0.00	3.45	0.00	4.99
NM_183031	Gpr183	G protein-coupled receptor 183	1.19	-0.92	0.02	-2.08	0.00	-3.82	0.17	-1.72	0.00	-4.54
NM_134116	Gpsm3	G-protein signalling modulator 3 (AGS3-like, C. elegans)	1.19	-0.99	1.00	-1.16	0.23	1.71	0.02	2.54	0.02	3.58
AK004932	Gpt	Glutamic pyruvic transaminase, soluble	0.92	-1.16	0.16	-1.58	0.12	-1.91	0.03	-2.19	0.06	-2.12
BB079812	Grik2	Glutamate receptor, ionotropic, kainate 2 (beta 2)	0.03	-1.96	0.32	1.47	0.05	-2.12	0.02	-2.04	0.06	2.76

NM_130455	Grin3b	Glutamate receptor, ionotropic, NMDA3B	0.64	-1.26	0.10	-1.73	0.17	-1.81	0.03	-2.15	0.41	-1.59
BE956571	Grit	Rho GTPase-activating protein	0.07	-1.77	0.29	-1.47	0.56	-1.41	0.05	-2.02	1.13	-0.95
BF320612	Grlf1	Glucocorticoid receptor DNA binding factor 1	0.02	2.14	0.83	1.18	0.80	-1.29	0.64	-1.33	0.10	-2.01
NM_010353	Gsg2	Germ cell-specific gene 2	0.86	1.08	0.05	-1.90	0.15	1.91	0.02	2.60	0.08	2.57
NM_008181	Gsta1	Glutathione S-transferase, alpha 1 (Ya)	0.98	1.03	0.46	1.37	0.00	-6.93	0.38	-1.48	0.16	-1.87
NM_008182	Gsta2	Glutathione S-transferase, alpha 2 (Yc2)	0.87	1.06	0.38	1.42	0.00	-7.17	0.75	-1.22	0.70	-1.37
NM_010357	Gsta4	Glutathione S-transferase, alpha 4	1.18	-0.95	1.19	-0.92	0.02	-2.40	1.07	-1.12	0.92	-1.24
NM_010358	Gstm1	Glutathione S-transferase, mu 1	0.79	-1.19	1.15	-1.04	0.01	-2.68	0.68	-1.31	0.87	-1.27
NM_010359	Gstm3	Glutathione S-transferase, mu 3	0.14	-1.55	0.65	-1.19	0.01	-2.69	0.40	1.46	1.05	-1.09
NM_133994	Gstt3	Glutathione S-transferase, theta 3	1.00	1.10	0.99	1.12	0.00	-3.25	0.44	-1.43	0.50	-1.49
AK028558	Gucy1a3	Guanylate cyclase 1, soluble, alpha 3	0.55	-1.30	0.05	-1.90	0.49	1.46	1.21	-0.95	1.08	-1.13
NM_145067	Gucy2c	Guanylate cyclase 2c	0.36	1.40	0.01	2.34	0.01	3.22	0.04	2.23	0.13	2.13
U48403	Gyk	Glycerol kinase	1.15	-1.05	0.38	-1.42	0.00	-3.07	0.32	-1.55	0.52	-1.49
BF608145	Gypa	Glycophorin A	0.32	1.41	0.89	1.08	1.00	1.13	0.66	-1.26	0.04	3.02
NM_010370	Gzma	Granzyme A	0.99	1.10	0.08	1.78	0.00	9.58	0.00	20.10	0.00	12.81
NM_013542	Gzmb	Granzyme B	1.19	-0.97	0.80	1.19	0.00	4.02	0.00	6.31	0.01	4.94
NM_010372	Gzmd	Granzyme D	0.08	1.73	0.04	1.94	0.34	1.57	0.45	1.43	1.12	-0.87
NM_031367	H28	Histocompatibility 28	0.90	-1.17	0.11	1.72	0.00	5.67	0.00	5.11	0.04	3.07
NM_010378	H2-Aa	Histocompatibility 2, class II antigen A, alpha	0.83	-1.21	0.73	1.23	0.00	4.22	0.00	6.02	0.00	10.22
NM_207105	H2-Ab1	Histocompatibility 2, class II antigen A, beta 1	0.17	1.59	0.13	1.63	0.00	8.22	0.00	12.17	0.00	18.88
NM_008199	H2-Bl	Histocompatibility 2, blastocyst	1.05	-1.14	1.19	-0.94	0.07	2.15	0.01	2.73	0.16	2.08
NM_010398	H2-D1	Histocompatibility 2, D region locus 1	1.06	-1.14	0.38	1.38	0.07	2.19	0.03	2.42	0.25	1.87
NM_010386	H2-DMa	Histocompatibility 2, class II, locus DMa	1.16	-1.06	0.00	2.69	0.00	5.81	0.00	3.30	0.20	1.88
NM_010387	H2-DMb1	Histocompatibility 2, class II, locus Mb1	1.19	-0.99	0.01	2.20	0.04	2.44	0.07	2.07	0.21	1.90
NM_010382	H2-Eb1	Histocompatibility 2, class II antigen E beta	0.86	-1.19	0.44	1.38	0.00	6.55	0.00	8.50	0.00	13.13
AI461836	H2-gs10	Histocompatibility 2, K1, K region	1.19	-0.96	0.02	2.07	0.70	-1.27	1.21	-0.91	0.64	1.44
AI326621	H2-K1	Histocompatibility 2, K1, K region	0.98	-1.14	0.54	1.30	0.04	2.43	0.03	2.40	0.15	2.13
NM_177636	H2-M1	Histocompatibility 2, M region locus 1	0.98	-1.06	0.02	2.18	0.05	2.28	0.15	1.78	0.99	1.21
NM_013819	H2-M3	Histocompatibility 2, M region locus 3	0.59	-1.30	0.12	1.68	0.03	2.60	0.03	2.44	0.08	2.48
NM_008205	H2-M9	Histocompatibility 2, M region locus 9	1.18	-1.00	0.64	1.25	0.01	3.14	0.00	3.46	0.06	2.72

BC025170	H2-Q6	Histocompatibility 2, Q region locus 8	0.97	-1.17	0.16	1.59	0.03	2.63	0.00	3.70	0.03	3.19
NM_010394	H2-Q7	Histocompatibility 2, Q region locus 7	0.54	1.26	0.49	1.31	0.01	3.27	0.00	5.26	0.01	4.52
NM_023124	H2-Q8	Histocompatibility 2, Q region locus 8	1.19	-1.02	0.63	1.28	0.11	2.00	0.00	3.44	0.05	2.80
NM_010395	H2-T10	Histocompatibility 2, T region locus 22	0.97	1.13	0.87	1.18	0.11	1.99	0.05	2.20	0.16	2.05
BB822862	H60a	Histocompatibility 60a	0.04	-1.90	1.18	-1.04	1.27	-0.89	1.21	-0.97	1.13	-0.96
AI466823	Hadhb	Hydroxyacyl-Coenzyme A dehydrogenase/3-ketoacyl-Coenzyme A thiolase/enoyl-Coenzyme A hydratase (trifunctional protein), beta subunit	1.03	-1.14	0.78	-1.24	0.03	-2.30	0.35	-1.52	0.31	-1.66
NM_019545	Hao3	Hydroxyacid oxidase 2	1.09	-1.11	0.04	-1.91	0.11	-1.97	0.01	-2.62	0.19	-1.77
BB370520	Hapln1	Hyaluronan and proteoglycan link protein 1	0.11	1.66	0.16	1.64	0.27	1.69	0.04	2.30	0.22	1.90
NM_134250	Havcr2	Hepatitis A virus cellular receptor 2	0.34	1.33	0.15	-1.62	0.05	2.37	0.01	2.80	0.10	2.42
NM_153198	Hbp1	High mobility group box transcription factor 1	0.59	-1.30	0.05	-1.92	0.00	3.64	0.00	9.00	0.00	18.63
NM_010407	Hck	Hemopoietic cell kinase	1.16	-1.05	0.15	1.62	0.00	3.78	0.00	4.69	0.00	5.15
NM_008225	Hcls1	Hematopoietic cell specific Lyn substrate 1	0.82	1.19	1.17	-1.02	0.01	3.38	0.00	4.60	0.01	4.62
NM_008230	Hdc	Histidine decarboxylase	0.59	1.29	0.00	2.91	0.00	4.60	0.00	6.31	0.03	3.39
AK083436	Hdx	Highly divergent homeobox	1.18	-1.03	0.62	-1.31	0.57	-1.42	0.04	-2.09	0.11	-2.01
AK011047	Herc5	Hect domain and RLD 5	0.89	-1.21	0.00	3.67	0.02	2.70	0.01	2.68	0.16	2.06
NM_138753	Hexim1	Hexamethylene bis-acetamide inducible 1	0.02	2.12	0.96	1.16	1.24	-0.99	1.20	-0.96	1.13	-0.89
NM_010423	Hey1	Hairy/enhancer-of-split related with YRPW motif 1	1.19	-1.01	0.00	-2.95	1.03	-1.18	1.17	-1.07	0.91	1.26
NM_008245	Hhex	Hematopoietically expressed homeobox	1.02	-1.07	0.05	-1.90	0.00	-4.62	0.01	-2.58	0.02	-2.58
AK033978	Hibadh	3-hydroxyisobutyrate dehydrogenase	0.62	1.15	0.05	1.93	0.21	-1.73	0.93	-1.22	0.79	1.32
NM_018792	Hils1	Histone H1-like protein in spermatids 1	0.43	1.35	0.04	1.95	0.03	-2.32	0.53	-1.36	0.30	-1.67
NM_145070	Hip1r	Huntingtin interacting protein 1 related	0.29	1.44	0.02	2.11	1.28	-0.97	0.88	-1.20	0.75	-1.36
NM_008255	Hmgcr	3-hydroxy-3-methylglutaryl-Coenzyme A reductase	0.04	1.84	0.12	1.65	1.26	-0.89	0.34	1.52	0.28	1.74
NM_145942	Hmgcs1	3-hydroxy-3-methylglutaryl-Coenzyme A synthase 1	0.00	-2.47	1.07	-1.04	0.36	-1.39	0.02	-2.26	0.21	-1.67
NM_010442	Hmox1	Heme oxygenase (decycling) 1	1.15	-0.90	0.27	1.48	0.02	2.61	0.01	3.01	0.02	3.56
NM_134032	Hoxb2	Homeo box B2	1.19	-0.94	0.02	2.08	1.26	-1.04	1.02	-1.13	0.63	-1.41
NM_010464	Hoxc13	Homeo box C13	0.02	-2.00	0.20	-1.52	0.18	-1.75	0.09	-1.83	0.36	-1.62
NM_146256	Hpdl	4-hydroxyphenylpyruvate dioxygenase-like	0.03	1.98	1.10	-1.02	0.00	15.07	0.00	12.80	0.00	12.24
NM_008284	Hras1	Harvey rat sarcoma virus oncogene 1	1.13	-0.90	1.19	-1.03	0.04	-2.25	0.05	-2.05	0.37	-1.61
AK038809	Hrasls3	Phospholipase A2, group XVI	1.16	-1.05	0.03	2.00	0.59	1.39	1.20	-0.91	0.81	-1.31

NM_008286	Hrh2	Histamine receptor H2	1.19	-0.99	0.30	-1.45	0.01	-2.82	0.01	-2.37	0.03	-2.41
NM_008290	Hsd17b2	Hydroxysteroid (17-beta) dehydrogenase 2	0.18	-1.51	0.04	-1.90	0.01	-2.68	0.08	-1.91	0.11	-2.03
NM_008291	Hsd17b3	Hydroxysteroid (17-beta) dehydrogenase 3	0.34	1.41	1.18	-0.95	0.02	2.60	0.02	2.55	0.22	1.85
NM_008293	Hsd3b1	Hydroxy-delta-5-steroid dehydrogenase, 3 beta- and steroid delta-isomerase 1	0.00	2.54	0.00	-3.22	0.71	-1.34	0.61	1.32	0.17	2.11
NM_153193	Hsd3b2	Hydroxy-delta-5-steroid dehydrogenase, 3 beta- and steroid delta-isomerase 3	1.15	-1.06	0.83	-1.19	0.00	-3.32	0.78	-1.27	0.75	-1.35
NM_008294	Hsd3b4	Hydroxy-delta-5-steroid dehydrogenase, 3 beta- and steroid delta-isomerase 4	0.00	-2.42	0.03	-2.01	0.26	1.67	0.17	1.75	0.13	2.13
NM_008295	Hsd3b5	Hydroxy-delta-5-steroid dehydrogenase, 3 beta- and steroid delta-isomerase 5	0.00	-4.59	0.00	-6.70	0.32	-1.62	0.63	-1.33	0.86	-1.25
NM_010480	Hsp90aa1	Heat shock protein 90, alpha (cytosolic), class A member 1	0.04	1.84	1.19	-0.92	0.16	1.88	0.01	2.74	0.06	2.71
NM_010479	Hspa1a	Heat shock protein 1A	0.14	1.55	0.01	2.54	0.00	8.43	0.00	11.70	0.00	12.40
M12573	Hspa1b	Heat shock protein 1B	0.01	2.44	0.00	4.92	0.07	2.14	0.01	3.10	0.03	3.11
NM_030704	Hspb8	Heat shock protein 8	0.22	1.48	0.00	2.75	0.00	4.51	0.00	6.04	0.00	6.58
M83997	Hspg2	Perlecan (heparan sulfate proteoglycan 2)	0.02	2.12	0.13	1.65	0.76	-1.23	0.40	1.53	0.40	1.71
NM_013559	Hsph1	Heat shock 105kDa/110kDa protein 1	0.00	3.16	0.09	1.77	0.93	1.23	0.19	1.68	0.57	1.43
NM_021358	Htr6	5-hydroxytryptamine (serotonin) receptor 6	1.08	-1.10	1.16	-1.05	0.00	5.36	0.42	1.47	0.54	1.47
NM_028752	Hvcn1	Hydrogen voltage-gated channel 1	0.70	1.23	0.00	-3.45	0.04	2.37	0.04	2.25	0.08	2.44
NM_021395	Hyou1	Hypoxia up-regulated 1	0.40	1.37	1.19	-0.96	0.03	2.57	1.18	-1.02	1.12	-0.98
NM_010493	Icam1	Intercellular adhesion molecule 1	1.13	-0.89	0.00	3.33	0.02	-2.43	0.01	-2.50	0.23	-1.77
NM_023892	Icam4	Intercellular adhesion molecule 4, Landsteiner-Wiener blood group	0.26	-1.46	0.34	1.43	0.01	3.38	0.91	-1.21	0.65	1.41
NM_017480	Icos	Inducible T-cell co-stimulator	1.07	-1.09	0.03	-1.97	0.30	-1.63	0.44	-1.47	0.29	-1.70
NM_010495	Id1	Inhibitor of DNA binding 1	0.09	1.70	1.13	-1.01	0.39	1.56	0.03	2.38	0.20	2.13
NM_133662	Ier3	Immediate early response 3	0.79	1.20	0.09	1.73	0.00	3.55	0.05	2.21	0.07	2.55
NM_008327	Ifi202b	Interferon activated gene 202B	0.88	-1.21	0.37	1.38	0.00	4.30	0.00	3.70	0.02	3.65
BC008167	Ifi203	Interferon activated gene 203	0.58	-1.30	0.41	1.38	0.01	3.05	0.02	2.65	0.07	2.60
NM_008329	Ifi204	Interferon activated gene 204	0.57	-1.31	0.33	1.42	0.04	2.39	0.06	2.16	0.13	2.22
NM_172648	Ifi205	Interferon activated gene 205	0.99	1.10	0.09	1.76	0.00	5.52	0.00	5.14	0.00	6.49
NM_023065	Ifi30	Interferon gamma inducible protein 30	0.97	1.14	1.19	-0.97	0.00	4.29	0.00	5.74	0.00	6.95
NM_027320	Ifi35	Interferon-induced protein 35	1.16	-1.06	0.12	1.66	0.03	2.48	0.27	1.59	1.12	-0.87

NM_133871	Ifi44	Interferon-induced protein 44	0.79	-1.22	0.00	2.67	0.03	-2.39	0.91	1.21	0.14	2.13
AI452181	Ifih1	Interferon induced with helicase C domain 1	1.04	-1.12	0.11	1.69	0.02	2.62	0.06	2.09	0.58	1.46
NM_008331	Ifit1	Interferon-induced protein with tetratricopeptide repeats 1	0.05	-1.85	0.00	4.15	0.93	1.20	0.34	1.53	0.14	2.22
NM_008332	Ifit2	Interferon-induced protein with tetratricopeptide repeats 2	1.07	-1.12	0.01	2.28	0.00	6.18	0.00	6.18	0.01	4.03
NM_010501	Ifit3	Interferon-induced protein with tetratricopeptide repeats 3	0.12	-1.63	0.00	5.72	0.24	1.74	0.78	1.19	1.10	-0.88
NM_026820	Ifitm1	Interferon induced transmembrane protein 1	0.83	1.18	0.15	1.61	0.03	2.51	0.12	1.86	0.40	1.61
AI386420	Ifitm6	Interferon induced transmembrane protein 6	0.71	-1.27	0.80	1.16	0.00	4.21	0.01	3.21	0.01	4.10
NM_028968	Ifitm7	Interferon induced transmembrane protein 7	0.27	1.45	0.07	1.78	0.01	3.45	0.07	2.03	0.33	1.68
NM_028742	Ifltd1	Intermediate filament tail domain containing 1	0.05	-1.83	0.56	1.31	0.00	4.34	0.00	3.54	0.08	2.50
NM_010511	Ifngr1	Interferon gamma receptor 1	1.10	-1.12	0.05	-1.91	0.25	1.71	0.02	2.48	0.07	2.65
AK020732	Igf1r	Insulin-like growth factor I receptor	1.15	-1.06	1.19	-1.03	0.04	-2.24	1.02	-1.17	0.86	-1.28
NM_008340	Igfals	Insulin-like growth factor binding protein, acid labile subunit	1.02	-1.12	0.16	-1.59	0.00	-3.30	0.32	-1.54	0.09	-2.03
NM_008342	Igfbp2	Insulin-like growth factor binding protein 2	1.16	-1.06	0.94	1.17	0.02	-2.49	0.72	-1.31	0.98	-1.22
NM_008343	Igfbp3	Insulin-like growth factor binding protein 3	0.54	-1.26	0.00	-3.07	0.01	3.41	0.02	2.49	0.08	2.48
NM_010518	Igfbp5	Insulin-like growth factor binding protein 5	0.00	2.67	0.05	1.85	0.92	1.16	0.58	1.40	0.66	1.46
BC031470	Igh-6	Immunoglobulin heavy chain 6 (heavy chain of IgM)	0.62	1.18	0.75	-1.17	0.96	-1.08	0.75	1.24	0.20	2.03
NM_030691	Igsf6	Immunoglobulin superfamily, member 6	1.19	-0.95	1.17	-1.01	0.05	2.36	0.00	3.49	0.00	6.63
NM_033608	Igsf9	Immunoglobulin superfamily, member 9	0.70	-1.18	0.03	-1.97	0.77	-1.32	1.19	-0.87	0.06	2.66
NM_018738	Igtp	Interferon gamma induced GTPase	0.48	-1.32	0.00	8.56	0.04	2.41	0.27	1.58	1.12	-0.91
AF177144	Ihpk1	Inositol hexaphosphate kinase 1	1.19	-0.99	0.00	2.55	0.00	-3.00	0.56	-1.36	0.71	-1.37
NM_021792	Iigp1	Interferon inducible GTPase 1	0.28	-1.45	0.00	3.24	0.50	1.42	0.46	1.39	0.56	1.48
NM_019440	Iigp2	Immunity-related GTPase family M member 2	0.20	-1.51	0.00	8.31	1.27	-0.94	0.29	1.59	0.56	1.47
NM_019777	Ikbke	Inhibitor of kappaB kinase epsilon	0.55	-1.30	0.86	1.18	0.02	2.59	0.23	1.65	0.43	1.57
NM_008348	Il10ra	Interleukin 10 receptor, alpha	0.17	1.52	0.97	1.06	0.04	2.51	0.00	3.58	0.00	5.36
NM_008352	Il12b	Interleukin 12b	0.98	1.13	1.17	-0.91	0.01	3.46	0.93	1.20	1.11	-0.85
NM_008357	Il15	Interleukin 15	0.94	1.10	0.02	2.11	0.23	-1.68	0.52	-1.39	0.27	-1.74
NM_145834	Il17c	Interleukin 17C	0.96	-1.16	1.19	-1.00	0.02	-2.41	0.00	-3.79	0.01	-2.80
NM_008359	Il17ra	Interleukin 17 receptor A	0.28	1.44	0.13	1.64	0.03	2.52	0.22	1.67	0.23	1.82
NM_010531	Il18bp	Interleukin 18 binding protein	1.09	-1.10	0.01	2.34	0.13	1.91	0.30	1.57	0.58	1.44
NM_008365	Il18r1	Interleukin 18 receptor 1	0.05	-1.85	1.05	-1.05	0.28	1.70	0.56	1.37	0.17	2.13

NM_001009940	Il19	Interleukin 19	0.96	-1.14	0.39	1.39	0.01	3.41	0.54	1.39	0.65	1.37
NM_010554	Il1a	Interleukin 1 alpha	1.14	-1.01	0.26	-1.49	0.02	2.75	0.08	1.98	0.35	1.72
NM_008361	Il1b	Interleukin 1 beta	0.96	1.05	0.07	1.83	0.00	4.15	0.00	3.33	0.00	5.58
AK009787	Il1f8	Interleukin 1 family, member 8	0.29	-1.45	0.02	-2.13	0.71	1.32	0.16	1.73	0.49	1.50
NM_008362	Il1r1	Interleukin 1 receptor, type I	0.17	1.54	0.10	1.75	0.00	5.17	0.33	1.59	0.04	2.87
NM_031167	Il1rn	Interleukin 1 receptor antagonist	0.25	1.47	0.12	1.67	0.00	13.50	0.00	3.68	0.01	3.88
BC030430	Il20rb	Interleukin 20 receptor beta	0.66	1.22	0.90	1.18	1.19	-1.05	0.02	-2.29	1.10	-0.99
NM_145636	Il27	Interleukin 27	1.14	-1.04	0.23	1.51	0.02	2.81	0.01	2.85	0.05	2.72
NM_013563	Il2rg	Interleukin 2 receptor, gamma chain	1.17	-1.05	0.04	1.94	1.18	-1.11	1.21	-0.93	0.89	1.25
NM_010556	Il3	Interleukin 3	1.18	-0.97	0.28	1.49	0.00	6.59	0.02	2.64	0.08	2.45
NM_029646	Il34	Interleukin 34	0.02	2.07	0.45	1.36	0.17	-1.80	0.09	-1.86	0.04	-2.27
NM_010215	Il4i1	Interleukin 4 induced 1	0.71	1.17	1.04	-1.04	0.01	-2.72	0.84	1.20	0.33	1.73
NM_010559	Il6ra	Interleukin 6 receptor, alpha	0.00	2.62	0.30	-1.49	0.98	-1.14	0.01	2.65	0.22	1.87
NM_010560	Il6st	Interleukin 6 signal transducer	1.17	-0.93	0.09	1.72	0.04	2.37	0.14	1.80	0.40	1.60
NM_008371	Il7	Interleukin 7	0.52	1.31	0.00	3.04	0.22	-1.67	0.01	-2.43	0.13	-1.94
NM_008372	Il7r	Interleukin 7 receptor	0.80	-1.19	1.01	-1.13	1.14	-1.14	1.21	-0.93	0.97	1.20
CA977449	Ilf2	Interleukin enhancer binding factor 2	0.15	-1.58	0.02	-2.07	0.01	3.07	0.00	3.41	0.03	3.25
NM_011829	Impdh1	Inosine 5'-phosphate dehydrogenase 1	1.14	-1.08	0.41	1.38	0.00	7.07	0.02	2.62	0.05	2.68
NM_008324	Indo	Indoleamine 2,3-dioxygenase 1	1.15	-0.96	1.02	-1.09	0.00	4.06	0.16	1.76	0.94	1.24
NM_010564	Inha	Inhibin alpha	0.26	-1.41	0.00	-2.84	0.46	-1.46	0.95	1.18	1.01	-1.14
NM_008380	Inhba	Inhibin beta-A	0.02	-2.00	0.00	-2.55	0.00	4.06	0.01	2.98	0.41	1.62
NM_010566	Inpp5d	Inositol polyphosphate-5-phosphatase D	0.31	1.35	0.26	1.49	0.03	2.62	0.01	3.11	0.01	4.50
NM_016721	Iqgap1	IQ motif containing GTPase activating protein 1	1.15	-1.06	0.98	1.11	0.02	2.88	0.01	3.22	0.02	3.74
NM_008390	Irf1	Interferon regulatory factor 1	0.91	-1.15	0.00	6.62	0.20	1.77	0.03	2.41	0.11	2.35
NM_016850	Irf7	Interferon regulatory factor 7	0.92	-1.13	0.00	2.65	0.04	-2.28	0.06	-1.99	0.02	-2.53
NM_008320	Irf8	Interferon regulatory factor 8	1.17	-0.93	0.00	10.17	0.01	3.49	0.00	4.86	0.01	4.22
NM_008326	Irgm1	Immunity-related GTPase family M member 1	0.66	-1.27	0.00	4.62	0.07	2.18	0.01	3.10	0.05	2.82
AK051117	Irgq	Immunity-related GTPase family, Q	0.01	2.32	0.01	2.53	0.24	1.73	1.21	-0.88	1.10	-0.96
AW212853	Irs1	Insulin receptor substrate 1	0.18	-1.52	0.03	-1.98	0.00	6.62	0.00	8.05	0.00	11.53
NM_018885	Irx4	Iroquois related homeobox 4 (Drosophila)	1.11	-1.06	1.05	-1.13	0.00	-3.48	0.01	-2.46	0.14	-1.89

NM_020583	Isg20	Interferon-stimulated protein	0.70	-1.24	0.08	1.77	0.00	4.73	0.05	2.18	0.48	1.53
NM_027397	Isl2	Insulin related protein 2 (islet 2)	0.02	2.13	0.07	1.90	0.74	-1.30	0.62	1.33	1.07	-1.11
NM_023627	Isyna1	Myo-inositol 1-phosphate synthase A1	1.18	-1.03	1.19	-0.93	0.00	21.06	0.00	5.83	0.00	5.77
NM_013565	Itga3	Integrin alpha 3	0.11	-1.64	0.19	-1.54	0.11	-1.94	0.01	-2.64	0.02	-2.58
AK085324	Itga9	Integrin alpha 9	0.62	-1.28	0.35	-1.45	0.03	-2.37	1.21	-0.94	0.58	1.48
NM_008400	Itgal	Integrin alpha L	1.19	-0.97	1.16	-0.91	0.06	2.16	0.00	3.66	0.02	3.72
AK009352	Itgb1bp3	Integrin beta 1 binding protein 3	0.04	1.99	0.16	1.64	0.10	1.99	0.13	1.81	0.15	2.05
NM_008404	Itgb2	Integrin beta 2	1.17	-1.03	1.19	-0.95	0.01	3.43	0.00	4.22	0.00	5.80
NM_021359	Itgb6	Integrin beta 6	0.01	-2.32	0.10	-1.74	0.90	1.24	0.42	1.48	0.75	1.34
AK018605	Itih5	Inter-alpha (globulin) inhibitor H5	0.80	-1.23	0.88	-1.16	0.07	-2.04	0.02	-2.24	0.13	-1.95
NM_172584	Itpk1	Inositol 1,3,4-triphosphate 5/6 kinase	1.07	-1.11	0.03	1.98	0.06	2.20	0.42	1.46	0.23	1.82
NM_010589	Jak3	Janus kinase 3	0.34	1.40	0.05	1.87	0.78	-1.07	0.92	1.21	1.12	-0.88
BB361206	Jarid1b	Lysine (K)-specific demethylase 5B	0.51	1.32	0.35	1.42	0.05	2.29	0.55	1.37	0.55	1.47
NM_030887	Jdp2	Jun dimerization protein 2	0.17	1.55	0.78	1.19	0.09	2.07	0.03	2.33	0.02	3.56
AI592182	Jmjd1c	Jumonji domain containing 1C	0.05	-1.84	0.05	-1.86	0.79	1.27	0.03	2.33	0.20	1.93
NM_010591	Jun	Jun oncogene	0.26	1.47	0.20	1.58	0.03	2.58	0.74	1.28	0.35	1.74
NM_008416	Junb	Jun-B oncogene	0.80	-1.22	0.00	3.71	0.15	1.87	0.15	1.77	0.82	1.31
NM_145983	Kcna5	Potassium voltage-gated channel, shaker-related subfamily, member 5	1.16	-1.05	0.13	-1.67	0.00	-4.45	0.00	-3.94	0.04	-2.29
NM_008420	Kcnb1	Potassium voltage gated channel, Shab-related subfamily, member 1	0.04	1.92	0.08	1.81	0.06	-2.11	0.70	-1.31	0.96	-1.21
BE949887	Kcnc1	Potassium voltage gated channel, Shaw-related subfamily, member 1	1.19	-1.02	0.95	1.16	0.01	2.88	0.94	1.19	0.96	1.21
NM_133207	Kcnh7	Potassium voltage-gated channel, subfamily H (eag-related), member 7	1.15	-1.06	1.17	-0.92	0.94	1.21	0.05	2.11	0.03	3.27
NM_010604	Kcnj16	Potassium inwardly-rectifying channel, subfamily J, member 16	0.64	1.25	0.00	-4.04	0.09	-2.03	0.25	-1.60	1.06	-1.06
NM_010606	Kcnj6	Potassium inwardly-rectifying channel, subfamily J, member 6	1.08	-1.09	0.04	-1.92	0.00	3.75	0.03	2.40	0.18	1.99
AK019376	Kcnk10	Potassium channel, subfamily K, member 10	0.03	1.93	0.12	1.75	0.01	3.10	0.00	3.66	0.00	5.59
NM_021542	Kcnk5	Potassium channel, subfamily K, member 5	0.03	1.99	0.22	-1.51	0.69	-1.32	0.86	1.23	1.13	-0.86
NM_008435	Kcns1	K+ voltage-gated channel, subfamily S, 1	1.02	-1.12	0.00	-2.47	0.00	-3.20	0.08	-1.91	0.00	-7.35
BC023820	Kdsr	3-ketodihydrosphingosine reductase	0.86	1.17	0.95	-1.17	0.00	-3.00	0.09	-1.90	0.34	-1.65
NM_029550	Keg1	Kidney expressed gene 1	0.95	-1.14	0.15	-1.61	0.00	-3.29	0.64	-1.34	0.16	-1.86

NM_010615	Kif11	Kinesin family member 11	0.63	-1.28	0.08	-1.77	0.38	1.54	0.40	1.48	0.74	1.35
NM_207682	Kif1b	Kinesin family member 1B	1.03	-1.15	1.00	-1.16	0.05	-2.20	0.36	-1.52	0.63	-1.43
NM_134471	Kif2c	Kinesin family member 2C	1.06	-1.09	0.25	-1.48	0.00	-11.19	0.26	-1.58	0.08	-2.07
NM_146182	Klc3	Kinesin light chain 3	1.16	-1.03	1.19	-0.98	1.25	-0.86	1.05	-1.00	0.02	-2.55
NM_013692	Klf10	Kruppel-like factor 10	0.71	-1.26	0.05	-1.87	0.05	-2.19	0.04	-2.08	0.14	-1.89
Y14295	Klf12	Kruppel-like factor 12	1.19	-0.97	0.87	1.18	0.02	2.58	0.57	1.37	0.54	1.46
NM_023184	Klf15	Kruppel-like factor 15	0.03	1.92	0.65	-1.26	1.28	-0.93	0.15	1.77	0.94	1.24
NM_010637	Klf4	Kruppel-like factor 4 (gut)	0.04	1.88	0.66	1.28	0.27	1.65	0.15	1.82	0.89	1.15
NM_008459	Klra10	Killer cell lectin-like receptor subfamily A, member 10	0.68	1.17	0.18	1.63	0.12	2.02	0.00	4.94	0.01	4.57
NM_008462	Klra2	Killer cell lectin-like receptor, subfamily A, member 2	1.17	-1.02	0.93	1.07	0.05	2.38	0.00	3.60	0.00	6.86
NM_010648	Klra3	Killer cell lectin-like receptor, subfamily A, member 3	0.83	1.13	0.71	0.97	0.01	2.94	0.00	7.33	0.00	6.40
NM_010652	Klrc1	Killer cell lectin-like receptor subfamily C, member 1	0.71	-1.23	0.87	-1.19	0.25	1.68	0.01	2.69	0.03	3.24
NM_033078	Klrk1	Killer cell lectin-like receptor subfamily K, member 1	0.31	-1.39	0.05	1.91	0.18	1.86	0.00	4.31	0.01	4.15
AK172905	Kntc1	Kinetochore associated 1	0.05	-1.80	0.08	-1.79	0.01	3.18	0.00	4.40	0.02	3.72
NM_010664	Krt18	Keratin 18	0.45	-1.33	0.01	2.24	0.01	-2.78	0.11	-1.79	0.11	-1.97
AI316362	Krt19	Keratin 19	1.18	-1.04	1.09	-1.11	0.03	-2.34	0.12	-1.80	0.60	-1.44
NM_008482	Lamb1-1	Laminin B1 subunit 1	0.04	1.92	0.00	2.83	0.00	4.33	0.00	4.46	0.01	4.34
NM_022964	Lat2	Linker for activation of T cells family, member 2	1.03	-1.01	1.09	-0.99	0.04	2.38	0.00	3.32	0.01	3.88
AF317517	Lbh	Limb-bud and heart	0.02	2.13	0.28	1.34	0.00	11.84	0.00	11.84	0.00	7.80
NM_008489	Lbp	Lipopolysaccharide binding protein	0.68	-1.25	1.17	-0.97	0.01	2.90	0.64	1.33	0.94	1.25
NM_010693	Lck	Lymphocyte protein tyrosine kinase	1.15	-0.92	0.94	1.17	0.13	1.90	0.01	2.93	0.02	3.51
NM_029959	Lcn9	Lipocalin 9	1.18	-0.98	0.92	1.17	0.01	3.04	0.61	1.35	0.93	1.24
NM_010696	Lcp2	Lymphocyte cytosolic protein 2	0.67	-1.24	0.20	1.57	0.00	3.92	0.00	4.72	0.00	5.63
NM_010701	Lect1	Leukocyte cell derived chemotaxin 1	0.47	-1.32	1.09	-1.09	0.00	-5.41	0.30	-1.55	0.04	-2.26
NM_008495	Lgals1	Lectin, galactose binding, soluble 1	1.18	-0.95	1.18	-0.96	0.02	2.65	0.02	2.51	0.12	2.21
NM_010712	Lhx4	LIM homeobox protein 4	1.17	-0.94	0.02	2.19	0.00	17.98	0.00	4.22	0.00	5.65
NM_013584	Lifr	Leukemia inhibitory factor receptor	0.49	-1.32	0.00	-2.66	0.87	1.16	0.07	2.04	0.46	1.60
NM_011095	Lilrb3	Leukocyte immunoglobulin-like receptor, subfamily B (with TM and ITIM domains), member 3	1.04	-1.13	0.11	-1.73	0.24	1.73	0.02	2.59	0.00	5.19
NM_013532	Lilrb4	Leukocyte immunoglobulin-like receptor, subfamily B, member 4	0.81	-1.16	0.13	1.63	0.06	2.21	0.02	2.62	0.01	4.36
NM_019980	Litaf	LPS-induced TN factor	1.17	-1.05	0.54	1.32	0.01	2.93	0.28	1.59	0.25	1.78

NM_144799	Lmcd1	LIM and cysteine-rich domains 1	0.01	2.20	0.74	1.14	1.06	-0.98	0.84	-1.12	0.15	-1.84
NM_010727	Lnx1	Ligand of numb-protein X 1	0.19	1.51	0.01	2.68	0.00	23.37	0.00	9.41	0.02	3.51
BG074664	LOC100042764	Zinc finger protein 523	0.08	-1.72	0.12	-1.68	0.15	-1.81	0.00	-3.83	0.01	-2.66
NM_010729	Loxl1	Lysyl oxidase-like 1	0.02	-2.01	0.03	-1.99	1.27	-0.97	0.79	-1.23	0.44	-1.56
NM_175271	Lpar4	Lysophosphatidic acid receptor 4	0.01	-2.29	0.06	-1.81	0.48	1.46	1.21	-0.90	0.76	-1.21
NM_173014	Lpcat2	Lysophosphatidylcholine acyltransferase 2	0.67	1.25	0.31	1.46	0.04	2.42	0.00	4.14	0.00	5.24
NM_172266	Lpgat1	Lysophosphatidylglycerol acyltransferase 1	0.79	1.20	1.06	-1.09	0.01	3.24	0.25	1.62	0.38	1.60
AF180471	Lpin1	Lipin 1	0.00	2.93	0.13	1.64	0.38	-1.54	0.08	-1.87	0.64	-1.31
NM_008509	Lpl	Lipoprotein lipase	0.02	-2.11	0.43	-1.41	0.12	-1.89	0.02	-2.25	0.09	-2.05
NM_146164	Lrch4	Leucine-rich repeats and calponin homology (CH) domain containing 4	0.90	-1.18	1.17	-0.91	0.52	1.44	0.45	1.43	1.13	-0.99
NM_029796	Lrg1	Leucine-rich alpha-2-glycoprotein 1	0.95	1.15	0.08	1.76	0.01	3.30	0.06	2.07	0.07	2.47
NM_008511	Lrmp	Lymphoid-restricted membrane protein	1.19	-0.96	0.83	-1.21	0.25	1.70	0.03	2.36	0.08	2.42
NM_019391	Lsp1	Lymphocyte specific 1	0.75	-1.24	1.16	-1.08	0.17	1.84	0.02	2.50	0.01	4.03
NM_146006	Lss	Lanosterol synthase	1.03	-1.09	0.04	1.97	0.01	-2.73	0.00	-3.77	0.00	-3.27
NM_010734	Lst1	Leukocyte specific transcript 1	1.18	-1.00	0.96	1.14	0.01	3.17	0.00	4.46	0.00	5.92
NM_008518	Ltb	Lymphotoxin B	1.16	-0.92	1.19	-0.97	0.02	2.64	0.01	2.81	0.01	4.59
NM_019919	Ltbp1	Latent transforming growth factor beta binding protein 1	0.69	-1.24	0.01	-2.31	0.00	22.54	0.00	15.32	0.00	10.52
NM_013589	Ltbp2	Latent transforming growth factor beta binding protein 2	1.09	-1.10	1.12	-1.07	0.02	-2.43	0.27	-1.59	1.11	-1.07
NM_175641	Ltbp4	Latent transforming growth factor beta binding protein 4	0.95	-1.16	0.58	-1.31	0.03	-2.35	0.00	-2.88	0.01	-2.77
NM_028190	Luc7l	Luc7 homolog (S. cerevisiae)-like	0.02	2.05	0.22	1.54	0.41	1.50	0.86	1.17	0.96	-1.16
NM_010738	Ly6a	Lymphocyte antigen 6 complex, locus A	0.16	-1.53	0.05	1.73	0.00	12.37	0.00	13.49	0.00	10.56
NM_010742	Ly6d	Lymphocyte antigen 6 complex, locus D	0.52	-1.29	0.82	-1.18	0.00	9.61	0.00	5.32	0.00	6.06
NM_020498	Ly6i	Lymphocyte antigen 6 complex, locus I	1.18	-1.02	0.97	1.11	0.02	2.75	0.02	2.67	0.06	2.72
NM_010745	Ly86	Lymphocyte antigen 86	1.16	-1.06	0.73	-1.26	0.01	3.02	0.00	3.43	0.01	4.34
NM_008534	Ly9	Lymphocyte antigen 9	1.19	-0.98	0.94	1.13	0.02	2.88	0.00	3.44	0.02	3.75
NM_008535	Lyl1	Lymphoblastomic leukemia 1	0.39	-1.38	0.01	-2.34	0.00	20.15	0.00	16.35	0.00	13.59
NM_053247	Lyve1	Lymphatic vessel endothelial hyaluronan receptor 1	0.02	2.12	0.24	-1.52	0.07	2.13	0.17	1.72	0.76	1.37
NM_011839	Mab21l2	Mab-21-like 2 (C. elegans)	0.98	0.98	0.92	1.01	0.02	-2.51	0.82	1.23	0.70	-1.33
NM_134147	Macrod1	MACRO domain containing 1	0.59	1.29	0.70	1.26	0.01	-2.61	0.81	-1.25	0.99	-1.19

NM_027985	Mad2l2	MAD2 mitotic arrest deficient-like 2 (yeast)	0.02	-2.02	0.25	-1.53	0.11	2.01	0.31	-1.54	0.76	-1.34
NM_010758	Mag	Myelin-associated glycoprotein	0.56	-1.27	0.70	1.25	0.06	2.16	0.01	3.06	0.04	2.82
NM_011943	Map2k6	Mitogen-activated protein kinase kinase 6	0.02	2.06	0.71	1.20	0.00	-9.97	0.87	-1.11	0.00	-3.55
NM_007746	Map3k8	Mitogen-activated protein kinase kinase kinase 8	0.64	1.26	0.11	1.69	0.22	1.73	0.01	2.66	0.05	2.70
NM_008279	Map4k1	Mitogen-activated protein kinase kinase kinase kinase 1	1.16	-1.06	0.58	1.29	0.05	2.34	0.00	3.35	0.03	3.28
BE864858	Map6d1	MAP6 domain containing 1	1.19	-0.98	0.36	-1.43	0.01	-2.68	0.01	-2.41	0.12	-1.96
CD742412	Mapk14	Mitogen-activated protein kinase 14	0.00	-2.91	0.37	-1.39	1.26	-0.98	0.59	1.36	0.41	1.57
NM_011952	Mapk3	Mitogen-activated protein kinase 3	1.07	-1.11	0.14	-1.64	0.01	-2.82	0.04	-2.07	0.21	-1.78
NM_010807	Marcksl1	MARCKS-like 1	0.18	-1.52	0.04	2.00	0.26	-1.67	0.01	-2.47	0.00	-4.93
NM_010766	Marco	Macrophage receptor with collagenous structure	0.46	1.35	0.05	1.84	0.00	5.50	0.00	6.41	0.00	20.24
AK042888	Mars2	Methionine-tRNA synthetase 2 (mitochondrial)	0.04	1.86	0.07	1.81	0.27	1.70	0.22	1.76	0.78	1.27
BB772766	Mc1r	Melanocortin 1 receptor	0.01	-2.29	0.00	-2.56	0.93	1.16	0.54	1.44	0.91	1.27
NM_178076	Mcf2l	Mcf.2 transforming sequence-like	0.58	1.27	0.34	1.45	0.00	8.99	0.02	2.52	0.06	2.65
NM_008563	Mcm3	Minichromosome maintenance deficient 3 (S. cerevisiae)	1.17	-0.93	0.65	1.27	0.06	2.20	0.01	3.03	0.14	2.19
NM_008565	Mcm4	Minichromosome maintenance deficient 4 homolog (S. cerevisiae)	0.88	1.16	1.17	-0.91	0.10	2.00	0.03	2.37	0.17	2.08
NM_008566	Mcm5	Minichromosome maintenance deficient 5, cell division cycle 46 (S. cerevisiae)	0.96	1.09	0.67	-1.27	0.01	2.99	0.00	3.33	0.06	2.80
NM_008567	Mcm6	Minichromosome maintenance deficient 6 (MIS5 homolog, S. pombe) (S. cerevisiae)	0.83	1.09	0.35	-1.39	0.04	2.43	0.01	3.21	0.01	4.93
NM_008568	Mcm7	Minichromosome maintenance deficient 7 (S. cerevisiae)	1.17	-1.05	0.04	-1.92	0.08	2.09	0.02	2.51	0.12	2.19
NM_026656	Mcoln2	Mucolipin 2	0.85	-1.06	0.53	1.32	0.04	2.44	0.00	4.13	0.04	2.83
NM_010783	Mdfi	MyoD family inhibitor	0.72	1.14	0.98	-1.03	0.02	2.63	0.30	1.59	0.42	1.60
NM_145494	Me2	Malic enzyme 2, NAD(+)-dependent, mitochondrial	1.12	-0.90	1.18	-0.90	0.15	1.86	0.02	2.53	0.08	2.42
AI429440	Med12	Mediator of RNA polymerase II transcription, subunit 12 homolog (yeast)	0.02	-2.09	0.20	-1.60	0.20	1.80	0.67	1.35	1.13	-0.85
NM_019453	Mefv	Mediterranean fever	0.11	1.66	0.02	2.19	0.00	3.67	0.01	3.02	0.04	2.90
NM_010791	Meox1	Mesenchyme homeobox 1	1.16	-1.04	0.97	-1.15	0.03	2.46	0.76	1.28	0.87	-1.19
NM_008589	Mesp2	Mesoderm posterior 2	1.18	-1.03	0.93	1.17	0.00	10.95	0.00	5.15	0.02	3.54
AK035332	Mgat4a	Mannoside acetylglucosaminyltransferase 4, isoenzyme A	0.79	-1.14	0.77	1.19	0.06	2.22	0.01	2.89	0.03	3.15
NM_011844	Mgll	Monoglyceride lipase	0.31	1.42	1.19	-0.99	0.01	-2.72	0.66	-1.33	0.70	-1.38
NM_025569	Mgst3	Microsomal glutathione S-transferase 3	0.53	1.31	0.82	1.22	0.01	-2.65	1.12	-1.09	0.78	-1.33

X82786	Mki67	Antigen identified by monoclonal antibody Ki 67	0.03	-1.99	0.00	-3.27	1.27	-0.94	0.85	1.24	0.78	1.32
NM_021462	Mknk2	MAP kinase-interacting serine/threonine kinase 2	0.00	2.84	0.02	2.09	0.00	-3.65	0.08	-1.92	0.01	-2.84
NM_027973	Mlf1ip	Myeloid leukemia factor 1 interacting protein	0.49	1.21	0.75	-1.14	0.21	1.78	0.01	2.89	0.04	3.06
AV381294	Mllt3	Myeloid/lymphoid or mixed-lineage leukemia (trithorax homolog, Drosophila); translocated to, 3	0.02	2.12	0.31	1.45	0.05	2.44	0.02	2.63	0.20	2.03
NM_019966	Mlycd	Malonyl-CoA decarboxylase	1.17	-0.93	1.20	-0.94	0.01	-2.59	0.26	-1.59	0.23	-1.73
NM_008605	Mmp12	Matrix metallopeptidase 12	0.02	2.14	0.44	-1.21	1.24	-1.06	1.15	-1.08	0.63	-1.43
NM_010809	Mmp3	Matrix metallopeptidase 3	0.00	-2.96	0.16	-1.61	0.73	-1.33	0.03	-2.22	0.13	-1.94
NM_010810	Mmp7	Matrix metallopeptidase 7	0.36	1.38	0.99	1.10	0.05	2.34	0.06	2.10	0.15	2.04
NM_008611	Mmp8	Matrix metallopeptidase 8	1.12	-1.06	0.53	1.33	0.00	5.37	0.01	2.90	0.00	5.68
L20315	Mpeg1	Macrophage expressed gene 1	1.14	-1.08	0.01	2.40	0.00	7.06	0.00	7.83	0.00	6.34
NM_010824	Mpo	Myeloperoxidase	0.55	-1.20	0.01	-2.27	0.12	-1.87	0.73	-1.23	0.70	-1.26
NM_001005423	Mreg	Melanoregulin	0.78	-1.22	0.03	-1.99	0.00	8.89	0.00	8.02	0.00	9.79
NM_145379	Mrgprf	MAS-related GPR, member F	0.65	-1.24	0.43	-1.38	0.11	-1.93	0.01	-2.46	0.36	-1.63
NM_007641	Ms4a1	Membrane-spanning 4-domains, subfamily A, member 1	0.03	-1.94	0.99	-1.13	0.00	5.60	0.00	7.98	0.00	6.39
NM_027209	Ms4a6b	Membrane-spanning 4-domains, subfamily A, member 6B	0.90	-1.15	0.60	1.23	0.00	4.22	0.00	5.37	0.00	5.72
BY495604	Ms4a6c	Membrane-spanning 4-domains, subfamily A, member 6C	0.42	1.28	0.13	1.67	0.00	5.24	0.00	6.71	0.00	6.96
NM_026835	Ms4a6d	Membrane-spanning 4-domains, subfamily A, member 6D	0.46	1.29	0.01	2.42	0.00	3.80	0.00	3.98	0.04	2.92
NM_022430	Ms4a8a	Membrane-spanning 4-domains, subfamily A, member 8A	0.93	1.13	1.08	-1.10	1.25	-1.02	0.09	1.96	0.01	4.50
NM_019544	Msgn1	Mesogenin 1	1.18	-0.92	1.15	-0.88	0.02	2.73	0.04	2.20	0.39	1.62
NM_018857	Msln	Mesothelin	1.09	-1.00	0.03	-2.00	0.18	-1.80	0.12	-1.81	0.65	-1.40
NM_031195	Msr1	Macrophage scavenger receptor 1	0.96	1.12	0.30	1.45	0.02	2.75	0.00	3.55	0.02	3.54
NM_029619	Msrb2	Methionine sulfoxide reductase B2	0.89	-1.19	0.00	-2.47	0.67	-1.27	0.96	1.18	0.75	1.38
NM_013601	Msx2	Homeobox, msh-like 2	0.97	-1.16	0.89	-1.20	0.21	-1.75	0.03	-2.17	0.50	-1.51
NM_010836	Msx3	Homeobox, msh-like 3	0.14	-1.59	0.10	-1.72	0.40	-1.53	0.00	-3.05	0.20	-1.81
NM_013602	Mt1	Metallothionein 1	0.61	1.27	0.05	1.85	0.02	2.63	0.02	2.52	0.10	2.28
NM_008630	Mt2	Metallothionein 2	0.02	2.10	0.00	4.40	0.98	-1.17	0.71	1.28	0.69	-1.33
NM_008638	Mthfd2	Methylenetetrahydrofolate dehydrogenase (NAD+ dependent), methenyltetrahydrofolate cyclohydrolase	1.19	-1.00	1.19	-0.94	0.01	3.02	0.02	2.44	0.24	1.84
AW110396	Mup1	Major urinary protein 1	0.02	-2.05	0.08	-1.71	0.38	-1.50	0.06	-1.99	0.71	-1.28

AW112931	Mup3	Major urinary protein 3	0.53	-1.28	0.67	-1.23	0.59	-1.40	0.02	-2.31	0.00	-4.06
NM_008648	Mup4	Major urinary protein 1	0.00	-3.09	0.01	-2.28	0.10	2.02	0.85	-1.16	0.54	1.46
NM_008649	Mup5	Major urinary protein 5	0.03	-1.95	0.12	-1.60	0.63	1.36	0.16	1.76	1.12	-0.84
NM_010846	Mx1	Myxovirus (influenza virus) resistance 1	0.65	-1.26	0.11	1.72	0.00	3.82	0.01	3.26	0.07	2.56
NM_013606	Mx2	Myxovirus (influenza virus) resistance 2	0.74	-1.23	0.00	3.88	0.12	2.00	0.17	1.80	0.60	1.49
NM_010751	Mxd1	MAX dimerization protein 1	1.18	-0.95	0.68	1.24	0.01	3.04	0.12	1.86	0.36	1.65
NM_008652	Mybl2	Myeloblastosis oncogene-like 2	0.11	1.61	0.06	1.97	0.03	2.64	0.00	3.59	0.06	2.64
NM_010850	Mycs	Myc-like oncogene, s-myc protein	0.67	1.24	0.06	-1.83	0.03	-2.38	0.26	-1.56	0.43	-1.52
NM_010851	Myd88	Myeloid differentiation primary response gene 88	1.12	-0.89	0.04	1.89	0.14	-1.83	0.23	-1.61	0.11	-1.98
NM_153789	Mylip	Myosin regulatory light chain interacting protein	1.18	-0.95	0.03	-2.01	0.64	-1.16	0.50	1.43	1.08	-0.86
AK016515	Myo18b	Myosin XVIIIb	1.16	-0.92	0.20	-1.56	0.00	-3.00	0.01	-2.38	0.13	-1.91
NM_053214	Myo1f	Myosin IF	0.70	-1.26	1.17	-1.06	0.02	2.65	0.00	3.45	0.01	4.70
NM_010866	Myod1	Myogenic differentiation 1	0.00	2.65	0.04	2.00	0.00	5.04	0.00	6.03	0.01	3.99
BB045598	Mysm1	Myb-like, SWIRM and MPN domains 1	0.03	2.03	0.12	1.66	0.07	-2.03	0.02	-2.37	0.21	-1.81
NM_025972	Naaa	N-acylethanolamine acid amidase	0.43	-1.36	1.18	-0.94	0.06	2.18	0.03	2.39	0.06	2.70
AK012899	Naaladl2	N-acetylated alpha-linked acidic dipeptidase-like 2	0.02	2.05	0.25	1.50	1.11	-1.12	0.41	1.46	0.22	1.84
BC004086	Nat13	N-acetyltransferase 13	0.25	1.46	0.58	1.31	0.04	2.32	0.02	2.41	0.19	1.92
NM_144818	Ncaph	Non-SMC condensin I complex, subunit H	1.06	-1.07	0.57	-1.30	0.25	1.70	0.02	2.45	0.29	1.82
NM_010876	Ncf1	Neutrophil cytosolic factor 1	0.06	1.78	0.64	1.20	0.01	3.16	0.00	3.99	0.00	5.33
NM_010877	Ncf2	Neutrophil cytosolic factor 2	1.18	-0.94	1.19	-0.97	0.20	1.79	0.01	2.83	0.01	4.51
NM_008677	Ncf4	Neutrophil cytosolic factor 4	0.95	1.14	0.36	1.43	0.02	2.79	0.00	3.77	0.00	5.21
NM_010746	Ncr1	Natural cytotoxicity triggering receptor 1	0.70	-1.20	0.36	1.41	0.00	4.14	0.00	6.41	0.01	4.67
NM_017464	Nedd9	Neural precursor cell expressed, developmentally down-regulated gene 9	0.94	1.14	0.85	1.18	0.01	2.89	0.05	2.12	0.13	2.19
NM_010892	Nek2	NIMA (never in mitosis gene a)-related expressed kinase 2	0.16	-1.56	0.02	-2.06	1.27	-0.98	1.16	-1.05	0.33	1.66
NM_016720	Neu3	Neuraminidase 3	0.01	2.42	0.05	1.94	0.11	-1.92	0.10	-1.84	0.11	-1.98
NM_028728	Nfam1	Nfat activating molecule with ITAM motif 1	1.16	-0.92	0.79	-1.24	1.26	-0.91	0.08	2.00	0.04	2.98
AV277440	Nfatc2ip	Nuclear factor of activated T-cells, cytoplasmic, calcineurin-dependent 2 interacting protein	0.28	1.44	0.21	1.53	0.00	9.09	0.00	4.41	0.03	3.14
NM_023699	Nfatc4	Nuclear factor of activated T-cells, cytoplasmic, calcineurin-dependent 4	0.02	-2.02	0.08	-1.79	0.01	3.12	0.09	1.95	0.14	2.12

NM_030612	Nfkbiz	Nuclear factor of kappa light polypeptide gene enhancer in B-cells inhibitor, zeta	0.39	1.34	0.03	2.03	0.20	1.77	0.14	1.80	0.39	1.59
NM_024253	Nkg7	Natural killer cell group 7 sequence	1.18	-1.01	0.48	1.35	0.00	5.09	0.00	8.68	0.00	7.45
NM_008701	Nkx2-9	NK2 transcription factor related, locus 9 (Drosophila)	0.56	1.19	0.17	-1.52	0.29	-1.61	0.00	-3.42	0.32	-1.67
AK035300	Nlrc4	NLR family, CARD domain containing 4	1.19	-0.95	1.20	-0.95	0.12	1.93	0.01	3.07	0.01	4.46
NM_145827	Nlrp3	NLR family, pyrin domain containing 3	0.22	1.39	0.11	1.76	0.01	3.42	0.00	4.02	0.00	5.41
NM_175188	NM_175188	Membrane-associated ring finger (C3HC4) 1	1.16	-1.07	0.76	1.18	0.01	3.17	0.00	3.99	0.00	5.60
NM_213614	NM_213614	Septin 5	1.14	-0.98	0.99	1.11	0.00	3.82	1.17	-0.93	0.69	1.36
NM_019401	Nmi	N-myc (and STAT) interactor	1.18	-0.93	0.03	2.00	0.00	-3.49	0.04	-2.11	0.01	-2.74
NM_010924	Nnmt	Nicotinamide N-methyltransferase	0.00	2.71	0.00	3.41	0.67	1.35	0.68	1.31	0.79	1.36
NM_172729	Nod1	Nucleotide-binding oligomerization domain containing 1	0.76	-1.24	0.08	1.77	0.04	2.38	0.04	2.22	0.10	2.31
NM_016708	Npy5r	Neuropeptide Y receptor Y5	0.94	-1.04	1.04	-1.02	0.30	-1.58	0.52	-1.35	0.03	-2.33
U12142	Nr1d2	Nuclear receptor subfamily 1, group D, member 2	0.05	1.81	0.06	1.87	0.00	31.72	0.00	12.41	0.00	13.79
NM_010936	Nr1i2	Nuclear receptor subfamily 1, group I, member 2	0.04	1.87	0.39	1.40	0.01	3.31	0.00	4.74	0.01	4.06
NM_009803	Nr1i3	Nuclear receptor subfamily 1, group I, member 3	1.18	-0.93	0.37	-1.43	0.00	-3.05	0.62	-1.36	1.10	-1.03
NM_010444	Nr4a1	Nuclear receptor subfamily 4, group A, member 1	0.04	-1.88	0.45	-1.34	0.00	4.15	0.31	1.60	0.11	2.29
NM_008734	Nrg3	Neuregulin 3	1.03	-1.13	0.16	-1.63	0.11	-1.92	0.01	-2.66	0.15	-1.90
NM_032002	Nrg4	Neuregulin 4	0.00	5.43	0.01	2.36	0.00	5.60	0.00	5.72	0.00	5.23
NM_008738	Nrtn	Neurturin	0.03	1.97	0.24	1.50	0.21	1.79	0.72	1.29	0.53	1.53
NM_028950	Nsun6	NOL1/NOP2/Sun domain family member 6	0.00	-2.51	0.97	-1.08	0.16	-1.83	0.00	-2.84	0.00	-3.51
BY467842	Nt5c	5',3'-nucleotidase, cytosolic	0.04	1.97	0.02	2.25	0.07	2.15	0.30	1.57	0.73	1.34
NM_011851	Nt5e	5' nucleotidase, ecto	1.18	-1.02	0.02	-2.09	0.02	2.65	0.27	1.65	0.29	1.80
NM_008745	Ntrk2	Neurotrophic tyrosine kinase, receptor, type 2	0.43	-1.30	0.00	-2.50	0.99	1.07	0.95	-1.09	0.63	-1.36
NM_028778	Nuak2	NUAK family, SNF1-like kinase, 2	1.19	-0.99	0.00	2.65	0.00	11.87	0.00	8.22	0.01	4.52
NM_023284	Nuf2	NUF2, NDC80 kinetochore complex component, homolog (S. cerevisiae)	0.26	-1.43	0.19	-1.57	0.06	2.27	0.02	2.48	0.14	2.26
CF536270	Numbl	Numb-like	0.04	1.90	0.03	2.18	0.01	3.50	0.01	3.01	0.13	2.21
NM_019738	Nupr1	Nuclear protein 1	0.30	-1.41	0.64	1.22	0.01	3.09	0.01	2.93	0.05	2.77
NM_133851	Nusap1	Nucleolar and spindle associated protein 1	0.21	-1.50	0.00	-2.45	0.27	1.65	0.62	1.36	0.56	1.46
NM_145227	Oas2	2'-5' oligoadenylate synthetase 2	0.19	-1.52	0.64	1.20	0.02	2.86	0.04	2.24	0.04	3.00
NM_145209	Oasl1	2'-5' oligoadenylate synthetase-like 1	0.23	-1.50	0.02	2.18	0.52	1.43	0.59	1.33	0.56	1.51

NM_028696	Obfc2a	Oligonucleotide/oligosaccharide-binding fold containing 2A	0.50	1.25	0.25	1.52	0.09	2.13	0.01	3.00	0.01	3.92
NM_013614	Odc1	Ornithine decarboxylase, structural 1	0.02	2.11	0.70	1.26	0.74	-1.32	1.21	-0.92	1.12	-0.93
NM_145746	Odf4	Outer dense fiber of sperm tails 4	0.38	1.39	0.86	1.16	1.24	-1.02	0.04	-2.08	0.88	-1.25
AK004916	Ogfod2	2-oxoglutarate and iron-dependent oxygenase domain containing 2	1.15	-1.04	1.09	-1.10	0.00	-4.79	0.00	-4.53	0.01	-3.04
NM_008760	Ogn	Osteoglycin	1.06	-1.13	0.00	-2.60	0.23	-1.74	1.08	-1.08	0.08	2.48
NM_153157	Olfm3	Olfactomedin 3	0.07	-1.77	0.32	-1.40	0.01	-2.85	0.97	-1.17	0.22	-1.79
NM_146571	Olfr1015	Olfactory receptor 1015	1.10	-1.07	1.20	-0.95	0.03	2.53	0.60	1.36	0.78	1.32
NM_146584	Olfr1026	Olfactory receptor 1026	0.01	-2.30	0.01	-2.22	1.24	-1.04	0.14	1.82	0.09	2.36
NM_146588	Olfr1030	Olfactory receptor 1030	0.10	1.65	0.30	1.45	0.04	2.35	0.92	1.18	1.08	-1.01
NM_147016	Olfr1049	Olfactory receptor 1049	0.19	-1.54	0.03	-2.00	0.44	1.49	1.20	-0.93	1.00	1.19
NM_147019	Olfr1054	Olfactory receptor 1054	1.18	-0.96	1.18	-0.94	0.10	-1.94	0.04	-2.09	0.28	-1.69
NM_147029	Olfr1120	Olfactory receptor 1120	0.03	1.93	0.03	2.06	0.05	2.31	0.09	1.93	0.43	1.55
NM_146349	Olfr1128	Olfactory receptor 1128	0.95	1.06	0.01	2.26	0.93	1.22	0.42	1.47	0.30	1.71
NM_146289	Olfr113	Olfactory receptor 113	0.24	1.42	0.30	1.47	0.01	3.52	0.91	1.18	0.64	1.43
NM_146848	Olfr1161	Olfactory receptor 1161	0.76	-1.22	0.25	-1.49	0.24	-1.68	0.01	-2.43	0.10	-2.01
NM_146917	Olfr1179	Olfactory receptor 1179	0.05	1.87	0.38	1.43	0.14	-1.86	0.05	-2.06	0.13	-1.93
NM_146288	Olfr122	Olfactory receptor 122	0.51	-1.28	1.10	-1.04	0.63	-1.38	0.02	-2.25	0.03	-2.38
NM_146902	Olfr1221	Olfactory receptor 1221	0.19	-1.53	0.04	-1.93	0.01	3.40	0.00	4.23	0.09	2.53
NM_146454	Olfr1231	Olfactory receptor 1231	0.42	1.30	0.02	2.22	0.01	2.98	0.02	2.59	0.32	1.69
NM_021368	Olfr1264	Olfactory receptor 1264	0.16	-1.55	0.90	-1.13	0.62	-1.35	0.01	-2.58	1.12	-0.97
NM_146448	Olfr1317	Olfactory receptor 1317	0.92	-1.14	1.18	-1.03	0.01	3.41	0.90	1.21	0.53	1.46
NM_146292	Olfr1324	Olfactory receptor 1324	1.19	-0.96	0.98	1.16	0.01	3.21	0.18	1.71	0.57	1.43
NM_146913	Olfr1348	Olfactory receptor 1348	0.32	-1.41	0.16	-1.60	0.02	-2.43	0.00	-4.65	0.00	-3.20
NM_146910	Olfr1378	Olfactory receptor 1378	0.54	-1.30	0.94	-1.17	0.48	-1.48	0.01	-2.44	0.32	-1.68
NM_146277	Olfr1412	Olfactory receptor 1412	0.23	1.50	0.01	2.35	0.00	7.63	0.00	8.10	0.00	8.98
NM_147038	Olfr1416	Olfactory receptor 1416	0.58	1.30	0.60	1.28	0.05	2.27	0.76	1.27	0.87	-1.18
NM_146301	Olfr1475	Olfactory receptor 1475	0.77	1.06	0.41	-1.34	0.28	-1.57	0.06	-1.97	0.00	18.27
NM_146505	Olfr148	Olfactory receptor 148	0.17	1.51	0.02	2.23	0.00	6.51	0.00	7.05	0.00	5.15
NM_146995	Olfr202	Olfactory receptor 202	0.39	1.39	0.04	1.99	0.30	1.64	0.02	2.67	0.14	2.24
NM_146446	Olfr215	Olfactory receptor 215	0.96	1.15	0.02	2.14	0.54	-1.40	1.19	-0.97	0.15	2.09

NM_146347	Olfr390	Olfactory receptor 390	1.15	-0.89	0.03	1.95	0.00	4.28	0.04	2.26	0.02	3.42
NM_146720	Olfr421	Olfactory receptor 421	0.36	-1.38	0.43	-1.38	0.02	-2.46	0.00	-2.95	0.15	-1.89
NM_146576	Olfr459	Olfactory receptor 459	0.15	1.58	0.99	1.08	0.05	2.30	0.02	2.56	0.03	3.02
NM_146734	Olfr478	Olfactory receptor 478	0.30	-1.43	0.01	2.57	0.33	1.64	0.24	1.71	0.96	1.21
NM_146736	Olfr491	Olfactory receptor 491	0.81	-1.20	0.87	-1.18	0.79	-1.30	0.04	-2.11	0.36	-1.63
NM_146356	Olfr521	Olfactory receptor 521	0.88	1.18	0.69	-1.27	0.06	-2.08	0.02	-2.24	0.12	-1.97
NM_146960	Olfr53	Olfactory receptor 53	0.75	1.23	0.62	1.29	0.02	2.81	0.03	2.36	0.17	2.00
NM_147104	Olfr550	Olfactory receptor 550	0.74	-1.23	0.15	-1.66	0.45	-1.50	0.01	-2.61	0.13	-1.95
NM_008330	Olfr56	Olfactory receptor 56	0.03	-1.95	0.00	5.03	0.01	3.02	0.00	3.64	0.05	2.88
NM_147091	Olfr568	Olfactory receptor 568	0.04	-1.85	0.90	-1.16	0.07	-2.07	0.01	-2.48	0.28	-1.69
NM_147114	Olfr575	Olfactory receptor 575	1.19	-0.93	0.18	-1.56	0.22	-1.71	0.02	-2.24	0.10	-2.02
NM_146380	Olfr593	Olfactory receptor 593	0.62	-1.24	0.06	-1.82	0.01	-2.69	0.05	-2.03	0.02	-2.47
NM_147080	Olfr615	Olfactory receptor 615	0.73	-1.18	1.17	-1.00	0.10	-1.97	0.04	-2.07	0.15	-1.95
NM_147119	Olfr632	Olfactory receptor 632	0.39	-1.35	0.23	-1.50	0.29	-1.62	0.04	-2.08	0.29	-1.69
NM_146379	Olfr654	Olfactory receptor 654	0.06	1.79	0.03	2.17	0.02	-2.44	0.00	-5.11	0.00	-3.20
NM_147033	Olfr714	Olfactory receptor 714	1.11	-1.02	1.19	-0.91	1.08	-1.15	0.03	-2.17	0.27	-1.70
NM_146929	Olfr807	Olfactory receptor 807	0.96	-1.14	0.92	-1.15	0.34	-1.59	0.01	-2.44	0.03	-2.40
NM_146777	Olfr818	Olfactory receptor 818	0.02	2.12	0.01	2.30	0.01	2.94	0.06	2.10	0.05	2.84
NM_146564	Olfr836	Olfactory receptor 836	0.04	-1.88	0.10	-1.73	0.96	-1.20	0.59	1.35	0.92	1.24
NM_146282	Olfr846	Olfactory receptor 846	1.13	-1.05	0.82	-1.21	0.77	-1.28	1.18	-0.87	0.02	-2.60
NM_146336	Olfr893	Olfactory receptor 893	0.49	-1.34	0.09	-1.75	0.06	-2.10	0.03	-2.17	0.02	-2.43
NM_146801	Olfr904	Olfactory receptor 904	0.07	1.75	0.04	1.93	0.19	1.78	0.31	1.56	0.46	1.54
NM_146330	Olfr958	Olfactory receptor 958	0.04	1.91	0.31	1.45	0.19	1.77	1.17	-0.86	1.11	-0.85
NM_053008	Olig3	Oligodendrocyte transcription factor 3	0.28	1.44	0.02	2.07	0.00	5.92	0.00	4.20	0.03	3.16
NM_011016	Orm2	Orosomucoid 2	1.17	-0.99	0.00	3.51	0.02	-2.51	0.07	-1.91	0.68	-1.34
NM_013623	Orm3	Orosomucoid 3	0.26	1.46	0.00	3.48	1.27	-0.88	0.93	1.20	1.11	-1.01
BB149074	Osbpl3	Oxysterol binding protein-like 3	0.12	-1.57	0.48	-1.23	0.59	-1.28	0.03	-2.19	0.21	-1.79
NM_024289	Osbpl5	Oxysterol binding protein-like 5	0.04	1.85	0.52	1.35	0.00	-5.31	0.22	-1.65	0.54	-1.48
NM_173350	Osbpl9	Oxysterol binding protein-like 9	0.44	1.35	0.03	1.97	0.00	-4.34	0.00	-2.89	0.00	-3.74
NM_011019	Osmr	Oncostatin M receptor	1.16	-1.05	0.29	1.47	0.00	3.92	0.41	1.49	0.19	1.94

NM_145932	Osta	Organic solute transporter alpha	1.16	-1.07	1.20	-1.00	0.01	2.91	0.06	2.07	0.36	1.61
NM_178933	Ostb	Organic solute transporter beta	1.00	1.07	0.00	2.57	0.00	7.22	0.00	3.84	0.00	5.46
NM_013624	Otog	Otogelin	0.73	1.20	0.04	1.99	0.02	2.66	0.01	3.08	0.05	2.76
CF165979	OTTMUSG00000010173	Predicted gene 13051	0.88	1.17	0.27	1.48	0.00	5.96	0.05	2.17	0.11	2.24
BC024323	OTTMUSG00000010657	Predicted gene, OTTMUSG00000010657	0.17	1.54	0.01	-2.16	0.00	6.84	0.00	5.06	0.00	5.57
NM_019935	Ovol1	OVO homolog-like 1 (Drosophila)	0.65	-1.23	0.54	-1.30	1.14	-1.13	0.03	-2.21	0.38	-1.62
NM_024188	Oxct1	3-oxoacid CoA transferase 1	1.19	-0.95	0.95	-1.13	0.01	2.94	0.00	4.02	0.02	3.52
NM_027571	P2ry12	Purinergic receptor P2Y, G-protein coupled 12	1.18	-0.96	0.03	-1.96	0.02	-2.46	0.21	-1.66	0.58	-1.45
NM_028808	P2ry13	Purinergic receptor P2Y, G-protein coupled 13	0.86	-1.22	0.69	1.23	0.06	2.22	0.00	3.35	0.01	4.09
NM_133200	P2ry14	Purinergic receptor P2Y, G-protein coupled, 14	0.25	1.47	0.14	1.63	0.00	3.94	0.00	4.46	0.01	4.34
NM_183168	P2ry6	Pyrimidinergic receptor P2Y, G-protein coupled, 6	1.19	-1.00	0.98	-1.18	0.26	1.69	0.05	2.20	0.02	3.67
NM_011061	Padi4	Peptidyl arginine deiminase, type IV	1.16	-0.93	1.19	-1.02	0.05	2.29	0.98	1.19	0.97	1.21
NM_008777	Pah	Phenylalanine hydroxylase	1.18	-0.97	0.86	-1.19	0.04	-2.24	0.76	-1.29	0.64	-1.41
NM_146169	Paip2b	Poly(A) binding protein interacting protein 2B	0.01	-2.12	0.05	-1.80	0.54	-1.44	1.19	-0.87	0.50	-1.50
AV151664	Pank3	Pantothenate kinase 3	0.78	-1.23	0.25	-1.51	0.04	-2.24	0.08	-1.91	0.21	-1.77
NM_019482	Panx1	Pannexin 1	1.16	-1.05	0.01	2.44	0.00	3.65	0.03	2.37	0.03	3.03
NM_011863	Papss1	3'-phosphoadenosine 5'-phosphosulfate synthase 1	0.50	1.31	0.25	1.51	0.03	2.56	0.10	1.96	0.50	1.56
NM_181402	Parp11	Poly (ADP-ribose) polymerase family, member 11	0.89	-1.20	0.03	1.98	0.04	-2.25	0.04	-2.13	0.11	-1.96
AK005563	Parp14	Poly (ADP-ribose) polymerase family, member 14	0.01	-2.39	0.00	3.10	0.09	2.03	0.15	1.75	0.28	1.72
NM_177460	Parp16	Poly (ADP-ribose) polymerase family, member 16	0.09	1.66	0.02	2.18	0.00	76.42	0.00	57.45	0.00	45.82
NM_030253	Parp9	Poly (ADP-ribose) polymerase family, member 9	0.99	-1.15	0.00	2.76	0.28	1.63	0.57	1.37	0.56	1.46
BQ174597	Parvb	Parvin, beta	1.19	-0.97	1.20	-0.97	0.47	1.47	0.04	2.22	0.11	2.22
NM_022321	Parvg	Parvin, gamma	1.03	-1.13	1.20	-0.99	0.03	2.58	0.00	3.40	0.03	3.16
NM_019574	Patz1	POZ (BTB) and AT hook containing zinc finger 1	1.18	-1.01	0.66	-1.25	0.01	-2.76	0.05	-1.99	0.47	-1.52
NM_011037	Pax2	Paired box gene 2	0.01	-2.36	0.08	-1.70	1.27	-0.89	0.19	1.71	0.38	1.66
BY476977	Pax3	Paired box gene 3	1.17	-0.94	0.37	1.40	0.00	5.08	0.15	1.77	0.19	1.90
NM_053144	Pcdhb19	Protocadherin beta 19	0.01	-2.34	0.12	-1.68	0.47	-1.47	0.05	-2.02	0.00	-3.06
AK019998	Pcgf5	Polycomb group ring finger 5	0.88	-1.17	0.35	1.43	0.03	-2.39	0.51	-1.40	0.89	-1.25
NM_146086	Pde6a	Phosphodiesterase 6A, cGMP-specific, rod, alpha	1.15	-0.92	0.00	3.09	0.02	2.61	0.08	2.00	0.51	1.52

NM_033614	Pde6c	Phosphodiesterase 6C, cGMP specific, cone, alpha prime	0.04	1.91	0.05	1.92	0.35	-1.58	0.28	-1.59	0.14	-1.90
NM_145630	Pdk3	Pyruvate dehydrogenase kinase, isoenzyme 3	1.17	-0.93	0.60	1.29	0.00	3.63	0.00	3.59	0.07	2.52
NM_010329	Pdpn	Podoplanin	0.29	1.44	0.58	1.31	0.05	2.32	0.31	1.58	0.56	1.48
NM_011066	Per2	Period homolog 2 (Drosophila)	0.00	2.84	0.00	2.61	0.00	18.75	0.00	12.21	0.00	7.02
NM_011067	Per3	Period homolog 3 (Drosophila)	0.00	2.85	0.01	2.47	0.20	-1.68	1.19	-0.95	0.49	-1.47
X98847	Pfkfb2	6-phosphofructo-2-kinase/fructose-2,6-biphosphatase 2	0.03	1.93	0.66	1.27	0.99	1.12	0.85	-1.12	0.73	-1.25
NM_173019	Pfkfb4	6-phosphofructo-2-kinase/fructose-2,6-biphosphatase 4	1.19	-1.00	0.39	1.41	0.01	2.95	0.00	3.60	0.01	4.74
NM_019703	Pfkp	Phosphofructokinase, platelet	0.63	-1.29	0.05	1.89	0.00	4.75	0.00	3.56	0.08	2.54
NM_019410	Pfn2	Profilin 2	0.56	-1.31	0.28	-1.48	0.03	2.45	0.41	1.49	1.00	1.21
NM_018774	Phc2	Polyhomeotic-like 2 (Drosophila)	1.12	-1.10	0.02	2.17	0.00	17.07	0.00	15.53	0.00	13.93
AK052150	Pi4kb	Phosphatidylinositol 4-kinase, catalytic, beta polypeptide	0.75	-1.22	0.46	-1.36	0.22	-1.71	0.01	-2.56	0.19	-1.82
AI608096	Pigq	Phosphatidylinositol glycan anchor biosynthesis, class Q	1.14	-1.08	0.66	-1.26	0.25	-1.69	0.00	-3.15	0.03	-2.41
AW741083	Pigs	Phosphatidylinositol glycan anchor biosynthesis, class S	0.03	1.93	0.08	1.79	0.00	-5.58	0.60	1.32	0.07	-2.14
NM_008840	Pik3cd	Phosphatidylinositol 3-kinase catalytic delta polypeptide	0.93	1.08	0.90	1.17	0.05	2.26	0.00	3.58	0.01	3.94
NM_153510	Pilra	Paired immunoglobin-like type 2 receptor alpha	1.16	-1.05	1.04	-1.14	1.26	-0.86	0.05	2.18	0.02	3.45
NM_008842	Pim1	Proviral integration site 1	0.36	-1.35	0.00	3.03	0.20	1.82	0.17	1.78	0.33	1.76
BU697303	Pira1	Paired-Ig-like receptor A1	1.19	-0.95	0.72	-1.27	0.39	1.54	0.05	2.16	0.04	3.02
NM_008848	Pira6	Leukocyte immunoglobulin-like receptor, subfamily B (with TM and ITIM domains), member 3	1.16	-1.01	0.04	-1.89	0.95	1.21	0.83	-1.26	1.13	-1.02
NM_008851	Pitpnm1	Phosphatidylinositol transfer protein, membrane-associated 1	1.14	-1.09	0.47	1.35	0.05	2.28	0.02	2.60	0.03	3.29
NM_008862	Pkia	Protein kinase inhibitor, alpha	0.04	1.91	0.04	2.01	0.01	3.10	0.00	4.45	0.05	2.79
NM_011099	Pkm2	Pyruvate kinase, muscle	0.85	1.15	0.99	1.08	0.00	5.83	0.00	5.86	0.01	4.89
NM_023058	Pkmyt1	Protein kinase, membrane associated tyrosine/threonine 1	1.14	-1.02	0.32	-1.45	0.02	2.66	0.00	3.38	0.28	1.93
NM_008869	Pla2g4a	Phospholipase A2, group IVA (cytosolic, calcium-dependent)	1.17	-1.05	0.72	1.23	0.01	3.48	0.00	4.60	0.01	4.25
NM_177845	Pla2g4e	Phospholipase A2, group IVE	1.07	-1.10	0.25	-1.52	0.14	-1.84	0.00	-2.91	0.19	-1.83
NM_001024145	Pla2g4f	Phospholipase A2, group IVF	0.37	1.27	0.02	2.31	0.07	-2.08	0.21	-1.66	0.04	-2.27
NM_013737	Pla2g7	Phospholipase A2, group VII (platelet-activating factor acetylhydrolase, plasma)	1.12	-0.90	0.29	-1.48	0.15	1.87	0.32	1.53	0.02	3.37
NM_008873	Plau	Plasminogen activator, urokinase	0.15	-1.57	1.10	-1.06	0.04	2.45	0.04	2.24	0.67	1.43
NM_011113	Plaur	Plasminogen activator, urokinase receptor	0.92	1.13	0.02	2.11	0.47	-1.48	0.70	-1.32	0.76	-1.35

NM_019677	Plcb1	Phospholipase C, beta 1	0.79	1.21	0.37	1.40	0.00	5.21	0.01	2.99	0.10	2.29
NM_008874	Plcb3	Phospholipase C, beta 3	1.08	-1.12	0.31	-1.47	0.00	-2.99	0.01	-2.44	0.22	-1.78
NM_172285	Plcg2	Phospholipase C, gamma 2	1.18	-1.04	0.90	1.18	0.24	1.69	0.02	2.58	0.04	2.84
NM_178911	Pld4	Phospholipase D family, member 4	1.17	-1.06	1.17	-1.05	0.07	2.15	0.00	3.71	0.00	5.72
NM_019549	Plek	Pleckstrin	0.68	-1.28	0.14	1.64	0.01	3.54	0.00	4.36	0.01	4.72
NM_153804	Plekhg3	Pleckstrin homology domain containing, family G (with RhoGef domain) member 3	0.09	-1.71	0.19	-1.60	0.05	-2.23	0.14	-1.73	0.28	-1.68
NM_025874	Plin5	Perilipin 5	0.01	2.32	0.91	1.15	0.19	1.81	0.76	1.25	1.12	-0.86
NM_152804	Plk2	Polo-like kinase 2 (Drosophila)	0.49	-1.32	0.02	-2.15	0.03	-2.30	0.00	-3.40	0.00	-4.04
BB807473	Plk3	Polo-like kinase 3 (Drosophila)	0.03	2.01	0.03	2.04	0.00	4.06	0.00	4.17	0.01	3.97
NM_026385	Pllp	Plasma membrane proteolipid	0.03	1.96	0.08	1.77	0.01	2.92	0.01	3.01	0.03	3.12
NM_011636	Plscr1	Phospholipid scramblase 1	0.36	-1.39	0.40	1.39	0.05	2.30	0.32	1.54	1.11	-0.84
NM_021451	Pmaip1	Phorbol-12-myristate-13-acetate-induced protein 1	0.50	1.26	0.29	1.46	0.04	2.50	0.01	2.96	0.01	4.62
NM_008884	Pml	Promyelocytic leukemia	0.18	-1.54	0.01	2.31	0.28	1.66	0.08	1.97	0.06	2.60
NM_011128	Pnliprp2	Pancreatic lipase-related protein 2	0.09	-1.66	0.14	-1.58	0.07	-2.07	0.00	-3.22	0.01	-2.78
NM_027002	Polr2d	Polymerase (RNA) II (DNA directed) polypeptide D	0.96	1.15	1.20	-0.96	0.03	2.55	0.17	1.73	0.64	1.40
NM_008898	Por	P450 (cytochrome) oxidoreductase	0.01	2.17	0.21	1.53	0.50	1.45	0.20	1.71	0.14	2.14
AK017664	Ppat	Phosphoribosyl pyrophosphate amidotransferase	0.04	1.88	0.08	1.75	1.28	-0.87	0.08	2.01	0.74	1.35
AK013818	Ppil6	Peptidylprolyl isomerase (cyclophilin)-like 6	0.86	1.18	1.14	-1.08	0.00	-3.11	1.10	-1.12	0.60	-1.44
NM_008909	Ppl	Periplakin	0.00	2.51	0.10	1.77	0.82	1.17	0.45	-1.27	0.91	-1.05
AK031654	Ppp1r10	Protein phosphatase 1, regulatory subunit 10	1.04	-1.11	0.01	-2.38	0.04	2.41	0.64	1.34	0.16	2.07
NM_133485	Ppp1r14c	Protein phosphatase 1, regulatory (inhibitor) subunit 14c	0.29	-1.27	0.05	-1.84	0.25	-1.67	1.17	-0.86	0.13	2.14
NM_177741	Ppp1r3b	Protein phosphatase 1, regulatory (inhibitor) subunit 3B	0.04	1.89	0.19	1.58	1.21	-1.09	1.21	-0.89	1.12	-0.88
NM_016854	Ppp1r3c	Protein phosphatase 1, regulatory (inhibitor) subunit 3C	0.02	-2.06	0.01	-2.36	0.26	1.75	0.09	2.16	0.22	2.10
NM_172994	Ppp2r2c	Protein phosphatase 2 (formerly 2A), regulatory subunit B (PR 52), gamma isoform	1.09	-1.04	0.47	-1.32	0.63	-1.36	0.01	-2.53	0.79	-1.32
NM_008917	Ppt1	Palmitoyl-protein thioesterase 1	1.18	-1.03	1.10	-1.11	0.04	2.43	0.01	2.71	0.15	2.09
NM_145150	Prc1	Protein regulator of cytokinesis 1	0.07	-1.74	0.00	-3.90	0.27	-1.66	0.00	-2.84	0.17	-1.87
BB224442	Prepl	Prolyl endopeptidase-like	0.01	2.31	0.18	1.58	0.00	5.80	0.41	1.48	0.69	1.38
NM_011073	Prf1	Perforin 1 (pore forming protein)	0.94	-1.10	0.57	1.29	0.00	4.22	0.00	8.61	0.01	4.84
NM_008855	Prkcb1	Protein kinase C, beta	1.16	-0.91	1.02	-1.14	0.15	1.87	0.01	2.72	0.06	2.66

NM_008859	Prkcq	Protein kinase C, theta	0.89	1.18	0.58	1.30	0.18	1.78	0.05	2.17	0.08	2.42
NM_030024	Prr15	Proline rich 15	1.19	-0.97	0.45	-1.36	0.00	-3.18	0.34	-1.53	0.15	-1.89
NM_133351	Prss8	Protease, serine, 8 (prostasin)	0.75	1.22	0.04	1.96	0.01	-2.65	0.20	-1.68	0.13	-1.99
NM_011178	Prtn3	Proteinase 3	0.12	1.16	0.00	7.25	0.01	2.98	0.00	3.54	0.03	3.39
NM_011180	Pscd1	Cytohesin 1	0.03	1.99	1.18	-0.95	0.69	-1.35	0.56	-1.38	0.05	-2.18
NM_028195	Pscd4	Cytohesin 4	1.19	-0.97	1.06	-1.11	0.18	1.80	0.02	2.55	0.03	3.18
BF661492	Pscdbp	Cytohesin 1 interacting protein	0.01	2.39	0.14	1.64	0.44	1.48	1.06	-1.14	0.99	1.18
NM_013640	Psmb10	Proteasome (prosome, macropain) subunit, beta type 10	1.17	-1.06	0.00	2.55	0.80	1.25	0.92	-1.14	0.59	1.47
NM_010724	Psmb8	Proteasome (prosome, macropain) subunit, beta type 8 (large multifunctional peptidase 7)	1.17	-1.05	0.01	2.51	0.00	4.24	0.00	3.91	0.06	2.61
NM_013585	Psmb9	Proteasome (prosome, macropain) subunit, beta type 9 (large multifunctional peptidase 2)	0.22	-1.50	0.00	4.63	0.43	1.49	0.41	1.48	0.44	1.62
NM_008949	Psmc3ip	Proteasome (prosome, macropain) 26S subunit, ATPase 3, interacting protein	0.11	1.66	0.80	1.10	0.03	2.48	0.00	3.31	0.04	3.03
BE956887	Psmd11	Proteasome (prosome, macropain) 26S subunit, non-ATPase, 11	0.03	1.99	0.26	1.49	0.00	-5.51	0.01	-2.54	0.02	-2.68
BB310829	Psmf1	Proteasome (prosome, macropain) inhibitor subunit 1	0.61	1.15	0.07	1.84	0.23	1.79	0.04	2.36	0.17	2.14
NM_019976	Psrc1	Proline/serine-rich coiled-coil 1	0.80	-1.22	1.16	-1.08	0.03	2.49	1.19	-0.89	0.97	1.23
NM_011193	Pstpip1	Proline-serine-threonine phosphatase-interacting protein 1	1.17	-1.04	1.18	-0.93	0.07	2.16	0.01	3.01	0.01	4.60
NM_008963	Ptgds	Prostaglandin D2 synthase (brain)	0.03	-1.94	0.07	-1.78	0.90	-1.25	0.41	1.47	0.58	1.42
NM_011198	Ptgs2	Prostaglandin-endoperoxide synthase 2	0.64	1.21	0.33	1.45	0.04	2.40	0.28	1.62	0.43	1.64
D84372	Ptpn11	Protein tyrosine phosphatase, non-receptor type 11	0.04	1.89	0.11	1.68	0.02	-2.57	0.44	-1.47	0.15	-1.88
NM_019933	Ptpn4	Protein tyrosine phosphatase, non-receptor type 4	0.75	1.22	1.15	-0.88	0.80	1.29	0.55	1.40	0.00	5.60
NM_011210	Ptprc	Protein tyrosine phosphatase, receptor type, C	1.19	-0.99	0.97	1.10	0.02	2.63	0.00	3.78	0.01	4.95
U62387	Ptpre	Protein tyrosine phosphatase, receptor type, E	0.21	-1.48	0.00	-4.05	0.65	1.36	0.49	1.41	0.91	1.25
W83004	Ptprf	Protein tyrosine phosphatase, receptor type, F	0.37	-1.38	0.90	-1.19	0.02	-2.56	0.20	-1.68	0.17	-1.84
NM_008988	Punc	Immunoglobulin superfamily, DCC subclass, member 3	0.01	-2.12	0.10	-1.68	0.03	2.54	0.02	2.57	0.17	2.06
NM_023258	Pycard	PYD and CARD domain containing	1.19	-1.01	0.18	1.55	0.00	5.68	0.00	5.48	0.02	3.60
NM_011224	Pygm	Muscle glycogen phosphorylase	0.04	1.97	0.67	1.22	0.57	1.40	0.61	1.33	0.86	1.28
NM_029781	Rab36	RAB36, member RAS oncogene family	0.01	-2.21	0.01	-2.22	0.20	1.84	0.02	2.61	0.10	2.42
M89777	Rab3d	RAB3D, member RAS oncogene family	0.07	1.75	0.49	1.27	0.05	2.48	0.12	1.97	0.58	1.50
NM_030566	Rabep2	Rabaptin, RAB GTPase binding effector protein 2	0.87	-1.17	0.62	-1.28	1.17	-1.12	0.03	-2.14	0.49	-1.51

NM_009008	Rac2	RAS-related C3 botulinum substrate 2	1.08	-1.11	1.17	-1.04	0.01	3.53	0.00	5.09	0.00	6.20
NM_011234	Rad51	RAD51 homolog (S. cerevisiae)	0.11	-1.62	0.22	-1.49	0.18	1.88	0.02	2.52	0.04	2.96
NM_009013	Rad51ap1	RAD51 associated protein 1	0.81	-1.16	0.25	-1.50	0.20	1.77	0.02	2.53	0.25	1.88
NM_009014	Rad51l1	RAD51-like 1 (S. cerevisiae)	0.06	1.81	0.00	2.71	0.00	17.98	0.00	15.81	0.00	9.43
NM_009015	Rad54l	RAD54 like (S. cerevisiae)	1.15	-1.02	0.00	-2.53	0.96	-1.17	1.19	-0.95	0.86	-1.23
NM_009058	Ralgds	Ral guanine nucleotide dissociation stimulator	1.16	-1.05	0.03	1.97	1.18	-1.08	0.03	2.27	0.77	1.31
BC025570	Ramp1	Receptor (calcitonin) activity modifying protein 1	0.01	2.25	0.13	1.68	0.00	5.56	0.01	2.99	0.58	1.48
NM_024457	Rap1b	RAS related protein 1b	0.52	1.31	0.30	1.45	0.11	1.97	0.05	2.18	0.11	2.24
NM_009026	Rasd1	RAS, dexamethasone-induced 1	0.08	1.72	0.00	2.84	0.98	-1.21	0.78	1.27	0.03	3.13
AK014511	Rasl12	RAS-like, family 12	0.01	-2.16	0.26	-1.44	0.36	-1.42	0.42	1.44	0.83	1.31
NM_175445	Rassf2	Ras association (RalGDS/AF-6) domain family member 2	0.04	1.86	0.11	1.71	0.07	2.27	0.09	2.05	0.38	1.63
NM_144917	Rbed1	ELMO/CED-12 domain containing 3	0.43	1.36	0.99	1.13	0.00	3.52	0.15	1.76	0.36	1.63
BU511360	Rbm3	RNA binding motif protein 3	0.46	1.36	0.04	1.99	0.25	1.71	0.04	2.34	0.19	2.07
NM_001024952	Rc3h1	RING CCCH (C3H) domains 1	0.92	1.14	0.98	1.15	1.03	-1.19	0.45	-1.45	1.09	-1.12
NM_009040	Rdh16	Retinol dehydrogenase 16	0.91	1.16	0.33	1.44	0.03	-2.37	1.21	-0.91	1.09	-1.08
NM_027301	Rdh20	4short chain dehydrogenase/reductase family 9C, member 7	1.14	-1.07	0.01	-2.23	0.30	1.64	0.02	2.54	0.01	4.45
NM_058214	Recql4	RecQ protein-like 4	0.04	1.90	0.05	2.00	1.21	-1.05	0.36	1.51	1.12	-0.86
NM_011261	Reln	Reelin	0.78	-1.23	1.15	-1.08	0.01	-2.94	0.01	-2.54	0.40	-1.58
NM_026159	Retsat	Retinol saturase (all trans retinol 13,14 reductase)	1.19	-0.97	0.93	1.17	0.00	-4.44	0.03	-2.18	0.13	-1.95
NM_027689	Rfx4	Regulatory factor X, 4 (influences HLA class II expression)	0.03	-1.95	0.14	-1.62	0.37	1.55	0.08	1.96	0.15	2.03
NM_021340	Rgr	Retinal G protein coupled receptor	0.01	2.17	0.09	1.75	1.13	-1.11	0.46	1.44	0.38	1.69
NM_011267	Rgs16	Regulator of G-protein signaling 16	0.88	1.05	0.59	1.26	0.33	-1.57	0.01	-2.50	0.00	-4.37
NM_026446	Rgs19	Regulator of G-protein signaling 19	1.13	-0.88	1.14	-1.05	0.04	2.32	0.00	3.50	0.03	3.14
NM_009061	Rgs2	Regulator of G-protein signaling 2	0.68	-1.27	1.04	-1.12	0.12	1.96	0.02	2.61	0.03	3.20
NM_009063	Rgs5	Regulator of G-protein signaling 5	0.77	1.21	1.04	-1.09	0.01	2.98	0.09	1.94	0.45	1.55
NM_011880	Rgs7	Regulator of G protein signaling 7	0.28	-1.40	0.17	-1.57	0.84	-1.21	0.02	-2.30	0.66	-1.37
NM_029879	Rgs7bp	Regulator of G-protein signalling 7 binding protein	0.87	1.19	0.05	-1.88	0.09	-1.95	0.88	1.21	1.03	-1.12
NM_007484	Rhoc	Ras homolog gene family, member C	1.16	-1.02	0.60	1.30	0.05	2.33	0.11	1.88	0.30	1.72
NM_175092	Rhof	Ras homolog gene family, member f	0.02	2.16	0.38	1.35	0.04	-2.18	1.00	-1.18	1.07	-1.13
AK122226	Rims3	Regulating synaptic membrane exocytosis 3	0.79	-1.24	0.01	-2.21	0.65	-1.38	1.11	-1.08	1.04	-1.05

NM_138952	Ripk2	Receptor (TNFRSF)-interacting serine-threonine kinase 2	1.16	-1.05	0.03	1.97	0.34	-1.58	1.09	-1.00	0.84	-1.23
NM_019955	Ripk3	Receptor-interacting serine-threonine kinase 3	1.17	-0.94	1.14	-1.08	0.04	2.37	0.00	4.23	0.00	5.29
NM_175448	Rlbp1l2	Retinaldehyde binding protein 1-like 2	0.05	-1.81	0.53	1.33	0.69	-1.27	0.02	-2.24	0.07	-2.13
NM_026301	Rnf125	Ring finger protein 125	0.00	-2.43	0.03	-2.05	1.14	-1.13	0.66	-1.34	0.66	-1.40
AK054424	Rock2	Rho-associated coiled-coil containing protein kinase 2	0.20	-1.53	0.01	-2.41	0.00	-4.64	0.00	-6.77	0.15	-1.89
NM_011281	Rorc	RAR-related orphan receptor gamma	0.00	2.87	0.00	2.65	0.00	18.85	0.00	12.80	0.00	9.82
AI549756	RP23-157O10.7	P140 gene	1.18	-0.95	0.13	-1.65	0.00	-8.26	0.00	-5.62	0.00	-4.00
NM_173431	Rpgrip1l	Rpgrip1-like	0.05	-1.82	0.01	-2.33	0.00	12.00	0.00	10.97	0.00	7.92
BQ443102	Rpl34	Ribosomal protein L34	0.29	-1.44	0.25	-1.51	0.10	-1.98	0.00	-2.78	1.01	-1.19
NM_016980	Rpl5	Ribosomal protein L5	0.83	1.21	0.73	1.25	0.74	1.32	0.94	1.20	1.12	-0.91
AK011587	Rspo2	R-spondin 2 homolog (Xenopus laevis)	0.21	-1.50	0.02	-2.07	0.05	-2.20	0.20	-1.67	0.69	-1.39
NM_080468	Rxfp2	Relaxin/insulin-like family peptide receptor 2	0.90	-1.17	0.67	-1.26	0.85	-1.26	0.02	-2.28	0.79	-1.33
NM_009112	S100a10	S100 calcium binding protein A10 (calpactin)	0.04	-1.89	0.15	-1.60	0.51	1.32	0.20	1.72	0.56	1.53
NM_016740	S100a11	S100 calcium binding protein A11 (calgizzarin)	0.90	-1.17	1.17	-0.92	0.01	3.23	0.17	1.74	0.23	1.84
NM_011313	S100a6	S100 calcium binding protein A6 (calcyclin)	1.19	-0.95	0.21	1.54	0.03	2.49	0.03	2.33	0.03	3.11
NM_013650	S100a8	S100 calcium binding protein A8 (calgranulin A)	0.56	1.30	0.12	1.68	0.00	11.09	0.00	6.27	0.00	10.98
NM_009114	S100a9	S100 calcium binding protein A9 (calgranulin B)	1.19	-0.94	0.12	1.70	0.00	13.08	0.00	5.41	0.00	10.35
NM_007901	S1pr1	Sphingosine-1-phosphate receptor 1	1.17	-1.04	0.00	-2.48	0.15	-1.82	0.27	-1.59	1.13	-0.93
NM_053190	S1pr5	Sphingosine-1-phosphate receptor 5	0.00	2.54	0.98	1.06	0.70	-1.33	1.00	1.14	0.83	-1.30
NM_020568	S3-12	Perilipin 4	0.00	3.26	0.77	1.21	0.36	1.57	0.01	2.89	0.01	4.22
NM_009117	Saa1	Serum amyloid A 1	0.02	-2.13	0.00	2.99	1.27	-0.99	0.01	-2.40	0.74	-1.35
NM_011314	Saa2	Serum amyloid A 2	0.76	0.60	0.00	7.92	0.25	1.68	0.32	1.53	0.36	1.68
NM_011315	Saa3	Serum amyloid A 3	0.20	1.52	0.05	1.86	0.00	57.58	0.00	31.67	0.00	19.67
U15635	Samhd1	SAM domain and HD domain, 1	0.87	-1.20	0.00	6.95	0.40	1.55	0.16	1.82	0.28	1.86
AK047823	Sap30bp	SAP30 binding protein	0.01	-2.23	0.18	-1.59	0.54	1.37	0.44	-1.39	0.84	-1.23
NM_172795	Sarm1	Sterile alpha and HEAT/Armadillo motif containing 1	1.17	-1.00	1.17	-1.01	0.03	2.51	0.23	1.63	0.65	1.37
NM_028773	Sash3	SAM and SH3 domain containing 3	1.17	-0.94	0.86	-1.21	0.04	2.38	0.00	3.98	0.00	5.03
NM_008759	Sebox	SEBOX homeobox	0.49	-1.26	1.16	-0.95	0.01	3.03	0.74	1.28	0.65	1.41
NM_011346	Sell	Selectin, lymphocyte	1.14	-1.07	0.83	1.20	0.02	2.77	0.00	3.26	0.03	3.05
NM_009151	Selplg	Selectin, platelet (p-selectin) ligand	0.85	-1.20	0.99	-1.17	0.06	2.19	0.01	3.15	0.01	4.63

BC010976	Sema3f	Sema domain, immunoglobulin domain (Ig), short basic domain, secreted, (semaphorin) 3F	0.72	-1.18	0.00	-2.69	0.41	1.44	0.10	-1.59	0.50	1.54
AK129018	Sema3g	Sema domain, immunoglobulin domain (Ig), short basic domain, secreted, (semaphorin) 3G	0.03	-2.00	0.36	-1.30	1.26	-0.91	0.89	1.17	0.22	1.96
AK173247	Sema4c	Sema domain, immunoglobulin domain (Ig), transmembrane domain (TM) and short cytoplasmic domain, (semaphorin) 4C	0.94	1.14	0.10	1.72	0.02	2.63	0.06	2.07	0.15	2.08
AK082711	Sema6a	Sema domain, transmembrane domain (TM), and cytoplasmic domain, (semaphorin) 6A	0.32	-1.41	0.01	-2.19	0.63	-1.26	1.08	-1.08	0.09	2.35
BQ934444	Senp3	SUMO/sentrin specific peptidase 3	0.86	1.16	1.16	-1.04	0.82	-1.28	0.04	-2.13	0.05	-2.22
AY862185	Serpina3g	Serine (or cysteine) peptidase inhibitor, clade A, member 3G	1.10	-1.05	0.00	19.57	0.00	-4.64	0.05	-2.05	0.18	-1.82
NM_009252	Serpina3n	Serine (or cysteine) peptidase inhibitor, clade A, member 3K	1.18	-1.01	0.72	1.24	0.04	2.44	0.69	1.32	0.41	1.58
NM_025429	Serpinb1a	Serine (or cysteine) peptidase inhibitor, clade B, member 1a	0.08	-1.70	0.19	-1.52	0.00	-3.63	0.36	-1.48	0.07	-2.11
NM_173052	Serpinb1b	Serine (or cysteine) peptidase inhibitor, clade B, member 1b	0.14	-1.60	0.18	-1.55	0.01	-2.79	0.47	-1.38	0.11	-1.98
BE686716	Serpinb9	Serine (or cysteine) peptidase inhibitor, clade B, member 9	0.90	-1.18	0.23	1.51	0.22	1.72	0.05	2.17	0.46	1.54
NM_009825	Serpinh1	Serine (or cysteine) peptidase inhibitor, clade H, member 1	0.82	1.16	1.13	-1.04	0.02	2.85	0.41	1.48	0.85	1.28
NM_018820	Sertad1	SERTA domain containing 1	0.04	1.86	0.45	1.40	0.34	1.61	0.01	2.99	0.02	3.74
U88566	Sfrp1	Secreted frizzled-related protein 1	0.12	1.65	0.00	2.72	0.19	1.79	0.02	2.60	0.07	2.48
NM_011890	Sgcb	Sarcoglycan, beta (dystrophin-associated glycoprotein)	1.07	-1.12	1.08	-1.10	0.01	3.44	0.02	2.67	0.12	2.29
NM_011892	Sgcg	Sarcoglycan, gamma (dystrophin-associated glycoprotein)	1.19	-0.96	0.21	-1.56	0.90	-1.23	0.44	-1.46	0.04	-2.39
AK031448	Sgms1	Sphingomyelin synthase 1	0.06	-1.79	0.60	-1.29	0.03	-2.32	0.25	-1.58	0.64	-1.34
NM_199007	Sgol2	Shugoshin-like 2 (S. pombe)	0.46	-1.34	0.16	-1.60	0.06	2.24	0.01	3.23	0.04	3.05
NM_021309	Sh2d2a	SH2 domain protein 2A	1.19	-0.99	0.76	-1.22	0.88	1.25	0.02	2.48	0.04	2.91
NM_021389	Sh3kbp1	SH3-domain kinase binding protein 1	1.14	-0.91	0.88	-1.18	0.54	1.42	0.05	2.14	0.03	3.12
NM_177364	Sh3pxd2b	SH3 and PX domains 2B	0.82	1.20	0.77	1.23	0.03	2.49	0.01	3.06	0.03	3.28
NM_011367	Shbg	Sex hormone binding globulin	0.24	-1.46	0.27	-1.47	0.22	-1.72	0.01	-2.47	0.17	-1.87
NM_011426	Siglec1	Sialic acid binding Ig-like lectin 1, sialoadhesin	0.61	-1.31	1.00	1.02	0.53	1.40	0.03	2.45	0.02	3.54
NM_007547	Sirpa	Signal-regulatory protein alpha	0.75	1.13	0.91	-1.17	0.05	2.29	0.07	2.05	0.04	2.95
NM_029415	Slc10a6	Solute carrier family 10 (sodium/bile acid cotransporter family), member 6	0.12	1.63	0.14	1.63	0.03	2.52	1.09	-1.02	0.75	1.37
AK037335	Slc10a7	Solute carrier family 10 (sodium/bile acid cotransporter family), member 7	0.10	-1.68	0.35	-1.40	0.05	-2.19	1.15	-0.95	1.08	-1.08
NM_013612	Slc11a1	Solute carrier family 11 (proton-coupled divalent metal ion transporters), member 1	0.90	1.14	1.19	-0.98	0.00	4.00	0.00	5.96	0.00	6.04

NM_008732	Slc11a2	Solute carrier family 11 (proton-coupled divalent metal ion transporters), member 2	0.77	1.20	0.68	1.25	0.05	2.33	0.85	1.24	1.12	-0.89
NM_019415	Slc12a3	Solute carrier family 12, member 3	0.21	1.51	0.08	1.75	0.01	-2.61	0.43	-1.46	0.19	-1.81
NM_022411	Slc13a2	Solute carrier family 13 (sodium-dependent dicarboxylate transporter), member 2	0.09	1.70	0.80	-1.17	0.03	-2.40	1.10	-1.07	0.01	-3.08
NM_054055	Slc13a3	Solute carrier family 13 (sodium-dependent dicarboxylate transporter), member 3	1.18	-0.99	0.29	1.44	0.00	7.96	0.00	3.87	0.01	4.52
NM_021301	Slc15a2	Solute carrier family 15 (H+/peptide transporter), member 2	1.17	-1.02	0.29	-1.48	0.02	-2.48	0.09	-1.90	0.22	-1.76
NM_023044	Slc15a3	Solute carrier family 15, member 3	0.48	-1.33	0.19	1.56	0.06	2.22	0.02	2.64	0.02	3.38
NM_133895	Slc15a4	Solute carrier family 15, member 4	0.00	3.06	0.18	1.57	0.01	3.31	0.38	1.53	0.91	1.25
NM_025807	Slc16a9	Solute carrier family 16 (monocarboxylic acid transporters), member 9	1.19	-0.99	1.01	-1.15	0.52	1.45	0.01	2.82	0.01	4.34
NM_182959	Slc17a8	Solute carrier family 17 (sodium-dependent inorganic phosphate cotransporter), member 8	0.16	1.57	0.63	-1.26	0.00	-4.32	0.11	-1.83	0.28	-1.67
NM_009201	Slc1a5	Solute carrier family 1 (neutral amino acid transporter), member 5	0.07	1.74	0.43	1.40	0.29	1.68	0.03	2.37	0.50	1.61
NM_144856	Slc22a7	Solute carrier family 22 (organic anion transporter), member 7	0.13	-1.60	0.35	-1.42	0.02	-2.47	1.21	-1.02	0.91	1.24
NM_172685	Slc25a24	Solute carrier family 25 (mitochondrial carrier, phosphate carrier), member 24	1.19	-0.98	1.20	-0.99	0.16	1.85	0.05	2.18	0.20	1.92
NM_146118	Slc25a25	Solute carrier family 25 (mitochondrial carrier, phosphate carrier), member 25	0.80	-1.15	0.02	-2.10	1.01	-1.21	0.43	-1.46	0.49	-1.52
NM_026232	Slc25a30	Solute carrier family 25, member 30	0.06	-1.77	0.00	-3.31	0.27	1.65	0.37	1.49	0.29	1.76
NM_028048	Slc25a35	Solute carrier family 25, member 35	0.32	-1.40	0.49	-1.32	0.69	-1.33	0.00	-2.90	0.24	-1.76
NM_178766	Slc25a40	Solute carrier family 25, member 40	0.21	-1.47	0.75	1.23	0.02	2.74	0.98	-1.13	1.12	-0.87
NM_031197	Slc2a2	Solute carrier family 2 (facilitated glucose transporter), member 2	0.92	1.15	0.86	-1.16	0.01	-2.69	0.85	-1.24	0.80	-1.32
NM_009204	Slc2a4	Solute carrier family 2 (facilitated glucose transporter), member 4	0.00	2.52	0.07	1.81	0.63	1.38	0.24	1.64	0.21	1.86
NM_022885	Slc30a5	Solute carrier family 30 (zinc transporter), member 5	0.26	1.46	0.44	1.37	0.03	2.52	0.20	1.68	0.38	1.61
AK017145	Slc38a2	Solute carrier family 38, member 2	0.02	-2.04	0.50	-1.29	0.99	-1.20	1.13	-1.10	1.12	-0.91
NM_028092	Slc39a5	Solute carrier family 39 (metal ion transporter), member 5	0.33	1.40	0.36	1.43	0.01	-2.69	0.91	1.13	1.13	-0.94
NM_009205	Slc3a1	Solute carrier family 3, member 1	0.25	-1.40	0.42	-1.32	0.02	2.83	0.03	2.35	0.11	2.20
NM_016917	Slc40a1	Solute carrier family 40 (iron-regulated transporter), member 1	1.19	-0.99	0.02	-2.09	0.06	2.22	0.45	1.47	0.23	1.86
NM_173865	Slc41a1	Solute carrier family 41, member 1	1.14	-1.07	0.09	1.72	0.02	2.59	0.74	1.29	0.40	1.58

AK033822	Slc41a2	Solute carrier family 41, member 2	0.13	-1.54	0.00	4.40	1.28	-0.96	0.85	-1.24	0.86	-1.29
NM_027868	Slc41a3	Solute carrier family 41, member 3	0.07	1.74	0.15	1.62	0.03	2.65	0.03	2.39	0.05	2.84
W58808	Slc43a1	Solute carrier family 43, member 1	0.08	1.70	0.04	1.91	1.22	-1.08	0.38	-1.49	0.40	-1.58
NM_053077	Slc45a2	Solute carrier family 45, member 2	0.60	1.25	0.94	1.13	0.02	2.63	0.08	1.98	0.28	1.76
NM_026183	Slc47a1	Solute carrier family 47, member 1	1.15	-0.90	0.80	-1.22	0.01	-2.76	0.37	-1.51	0.47	-1.53
AI875486	Slc5a10	Solute carrier family 5 (sodium/glucose cotransporter), member 10	1.17	-0.94	0.61	1.29	0.02	2.60	0.60	1.35	1.11	-0.85
NM_146198	Slc5a11	Solute carrier family 5 (sodium/glucose cotransporter), member 11	0.64	-1.25	1.13	-1.07	0.49	-1.45	0.03	-2.21	0.47	-1.54
NM_144512	Slc6a13	Solute carrier family 6 (neurotransmitter transporter, GABA), member 13	0.95	1.15	0.98	-1.13	0.01	-2.71	0.70	-1.31	0.71	-1.37
NM_201353	Slc6a7	Solute carrier family 6 (neurotransmitter transporter, L-proline), member 7	0.00	-2.59	0.00	-2.76	0.06	2.23	0.22	1.67	0.55	1.47
NM_007514	Slc7a2	Solute carrier family 7 (cationic amino acid transporter, y+ system), member 2	0.03	1.98	0.03	1.99	0.02	2.58	0.18	1.72	0.55	1.44
NM_011404	Slc7a5	Solute carrier family 7 (cationic amino acid transporter, y+ system), member 5	0.51	1.32	0.57	1.30	0.03	2.55	0.03	2.40	0.29	1.76
NM_011406	Slc8a1	Solute carrier family 8 (sodium/calcium exchanger), member 1	0.85	1.18	0.97	1.12	0.04	2.33	0.09	1.93	0.40	1.59
NM_013797	Slco1a1	Solute carrier organic anion transporter family, member 1a1	0.07	-1.75	0.00	-2.58	0.05	2.28	0.04	2.22	0.13	2.14
NM_030687	Slco1a4	Solute carrier organic anion transporter family, member 1a4	1.18	-0.92	0.95	1.15	0.00	-5.98	1.07	-1.13	1.00	-1.18
NM_021471	Slco1c1	Solute carrier organic anion transporter family, member 1c1	1.06	-1.12	0.13	-1.68	0.14	-1.84	0.01	-2.42	0.27	-1.72
NM_023908	Slco3a1	Solute carrier organic anion transporter family, member 3a1	1.18	-0.97	0.12	1.66	0.01	2.97	0.02	2.44	0.21	1.92
NM_011407	Slfn1	Schlafen 1	0.73	-1.24	0.20	1.56	0.00	3.72	0.00	3.68	0.03	3.29
NM_011408	Slfn2	Schlafen 2	1.18	-1.01	0.08	1.78	0.00	3.57	0.00	4.39	0.00	5.60
NM_011409	Slfn3	Schlafen 3	0.69	1.13	0.24	1.47	0.02	2.81	0.02	2.66	0.15	2.20
NM_172796	Slfn9	Schlafen 9	0.24	-1.48	0.80	1.20	0.03	2.45	0.39	1.49	0.82	1.33
NM_011414	Slpi	Secretory leukocyte peptidase inhibitor	0.80	-1.17	0.52	1.30	0.00	3.99	0.10	2.00	0.48	1.59
AF016189	Smad3	MAD homolog 3 (Drosophila)	0.04	-1.84	0.79	-1.11	0.20	-1.73	0.48	1.41	0.90	1.24
NM_080470	Smc1b	Structural maintenance of chromosomes 1B	1.17	-1.04	0.87	1.18	0.06	2.21	0.00	3.80	0.04	2.85
NM_133888	Smpdl3b	Sphingomyelin phosphodiesterase, acid-like 3B	0.76	1.20	0.05	1.83	0.04	2.35	0.06	2.10	0.14	2.08
BM938145	Snapc5	Small nuclear RNA activating complex, polypeptide 5	1.16	-0.98	0.06	-1.87	0.02	-2.48	0.42	-1.44	0.30	-1.65
NM_172463	Sned1	Sushi, nidogen and EGF-like domains 1	0.14	-1.61	0.18	-1.59	0.02	-2.56	0.05	-2.04	0.33	-1.64

NM_010831	Snf1lk	Salt inducible kinase 1	0.04	1.91	0.24	1.51	1.22	-1.00	1.21	-0.92	1.12	-0.85
NM_009229	Sntb2	Syntrophin, basic 2	0.54	1.31	0.19	1.56	0.02	2.60	0.03	2.30	0.15	2.07
NM_009896	Socs1	Suppressor of cytokine signaling 1	1.19	-1.00	0.00	10.36	0.06	2.24	0.08	2.02	0.36	1.68
BB376896	Socs2	Suppressor of cytokine signaling 2	1.08	-1.12	1.17	-0.93	0.03	-2.30	0.10	-1.85	0.36	-1.64
NM_007707	Socs3	Suppressor of cytokine signaling 3	1.17	-1.02	0.00	3.11	1.28	-0.97	0.48	1.43	0.89	1.26
AV329117	Socs6	Suppressor of cytokine signaling 6	0.19	-1.49	0.76	-1.18	0.07	-2.04	0.00	-4.00	0.00	-5.15
NM_009166	Sorbs1	Sorbin and SH3 domain containing 1	0.33	-1.42	0.01	-2.32	0.00	20.78	0.00	16.34	0.00	9.87
NM_175397	Sp110	Sp110 nuclear body protein	0.55	-1.31	0.02	2.11	0.11	-1.98	0.49	-1.40	0.80	-1.22
NM_029160	Spag16	Sperm associated antigen 16	0.07	-1.75	0.02	-2.14	0.01	-2.81	0.00	-4.16	0.01	-2.95
NM_017407	Spag5	Sperm associated antigen 5	0.55	-1.30	0.04	-1.91	1.26	-0.90	0.08	1.96	0.22	1.84
NM_010097	Sparcl1	SPARC-like 1	1.17	-1.02	1.07	-1.11	0.00	-3.13	0.00	-3.21	0.03	-2.37
NM_011461	Spic	Spi-C transcription factor (Spi-1/PU.1 related)	1.17	-0.91	0.32	-1.44	0.05	2.28	0.00	3.66	0.00	4.98
NM_009258	Spink3	Serine peptidase inhibitor, Kazal type 3	0.13	1.60	0.05	1.91	0.00	4.29	0.00	6.15	0.01	4.30
NM_011463	Spink4	Serine peptidase inhibitor, Kazal type 4	0.02	2.06	0.78	1.10	0.75	-1.30	0.65	1.32	0.89	-1.24
NM_133903	Spon2	Spondin 2, extracellular matrix protein	0.00	-2.94	0.17	-1.61	0.83	1.17	0.09	2.05	0.11	2.45
NM_033523	Spred2	Sprouty-related, EVH1 domain containing 2	1.11	-1.04	0.46	-1.36	0.37	-1.55	0.02	-2.29	0.22	-1.77
NM_011896	Spry1	Sprouty homolog 1 (Drosophila)	1.13	-1.07	0.24	-1.52	0.02	-2.52	0.10	-1.84	0.61	-1.43
NM_145134	Spsb4	SplA/ryanodine receptor domain and SOCS box containing 4	0.58	-1.18	0.41	-1.27	0.01	-2.72	0.18	-1.65	0.23	-1.74
AB017337	Srebf1	Sterol regulatory element binding transcription factor 1	0.00	3.10	0.13	1.64	0.01	-2.87	0.02	-2.29	0.44	-1.50
NM_080448	Srgap3	SLIT-ROBO Rho GTPase activating protein 3	0.04	-1.81	0.01	-2.29	0.27	-1.64	1.21	-0.96	0.91	-1.26
NM_019684	Srpk3	Serine/arginine-rich protein specific kinase 3	0.85	-1.13	0.80	-1.14	0.14	-1.82	0.05	-2.03	0.72	-1.32
NM_011375	St3gal5	ST3 beta-galactoside alpha-2,3-sialyltransferase 5	0.00	3.20	0.41	1.42	0.44	1.50	0.34	-1.53	0.48	-1.52
D16106	St6gal1	Beta galactoside alpha 2,6 sialyltransferase 1	0.76	1.21	0.93	-1.08	0.01	2.98	0.22	1.66	1.13	-0.89
NM_011373	St6galnac4	ST6 (alpha-N-acetyl-neuraminyl-2,3-beta-galactosyl-1,3)-N-acetylgalactosaminide alpha-2,6-sialyltransferase 4	0.56	1.30	0.02	2.14	1.27	-0.91	1.20	-1.00	0.01	3.82
X80502	St8sia3	ST8 alpha-N-acetyl-neuraminide alpha-2,8-sialyltransferase 3	0.70	-1.16	0.12	-1.69	0.41	-1.44	0.84	-1.10	0.04	-2.35
NM_016964	Stag3	Stromal antigen 3	0.59	-1.27	0.32	-1.45	0.36	-1.57	0.01	-2.37	0.23	-1.75
AK020229	Stambpl1	STAM binding protein like 1	0.09	-1.69	1.12	-1.09	0.03	-2.38	0.43	-1.47	1.11	-0.83
NM_019992	Stap1	Signal transducing adaptor family member 1	0.33	-1.41	0.01	-2.19	0.82	1.28	1.18	-0.86	1.09	-1.06
BB232688	Stat1	Signal transducer and activator of transcription 1	0.35	0.95	0.00	11.62	0.08	2.21	0.15	1.86	0.40	1.60
NM_011486	Stat3	Signal transducer and activator of transcription 3	1.15	-0.91	0.01	2.30	0.00	4.40	0.01	3.15	0.05	2.84

NM_009185	Stil	Scl/Tal1 interrupting locus	0.34	-1.38	0.88	-1.16	0.16	-1.78	1.16	-1.01	0.02	-2.61
NM_133810	Stk17b	Serine/threonine kinase 17b (apoptosis-inducing)	0.55	1.27	0.69	-1.29	0.31	1.62	0.04	2.33	0.03	3.27
NM_016866	Stk39	Serine/threonine kinase 39, STE20/SPS1 homolog (yeast)	0.73	1.23	1.17	-0.92	0.05	2.30	0.02	2.43	0.39	1.61
NM_019641	Stmn1	Stathmin 1	1.13	-1.01	0.01	-2.35	0.00	8.78	0.00	7.16	0.00	5.70
NM_009292	Stra8	Stimulated by retinoic acid gene 8	0.04	1.83	0.32	1.47	1.22	-0.99	0.67	1.34	0.40	1.66
NM_011502	Stx3	Syntaxin 3	0.32	1.41	0.09	1.74	0.02	2.81	0.00	3.72	0.01	4.56
AK016060	Sucla2	Succinate-Coenzyme A ligase, ADP-forming, beta subunit	0.01	-2.15	0.87	1.19	0.58	-1.41	0.61	-1.36	0.62	-1.42
NM_032400	Sucnr1	Succinate receptor 1	0.12	-1.61	0.02	-2.02	0.00	15.28	0.00	12.20	0.00	8.56
NM_172294	Sulf1	Sulfatase 1	0.03	1.98	0.01	2.31	0.00	4.26	0.04	2.33	0.42	1.61
NM_028072	Sulf2	Sulfatase 2	1.12	-0.89	1.20	-0.95	0.01	-2.96	0.24	-1.61	0.31	-1.66
NM_019878	Sult1b1	Sulfotransferase family 1B, member 1	1.16	-0.91	1.00	-1.12	0.02	-2.46	0.24	-1.63	0.28	-1.69
NM_018751	Sult1c1	Sulfotransferase family, cytosolic, 1C, member 1	1.16	-1.07	0.69	-1.28	0.01	-2.97	0.01	-2.53	0.02	-2.56
NM_026935	Sult1c2	Sulfotransferase family, cytosolic, 1C, member 2	0.97	1.15	0.60	-1.24	0.02	-2.48	0.55	-1.37	0.03	-2.38
NM_023135	Sult1e1	Sulfotransferase family 1E, member 1	0.00	3.22	0.00	3.02	0.00	5.42	0.00	6.76	0.00	13.71
NM_020565	Sult3a1	Sulfotransferase family 3A, member 1	0.22	-1.48	0.00	-3.23	1.27	-0.89	0.46	1.45	0.85	1.26
NM_020564	Sult5a1	Sulfotransferase family 5A, member 1	0.01	-2.38	0.00	-6.74	0.03	-2.29	0.02	-2.34	0.24	-1.75
NM_011518	Syk	Spleen tyrosine kinase	1.10	-1.08	0.72	-1.26	0.64	1.37	0.05	2.14	0.01	3.77
AK046627	Syt12	Synaptotagmin XII	1.18	-1.02	1.14	-0.89	0.03	2.51	1.19	-0.87	0.91	1.24
CD802855	Syt14	Synaptotagmin XIV	0.02	2.15	0.04	2.07	0.36	-1.58	0.69	-1.32	1.11	-1.02
NM_021314	Tacc2	Transforming, acidic coiled-coil containing protein 2	0.95	1.11	0.02	2.15	0.00	10.58	0.00	5.55	0.01	3.95
NM_009314	Tacr2	Tachykinin receptor 2	0.83	1.20	0.92	1.18	0.00	10.50	0.06	2.13	0.11	2.23
NM_027592	Taf9	TAF9 RNA polymerase II, TATA box binding protein (TBP)-associated factor	0.01	2.41	0.03	2.03	0.02	2.62	0.04	2.23	0.41	1.59
NM_178598	Tagln2	Transgelin 2	0.05	1.84	0.34	1.43	0.00	4.18	0.01	2.82	0.19	1.94
NM_013683	Tap1	Transporter 1, ATP-binding cassette, sub-family B (MDR/TAP)	0.35	-1.41	0.00	8.17	0.05	2.31	0.10	1.90	0.57	1.44
NM_011530	Tap2	Transporter 1, ATP-binding cassette, sub-family B (MDR/TAP)	1.11	-1.11	0.00	2.70	0.22	1.72	0.19	1.71	0.39	1.64
NM_009318	Tapbp	TAP binding protein	1.19	-0.94	0.57	1.29	0.00	3.77	0.01	2.72	0.36	1.69
NM_145391	Tapbpl	TAP binding protein-like	1.18	-1.03	0.00	2.79	1.24	-1.00	0.94	1.18	1.13	-0.90
NM_198100	Tbkbp1	TBK1 binding protein 1	0.58	1.29	0.01	2.26	1.28	-0.95	0.11	1.85	0.16	2.04
NM_001001320	Tbx10	T-box 10	1.19	-1.00	1.16	-0.93	0.01	3.38	0.02	2.44	0.16	1.99

AK031708	Tbx3	T-box 3	0.08	-1.74	0.02	-2.17	0.00	-5.91	0.00	-6.46	0.00	-5.80
NM_011539	Tbxas1	Thromboxane A synthase 1, platelet	0.75	-1.23	0.87	1.18	0.01	3.20	0.00	4.19	0.01	3.87
NM_031198	Tcfec	Transcription factor EC	0.17	1.54	0.95	1.04	0.02	2.71	0.00	3.63	0.00	5.63
AK005842	Tekt4	Tektin 4	0.04	1.85	1.19	-0.99	0.41	1.54	0.42	1.48	0.90	-1.11
NM_009356	Tesp2	Protease, serine, 40	0.03	1.91	0.02	2.08	0.02	2.58	0.10	1.90	0.29	1.71
AK080016	Tet2	Tet oncogene family member 2	0.03	-1.94	0.03	-2.02	0.03	2.53	0.07	2.01	0.18	1.95
X57349	Tfrc	Transferrin receptor	0.04	1.86	0.62	1.30	0.31	-1.58	0.00	-3.17	0.04	-2.30
NM_019984	Tgm1	Transglutaminase 1, K polypeptide	0.41	1.37	0.02	2.16	0.00	11.09	0.00	9.51	0.00	12.30
AF076928	Tgm2	Transglutaminase 2, C polypeptide	0.74	1.22	0.26	1.48	0.00	3.90	0.02	2.58	0.24	1.85
NM_011579	Tgtp	T-cell specific GTPase	0.03	-2.18	0.00	13.53	0.13	-1.85	1.20	-0.98	1.10	-0.93
NM_027919	Tha1	Threonine aldolase 1	0.61	1.28	0.32	1.44	0.04	2.39	1.19	-0.86	1.13	-0.96
NM_011583	Theg	Testicular haploid expressed gene	1.17	-1.04	1.04	-1.13	0.04	-2.22	0.13	-1.77	0.38	-1.60
NM_009381	Thrsp	Thyroid hormone responsive SPOT14 homolog (Rattus)	0.00	2.67	0.13	1.69	0.14	1.92	0.02	2.60	0.02	3.69
NM_009384	Tiam1	T-cell lymphoma invasion and metastasis 1	1.11	-1.07	0.11	-1.70	0.08	-2.01	0.03	-2.17	0.87	-1.28
NM_145133	Tifa	TRAF-interacting protein with forkhead-associated domain	0.75	-1.24	0.00	2.55	0.01	3.40	0.00	4.45	0.00	7.41
NM_178892	Tiparp	TCDD-inducible poly(ADP-ribose) polymerase	0.39	1.38	0.02	2.22	0.00	4.23	0.04	2.33	0.07	2.50
NM_009389	Tle3	Transducin-like enhancer of split 3, homolog of Drosophila E(spl)	0.61	1.27	0.18	1.58	0.04	2.33	0.33	1.53	0.23	1.83
NM_011600	Tle4	Transducin-like enhancer of split 4, homolog of Drosophila E(spl)	0.54	1.26	0.04	1.99	0.10	-1.96	0.04	-2.07	0.04	-2.28
NM_030682	Tlr1	Toll-like receptor 1	1.19	-0.99	0.89	1.14	0.02	2.75	0.00	4.57	0.00	6.28
AI646605	Tlr11	Toll-like receptor 11	0.31	-1.37	0.86	1.08	0.00	4.99	0.00	5.78	0.00	5.86
NM_205823	Tlr12	Toll-like receptor 12	1.00	-1.14	0.05	1.88	0.71	1.33	0.14	1.83	0.36	1.69
NM_011905	Tlr2	Toll-like receptor 2	1.12	-1.10	0.00	3.36	0.00	-7.97	0.00	-4.35	0.32	-1.70
NM_126166	Tlr3	Toll-like receptor 3	1.16	-0.91	0.00	3.56	0.06	2.18	0.13	1.87	0.58	1.45
NM_021297	Tlr4	Toll-like receptor 4	0.46	1.32	0.93	-1.10	0.05	2.30	0.00	3.32	0.01	4.36
NM_133211	Tlr7	Toll-like receptor 7	1.12	-1.08	0.96	-1.17	0.00	5.90	0.01	3.01	0.02	3.69
NM_029422	Tm7sf4	Transmembrane 7 superfamily member 4	0.60	-1.28	0.78	-1.22	0.53	-1.45	0.05	-2.03	0.38	-1.61
NM_178642	Tmem16a	Anoctamin 1, calcium activated chloride channel	0.36	-1.41	0.11	-1.69	0.01	-2.78	0.04	-2.11	0.16	-1.87
AK089405	Tmem173	Transmembrane protein 173	0.86	-1.19	0.03	1.98	0.00	3.55	0.01	2.98	0.14	2.14
NM_144534	Tmem38a	Transmembrane protein 38A	0.02	2.04	0.02	2.13	1.02	-1.19	0.05	-2.03	0.04	-2.29
NM_138758	Tmlhe	Trimethyllysine hydroxylase, epsilon	0.88	-1.17	0.61	-1.27	0.04	-2.22	0.55	-1.38	0.56	-1.46

NM_011607	Tnc	Tenascin C	0.20	-1.50	0.61	-1.27	0.29	-1.63	0.05	-2.05	1.09	-1.04
NM_027206	Tnfaip8l2	Tumor necrosis factor, alpha-induced protein 8-like 2	0.85	1.14	0.11	-1.72	0.10	2.06	0.01	3.02	0.00	6.00
BI079188	Tnfrsf11a	Tumor necrosis factor receptor superfamily, member 11a	0.70	-1.27	0.83	-1.23	0.30	1.64	0.02	2.58	0.06	2.74
NM_013749	Tnfrsf12a	Tumor necrosis factor receptor superfamily, member 12a	0.05	1.83	0.68	1.27	0.98	-1.17	0.75	1.27	0.73	-1.30
BI217232	Tnfrsf14	Tumor necrosis factor receptor superfamily, member 14 (herpesvirus entry mediator)	1.19	-0.93	0.08	1.76	0.05	2.29	0.01	3.12	0.09	2.41
NM_009400	Tnfrsf18	Tumor necrosis factor receptor superfamily, member 18	0.15	1.35	0.24	1.51	0.09	2.30	0.03	2.61	0.01	4.24
M60469	Tnfrsf1b	Tumor necrosis factor receptor superfamily, member 1b	0.01	2.22	0.12	1.72	0.83	1.26	1.19	-1.01	0.52	1.53
CB318883	Tnfrsf23	Tumor necrosis factor receptor superfamily, member 23	1.18	-0.98	0.95	-1.14	0.01	3.39	0.06	2.05	0.18	1.96
NM_175649	Tnfrsf26	Tumor necrosis factor receptor superfamily, member 26	0.63	1.19	0.84	1.13	0.28	1.69	0.01	3.18	0.02	3.75
NM_011659	Tnfrsf4	Tumor necrosis factor receptor superfamily, member 4	1.15	-1.06	1.15	-0.90	0.02	2.84	0.36	1.51	0.64	1.40
NM_145390	Tnpo2	Transportin 2 (importin 3, karyopherin beta 2b)	0.09	1.70	1.12	-1.01	1.27	-0.95	0.37	-1.48	0.00	-3.12
AV321031	Tnrc18	Trinucleotide repeat containing 18	1.19	-0.99	0.87	1.20	0.02	2.76	0.45	1.44	0.35	1.64
NM_009427	Tob1	Transducer of ErbB-2.1	0.52	1.22	0.12	-1.67	0.69	-1.29	0.51	-1.38	0.75	-1.28
NM_020507	Tob2	Transducer of ERBB2, 2	0.21	1.48	0.22	-1.50	1.08	-1.08	1.15	-1.01	1.10	-0.95
NM_011623	Top2a	Topoisomerase (DNA) II alpha	0.16	-1.56	0.01	-2.29	0.05	-2.12	0.03	-2.16	0.60	-1.43
NM_145711	Tox	Thymocyte selection-associated high mobility group box	0.82	1.20	0.79	1.22	0.00	7.37	0.00	4.91	0.02	3.72
NM_009417	Tpo	Thyroid peroxidase	1.17	-1.02	0.96	-1.14	0.83	-1.28	0.04	-2.07	0.45	-1.54
NM_026481	Tppp3	Tubulin polymerization-promoting protein family member 3	0.85	1.07	0.25	1.51	0.19	1.83	0.03	2.33	0.25	1.89
AK014457	Traf3ip1	TRAF3 interacting protein 1	1.18	-0.95	0.70	-1.24	0.02	-2.56	0.23	-1.63	0.34	-1.64
NM_172275	Trafd1	TRAF type zinc finger domain containing 1	0.53	-1.33	0.01	2.37	0.00	6.58	0.00	4.72	0.26	1.90
NM_011637	Trex1	Three prime repair exonuclease 1	0.82	-1.22	0.04	1.94	0.04	2.40	0.07	2.04	0.37	1.61
BU840016	Trim28	Tripartite motif-containing 28	0.05	1.86	0.04	1.96	0.05	-2.17	0.04	-2.11	0.37	-1.61
NM_009099	Trim30	Tripartite motif-containing 30	1.09	-1.11	0.03	2.03	0.88	1.24	0.49	1.41	0.42	1.56
NM_030684	Trim34	Tripartite motif-containing 34	0.19	-1.56	0.01	2.27	0.01	3.04	0.00	4.37	0.01	3.95
NM_019510	Trpc3	Transient receptor potential cation channel, subfamily C, member 3	1.18	-1.00	0.00	-2.61	0.98	1.19	0.56	1.38	0.95	1.24
NM_016984	Trpc4	Transient receptor potential cation channel, subfamily C, member 4	0.02	2.07	0.18	1.62	0.00	-4.90	0.00	-3.81	0.08	-2.14
NM_020277	Trpm5	Transient receptor potential cation channel, subfamily M, member 5	0.00	-2.70	0.04	-1.93	0.01	3.15	0.04	2.18	0.34	1.64
NM_011706	Trpv2	Transient receptor potential cation channel, subfamily V,	0.82	1.18	0.52	1.34	0.20	1.76	0.01	2.78	0.03	3.28

		member 2										
NM_009366	Tsc22d1	TSC22 domain family, member 1	0.10	-1.66	0.00	-2.76	1.07	-1.14	1.21	-0.90	1.11	-0.97
NM_029836	Tspyl2	TSPY-like 2	0.22	-1.50	0.06	-1.86	0.52	1.44	0.03	-2.16	1.13	-0.98
NM_009445	Ttk	Ttk protein kinase	0.08	-1.71	0.00	-3.15	0.03	2.61	0.01	2.99	0.03	3.21
AK014557	Ttll4	Tubulin tyrosine ligase-like family, member 4	0.50	1.28	0.20	1.58	0.00	3.80	0.04	2.27	0.22	1.89
AK083236	Ttll7	Tubulin tyrosine ligase-like family, member 7	0.88	1.18	0.99	1.15	0.00	4.07	0.04	2.18	0.25	1.76
NM_011652	Ttn	Titin	1.11	-1.00	0.37	-1.35	0.91	-1.16	0.60	-1.31	0.04	-2.30
NM_181734	Ttpal	Tocopherol (alpha) transfer protein-like	0.00	2.44	0.15	1.60	0.02	-2.51	0.00	-5.22	0.00	-3.34
NM_017379	Tuba8	Tubulin, alpha 8	0.24	1.41	0.00	4.35	0.98	-1.21	1.21	-1.00	1.08	-1.00
NM_011876	Twf2	Twinfilin, actin-binding protein, homolog 2 (Drosophila)	1.04	-1.10	0.99	-1.14	0.44	1.51	0.05	2.18	0.13	2.17
NM_013698	Txk	TXK tyrosine kinase	1.13	-0.90	1.18	-0.95	0.09	2.06	0.00	3.21	0.03	3.27
NM_138302	Tymp	Thymidine phosphorylase	0.08	-1.74	0.02	-2.09	0.09	2.08	0.02	2.62	0.10	2.27
NM_011662	Tyrobp	TYRO protein tyrosine kinase binding protein	1.19	-0.97	1.16	-1.06	0.04	2.37	0.00	3.44	0.00	5.37
NM_023137	Ubd	Ubiquitin D	0.61	1.27	0.00	8.32	0.11	2.06	1.00	-1.04	0.97	-1.08
NM_023738	Ube1l	Ubiquitin-activating enzyme E1-like	0.97	-1.13	0.01	2.56	0.05	2.31	0.37	1.50	1.11	-0.86
NM_026785	Ube2c	Ubiquitin-conjugating enzyme E2C	0.24	-1.48	0.02	-2.16	0.00	-3.31	0.00	-4.88	0.01	-2.81
AA673621	Ube2l3	Ubiquitin-conjugating enzyme E2L 3	0.03	1.95	0.13	1.68	1.28	-0.96	1.12	-1.09	0.98	-1.22
NM_019949	Ube2l6	Ubiquitin-conjugating enzyme E2L 6	1.02	-1.14	0.05	1.90	0.01	3.00	0.02	2.56	0.37	1.72
NM_026024	Ube2t	Ubiquitin-conjugating enzyme E2T (putative)	0.69	-1.19	0.02	-2.12	0.36	1.56	0.63	1.33	0.66	1.39
NM_016723	Uchl3	Ubiquitin carboxyl-terminal esterase L3 (ubiquitin thiolesterase)	0.26	-1.46	1.19	-0.97	1.12	-1.09	0.03	-2.13	0.49	-1.52
NM_028094	Ugt2a3	UDP glucuronosyltransferase 2 family, polypeptide A1	1.17	-1.04	0.09	-1.72	0.00	-4.11	0.09	-1.86	0.18	-1.82
NM_152811	Ugt2b1	UDP glucuronosyltransferase 2 family, polypeptide B1	0.95	-1.14	0.09	-1.73	0.00	-3.18	0.05	-2.01	0.06	-2.13
NM_053215	Ugt2b37	UDP glucuronosyltransferase 2 family, polypeptide B37	0.75	-1.23	0.01	-2.17	0.07	2.14	0.07	2.06	0.21	1.94
NM_133894	Ugt2b38	UDP glucuronosyltransferase 2 family, polypeptide B38	0.15	-1.57	0.01	-2.23	0.22	-1.70	0.11	-1.82	0.80	-1.33
NM_144845	Ugt3a2	UDP glycosyltransferases 3 family, polypeptide A2	0.84	-1.20	0.42	-1.40	0.04	-2.25	0.12	-1.80	0.43	-1.56
NM_010931	Uhrf1	Ubiquitin-like, containing PHD and RING finger domains, 1	0.34	-1.36	0.73	-1.23	0.02	2.85	0.00	4.10	0.11	2.40
AI837521	Unc13c	Unc-13 homolog C (C. elegans)	0.01	2.30	0.27	1.42	0.00	4.14	0.00	5.17	0.00	10.58
NM_011677	Ung	Uracil DNA glycosylase	0.16	1.57	0.02	2.05	0.61	1.35	0.67	1.28	0.87	1.26
NM_009477	Upp1	Uridine phosphorylase 1	0.94	1.15	0.00	3.04	0.00	5.66	0.00	3.32	0.31	1.76
NM_144940	Uroc1	Urocanase domain containing 1	1.18	-0.95	0.90	1.19	0.03	-2.37	0.98	-1.17	1.00	-1.18

NM_011909	Usp18	Ubiquitin specific peptidase 18	0.19	-1.53	0.00	3.39	0.08	-2.01	0.01	-2.48	0.25	-1.73
NM_016808	Usp2	Ubiquitin specific peptidase 2	0.00	5.26	0.03	2.04	0.54	-1.42	1.22	-0.94	1.12	-0.89
NM_028846	Usp20	Ubiquitin specific peptidase 20	0.15	1.59	0.10	1.76	0.84	-1.17	0.05	2.21	0.99	1.24
NM_031388	Usp26	Ubiquitin specific peptidase 26	0.81	-1.14	0.02	-2.02	0.00	5.52	0.00	6.29	0.00	6.69
AK029782	Ust	Uronyl-2-sulfotransferase	1.01	-1.14	0.99	1.15	0.02	2.70	0.09	1.92	0.18	1.95
NM_134165	V1rc10	Vomeronasal 1 receptor, C10	1.16	-1.05	1.20	-1.00	0.01	-2.92	0.32	-1.54	0.65	-1.40
NM_053235	V1rc5	Vomeronasal 1 receptor, C5	0.80	0.41	0.67	0.52	0.01	-2.50	0.00	-2.54	0.00	5.48
NM_030740	V1rd3	Vomeronasal 1 receptor, D3	0.54	1.30	1.19	-0.99	0.02	-2.46	0.00	-3.00	0.02	-2.50
NM_030735	V1rd9	Vomeronasal 1 receptor, D9	0.00	-4.01	0.00	-3.58	0.01	3.03	0.00	4.81	0.03	3.33
NM_134207	V1rg6	Vomeronasal 1 receptor, G6	0.85	-1.18	0.02	-2.03	0.07	2.12	0.01	2.75	0.17	1.98
NM_134209	V1rg8	Vomeronasal 1 receptor, G8	0.96	-1.14	1.08	-1.09	0.04	-2.24	1.06	-1.10	0.65	-1.41
NM_134214	V1rh5	Vomeronasal 1 receptor, H5	0.10	-1.63	0.52	-1.23	0.23	-1.66	0.01	-2.62	0.03	-2.52
NM_134226	V1rj2	Vomeronasal 1 receptor, J2	0.29	-1.43	0.18	-1.59	0.13	-1.88	0.00	-3.25	0.02	-2.51
NM_134228	V1rl1	Vomeronasal 1 receptor, L1	1.17	-1.05	1.20	-0.97	0.00	4.54	0.01	2.81	0.10	2.33
CB525165	Vac14	Vac14 homolog (S. cerevisiae)	0.30	1.43	0.06	1.80	0.02	2.67	0.04	2.25	0.18	1.95
NM_011691	Vav1	Vav 1 oncogene	1.18	-1.01	0.53	1.29	0.00	3.72	0.00	4.58	0.00	5.61
NM_009500	Vav2	Vav 2 oncogene	0.85	-1.20	0.85	-1.22	0.04	-2.24	0.00	-3.40	0.02	-2.57
NM_011912	Vax2	Ventral anterior homeobox containing gene 2	1.15	-1.06	0.00	2.58	0.00	9.11	0.00	12.66	0.00	16.10
D28599	Vcan	Versican	0.55	1.18	0.65	1.24	0.01	3.16	0.10	1.98	0.08	2.39
NM_011701	Vim	Vimentin	1.16	-1.00	1.18	-0.91	0.02	2.80	0.00	3.24	0.01	3.81
NM_027260	Vrk2	Vaccinia related kinase 2	1.17	-1.05	1.10	-1.10	0.25	1.69	0.03	2.34	0.09	2.40
NM_177723	Vsig8	V-set and immunoglobulin domain containing 8	1.15	-0.91	0.96	-1.16	0.01	-2.84	0.07	-1.92	0.18	-1.84
NM_011710	Wars	Tryptophanyl-tRNA synthetase	1.19	-1.00	0.04	1.93	0.64	1.35	0.78	1.24	0.60	1.44
NM_145155	Wasf3	WAS protein family, member 3	1.19	-0.95	1.19	-0.94	0.03	2.48	0.05	2.18	0.17	2.02
NM_145218	Wbscr17	Williams-Beuren syndrome chromosome region 17 homolog (human)	1.14	-0.92	0.93	1.17	1.26	-0.92	0.07	2.03	0.03	3.07
NM_009516	Wee1	WEE 1 homolog 1 (S. pombe)	0.00	4.07	0.13	1.68	0.02	2.90	0.01	3.13	0.04	3.00
NM_018865	Wisp1	WNT1 inducible signaling pathway protein 1	0.01	-2.17	0.01	-2.21	0.00	-3.17	0.10	-1.81	0.07	-2.15
NM_016873	Wisp2	WNT1 inducible signaling pathway protein 2	1.11	-1.09	1.19	-0.97	0.00	8.36	0.00	5.99	0.01	4.20
BC030370	Wnk1	WNK lysine deficient protein kinase 1	0.04	1.91	1.05	-1.05	1.19	-1.11	0.53	1.40	0.80	1.32
NM_023653	Wnt2	Wingless-related MMTV integration site 2	1.12	-1.09	0.70	-1.26	0.11	-1.93	0.04	-2.11	0.12	-1.95

NM_009525	Wnt5b	Wingless-related MMTV integration site 5B	0.00	2.51	0.35	1.44	0.46	-1.48	0.58	-1.36	0.94	-1.23
NM_019653	Wsb1	WD repeat and SOCS box-containing 1	0.01	-2.35	0.58	-1.31	0.03	2.48	0.04	2.24	0.16	2.05
NM_019573	Wwox	WW domain-containing oxidoreductase	0.89	1.17	0.45	1.37	0.12	-1.91	1.21	-0.98	1.10	-1.06
BG092359	Xaf1	XIAP associated factor 1	0.45	-1.38	0.05	1.90	0.08	2.13	0.04	2.29	0.43	1.62
NM_008510	Xcl1	Chemokine (C motif) ligand 1	1.16	-1.06	0.67	1.26	0.04	2.38	0.03	2.29	0.17	1.98
NM_011723	Xdh	Xanthine dehydrogenase	0.75	1.23	0.01	2.32	0.01	2.94	0.06	2.15	0.20	1.90
NM_134014	Xpo1	Exportin 1, CRM1 homolog (yeast)	1.16	-1.02	1.18	-0.93	0.03	2.49	0.14	1.81	0.50	1.52
NM_020506	Xpo4	Exportin 4	1.19	-0.93	0.86	1.20	0.00	5.75	0.01	2.76	0.08	2.46
Y17040	Xrcc2	X-ray repair complementing defective repair in Chinese hamster cells 2	1.05	-1.13	0.75	-1.26	0.25	-1.68	0.04	-2.07	0.72	-1.37
NM_009539	Zap70	Zeta-chain (TCR) associated protein kinase	0.98	1.13	1.05	-1.11	0.04	-2.22	0.80	-1.25	0.92	-1.24
AA882005	Zbtb16	Zinc finger and BTB domain containing 16	0.00	2.80	0.01	2.43	1.09	-1.16	1.15	-1.09	0.79	1.32
NM_019778	Zbtb20	Zinc finger and BTB domain containing 20	1.11	-1.10	1.19	-1.00	0.00	4.49	0.01	3.00	0.13	2.15
NM_172765	Zbtb44	Zinc finger and BTB domain containing 44	0.81	1.20	1.17	-1.06	0.00	-9.31	0.00	-4.54	0.00	-3.61
NM_028864	Zc3hav1	Zinc finger CCCH type, antiviral 1	0.30	-1.43	0.01	2.43	0.00	6.53	0.00	6.96	0.01	4.59
NM_199309	Zdhhc19	Zinc finger, DHHC domain containing 19	0.84	1.18	0.99	-1.10	1.27	-0.95	0.03	-2.23	1.11	-1.03
NM_178395	Zdhhc2	Zinc finger, DHHC domain containing 2	0.21	1.47	1.08	-1.04	0.01	3.18	0.00	3.88	0.07	2.57
BG803382	Zfand5	Zinc finger, AN1-type domain 5	0.92	-1.16	0.17	-1.58	0.01	-2.62	0.05	-2.04	0.17	-1.84
NM_024467	Zfp319	Zinc finger protein 319	0.06	1.73	0.16	1.57	0.03	2.78	0.05	2.40	0.13	2.41
NM_009555	Zfp40	Zinc finger protein 40	1.18	-1.02	1.08	-1.08	0.01	-2.57	0.12	-1.80	0.18	-1.83
BM730596	Zfp456	Zinc finger protein 456	0.18	1.54	0.03	2.08	0.00	-4.23	0.00	-2.80	0.12	-2.03
NM_207255	Zfp532	Zinc finger protein 532	0.55	-1.31	0.12	-1.70	0.01	-2.72	1.10	-1.12	0.90	1.25
NM_182996	Zfp692	Zinc finger protein 692	0.48	-1.33	0.46	-1.38	0.00	-3.13	0.03	-2.19	0.11	-1.99
NM_001012448	Zfp708	Zinc finger protein 708	0.04	1.89	0.42	1.39	0.00	-4.59	0.00	-4.69	0.00	-5.28
NM_023750	Zfp84	Zinc finger protein 84	0.65	1.28	0.71	1.22	0.00	3.60	0.58	1.40	0.54	1.50
NM_026507	Zwilch	Zwilch, kinetochore associated, homolog (Drosophila)	1.15	-1.03	1.16	-1.01	0.01	3.35	0.02	2.56	0.21	1.97

Group	Na (mMol/l)	K (mMol/l)	Ca (mMol/l)	Cl (mMol/l)	Glucose (mg/dl)	LDH (U/l)	GOT (U/l)
Control	150	6,1	2,5	116	184	1172	282
Control	146	8,9	2,5	111	257	2363	566
Control	149	9,2	2,6	114	228	2533	712
4h	146	7,6	2,3	115	213	2346	257
4h	148	8,4	2,5	116	211	2646	424
4h	147	8,2	2,3	115	273	2620	715
1d	150	7	2,7	112	221	1122	222
1d	144	9,6	2,5	113	249	2334	424
1d	148	6,9	2,8	111	261	664	135
2d	147	8,2	2,5	108	221	1530	247
2d	149	7,2	2,6	109	227	1176	239
2d	150	8,5	2,6	110	227	1609	193
3d	152	6,9	2,8	111	218	672	239
3d	150	6,6	2,6	110	191	461	174
3d	148	6,7	2,7	110	231	690	283

Group	GPT (U/l)	de-Ritis (GOT/GPT)	GGT (U/l)	CHE (U/l)	Cholesterol (mg/dl)	TRIG (mg/dl)
Control	119	2,369748	6	6434	82	251
Control	236	2,398305	6	6772	95	170
Control	482	1,477178	6	7066	100	159
4h	48	5,354167	6	6254	97	114
4h	184	2,304348	6	6222	84	134
4h	383	1,866841	6	5936	86	141
1d	43	5,162791	6	6486	84	273
1d	63	6,730159	6	6568	90	363
1d	62	2,177419	6	7152	89	303
2d	81	3,049383	6	7167	90	98
2d	133	1,796992	16	6987	104	160
2d	54	3,574074	6	6462	106	127
3d	140	1,707143	6	8176	91	207
3d	109	1,59633	6	7911	88	185
3d	180	1,572222	6	7821	85	172

Table S2: Biochemical serum parameters for control and experimental groups.

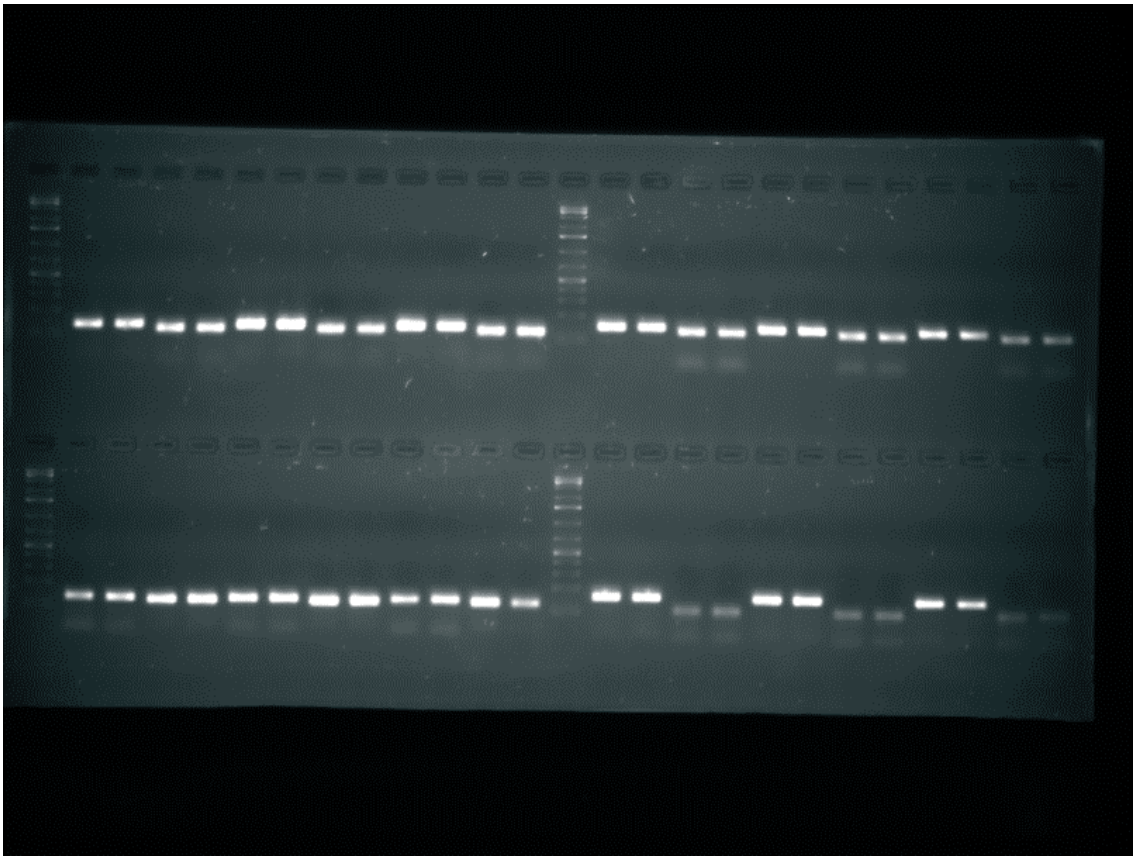

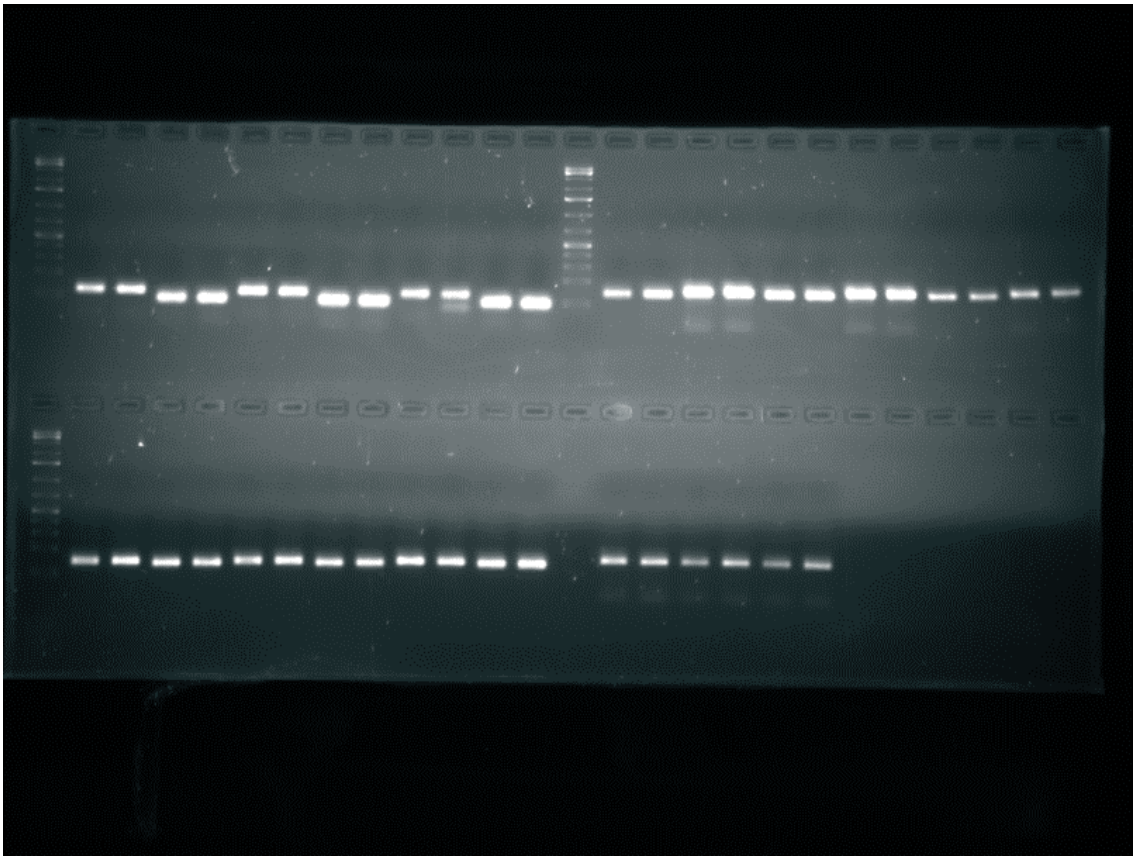

Figure S1: Gel-eclectrophoresis of primer pairs to test specificity of primer products. Single bands indicate that no unspecific DNA was measured during qRT-PCR. Primers for the following genes were used in this study: ACOT1 (Acyl-CoA thioesterase 1), acyl-CoA thioesterase 3 (ACOT3), activin A receptor type II-like 1 (ALK-1), baculoviral IAP repeat-containing 5 (BIRC5), chemokine (C-C motif) ligand 24 (CCL24), chemokine (C-C motif) ligand 5 (CCL5), CD5 molecule-like (SP-α), cyclin-dependent kinase 1 (CDK1), cathelicidin antimicrobial peptide (CRAMP), cytochrome P450, family 7, subfamily A, polypeptide 1 (CYP7A1). G6PD, B2M, PPIA and RPLP2 were used as controls and housekeeping genes, respectively

édition scientifique
VVB LAUFERSWEILER VERLAG

VVB LAUFERSWEILER VERLAG
STAUFENBERGRING 15
D-35396 GIESSEN

Tel: 0641-5599888 Fax: -5599890
redaktion@doktorverlag.de
www.doktorverlag.de

ISBN: 978-3-8359-6007-7